Neuroprosthetic Rehabilitation and Translational Mechanism after Severe Spinal Cord Injury

THÈSE N^{O} 6364 (2014)

PRÉSENTÉE LE 9 DÉCEMBRE 2014

À LA FACULTÉ DES SCIENCES DE LA VIE

CHAIRE IRP EN RÉPARATION DE LA MOËLLE ÉPINIÈRE

PROGRAMME DOCTORAL EN NEUROSCIENCES

ÉCOLE POLYTECHNIQUE FÉDÉRALE DE LAUSANNE

POUR L'OBTENTION DU GRADE DE DOCTEUR ÈS SCIENCES

PAR

Lucia Florinda FRIEDLI WITTLER

acceptée sur proposition du jury:

Prof. M. D. C. Sandi Perez, présidente du jury
Prof. G. Courtine, directeur de thèse
Prof. O. Blanke, rapporteur
Dr J. Bloch, rapporteuse
Prof. E. Rouiller, rapporteur

ÉCOLE POLYTECHNIQUE
FÉDÉRALE DE LAUSANNE

Suisse
2014

Summary

This thesis is a collection of studies, both published and in reparation for publication, that uncover mechanisms of recovery after severe but incomplete spinal cord injuries (SCI). The gradual development of multi-system rehabilitation is illustrated in detail as well as the application in a more clinical relevant setting. Finally, a translational mechanism after SCI is investigated and clinical implications discussed.

Traumatic SCIs have long-term health, economic and social consequences, stressing the urgency to develop interventions to improve recovery after such injuries. Today, the only proven effective interventions to enhance recovery after neuromotor disorders are activity-based rehabilitation therapies, such as locomotor training. However, locomotor training shows no or very limited efficacy to improve function after a severe SCI that induces paralysis of the limbs (ASIA A-B). To mimic the outcome of severe but incomplete SCI in rodents, we developed a model of double opposite-side lateral hemisections termed staggered hemisection in adult rats. This model induced permanent paralysis below the level of injury but leaves an intervening gap of intact neural tissue that provides a substrate for recovery. We showed that this SCI leads to degradation of motor functions, which correlates with the formation of aberrant neuronal connections below the lesion.

Robotic bodyweight support systems used in clinical settings to facilitate rehabilitation generally provide unilateral support under treadmill-restricted conditions. These robotic devices should instead act as propulsive or postural neuroprosthesis allowing training under more natural conditions. We introduced a novel versatile robotic interface that meets these criteria. The robot provides multidirectional bodyweight support during overground locomotion in rats. In evaluation mode, the robotic interface allows detailed assessments of pattern generation and dynamic equilibrium after SCI and stroke. In enabling mode, the robot acts as a propulsive or postural neuroprosthesis that instantly promotes unexpected locomotor capacities. In training mode, the robot enables bipedal and quadrupedal overground rehabilitation.

We next evaluated the effects of robot-assisted gait training enabled by electrochemical neuromodulation of spinal circuits to restore locomotion after staggered hemisection SCI. We found that after two months of daily training, paralyzed rats recovered the ability to initiate, sustain and adjust bipedal locomotion while supported in the robot under electrochemical stimulation. This recovery correlated with ubiquitous reorganization of corticospinal, brainstem, and intraspinal fibers.

We next evaluated whether this treatment paradigm was capable of restoring supraspinal control of locomotion after a more clinically relevant SCI. Rats received a severe contusion of the thoracic spinal cord that spared less than 10% of white matter tissue. Robot-assisted rehabilitation under electrochemical stimulation restored weight-bearing locomotion in all the trained rats. Additionally, a subset of trained rats regained weight-bearing plantar steps in the absence of any enabling factors. Tract-tracing experiments revealed that training promoted reorganization of axonal projections from reticulospinal fibers below the contusion. Virus-mediated silencing of reticulospinal neurons projecting to lumbar segments demonstrated that these inputs were necessary to initiate and sustain walking after training. When delaying the onset of training by two months, in the chronic stage, all the rats regained voluntary locomotor movements but the extent of the recovery was reduced compared to rats trained early after SCI. These combined results confirm the potential of neuroprosthetic training to improve motor function after SCI, and advance our understanding of the mechanisms underlying this recovery. The results provide a strong rationale to evaluate the impact of neuroprosthetic training to improve motor functions in human patients with incomplete SCI.

Translation of treatment paradigms developed in rodent models into effective clinical applications remains a major challenge in biomedical research. Preclinical research studies are often performed in conditions that are poorly comparable to those found in clinical settings. Here, we studied recovery of motor functions in more than 400 quadriplegic patients who presented various degree of spinal cord damage laterality. We found that recovery increases with the asymmetry of early motor deficits. We then compared the recovery of motor functions in animal models and human patients with similar spinal cord damage. We selected patients with the most extreme type of lateralized SCI, termed Brown-Séquard syndrome. We modeled this SCI in cohorts of rhesus monkeys and rats using a lateral cervical hemisection. Kinematic and electromyographic analyses were conducted during locomotion and skilled hand manipulation to investigate recovery in animal models compared to Brown-Séquard patients. Bilateral corticospinal projections were examined in animal models, while motor cortex stimulation was performed both in animal models and Brown-Séquard patients. Surprisingly, we found superior recovery in human patients and hemisected monkeys compared to hemisected rats, both for locomotion and hand function. Multivariate analyses uncovered robust correlations between functional recovery and corticospinal tract reorganization in monkey and humans, but not in rats. We conclude that emergence of spinal cord decussating corticospinal fibers and bilateral motor cortex projections during mammalian evolution supports greater recovery after lateralized SCI primates

compared to rodents. Novel experimental models and dedicated therapeutic strategies are necessary to take advantage of this powerful neuronal substrate for recovery after SCI.

Key words: Spinal cord injury, neurorehabilitation, locomotor training, neuroprosthesis, gait analysis, use-dependent plasticity, epidural electrical stimulation, pharmacological spinal cord stimulation, translational mechanisms, rats.

Kurzfassung in Deutsch

Diese Arbeit ist eine Kollektion wissenschatlicher Studien, publizierte und Manuskripte in Vorbereitung zur Publikation, die Mechanismen von Erholung nach Rückenmarksverletzungen aufzeigen und diskutieren. Grosse Aufmerksamkeit wird weiterhin der Entwicklung von „neuroprothetischem Training“ und der Applikation in ein prä-klinisches Umfeld gewidmet. Die Entwicklung eines neuen neuroprothetischen Trainingsystems, das Gangfunktionen nach Rückenmarksverletzungen (RMV) verbessern soll, wird im Detail und schrittweise erläutert. Schlussendlich wird ein Erholungsmechanismus nach RMV bei verschiedenen Spezien untersucht und die Umsetzungen präklinischer Methoden und Resultate in klinische Therapien diskutiert.

Traumatische RMV haben schwerwiegende langzeit-, gesundheitliche, ökonomische und soziale Konsequenzen. Dadurch ergibt sich die Notwendigkeit neue effektive Behandlungsmethoden zu entwickeln. Die einzige wissenschaftlich bewiesene wirkungsvolle Methode um gegen die Folgen von RMV entgegen zu wirken, sind aktivitätsbasierte Rehabilitationsmethoden wie etwa Lauftraining. Patienten mit einer kompleten Querschnittslähmung profitieren kaum von konventionellem Lauftraining, was auf ein Mangel an gesundem neuronalem Gewebe in diesen Patienten hinweist. Anatomische Studien haben jedoch gezeigt, dass auch bei diesen Patienten intaktes Gewebe neben der Rückenmarksläsion vorhanden ist. Dadurch ist der Begriff der funktionell kompletten jedoch anatomisch inkompeten RMV entstanden. Um die Auswirkung einer solchen RMV zu studieren, haben wir ein Tiermodell entwickelt, das aus zwei gestaffelten entgegen gesetzten Hemisektionen besteht. Diese Art der RMV is unter anderem charakterisiert durch eine massive, graduelle Verschlechterung des Laufmusters. Weiterhin haben wir festgestellt, dass diese Degradation von extensiver Plastizität anormalen spinaler Nervenkreisläufen und Reflexaktivitäten begleitet wird. Eine ähnliche Degradation kann auch bei Patienten mit schweren RMV beobachtet werden.

Robotische Rehabilitationssysteme, wie etwa Gangroboter, werden heute häufig in der Physiotherapie nach RMV eingesezt. Diese Rehabilitationsroboter sollten antreibend und gleichzeitig haltungsunterstützend wirken und das Training natürlichen Laufens auf offenen Oberflächen ermöglichen. Die heute erhältlichen Gangorthesen unterstützen jedoch Patienten vorwiegend beim Lauftraining auf einem Laufband. Der nächste Schritt dieser Doktorareit widmet sich daher der Charakerisierung eines neuen Rehabilitationsroboters, der das Laufen und Gleichgewichtsfunktionen bei Tieren mit Gangstörungen zu trainieren oder evaluieren vermag. Der Evaluationsmodus des

Roboters is in der Lage das Gangmusters sowohl als auch die Balancekontrolle im Detail zu untersuchen. Im Trainingsmodus arbeitet der Roboter als antreibende und haltungsunterstützende Neuroprothese und erlaubt Lauftraining auf einer offenen Oberfläche.

Als nächstest entwickelten wir eine neue Rehabilitationsmethode um willentliche Bewegung nach einer gestaffelten doppelten Hemisektion bei Ratten wieder herzustellen. Dieses neuroprothetische Training beinhaltet bipedales Lauftraining, das durch das oben beschriebene neuroprothetische robotische System und elektrochemischer Stimulation des Rückenmarkes (elektrochemische neuroprothese genannt) ermöglicht wird. Nach zwei Monaten Training haben die Ratten gelernt selbstständig laufen zu initiieren und zu kontrollieren solange sie mit der Haltungs- (Roboter) und elektrochemischer Neuroprothese unterstütz wurden. Die Ergebnisse dieser Studie sind wegweisend in der Rückenmarksforschung da zum ersten Male nach einer schweren Querschnittslähmung eine Wiederherstellung willentlicher Bewegung nachgewiesen werden konnte. Diese bemerkenswerte Erholung assoziierten wir mit einer plastischen Reorganisation von kortikospinalen und auch intraspinalen Nervenfasern an verschiedenen Positionen im Hirnstamm und im Rückenmark.

Obwohl die Resultate dieser Studie in vieler Hinsicht bemerkenswert sind, kann man doch bemängeln, dass eine derartige Läsion von doppelter Hemisektionen im Menschen, zumindest anatomisch betrachtet, nicht vorkommt. Daher haben wir in einem nächsten Schritt den Effekt des neuroprothetischen Trainings in einem klinisch relevanteren Rahmen getestet. Hierfür haben wir Ratten nach einer Rückenmarksquetschung mit der selben Methode für zwei Monate trainiert. In dieser Studie sahen wir, dass auch hier alle Ratten willentliches Laufen wieder erlernt haben. Von besonderen Bedeutung ist, dass wir in gut zwei Drittel der Tiere die Erholung unabhängig der elektochemischen Stimulation war. Somit zeigen wir einen sogenannten „carry-over“ Effekt, also der Loslösung von der Interventionsmethode in ein natürliches Umfeld. Die funktionelle Verbesserung wird begleitet von der Reorganisation retikulospinaler Fasern. Mittels virusinduzierte Deaktivierung haben wir schliesslich die essenzielle Rolle dieses Systems für willkürliches Gehen in diesen Tieren bestätigt. Weiter wollten wir der Frage nachgehen, ob diese Rehabilitationsmethode auch bei Ratten mit chronischen RMV zu einem verbesserten Gang führt. Auch hier konnte die Wiederherstellung willkürlicher Bewegung gezeigt werden; der Umfang der Erholung war jedoch vermindert verglichen mit Tieren, die akut trainiert wurden. So blieben die Ratten, die erst im chronischen Zustand trainiert wurden von der elektrochemischen Prothese abhängig; spontane willkürliche Bewegung konnten wir bei diesen Tieren nicht nachweisen. Die Resultate

dieser Studie bestätigen einerseits das Potential unseres neuroprothetischen Systems motorische Fähigkeiten nach einer schweren RMV wieder herzustellen und fördert gleichzeitig unser Verständnis über den Mechanismus der Erholung nach einer Rückenmarksquetschung.

Die Umsetzung präklinische erfolgreicher Therapien in effektive klinische Anwendungen, auch Bench-to-Bedside Problematik genannt, ist eine sehr grosse Herausforderung in der Forschung. Der Grund dafür liegt häufig darin, dass die Bedingungen im Labor und in der Klinik nicht die selben sind. Um das klinische Potenzial präklinischer Studien besser zu verstehen, haben wir die Mechanismen einer spontanen Erholung nach einer RMV in verschiedenen Spezien untersucht und direkt verglichen. Als erstes haben wir die Erholung von Patienten mit Halbseitenlähmung, Brown-Séquard-Syndrom genannt, untersucht. Hierfür wurden die neurologischen, elektrophysiologischen, lokomotorischen und manuellen Fähigkeiten rapportiert. Als nächstes haben wir dieses Syndrom in Ratten und Rhesusaffen imitiert indem wir eine zervikale Hemisektion angewendet haben. Kinematische und elektromyographische Analysen wurden gemacht und mit denen der Brown-Séquard Patienten verglichen. Die kortikospinalen Projektionen im Rückenmark untersuhten wir mittels neuronalen tracing Methoden und der Studie motorisch evozierter Potentiale. Erstaunlicherweise, zeigten die Resultat eine erhöhte Erholung motorischer Fähigkeiten bei den Affen und Patienten verglichen mit den Ratten. Dies zeigte sich bei der Untersuchung des Ganges und der Handfunktion, die unterschiedliche Erholung zwischen den Spezien war jedoch ausgeprägter bei der Handfunktion. Affen habe im dorsolateralen Trakt bilateral projezierende kortikospinale Axone. Diese Neurite zeigten ein substanzielles Wachstum unterhalb der Läsion. Wir konnten zeigen, dass diese Fasern vom linken, intakten dorsolateralen Kortikospinaltrakt aus über die Mittellinie wuchsen und ein grosses Mass an Neuritverzweigungen aufzeigten in Laminae, die Motoneurone enthalten, die Handmuskeln innervieren. Da Ratten vorwiegend unilateral projezierende kortikospinalen Axone haben sind diese nach einer solchen Verletzung permanent unterbrochen. Multivariate stattistische Verfahren (Hauptkomponentenanalyse) ergaben Korrelationen zwischen Reorganisation von kortikospinalen Axonen und funktioneller Erholung sowohl bei Patienten als auch bie Affen aber nicht bei Ratten. Unsere Untersuchungen haben gezeigt, dass die im Verlaufe der Evolution entstandenen bilateralen Projektionen des Motorkortex die Erholung nach lateraler RMV bei Primaten unterstüzt. Weiterführende experimentelle Untersuchungen und auch therapeutische Ansätze sollten daher von dieser Besonderheit Gebrauch machen und dieses neuronale Substrat sinnvol nutzen.

Schlüsselwörter: Rückenmarksverletzung, eperimentelle Neurorehabilitation, Gang training, Neuroprothetik, neuronales sprouting, epidurale Elektrostimulation, harmakologische Rückenmarksstimulation Ganganalyse, Ratten.

Table of content

SUMMARY **1**

KURZFASSUNG IN DEUTSCH **5**

TABLE OF CONTENT **10**

1 INTRODUCTION **13**

1.1 Spinal cord injury *13*

1.2 Spinal cord injury an ailment not to be treated *15*

1.3 Historical perspectives on locomotion and concepts for neurorehabilitation *18*

1.3 Gaining access to dormant spinal locomotor circuitries after SCI *21*

1.4 Learning in spinal Locomotor circuitries after SCI *28*

1.5 Control of spinal motor circuitries after SCI *31*

1.6. Multi-systems rehabilitation in humans with SCI *35*

2 AIMS OF THE THESIS **37**

3 UNDIRECTED COMPENSATORY PLASTICITY CONTRIBUTES TO NEURONAL DYSFUNCTION AFTER SPINAL CORD INJURY **39**

3.1 Abstract *40*

3.2 Introduction *41*

3.3 Methods *43*

3.4 Results *48*

3.5 Discussion *61*

4 VERSATILE ROBOTIC INTERFACE TO EVALUATE, ENABLE AND TRAIN LOCOMOTION AND BALANCE AFTER NEUROMOTOR DISORDERS **65**

4.1 Abstract *66*

4.2 Introduction *67*

4.3 Methods *69*

4.3 Results *74*

4.4 Discussion *83*

5 RESTORING VOLUNTARY CONTROL OF LOCOMOTION AFTER PARALYZING SPINAL CORD INJURY **85**

5.1 Abstract *86*

5.2 Introduction *87*

5.3 Methods *88*

5.4 Results *92*

5.5 Discussion *100*

6 RETICULAR FORMATION MEDIATES MOTOR FUNCTION RECOVERY AFTER SEVERE SPINAL CORD CONTUSION 101

6.1 Abstract 102

6.2 Introduction 103

6.3 Methods 105

6.4 Results 111

6.5 Discussion 125

7 REORGANIZATION OF CORTICOSPINAL FUNCTION INCREASES RECOVERY AFTER LATERALIZED SPINAL CORD INJURY 129

7.1 Summary 130

7.2 Introduction 131

7.3 Methods 133

7.4 Results 141

7.5 Discussion 153

8 INTEGRATION AND FUTURE APPROACHES IN SPINAL CORD MEDICINE 157

8.1 Neuroposthetic training after SCI 158

8.2 Use-dependent plasticity 161

8.3 Primate specific recovery after SCI 162

8.4 Clinical implementations 163

8.5 Future approaches in spinal cord medicine 165

9 ABBREVIATIONS 168

10 ANNEX AND SUPPLEMENTARY FIGURES 171

10.1 ASIA impairment scale 171

10.2 Supplementary information chapter 4 172

10.3 Supplementary information chapter 5 186

10.4 Supplementary information chapter 6 202

10.5 Supplementary information chapter 7 204

11 REFERENCES 215

12 ACKNOWLEDGMENT 237

13 CURRICULUM VITAE 239

1 Introduction

1.1 Spinal cord injury

The term “spinal cord injury (SCI)” refers to damage of the spinal cord resulting from trauma (e.g. accident, fall), diseases or degeneration (e.g. cancer, vascular disorder, vertebral column degenerative disorders) of spinal tissue. The annual incidence of SCI including pre-hospital fatalities varies in region from < 20 per million people to > 50 per million people; Swiss incidence has been estimated at 15 per million inhabitants (Bernhard *et al.*, 2005; Fawcett *et al.*, 2007; Lee *et al.*, 2014). In the United States alone, it is estimated that 20’000 cases occur every year, of which about 20% of these patients die before they are admitted to the hospital. Since 50 to 70% of new SCI patients are between 15 and 35 years old and the life expectancy is growing after SCI, the worldwide number of survivors has continued to grow over 2 million people; in the USA, SCI population is over 200’000 people. Healthcare for these individuals creates costs of about US$ 4 billion per year, whereas lifetime costs vary from 0.5 to 3 million US$ per patient depending on the severity degree of the SCI. Thus, SCI displays not only a major cause of mortality and morbidity but also a significant economic burden for the society, not to mention the physiological, psychological and social suffering of these patients (Anderson, 2004; Bernhard *et al.*, 2005; Fawcett *et al.*, 2007).

Traumatic SCI can be due to different causes, in developed countries most frequent are motor vehicle accidents (40%), falls (21%), acts of violence (15%), and sports-related activities (13%) (Bernhard *et al.*, 2005), yet the proportion of SCI causes is highly variable from region to region. But there are general trends described between developing and developed countries. SCIs resulting from motor vehicle accidents are stable or even decreasing in developed countries, but are significantly increasing in developing countries. Violence-related SCI occurs in regions of conflict or high availability of weapons (South Africa, North and South America, Middle East). Demographic and economic differences between developed and developing countries were also found in incidence of SCI from low and high falls. Low falls (1-meter or less or on the same level) in elderly are on the increase in developed countries with aging population (Lee *et al.*, 2014).

Generally, SCIs can be classified in two dimensions. First dimension is the injury level and whereas the second level is characterized by the injury severity. The injury level is defined by the neurological level of the injury and classifies the patient roughly into a group of paraplegia (lower limbs are affected) and tetraplegia (upper and lower limbs are

affected). Although the injury level is also varying strongly between regions, overall there are about 50% of SCIs due to injury to the cervical spinal cord resulting in tetraplegia (Ackery, 2004; Lee *et al.*, 2014). The injury severity can superficially divided into two groups, complete (loss of all function, sensory and motor) and incomplete (partial motor function and/or sensory functions). The impairment scale of the American Spinal Injury Association **(**ASIA, **annex 1)** is the most frequent used assessment tool to measure neurological damage. The ASIA scale assesses separately the sensory and motor scores at the different neurological levels. Patients are graded from A (sensorimotor complete – loss of all function) to B (motor complete sensory incomplete), C and D (motor and sensory incomplete), whereas E stands for normal. The International Campaign for Cures of Spinal Cord Injury Paralysis (ICCP) reported a considerable degree of recovery during the first year after SCI, the vast of majority of recovery occurs in the first 3 months though. While the spontaneous recovery of motor function in patients with motor-complete SCI is fairly limited and predictable, recovery in motor-incomplete SCI patients (ASIA C and D) is both more substantial and highly variable and therefore more difficult to predict following conventional neurorehabilitation. Whereas only 17% of patients classified as ASIA A are converting into ASIA B, 80% of ASIA C patients (motor incomplete) are becoming ASIA D or even E (normal). If only sensory functions are preserved (ASIA B), almost half of the patients converted into motor-incomplete (ASIA C mainly, 40%). Together, these results highlight the importance of preserved neuronal tissue for functional recovery (Fawcett *et al.*, 2007; Steeves *et al.*, 2007). In order to reduce lesion severity, pharmacological interventions, like the anti-inflammatory drug methylprednisolone, are already used acutely (1-3 days) after SCI. Further improved understanding of the different elements of reactive process involved in the progression of lesion development could provide opportunities for future interventions (Kakulas, 1999).

1.2 Spinal cord injury an ailment not to be treated

The history of SCI has a rich and absorbing past and goes back to ancient Egyptian times. The "Edwin Smith Papyrus", which dates to ca. 1'500 BCE, is a medical and surgical instruction on trauma. It discusses 48 traumatic cases amongst two are clearly injuries to the spinal cord. The scroll is the first known record that can be called a scientific document and medical document describing treatment methods and is the oldest documentation of cases of SCI. The instructions of handling those two cases of SCI are clear, the injury is not to be treated ("an ailment not to be treated" (Hughes, 1988))(Donovan, 2007). This therapeutic nihilism was followed down through more than a millennium until the early part of the 20th century. Historical examples for this nihilistic philosophy can be cited from the historical records of the 19th century. An example in the 19th century is the case of Lord Admiral Sir Horation Nelson (1758-1805). In the battle of Trafalgar 1805 he was hit by a sniper's bullet that entered his shoulder and spinal cord at the level of the 6th and 7th thoracic vertebrae. After examining the admiral and confirming his SCI, the surgeon's prognosis was unambiguous, he said: "My Lord, unhappily for our country, nothing can be done for you" (Donovan, 2007).

In the early 20th century, the first group expressing their interests for ameliorating the treatment after SCI, were surgeons. Despite advanced knowledge of sterilization and the "germ theory", the mortality rate remained high acutely after injuries to the spine. Records from World War I show that about 70-80 % of soldiers whose spinal cord was hit died within the first 3 weeks (Silver JR 2005) Only the inauguration of the antibiotic era with the discovery of penicillin in 1928 increased substantially the survival rate after SCI. The stabilization of the spinal column remains till today an important aspect of treatment after spinal cord injury (Hughes, 1988; Donovan, 2007). The Dogma of untreatable CNS damage persisted until the late 20th century, but was overturned in the early 1980s when experiments in rats showed that many types of CNS neurons could re-grow their axons under specific laboratory conditions. Researchers now turned their attention towards identifying factors that inhibit the re-growth of CNS tissue. The era of spinal cord research finally was launched by the discovery of both growth-inhibiting factors like Nogo (Schnell & Schwab, 1990) and the discovery of spinal locomotor networks that can produce stepping movements without the input of supraspinal centers and the usage of these circuits to promote use-dependent plasticity through locomotor training (Grillner, 1985; Lovely *et al.*, 1986; Barbeau & Rossignol, 1987).

In the following part of this chapter we reviewed the development current state and potential future of rehabilitative interventions to restore motor functions after severe SCI.

Original article:

Multi-system rehabilitative strategies to restore motor functions following severe spinal cord injuries"

Pavel Musienko[1,2,3,]*, Janine Heutschi[1,2,]*, Lucia Friedli[1,2], Rubia van den Brand[1,2], and Grégoire Courtine[1,2]

Experimental Neurology. 2012 May;235(1):100-9

1. Neurology Department, University of Zurich, Zurich, Switzerland
2. Rehabilitation and Technology Initiative Zurich (RITZ), Zurich, Switzerland
3. Motor Physiology Laboratory, Pavlov Institute of Physiology, St. Petersburg, Russia

*These authors contributed equally to this work

The PhD candidate's contribution: The student contributed to data acquisition and figure preparation

1.3 Historical perspectives on locomotion and concepts for neurorehabilitation

Severe spinal cord injury (SCI) significantly impacts the ability of affected individuals to produce functional standing and walking movements. However, a century of research on the organization of the neural processes that control movements in mammals has demonstrated that the basic neuronal circuitries sufficient to generate efficient stepping patterns and independent standing are embedded within lumbosacral segments (Philippson, 1905; Sherrington, 1910a; Grillner & Zangger, 1984), i.e. caudal to the level of most human SCI. Therefore, the question becomes: how can we transform nonfunctional spinal motor circuitries into highly functional and adaptive states after a severe SCI to restore motor functions in paralyzed subjects?

At the beginning of the past century, Philippson (Philippson, 1905) and Sherrington (Sherrington, 1910a) reported unexpected observations that revolutionized our conception of neural control of movements. They showed that after a complete transection of the thoracic spinal cord in cats and dogs, the hindlimbs could still exhibit a range of motor patterns in response to changing sensory inputs. These observations led Sherrington to conceive the production of movements as “a train of motor acts resulting from a train of successive external situations” (Sherrington, 1910a). Notwithstanding Graham-Brown’s work demonstrating the intrinsic capacity of spinal circuitries to generate rhythmic outputs in the absence of sensory inputs (Graham-Brown, 1911), Sherrington reaffirmed his view on the crucial importance of afferent information in allowing, selecting, and controlling spinal motor outputs in a lecture he gave in 1947 (see discussions in Burke, 2007).

In the mid-70s, Edgerton and Rossignol visited the Karolinska Institute where Grillner sought to unravel the functional architecture of the spinal neuronal networks that can autonomously organize the alternating recruitment of flexor and extensor motor pools—i.e., the circuitries originally conceptualized by Graham-Brown and currently termed central pattern generators or CPGs (Grillner & Zangger, 1979; Grillner, 2006). However, beyond the fascination for the capacities of isolated spinal circuits to produce step-like patterns, Edgerton and Rossignol were puzzled that, to obtain optimal locomotion for experimental recordings, Grillner routinely exposed the spinal kittens to repetitive sensory stimulations, i.e. treadmill training.

Upon their return to their respective laboratories in Los Angeles and Montreal, these observations compelled both researchers to evaluate the full potential of intense daily exercise for improving the functional capacities of adult cats with complete spinal cord

transections. They simultaneously reported that after several months of daily step training, spinal cats could regain the impressive ability to produce full weight bearing locomotion on a treadmill for extended periods of time (Lovely *et al.*, 1986; Barbeau & Rossignol, 1987). Fueled by these findings, Edgerton and his team further challenged the potential of rehabilitative training and weight-bearing afferent inputs to improve function after SCI by evaluating the ability of spinal cats to develop the capacity to stand (De Leon *et al.*, 1998a). They discovered a surprising property of spinal circuitries: cats that had intensively been trained to stand developed the remarkable ability to support their entire body weight for up to one hour, but they stepped very poorly on the treadmill—the spinal cord learned the sensorimotor task that was specifically practiced and trained (Tillakaratne *et al.*, 2002). These results led Edgerton to formulate the concept of activity-dependent plasticity: as repetitive activation of a synapse can change its properties within a timeframe that ranges from milliseconds to months (Hebb, 1949), the repetitive activation of certain sensory and motor pathways with task-specific training can select and reinforce those circuits and connections in a way that significantly improves their ability to perform the practiced movement successfully (Cai *et al.*, 2006a; Edgerton *et al.*, 2008). This system level Hebbian plasticity predicts that the outcome of a neurorehabilitative program will strongly depend upon the type and quality of the motor function that is trained. Moreover, this concept emphasizes the crucial importance of sensory information in shaping the functional remodeling of spinal circuitries with training.

Following these promising discoveries, there has been substantial success in translating activity-based rehabilitation therapies from cats to humans with partial SCI (Dietz & Harkema, 2004). Improvements of ambulatory function in response to locomotor training therapy in patients with incomplete SCI have been reported in several studies from different laboratories (Wernig & Muller, 1992; Dietz *et al.*, 1994; Barbeau *et al.*, 1999; Behrman & Harkema, 2000). A recent clinical trial demonstrated that with weight-bearing training, 92% of subjects with an incomplete SCI (ASIA C or D) regained the ability to walk at a functional speed within three months (Dobkin *et al.*, 2007). On the contrary, locomotor training has not resulted in successful overground walking even with the aid of any walking device in people with a severe SCI classified as ASIA A, B or C with low lower limb motor scores (Dietz *et al.*, 1994; Dietz, 2009). Why does locomotor training fail to significantly ameliorate motor functions in severely affected individuals? The response may be deceivingly simple: robust activity needs to be present for activity-dependent plasticity to occur. However, contrary to individuals with incomplete SCI who progressively regain basic walking capacities after recovering from the initial spinal shock, patients with severe SCI exhibit limited or no residual function to be trained (Dietz

et al., 1994), and locomotor rehabilitation thus fails to promote useful plasticity in sensorimotor pathways (Harkema, 2008). Therefore, the next logical step was to elaborate interventions to gain access to the dormant spinal locomotor circuitries with the aim to reanimate the paralyzed limbs during rehabilitation in order to mediate use-dependent plasticity in the trained neuronal networks.

1.3 Gaining access to dormant spinal locomotor circuitries after SCI

A severe lesion of the spinal cord significantly compromises the degree of sustainable excitability in lumbosacral circuitries. Thus, the inability to produce standing and stepping patterns after a severe SCI is not only due to the interruption of the descending motor commands, but also and above all to the markedly depressed state of spinal neuronal networks (Harkema, 2008). Consequently, in the past decade much effort has been placed on developing paradigms to tune the physiological state of spinal circuits to a level sufficient for stepping and standing to occur. Various strategies including electrical stimulations of the muscles (Mushahwar & Horch, 2000; Mushahwar *et al.*, 2007) or dorsal roots (Barthelemy *et al.*, 2007), epidural (Musienko *et al.*, 2005; Lavrov *et al.*, 2008b; Musienko *et al.*, 2010) or intraspinal (Barthelemy *et al.*, 2007; Mushahwar *et al.*, 2007) electrical spinal cord stimulation, and a variety of pharmacological agents (Rossignol *et al.*, 2001; Landry *et al.*, 2006; Gerasimenko *et al.*, 2007; Lapointe & Guertin, 2008; Courtine *et al.*, 2009a) have shown the capacity to facilitate standing and stepping after a severe SCI. In this review, we specifically focus on the ability of and mechanisms through which epidural spinal cord stimulation and monoamine agonists enable locomotor permissive states in rats with complete SCI (**Figure 1.1**). The reader is referred to other references for a comprehensive review of alternative approaches (Prochazka *et al.*, 2001; Fong *et al.*, 2005; Mushahwar *et al.*, 2006; Guertin, 2009).

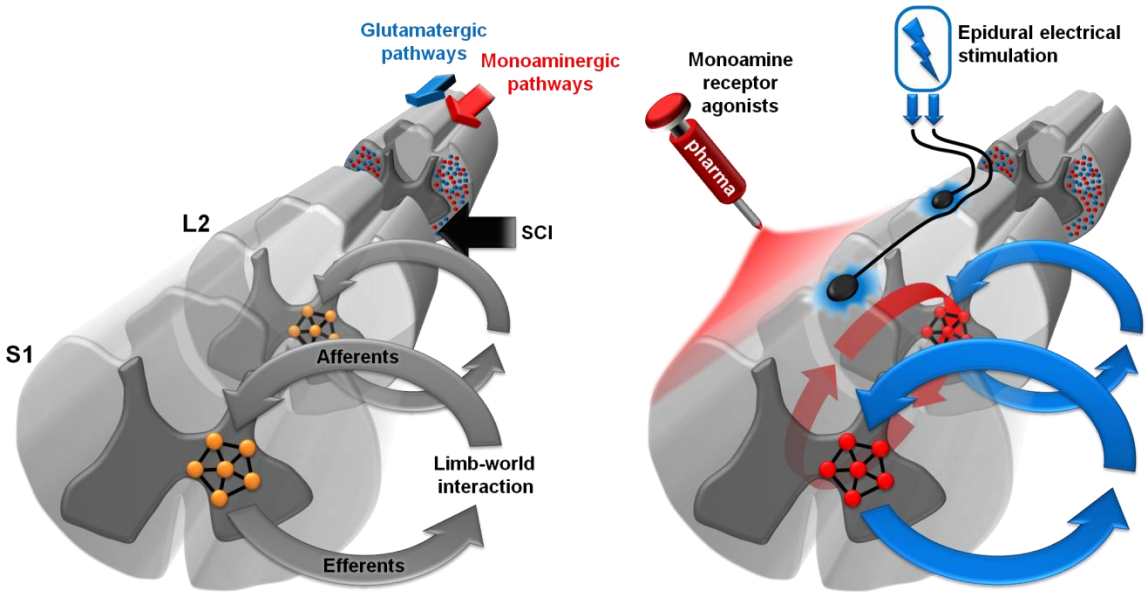

Figure 1.1 Transformation of dormant spinal locomotor circuitries into highly functional states after the loss of supraspinal input.
Schematic drawings of locomotor circuits are shown after a spinal cord transection at the thoracic level that completely interrupts both glutamatergic (blue) and monoaminergic (red) descending pathways originating from various brainstem areas. Without any intervention the lumbosacral circuitries for stepping are in a quiescent state; no or limited locomotor movements can be generated (left). The combination of monoamine receptor agonists and epidural electrical stimulation (EES) at the L2 and S1 levels can transform the physiological state of spinal circuits to a level sufficient for stepping and standing to occur. Tonic EES (blue) replaces the excitatory drive provided by glutamatergic pathways under normal conditions while pharmacological agents (red) mimic the modulatory action of monoaminergic systems (right). The generation of efficient locomotor movements relies on the capacity of spinal circuitries to ensure a continuous match between afferent input and efferent output defining optimal motor states.

Tonic epidural electrical stimulation (EES) applied over the dorsal surface of virtually any lumbar or sacral segment (Ichiyama *et al.*, 2005) have shown the ability to encourage stepping on a treadmill as well as standing in rats (Gerasimenko *et al.*, 2007; Musienko *et al.*, 2009), cats (Musienko *et al.*, 2007), and humans with severe SCI (Minassian *et al.*, 2004; Harkema *et al.*, 2010). The mechanisms underlying the facilitation of motor activities with EES are not yet fully understood (Gerasimenko *et al.*, 2008). Electrophysiological recordings (Gerasimenko *et al.*, 2006) and computer simulations (Holsheimer, 1998; Rattay *et al.*, 2000; Capogrosso *et al.*, 2013), however, suggest that the electrical stimulation engages spinal circuits primarily by recruiting posterior root fibers at their entry into the spinal cord as well as along the longitudinal portions of the fiber trajectories. During quiet standing, EES induces three well-defined motor responses in lower limb muscles that can be classified based on their respective latencies (**Figure 1.2A**): the early response (ER), which only appears at higher intensities when simulating

the more caudal segments, results from the direct stimulation of motoneurons and/or motor nerves. The middle (MR) response is essentially mediated by the monosynaptic connections between Ia fibers and motoneurons, i.e., a response equivalent to the H-Reflex (Gerasimenko *et al.*, 2006; Courtine *et al.*, 2007b). The neural elements associated with the long latency response (LR) remain undetermined, but are likely to rely on multiple systems. Based on the electrophysiological signature of these responses, we argued that the LR in part relies on the disynaptic and/or oligosynaptic connections between group-II fibers and motoneurons (Gerasimenko *et al.*, 2006; Lavrov *et al.*, 2008b). We also surmise that EES recruits thick cutaneous afferent fibers that contact multisensorial interneurons (**Figure 1.2A**), facilitate transmission in group Ib and II pathways (Schomburg *et al.*, 1999), and can elicit coordinated bilateral motor responses in flexor and extensor muscles (Rossignol *et al.*, 2006). How do these motor responses translate into functional patterns of EMG activity during stepping and standing under the influence of continuous EES?

When a spinal rat is positioned bipedally on a stationary treadmill belt, continuous EES applied at the sacral level (S1) induces tonic levels of EMG activity in extensor muscles, which enable the maintenance of a continuous standing posture (**Figure 1.2B**) (Courtine *et al.*, 2009a). A close inspection of muscle EMG traces reveals that the sustained EMG activity in extensors is composed of a succession of motor responses that are locked to the electrical stimulation (**Figure 1.2B**). When treadmill belt motion is initiated, all hindlimb joints undergo changes toward extension (limb moving backward), creating dynamic proprioceptive input that immediately transforms the motor patterns from a tonic to a rhythmic state (**Figure 1.2B**). Under such locomotor states, we found that EMG bursts are essentially built from a sequence of MR responses in extensor muscles, and MR and LR responses in flexor muscles (**Figure 1.2B**) (Lavrov *et al.*, 2008b). Both responses are markedly modulated in amplitude throughout the gait cycle according to the phase of the movement (Gerasimenko *et al.*, 2006; Courtine *et al.*, 2007b; Lavrov *et al.*, 2008b) (**Figure 1.2B**). This phase-dependent modulation of EES-evoked motor responses in flexor and extensor muscles creates rhythmic and alternating bursts of EMG activity sufficient to sustain continuous hindlimb locomotion on a treadmill (Lavrov *et al.*, 2008b). MR and LR motor components show similar behaviors when eliciting step-like patterns with EES in the paralyzed legs of human subjects (Minassian *et al.*, 2004). Together, these data indicate that central mechanisms dynamically update the level of excitability in motor pools and strictly tune the gain in afferent pathways based on the current sensory and motor states of the locomotor apparatus (Hultborn, 2001). Although experimental evidences are still lacking, EES seems to play a crucial

role in augmenting the excitability of the spinal circuitries that underlie and control these operations.

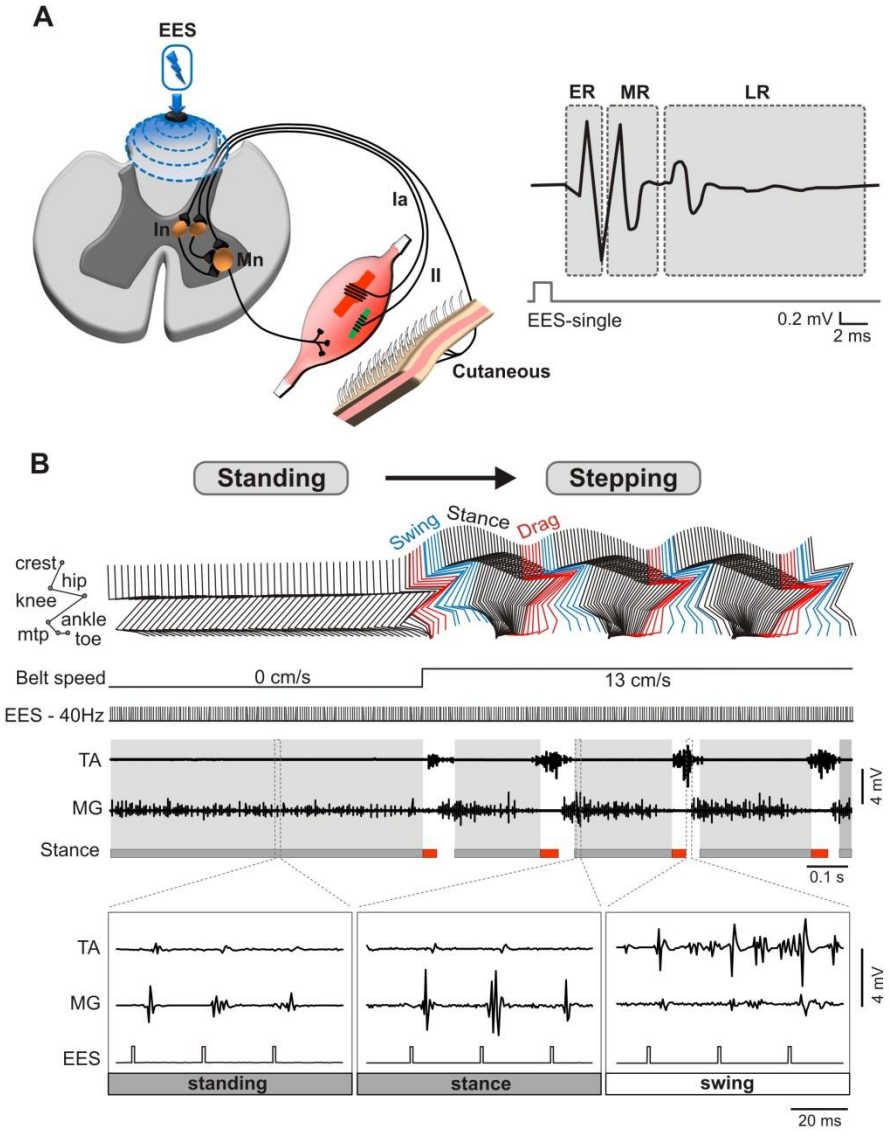

Figure 1.2 Recruitment and modulation of spinal circuits with EES during standing and stepping. **(A)** Schematic illustration of the afferent systems putatively recruited when delivering single-pulse EES. EES typically elicits three responses in all hindlimb muscles. The responses are termed early response (ER), middle response (MR), and late response (LR) based on their respective latencies. **(B)** Hindlimb kinematics and EMG activity from tibialis anterior (TA) and medial gastrocnemius (MG) muscles are shown for a spinal rat receiving continuous (40Hz) EES at the sacral (S1) level. During the represented sequence, the treadmill belt abruptly switches from static (no motion) to dynamic (13 cm/s) conditions. The lower insets display the responses occurring during the highlighted region of the EMG recordings. During standing, the sustained EMG activity in extensor muscles (left inset) is composed of a succession of MR responses that are locked to the EES pulses. The emergence of dynamic state (belt motion) induces the immediate modulation of EES-evoked motor responses whereby the MR in the MG is facilitated during stance (middle inset) and inhibited during swing (right inset), whereas the MR and LR are suppressed in flexor muscles during stance but substantially facilitated during swing. In, interneuron; Mn, motoneuron.

Analysis of EMG activity during standing and stepping showed that EES engages motor pools through the recruitment of afferent pathways, which follow a strict muscle-specific architecture along the rostro-caudal extent of the spinal cord (Vrieseling & Arber, 2006). Thus, can EES delivered at specific locations elicit distinct patterns of motor responses in lower limb muscles? In order to test this hypothesis we applied EES over lumbar (L2) versus sacral (S1) segments during both standing and stepping in spinal rats (Courtine *et al.*, 2009a). Consistent with the rostrocaudal anatomical gradient of flexor and extensor motor pools, we observed a facilitation of flexion with lumbar EES, whereas stimulation applied at the sacral level primarily facilitated extension, both during standing (**Figure 1.3A**) and stepping (**Figure 1.3B**). Moreover, the combination of two (Courtine *et al.*, 2009a), and even more efficiently three (Musienko *et al.*, 2009), sites of EES promoted clear synergistic facilitation of stepping which was evident in the increased consistency of hindlimb kinematics and enhanced body weight support (BWS) capacities (**Figure 1.3C**).

Under normal conditions glutamatergic reticulospinal neurons provide the tonic excitatory drive to engage spinal locomotor networks (Hagglund *et al.*, 2010). Here, we summarized results from various studies that collectively demonstrate the powerful ability of basic spinal cord electrical stimulations to replace the tonic descending source of excitation to facilitate standing and stepping in paralyzed subjects with severe SCI. However, EES alone fails to promote substantial levels of weight bearing with plantar placements of the feet on the treadmill belt (Courtine *et al.*, 2009a). Along the same lines, descending glutamatergic inputs alone fail to elicit long-lasting step-like patterns in mice without the presence of monoamines (Hagglund *et al.*, 2010).

Indeed, spontaneous locomotor activity is associated with a substantial release of monoamines within most laminae of the lumbosacral segments (Hentall *et al.*, 2006). These monoaminergic inputs are not restricted to the classical, hard-wired synaptic communication, but also and primarily operate peri-synaptically through 3-dimensional signal diffusion, i.e., volume transmission (Agnati *et al.*, 2010). Monoaminergic neurotransmitters easily escape the synaptic cleft, enter the extracellular space, and reach extra-synaptic G-protein-coupled receptors located on the surface membrane of neighboring cells. This signaling transduction pathway profoundly alters cell properties over timescales that span from minutes to hours (Agnati *et al.*, 2010). Volume transmission communication suggests that pharmacological agents mimicking the action of monoamines could act in concert with EES to orchestrate the functional tuning of spinal circuitries.

We directly tested this hypothesis in adult rats with a complete SCI (Courtine *et al.*, 2009a). We selected agonists to $5HT_{1A}$ and $5H_{T7}$ (8-OHDPAT) and $5HT_{2A/C}$ (quipazine) receptors since these pharmacological agents previously showed the ability to facilitate locomotion in rodents with SCI (Landry *et al.*, 2006; Gerasimenko *et al.*, 2007). In the sub-acute phase after the injury, the functional state of spinal circuitries is markedly depressed. Accordingly, neither EES nor serotonin agonists could induce functional states that would enable stepping movements on the treadmill at one week post injury. In striking contrast, the combination of dual-site EES and serotonergic agonists promoted coordinated locomotion with plantar placement and substantial levels of weight bearing on the treadmill (**Figure 1.3C**). Detailed statistical analyses revealed that each pharmacological or electrical intervention modulates distinct aspects of locomotor movements, suggesting the fine-tuning of selective functional circuits. For example, $5HT_{2A/C}$ receptors primarily facilitated extension and weight bearing capacities whereas $5HT_{1A}$ and $5HT_{7}$ receptors facilitated rhythmic components and promoted stepping patterns biased towards flexion (**Figure 1.3C**). The functional specificities of electrical and pharmacological stimulations, in turn, provided the means for the exquisite synergy between both paradigms, such that only combinations of serotonin agonists and EES were able to engage spinal locomotor networks as early as one week after a complete SCI (**Figure 1.3C**). We recently investigated whether this receptor-specific functional tuning of gait could apply to a broader range of monoaminergic receptors. Using advanced neurobiomechanical analyses, we could demonstrate the intriguing ability of serotonergic, dopaminergic, and noradrenergic receptor subtypes to modulate stepping behavior in qualitatively unique ways in adult spinal rats (Musienko *et al.*, 2008). Thus, stimulation of spinal monoaminergic receptors pharmacologically and recruitment of spinal circuits electrically can modulate recognizable qualitative features of locomotion independently as well as synergistically in rats deprived of any supraspinal influences.

Collectively, these findings support the viewpoint that the spinal motor infrastructure is composed of a widely distributed and heterogeneous, but highly integrated and synergistic, system of neural circuits and receptors that can generate a range of stepping behaviors when recruited in different combinations (Giszter *et al.*, 2007). Under normal conditions, glutamatergic and monoaminergic pathways originating from the brainstem engage and modulate those spinal locomotor networks (Jordan *et al.*, 2008; Hagglund *et al.*, 2010). Our data show that electrical and pharmacological stimulations can efficaciously compensate for the lost activating and modulating commands after a severe SCI (Courtine *et al.*, 2009a). These paradigms allow getting highly functional access to specific spinal circuitries and receptors, thus promoting distinct stepping behaviors

including weight-bearing locomotion with appropriate patterns of coordination in paralyzed rats (**Figure 1.1**). In the following section, we address the next logical question: can the repeated activation of spinal sensorimotor systems with different combinations of EES, pharmacological agents and locomotor rehabilitation promote activity-dependent functional changes in the trained neuronal networks?

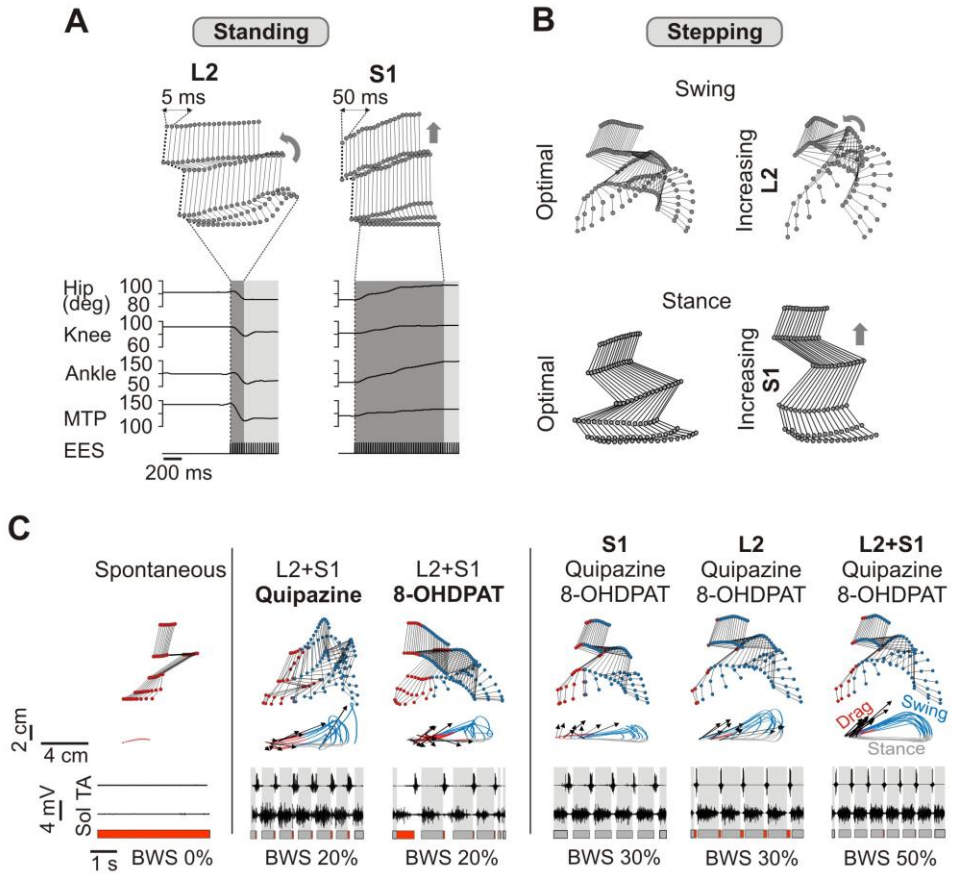

Figure 1.3 Specific modulation of hindlimb movements mediated by EES and serotonergic agonists during standing and stepping.
(A) Stick diagram decomposition of hindlimb movements and associated time course of changes in hindlimb joint angles (increase toward extension) when delivering EES at L2 (left) or S1 (right) during standing**. (B)** Effects of increasing EES at L2 during swing (top) and at S1 during stance (bottom) on hindlimb stepping movements enabled by dual-site EES and serotonin agonists. **(C)** Representative features of locomotion recorded in spinal rats at 7 days post-injury under various pharmacological and EES stimulations. A representative stick diagram decomposition of hindlimb motion during swing is shown for each condition with the successive color-coded trajectories of limb endpoint. Vectors represent the direction and intensity of the limb endpoint velocity at swing onset. A sequence of raw EMG activity from TA and soleus (Sol) muscles is displayed at the bottom. Grey and red bars indicate the duration of stance drag phases, respectively. The level of body weight support (BWS) is indicated for each condition. Stimulation of different serotonin receptors pharmacologically and/or spinal segments electrically each facilitates distinct features of gait. Stimulation-specific modulations combine synergistically when delivering multiple stimulations simultaneously.

1.4 Learning in spinal Locomotor circuitries after SCI

Before addressing issues related to the efficacy of neurorehabilitative interventions to improve function, the impact of the chronic absence of weight bearing and activity on the functional capacities of spinal locomotor systems should be considered. Indeed, there is overwhelming evidence that the spinal circuitries responsible for the control of stepping and standing undergo a major remodeling after the partial or complete loss of descending input, a process that continues to evolve for years after the SCI (Dietz, 2010). Notably, a series of anatomical and neurophysiological observations in animals (Hou *et al.*, 2008) and humans (Calancie *et al.*, 2005; Dietz *et al.*, 2009) suggest that, after a severe SCI, the severed axonal fibers degenerate, creating vacant synaptic territories that become partially re-occupied by sprouting intraspinal fibers. These new synaptic connections likely lead to the formation of aberrant circuits that may misdirect neural information towards inappropriate motor networks during movement execution (Maegele *et al.*, 2002; Fong *et al.*, 2009). Indeed, we observed that rats with complete SCI show a significant deterioration of stepping capacities in the chronic state of the injury (Courtine *et al.*, 2009a): whereas the combination of electrical and pharmacological stimulations enabled coordinated locomotion with plantar placements at 1 week after the injury, the same rats exhibit poorly coordinated stepping patterns with large variability when tested at 9 weeks post-lesion (**Figure 1.4 A-B**). Compared to non-injured rats, these animals displayed a large increase in the expression pattern of the activity-dependent neuronal marker c-fos in all lumbar and sacral segments (**Figure 1.4C**) (Courtine *et al.*, 2009a). This drastic increase in the number of cells contributing to stepping in chronic spinal animals suggests that new nonfunctional circuits progressively form after a severe SCI, and that these abnormal connections engage inappropriate circuits to produce locomotor patterns when pharmacological and EES interventions are delivered. These results are compatible with the emergence of abnormal reflexes (Calancie *et al.*, 2005; Dietz *et al.*, 2009), unintended movements (Maegele *et al.*, 2002) and spasticity (Hiersemenzel *et al.*, 2000) in the chronic state of the injury in humans.

Can step training enabled by locomotor permissive interventions direct the chaos of plasticity that spontaneously takes place after SCI towards useful changes associated with improved functional capacities? In our first attempts, we only used a combination of lumbar (L2) EES and $5HT_{2A/C}$ agonists (quipazine) to facilitate locomotion during training (Ichiyama *et al.*, 2008). As mentioned above, each locomotor permissive system modulates distinct features of stepping behaviors. Accordingly, this specific combination

promotes unique patterns of locomotion including enhanced extension components, in particular in the distal extremities (Gerasimenko *et al.*, 2007).

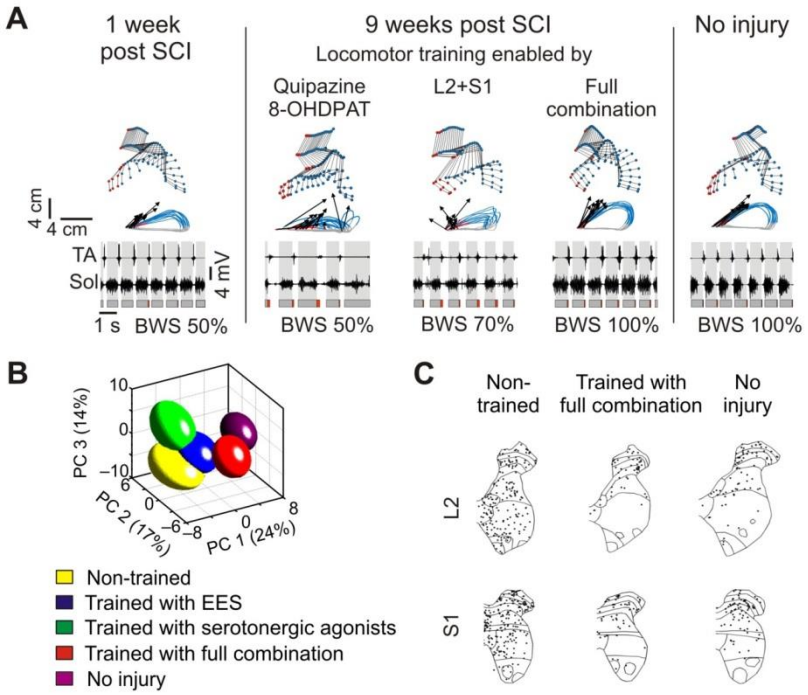

Figure 1.4 Locomotor training enabled by selective pharmacological and/or EES paradigms promotes the recovery of intervention-specific gait patterns in rats deprived of supraspinal input. **(A)** Representative illustrations of EMG and kinematic features during stepping under the full combination (EES at S1 plus L2 and quipazine plus 8-OHDPAT) 1 week post-injury (before training; left) and after 8 weeks of training enabled by pharmacological and/or electrical stimulation (middle). A similar representation is shown for a non-injured rat (right). Conventions are the same as in **Figure 1.3**. **(B)** Three-dimensional statistical representation of locomotor patterns based on principal component analysis applied on a large number of gait parameters (n=135). Each group clustered in distinct locations, revealing that each locomotor training paradigm promoted the recovery of unique stepping patterns. **(C)** Representative camera lucida drawings of FOS-positive neurons in spinal segments L2 and S1 of a non-trained SCI rat (left), a SCI rat trained with the full combination (middle) and a non-injured rat (right).

After 2 months of training, the rats displayed improved locomotor movements characterized by low variability of kinematic features and the capacity to step for extended period of time on the treadmill under the presence of pharmacological and EES interventions. However, the rats developed exaggerated stance phases with marked extension of the foot and toes during swing. The chronic repetition of a certain type of movements thus reinforced and indeed amplified the specifically trained stepping behavior. More recently, we tested the therapeutic potential of locomotor training enabled by lumbar (L2) plus sacral (S1) EES and agonists to $5HT_{1A}$, $5HT_{2A/C}$, and $5HT_7$ receptors

(quipazine and 8-OHDPAT) (Courtine *et al.*, 2009a). Compared to lumbar EES and quipazine alone (Ichiyama *et al.*, 2008), this combination enables more physiologically normal stepping patterns, and can effectively promote locomotion as early as one week post-injury. On the contrary, the combination of lumbar EES and quipazine is not effective to encourage locomotion until 2-3 weeks post-SCI (Lavrov *et al.*, 2008a). After 9 weeks of neurorehabilitation, the spinal rats recovered the impressive capacity to perform full weight bearing locomotion with features that were nearly indistinguishable from those underlying walking patterns of the same rats recorded before the injury (**Figure 1.4A**). Rats trained with EES alone or serotonin agonists alone developed specific patterns of locomotion but these interventions failed to prevent the deterioration of functional capacities in the chronic state of the injury (**Figure 1.4A-B**). Collectively, these results suggest that the repetitive activation of unique combinations of sensorimotor circuits under the influences of distinct electrical and pharmacological stimulations and through task-specific sensory patterns leads to the selection and reinforcement of those neuronal networks in an activity-dependent manner (Edgerton *et al.*, 2008). As elegantly exemplified in cats (Tillakaratne *et al.*, 2002), the rodent spinal motor circuitries deprived of any supraspinal influences can learn the task that is trained and practiced.

This concept of Hebbian-like plasticity among spinal sensorimotor pathways is consistent with the changes in c-fos expression patterns underlying continuous locomotion of trained rats. Regardless of the intervention used to facilitate stepping, we found that rats exposed to locomotor rehabilitation exhibited a substantial decrease in the number of c-fos+ neurons compared to non-trained animals (Ichiyama *et al.*, 2008; Courtine *et al.*, 2009a) (**Figure 1.4C**). However, the detailed features of c-fos expression patterns in lumbar and sacral segments significantly depended on the selective intervention provided during training—each neurorehabilitation procedure promoted specific gait patterns that were produced by unique combinations of neuronal networks. These results reveal that the recovery of stepping ability after a complete SCI does not result from the activation of an ontogenetically defined hardwired circuitry that persists and recovers post-injury. Instead, specific combinations of locomotor training, pharmacological and electrical stimulation interventions induce novel activity-dependent anatomical states that reflect the ability of spinal circuits to learn, and that can promote unexpectedly high levels of functional recovery without any supraspinal inputs in adult rats.

1.5 Control of spinal motor circuitries after SCI

After the complete loss of brain input, where is the source of control for stepping and standing originating from? As summarized in the first section of this review, Sherrington originally introduced the idea that sensory ensembles dictate the properties of spinal locomotion *in vivo* (Sherrington, 1910a). This viewpoint, historically reduced to the "chain of reflex" hypothesis, predicts that the succession of external situations detected by afferent systems allows, determines, and actually controls the characteristics of centrally generated motor outputs. Currently, sensory input is instead regarded as part of reflex subsystems that modulate but are under the control of CPG networks (Pearson, 2004; Rossignol *et al.*, 2006). Thus, is sensory information a source of modulation or a source of control after the loss of brain influences? At first sight, this distinction may essentially appear semantic for spinal sensorimotor processes are so intricately intermingled that they can hardly be dissociated *in vivo* (Hultborn, 2006). However, this conceptual difference is crucial for the optimized design of neurorehabilitative interventions and robotic systems that efficiently capitalize on task-specific sensory cues for the training of spinal motor circuitries (Harkema, 2001). Indeed, most of the existing rehabilitative robots fail to maximally exploit sensory input to facilitate motor training, thus revealing that this view is not sufficiently recognized. Here, we provide a few examples that illustrate the ability of multisensory information to control spinal motor outputs with an astonishing degree of precision.

In the absence of treadmill motion, but under weight-bearing conditions, electrical and pharmacological stimulations allow spinal rats to maintain a tonic posture behaviorally apparent as standing (**Figure 1.5A**). However, when the treadmill belt is initiated, spinal circuits detect the emergence of dynamic conditions and immediately transform the motor patterns from a tonic to a rhythmic state (Courtine *et al.*, 2009a). Likewise, spinal locomotor systems can accommodate limb kinematics and EMG patterns to changing treadmill belt speeds within a single step, even at running velocities (**Figure 1.5A**). Strikingly, while spinal rats are sprinting on the treadmill, the sudden stop of the belt abruptly terminates flexor bursting and results in sustained tonic activity of extensor muscles (Courtine *et al.*, 2009a). Spinal sensorimotor systems are thus capable of recognizing a deviation from expected task-specific patterns of proprioceptive input within milliseconds, hence allowing the immediate switch from a running to a standing state without any supraspinal influences. Similar modulation of locomotor patterns can be found in decerebrated and spinal cats (Musienko *et al.*, 2007) as well as humans with severe SCI during manually assisted stepping on a treadmill (Harkema *et al.*, 1997;

Beres-Jones & Harkema, 2004). Along the same line, spinal rats show the remarkable ability to adjust limb movements to a sudden change in the direction of the treadmill belt from forward to backward, or to a progressive rotation of the body in the sideward direction (**Figure 1.5B**). In both situations, spinal circuitries respond to changing external conditions with a complete reorganization of hindlimb kinematic and muscle activity patterns in order to produce continuous locomotion in virtually any direction of space (Courtine *et al.*, 2009a).

During the execution of these various motor tasks, we found a continuous match between the spatiotemporal patterns of sensory inputs (external situations) and the characteristics of the motor outputs (Courtine *et al.*, 2009a). The precision and versatility of these complex tuning patterns cannot be explained by any of the spinal reflex responses that have been described to date. Together these data suggest that the ensemble of afferent systems sensitive to load, direction, and velocity collectively contributes to elaborate a detailed representation of the locomotor state that allows for the continuous selection of the combination of motor circuits appropriate to perform the current task successfully. These observations imply that, after the loss of brain input, sensory information is instructive in a functional, primarily feed forward manner (Edgerton *et al.*, 2008).

The recovery of hindlimb locomotion in animals with SCI is usually attributed to the neuronal networks responsible for central pattern generation, i.e., CPG networks (Barriere *et al.*, 2008; Guertin, 2009). Even in humans, the recovery of locomotor function after severe SCI is still thought to heavily rely on whether CPGs are present in the human spinal cord (Van de Crommert *et al.*, 1998). We instead argue that the recovery of impressive locomotor capacities with step training under the presence of electrical and pharmacological stimulations rely on the ability of spinal circuitries to utilize sensory ensembles as a continuing source of motor control and as a substrate for learning (Edgerton *et al.*, 2008). Indeed, the data presented in this review (Rossignol *et al.*, 2006) show that the spinal cord acts as a smart processing interface that continuously integrates multisensory input to control its motor output, both acutely and chronically. Thus, beyond representing automated machinery that produces stereotyped reflexes and CPG-like activity, we argue that evolutionary pressures engineered the spinal brain to process complex patterns of afferent inputs and utilize this information to make decisions about how to maintain successful locomotor conditions. Moreover, repetitive exposure to specific sensory patterns with practice allows for the significant optimization of these sensorimotor processes whereby spinal circuitries can learn to produce optimal motor states in the total absence of brain input. Here, the concept of optimal motor states is not

restricted to stereotyped stepping patterns with alternation between extensor and flexor muscles, but instead encapsulates the rich repertoire of motor behaviors underlying activities of daily living. In fact, even when deprived of any supraspinal influences, spinal circuitries can recognize task-specific sensory input and instantly modulate or transform the patterns of muscle activity in order to execute a variety of motor tasks ranging from standing to walking, running, stepping backward or even jogging in the sideward direction (Courtine *et al.*, 2009a).

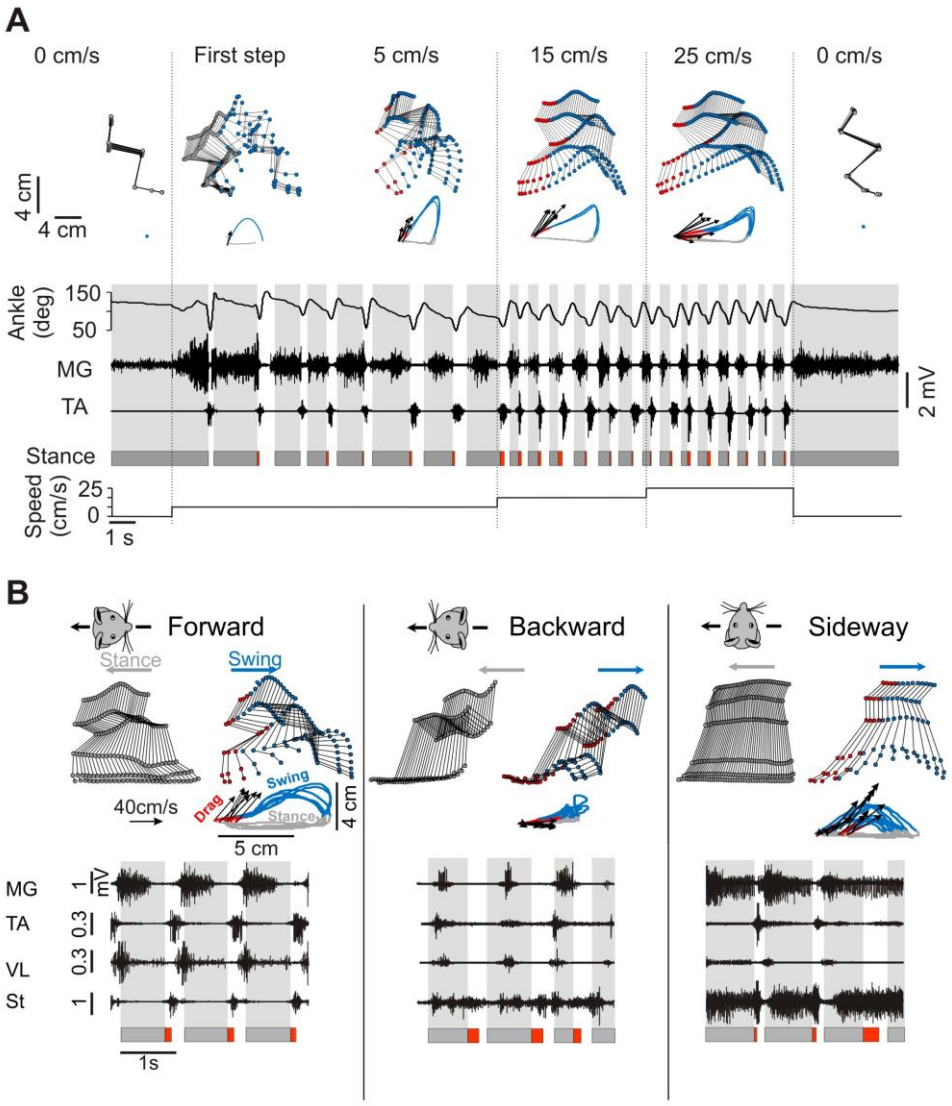

Figure 1.5 Effects of velocity- and direction-sensitive afferent input on the characteristics of hindlimb movements in spinal rats.

(A) Representative example of hindlimb kinematics and EMG activity recorded from a continuous sequence of steps during a gradual increase of treadmill belt speed including running velocities. Stick diagram decomposition of the first step shows the smooth transition from standing to stepping. Conventions are the same as in **Figure 1.3**. **(B)** Representative example of hindlimb kinematics and EMG activity recorded during continuous locomotion in the forward (left), backward (middle) and sideways (right) direction. The same limb from the same rat corresponding to the leading (front) limb during sideway stepping is shown for the three conditions. Data are represented as in **Figure 1.3**, except that stick diagrams are shown in three dimensions, with the main plane oriented with the direction of treadmill belt motion. VL, vastus lateralis; ST, semitendinosus.

1.6. Multi-systems rehabilitation in humans with SCI

What is the potential for these interventions to translate into viable clinical applications? The capacity of task-specific rehabilitation to improve motor functions in humans with SCI is well established (Harkema, 2001; Dietz & Harkema, 2004). There is also growing evidence that epidural spinal cord stimulation can restore standing capacities and stepping-like activity during assisted treadmill locomotion in humans with a motor complete SCI (Harkema *et al.*, 2010). Consequently, we argue that the aggressive design of multi-pronged neurorehabilitative interventions may pave the way towards efficacious therapeutic strategies to improve the recovery of motor capacities and other key physiological functions in individuals with severe SCI.

How should these interventions be designed to attain useful functional outcomes? Firstly, the ability of EES and monoaminergic agonists to modulate specific and synergistic functions in the production of gait provides a strong rationale for the design of *neuroprosthetic electrode* and *chemotrode arrays* (Musienko *et al.*, 2009). Electrode configurations with dense 2D-spatial resolutions will allow delivering electrical stimulation over distinct lumbosacral locations, thus evolving from non-specific tonic excitation of spinal networks to selective phase-dependent (phasic) recruitment of distinct motor circuits. Future studies will thus develop *closed-loop control systems* to capitalize on the full range of spatiotemporal modulatory capabilities afforded with flexible multi-electrode arrays. Along the same lines, the concurrent manipulation of multiple monoaminergic systems will be necessary to promote highly functional motor states adapted to the specifically trained function, e.g. standing vs. stepping. Clearly, both electrical and pharmacological stimulation paradigms will require labor-intensive customization processes to tailor electrode and chemotrode neuroprosthetic systems to the specific pathophysiological condition and need of each patient. Since electrical and pharmacological stimulations enable *sensory systems* to control movement instead of inducing movement per se, we term these interventions *locomotor permissive systems*. Finally, the optimized use of task-specific sensory cues to facilitate movement execution and learning encourages the design of *smart robotic systems* to provide conditions that favor the recruitment of both lumbosacral circuitries and spared supraspinal connections during rehabilitation. The underlying objective is to promote the recovery of supraspinal control of spinal circuitries through activity-dependent mechanisms (Courtine *et al.*, 2008). Therefore, *neuroprosthetic systems*, *locomotor permissive systems*, *sensory systems* and *robotic systems* need to be deployed in concert to orchestrate *multi-systems neurorehabilitation*, i.e., a technology-intensive but physiology-based therapeutic

approach that may restore a range of motor functions following severe SCI and other neuromotor disorders (Fuentes *et al.*, 2009) in humans. Although the medical and technological challenges are tremendous, these are “solutions truly staring us in the face” (Fong *et al.*, 2009).

2 Aims of the thesis

Despite of improved rehabilitation approaches after incomplete SCI, most SCI patients suffering from a severe injury are unlikely to recover extensive locomotor functions and often remain wheelchair bound (Dietz & Harkema, 2004). After such severe injury, most of supraspinal inputs are interrupted, and the spontaneous capacity to engage spinal locomotor networks is lost. However, most SCIs of such human patients remain anatomically incomplete. Instead intraspinal neuronal connections (Lammertse *et al.*, 2007) are spared throughout the scattered injuries. The first three aims of this thesis focus on the development of holistic novel rehabilitative strategies to counteract neuronal degradation after paralyzing SCI in rat rodent models. The first aim was to develop an experimental SCI model that mimics severe yet anatomically incomplete SCIs in adult rats. This was reached with the development and characterization of staggered hemisection SCI. The next aim was to investigate a robotic system that is able to evaluate, train and assess locomotor functions during natural walking overground in rats with neuromotor disorders. The third aim was to integrate previously developed neuromodulation (Musienko *et al.*, 2011c) with bipedal step training using the robotic interface (neuroprosthetic training) to restore voluntary locomotion after staggered hemisection SCI. These studies resulted in three high-profile co-author publications (Beauparlant *et al.*, 2013), *(Dominici et al., 2012a),* (van den Brand *et al.*, 2012) and are presented in *chapter 3 to 5* of this thesis.

Although sharing much functional similarity with SCIs in humans, staggered hemisection SCI remain an artificial SCI and clinical validity is difficult to predict. We subsequently aimed to exploit the potential of the novel neurorehabilitation in a more clinically relevant setting. Neuroprosthetic training was used to enhance voluntary locomotor functions following severe contusion SCI. Further we sought to address the concerns of clinical implementation of the chemical prosthesis as well as the effect of neuroprosthetic rehabilitation on chronic SCIs. The results of this study (manuscript *in preparation*) are presented in *chapter 6* of this thesis.

Both in public and scientific environment, spontaneous recovery after SCI is often perceived to be superior in phylogenetic lower mammals (e.g. rats) than in phylogenetic higher mammals (e.g. monkeys or humans). However, to date a direct comparison of recovery is missing. As the last step of this thesis, we sought to uncover a translational mechanism of spontaneous recovery after lateralized SCI. We compared recovery

process after comparable lateralized SCIs in different species by using detailed kinematic, muscle activity and multivariate analyses. The results of this comparative study (manuscript *in submission*) are presented in *chapter 7* of this thesis.

3 Undirected compensatory plasticity contributes to neuronal dysfunction after spinal cord injury

Original article:

"Undirected Compensatory plasticity contributes to neuronal dysfunction after spinal cord injury"

Janine Beauparlant[1,2,*], Rubia van den Brand[1,2,*], Quentin Barraud[1,2], Lucia Friedli[1,2], Pavel Musienko[1,2,3], Volker Dietz[4], and Grégoire Courtine[1,2]

Brain 2013 Nov;136(Pt11):3347-61

1. Neurology Department, University of Zurich, Zurich, Switzerland

2. Center for Neuroprosthetics and Brain Mind Institute, Swiss Federal Institute of Technology (EPFL), Lausanne, Switzerland

3. Russian Academy of Sciences, Pavlov Institute of Physiology, St Petersburg, Russia

4. Spinal Cord Injury Center, University Hospital Balgrist, Zurich, Switzerland

* These authors contributed equally to this work.

The PhD candidate's contribution: performance of surgeries, performance and analysis of behavioral and electrophysiological experiments

3.1 Abstract

Severe spinal cord injury in humans leads to a progressive neuronal dysfunction in the chronic stage of the injury. This dysfunction is characterized by premature exhaustion of muscle activity during assisted locomotion, which is associated with the emergence of abnormal reflex responses. Here, we hypothesize that undirected compensatory plasticity within neural systems caudal to a severe spinal cord injury contributes to the development of neuronal dysfunction in the chronic stage of the injury. We evaluated alterations in functional, electrophysiological, and neuromorphological properties of lumbosacral circuitries in adult rats with a staggered thoracic hemisection injury. In the chronic stage of the injury, rats exhibited significant neuronal dysfunction, which was characterized by co-activation of antagonistic muscles, exhaustion of locomotor muscle activity, and deterioration of electrochemically enabled gait patterns. As observed in humans, neuronal dysfunction was associated with the emergence of abnormal, long-latency reflex responses in leg muscles. Analyses of circuit, fiber and synapse density in segments caudal to the spinal cord injury revealed an extensive, laminae-specific remodeling of neuronal networks in response to the interruption of supraspinal input. These plastic changes restored a near-normal level of synaptic input within denervated spinal segments in the chronic stage of injury. Syndromic analysis uncovered significant correlations between the development of neuronal dysfunction, emergence of abnormal reflexes, and anatomical remodeling of lumbosacral circuitries. Together, these results suggest that spinal neurons deprived of supraspinal input strive to reestablish their synaptic environment. However, this undirected compensatory plasticity forms aberrant neuronal circuits, which may engage inappropriate combinations of sensorimotor networks during gait execution.

3.2 Introduction

More than half of human spinal cord injuries (SCI) lead to permanent paralysis below the level of the injury, as well as severe bladder, bowel, sexual, and immune dysfunction (Fawcett *et al.*, 2007; Riegger *et al.*, 2009). There is overwhelming evidence that the dramatic consequences of a severe SCI expand beyond these apparent deficits (Hiersemenzel *et al.*, 2000; Dietz & Muller, 2004; Calancie *et al.*, 2005; Courtine *et al.*, 2009a; Dietz *et al.*, 2009; Boulenguez *et al.*, 2010; Murray *et al.*, 2010; Horst *et al.*, 2012). Various electrophysiological studies have suggested that neuronal circuits deprived of supraspinal input undergo a progressive and extensive remodeling (Calancie *et al.*, 1996; Calancie *et al.*, 2000; Maegele *et al.*, 2002; Beres-Jones *et al.*, 2003; Calancie *et al.*, 2005; Harkema, 2008); a process that continues to evolve for years after the SCI (Dietz, 2010). These alterations have been associated with the development of neuronal dysfunction in chronically paralyzed individuals. This clinical syndrome is characterized by pre-mature exhaustion of the overall motoneuronal output and poorly coordinated muscle activation patterns during assisted stepping on a treadmill (Dietz & Muller, 2004; Dietz *et al.*, 2009).

Restoration of motor function after severe SCI has been interpreted as the need to regenerate severed fibers to their original target (Tuszynski & Steward, 2012). However, the progressive neuronal dysfunction observed in paralyzed individuals emphasizes that recovery of useful sensorimotor capacities after severe SCI will rely on the ability to design interventions that will additionally preserve the integrity of neuronal networks caudal to the injury (Dietz, 2010; Roy & Edgerton, 2012).

A deeper understanding of the mechanisms leading to neuronal dysfunction after severe SCI may contribute to conceptualizing therapeutic strategies capable of counteracting the development of neuronal dysfunction. Various studies in experimental animals uncovered a mosaic of injury-induced molecular and cellular changes in segments caudal to a SCI (Krenz & Weaver, 1998; Ballermann & Fouad, 2006; Kitzman, 2006; 2007; Soares *et al.*, 2007; Hou *et al.*, 2008; Tan *et al.*, 2008; Hou *et al.*, 2009; Boulenguez *et al.*, 2010; Murray *et al.*, 2010; Ichiyama *et al.*, 2011; Singh *et al.*, 2011; Kapitza *et al.*, 2012; Tan *et al.*, 2012). Depending upon the SCI model and specific functional assessments, these alterations in the properties of neuronal circuits have alternatively been classified as beneficial or detrimental. Therefore, the general impending biological principles through which the development of neuronal dysfunction occurs remain unclear.

Although previous studies reported contrasting and variable conclusions, they consistently highlighted the progressive upregulation of receptor (Murray *et al.*, 2010), synapse (Kitzman, 2006; Ichiyama *et al.*, 2011; Kapitza *et al.*, 2012; Tan *et al.*, 2012), and fiber density (Krenz & Weaver, 1998; Ballermann & Fouad, 2006; Hou *et al.*, 2008; Hou *et al.*, 2009) in response to the interruption of supraspinal input. Likewise, ablation of afferent pathways in the brain provokes the formation of new fiber arborizations and spines in the affected region (Kirov & Harris, 1999). This compensatory mechanism has been described as homeostatic plasticity (Turrigiano *et al.*, 1998), a process that strives to maintain the number and strength of synaptic inputs within denervated neuronal circuits. After incomplete SCI that leaves residual motor capacities, activity-dependent mechanisms steer compensatory plasticity in order to restore useful functional capacities (Raineteau & Schwab, 2001; Weidner *et al.*, 2001; Edgerton *et al.*, 2004; Courtine *et al.*, 2008; Rosenzweig *et al.*, 2010). In contrast, more severe SCIs impair the ability to produce movements, which prevents activity-dependent mechanisms from contributing to the remodeling of denervated neuronal networks in a useful direction. The resulting undirected compensatory plasticity may potentially lead to detrimental changes in neuronal circuit properties.

To test this hypothesis, we developed a new rodent model of SCI (Courtine *et al.*, 2008; van den Brand *et al.*, 2012) that replicated the key characteristics of neuronal dysfunction observed in severely paralyzed human subjects. Using a range of multifaceted assessments and novel syndromic analysis (Ferguson *et al.*, 2013), we provide evidence suggesting that undirected compensatory plasticity contributes to the development of neuronal dysfunction in the chronic stage of severe SCI.

3.3 Methods

Experimental setup

Experiments were conducted on adult female Lewis rats (~220 g body weight). Animals were housed individually on a 12 h light/dark cycle, with access to food and water ad libitum. Temperature (22 ± 1 °C) and humidity (40 - 60 %) in the animal facilities were maintained constant in accordance to Swiss regulations for animal housing. All animals were handled daily for at least two weeks prior to the first surgeries. Animal care, including manual bladder voiding, was performed twice daily throughout the post-injury period. All procedures and surgeries were approved by the Veterinarian Office of the cantons of Zurich and Vaud, Switzerland.

Surgical procedures and post-surgical care

All surgical procedures used have been described previously (Courtine *et al.*, 2009c; Musienko *et al.*, 2011c; van den Brand *et al.*, 2012). Under aseptic conditions and general anesthesia, a partial laminectomy was performed over spinal segments L2 and S1. Stimulating electrodes were created by removing a small part (~1 mm notch) of insulation from Teflon-coated stainless steel wires (AS632, Cooner Wire, Chatsworth, CA, USA), which were subsequently secured at the midline overlying spinal level L2 and S1 by suturing the wires to the dura. A common ground wire (~1 cm of Teflon removed at the distal end) was inserted subcutaneously over the right shoulder. Bipolar intramuscular EMG electrodes, using the same wire type, were inserted bilaterally in the medial gastrocnemius (MG) and tibialis anterior (TA) muscles. All electrode wires were connected to a percutaneous amphenol connector (Omnetics Connector Corporation, Minneapolis, USA) fixed to the skull of the rat. Analgesia (buprenorphine Temgesic®, ESSEX Chemie AG, Lucerne, Switzerland, 0.01-0.05 mg per kg, s.c.) and antibiotics (Baytril® 2,5%, Bayer Health Care AG, Germany, 5-10 mg per kg, s.c.) were provided for 5 days post-surgery. After the completion of pre-injury recordings, a second surgery was performed. Partial laminectomies were made at mid-thoracic levels and two lateral hemisections were placed on opposite sides at the T7 (left) and T10 (right) spinal segments. This SCI completely interrupted all direct supraspinal input. The completeness of spinal cord lesions was verified histologically post-mortem.

Kinematic, kinetic and EMG recordings

The same rats (n = 11) participated in kinematic, kinetic and EMG recordings before injury, and one week (sub-acute SCI) as well as 9 weeks (chronic SCI) after injury. Stepping capacities were recorded on a motorized treadmill belt set at a constant speed

of 9 cm/s. Animals wore a custom-made jacket especially designed for either bipedal or quadrupedal locomotion (Dominici et al., 2012) that was connected to an automated, servo-controlled body-weight support system (Robomedica Inc., CA, USA). The optimal amount of body weight support was determined visually. Spontaneous (no facilitation) stepping capacities were recorded under both quadrupedal and bipedal postures, before injury as well as one and nine weeks post-injury. To evaluate the functional capacities of lumbosacral circuits in paralyzed rats, we applied an electrochemical neuroprosthesis that transformed lumbosacral circuits from non-functional to highly functional networks (Courtine et al., 2009, Musienko et al., 2011, Musienko et al., 2012, van den Brand et al., 2012). Chemical stimulations consisted of a systemic administration of the 5-HT_{2A} receptor agonist quipazine (0.2–0.3 mg per kg, i.p.) and the 5-$HT_{1A,7}$ receptor agonist 8-OHDPAT (0.05–0.3 mg per kg, s.c.). The agonists were injected 5 min prior to behavioral testing. Epidural electrical stimulations (EES; 0.2 ms duration, 100-500 µA, 40 Hz) consisted of continuous series of rectangular pulses delivered at 40 Hz over spinal segments L2 and S1 through the chronically implanted electrodes. To evaluate the capacity of lumbosacral circuits to sustain stepping in the chronic stage of SCI, locomotor output was recorded every 7 min in a separate group of rats (n = 4) during a bout of continuous stepping (14 min) enabled by EES alone. In this condition no chemical stimulations were delivered in order to avoid time-dependent effects of pharmacological agents.

Kinematic, kinetic and EMG analyses

All procedures used have been detailed previously (Courtine et al., 2009, Musienko et al., 2011, van den Brand et al., 2012). Kinematics of hindlimb stepping were captured by the high speed motion capture system Vicon (Vicon Motion Systems, Oxford, UK), consisting of 10 infrared cameras (MX-3+, 200Hz). Reflective markers were attached bilaterally at the iliac crest, the greater trochanter (hip joint), the lateral condyle (knee joint), the lateral malleolus (ankle), the distal end of the fifth metatarsophalangeal (MTP) joint and the tip of the forth toe. The body was modeled as an interconnected chain of rigid segments, and joint angles were generated accordingly. Vertical ground reaction forces (vGRF) were recorded using a biomechanical force plate (2 kHz; HE6X6, AMTI) located below the treadmill belt. EMG signals (2 kHz) were amplified, filtered (10-1000 Hz bandpass), stored and analyzed offline to compute the amplitude, duration and timing of individual bursts. For both the left and right hindlimbs, ten successive step cycles were extracted from a continuous sequence of stepping on a treadmill for each rat under each condition. A 10-s interval was used when no or very minimal stepping movements were

observed. A total of 147 parameters quantifying gait, kinematics, kinetics, and EMG features were computed for each limb and gait cycle according to methods described in detail previously (Courtine *et al.*, 2008; Courtine *et al.*, 2009c; Musienko *et al.*, 2011c; van den Brand *et al.*, 2012)

Electrophysiological experiments

Spinal reflexes were assessed in fully awake rats (n = 10). During testing, the animals were suspended in the air (no contact with the ground) using the trunk harness and robotic systems described above. To elicit reflexes, we delivered single rectangular pulses (0.5 ms duration) through the chronically implanted S1 electrode at 0.2 Hz. Before the injury, we identified the stimulus intensity (typically ~160-200 µA) that elicited the largest monosynaptic responses in the absence of direct muscle responses (direct stimulation of the motor nerve, equivalent to M waves), typically 1.5–2-fold above motor threshold (Gerasimenko et al., 2006), and used this intensity to test reflexes at 1 and 9 weeks post-injury. The compound motor-evoked potentials were recorded in both left and right TA muscles (10 kHz), and the onset latency, peak-to-peak amplitude, and integral of the averaged (n = 5) reflex responses were determined.

Tracing procedures

Under general anesthesia, a laminectomy over L1-L2 spinal level was performed to expose the dorsal aspect of the spinal cord. In a subset of chronic SCI rats (n = 6), a 10% suspension of Tetramethylrhodamine-conjugated dextran 3000 MW (TMR) (Invitrogen AG, Eugene, OR, USA) was stereotaxically injected into the spinal cord, using a 33G needle on a 10 µl Hamilton syringe (1701 RN, Hamilton Company, Reno, NV, USA) attached to an UltraMicroPump (World Precision Instruments, Sarasota, FL, USA). Six injections of 200 nl TMR separated by 700 µm were performed in each hemicord. The injection coordinates were 800 µm lateral of the midline and approximately 700 µm above the ventral surface of the spinal cord.

To elicit locomotor-related expression of c-fos, the remaining chronic SCI rats (n = 5) stepped bipedally on a treadmill during 45 min with the electrochemical neuroprosthesis. Rats were returned to their cages and perfused exactly 60 min after stepping (Ichiyama et al., 2008, Courtine et al., 2009). All animals were deeply anesthetized by an i.p. injection of 0.5 ml Pentobarbital-Na (50 mg/mL) and transcardially perfused with approximately 80 ml Ringer's solution containing 100'000 IU/L heparin (Liquemin, Roche, Basel, Switzerland) and 0.25% $NaNO_2$ followed by 300 ml of cold 4% phosphate buffered paraformaldehyde, pH 7.4 containing 5% sucrose. The brain and spinal cord were removed and postfixed overnight in the same fixative before they were transferred

to 30% sucrose in phosphate buffer (PB) for cryoprotection. The tissue was embedded in Tissue Tek O.C.T (Sakura Finetek Europe B.V., Zoeterwoude, The Netherlands), frozen at -40°C, and cut to a thickness of 30 µm or 40 µm.

Immunohistochemistry

Mounted or free-floating sections were washed 3 times in 0.1M PBS and blocked in 5% normal goat serum containing 0.3% Triton. For c-fos and Neurofilament stainings, slices were pretreated with H2O2 and cold methanol (100%), respectively. Sections were then incubated in primary antibody diluted in the blocking solution overnight at 4°C (c-fos) or room temperature (Neurofilament, vGlut1, vGlut2). TMR visualization incubation time was carried out over 48 hours at 4°C. The primary antibodies used were rabbit anti-c-fos (1:5000; Santa Cruz Biotechnologies, Santa Cruz, CA, USA) and anti-TMR (1:1000; Molecular Probes, Life Technologies, Grand Island, NY, USA), mouse anti-Neurofilament (1:10,000; Millipore, Billerica, MA, USA) and anti-vGlut2 (1:5000; Millipore, Billerica, MA, USA), and guinea pig anti-vGlut1 (1:2000; Millipore, Billerica, MA, USA) antibodies. Sections were again washed 3 times in 0.1M PBS and incubated with the appropriate secondary antibody diluted 1:200 (Alexa fluor® 488 or Alexa fluor® 555; Molecular Probes, Life Technologies, Grand Island, NY, USA) in blocking solution. Sections were washed again, mounted onto glass slides, and coverslipped with Mowiol.

Neuromorphological evaluations

TMR-labeled fibers and c-fos-positive neurons were counted using image analysis software (Neurolucida, MicroBrightField, Williston, VT, USA) on 4-5 transverse slices per animal. For TMR-labeled fibers, a rectangular grid half the size of the ventral horn was overlaid and intersecting fibers within the grey matter were counted. C-fos-positive neurons were quantified with respect to the Rexed laminae defined by Molander et al.(Molander *et al.*, 1984). Neurofilament and vesicular glutamate transporter (vGlut1, vGlut2) density was measured using 3-5 confocal image stacks per region per rat acquired with standard imaging settings and analyzed using custom-written Matlab (MathWorks, Natick, MA, USA) scripts according to previously described methods (Carmel et al., 2010, van den Brand et al., 2012). Confocal output images were divided into square regions of interest (ROI), and densities computed within each ROI as the ratio of traced fibers (amount of pixels) per ROI area. Both manual and computerized counts were performed blindly. Image acquisition was performed using a Leica TCS SPE or SP5 laser confocal scanning microscope and the LAS AF interface (Leica Microsystems, Wetzlar, Germany) and stacks were processed offline using the Imaris software (Bitplane, South Windsor, CT, USA).

Principal component analysis

To evaluate the characteristics underlying stepping for the different experimental conditions, we implemented a multi-step statistical procedure based on principal component (PC) (Courtine *et al.*, 2009c; Musienko *et al.*, 2011c; Dominici *et al.*, 2012a). The various steps, methods, typical results, and interpretation of the analysis are detailed in Figure 2 and Figure 3. The same procedure was applied for the syndromic analysis; all the collected kinematic, kinetic, EMG, electrophysiological, neuromorphological and immunohistochemical parameters of SCI animals (n = 6) were manually curated and combined in a single matrix.

Comparisons with neuronal dysfunction in humans with severe SCI

Electrophysiological recordings of leg muscle activity and spinal reflex behavior were conducted in individuals with motor complete (Dietz *et al.*, 2009; Hubli *et al.*, 2012) or motor incomplete SCI (Dietz *et al.*, 2009; Hubli *et al.*, 2012). To evaluate the capacity of spinal neuronal networks to sustain locomotion, we recorded the EMG activity of the TA and MG muscles during 10-15 min of robotically assisted stepping at a constant speed of 2.0 km/h and 65-75% body weight support. Spinal reflex behavior was assessed in healthy subjects, as well as in spinal cord injured individuals in the early and late stage of SCI. Non-noxious electrical stimuli were randomly applied to the distal part of the tibial nerve in subjects wearing a harness in an upright, unloaded position, as performed in the rats. Each stimulation was composed of a series of 8 biphasic rectangular stimuli with 2 ms single stimulus duration and a frequency of 200 Hz. Stimulation intensity was set at two times motor threshold. Reflex responses were recorded from the ipsilateral TA muscle.

Statistical procedures

All data are reported as mean values ± s.e.m. Statistical evaluations were performed using one-way ANOVA for neuromorphological evaluations, and one- or two-way repeated-measures ANOVA for functional assessments. The post hoc Tukey's or Fisher LSD test was applied when appropriate. Pearson's correlation coefficients were used to evaluate univariate correlations, except for patient data where the Spearman's rank correlation coefficient was computed. The significance level was set as $|R \text{ value}| > 0.45$ and $p < 0.05$, respectively.

3.4 Results

Staggered hemisection SCI leads to complete and permanent paralysis

Adult rats received a severe SCI consisting of a left lateral hemisection at T7 and right lateral hemisection at T10, which interrupted all the direct supraspinal input to lumbosacral circuits (van den Brand *et al.*, 2012). To test the functional impact of the SCI, we positioned the rats bipedally and quadrupedally on a motorized treadmill (9 cm/s) with robot-assisted vertical support (% of BWS). In both postures, the rats showed continuous dragging of both hindlimbs along the treadmill belt, which was associated with the absence of EMG activity in flexor and extensor muscles of the ankle **(Figure 3.1B-C).** Occasionally, some of the tested rats exhibited spontaneous hindlimb oscillations, either unilateral or bilateral, which rapidly extinguished after a few cycles, as previously observed in rats with complete SCI (Courtine *et al.*, 2009a).

Staggered hemisection SCI leads to neuronal dysfunction in the chronic stage

We sought to evaluate the functional properties of lumbosacral locomotor circuits in the sub-acute (1 week post-injury) and chronic stage (9 weeks post-injury) of the SCI (n = 9). To enable locomotion of the paralyzed hindlimbs, we applied an electrochemical neuroprosthesis that transformed lumbosacral circuits from non-functional to highly functional networks (Courtine *et al.*, 2009c; Musienko *et al.*, 2012). By increasing the general level of spinal excitability, this electrochemical spinal neuroprosthesis enables sensory information to become a source of control for stepping. In consequence, the recorded motor patterns were exclusively generated within lumbosacral circuits, without contribution from supra-lesional input (Courtine *et al.*, 2009a; van den Brand *et al.*, 2012). As early as 1 week post-lesion, electrochemical stimulations promoted coordinated locomotion with appropriate timing of left and right limb alternation, and reciprocal activation between flexor and extensor muscles **(Figure 3.1A-B).** In striking contrast, the same rats exhibited highly variable stepping patterns with poor inter- and intra-limb coordination in the chronic stage of the SCI **(Figure 3.1C).**

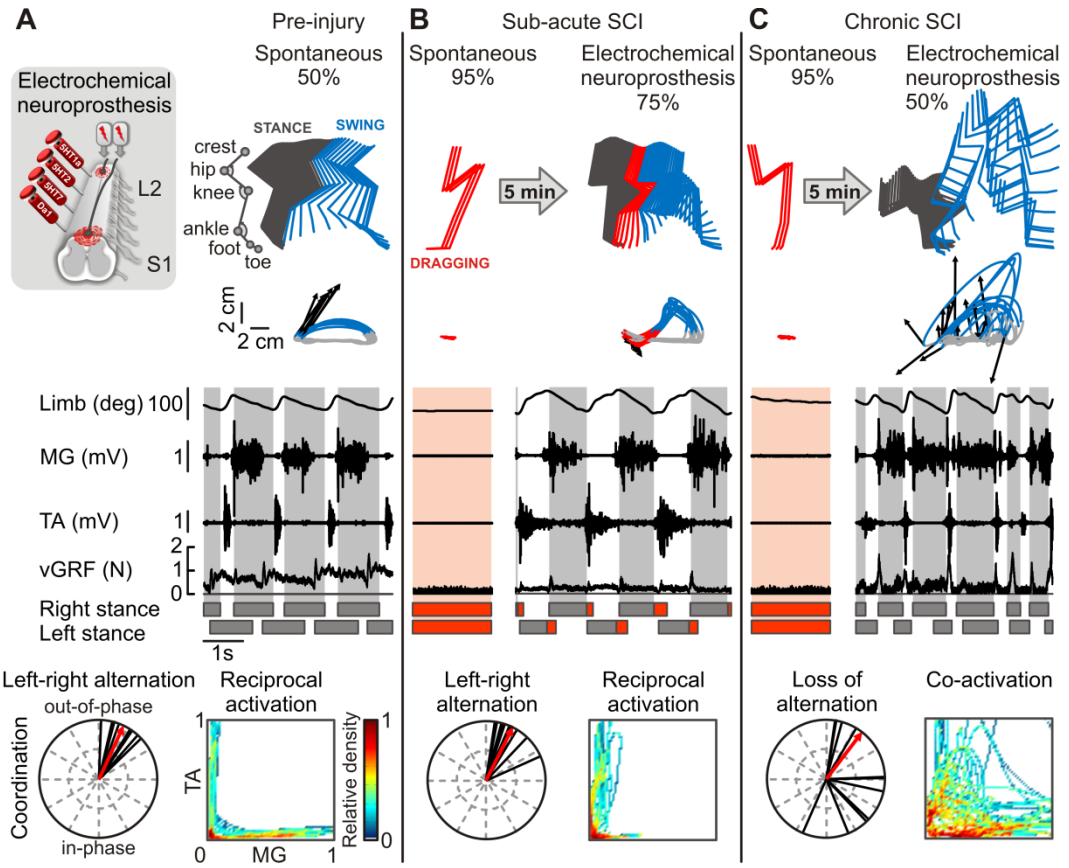

Figure 3.1 The staggered lateral hemisection SCI led to deterioration of locomotor function in the chronic stage.

(A) Diagram of the electrochemical neuroprosthesis. Rats were positioned bipedally over a moving treadmill belt and provided with body weight support (BWS). A representative locomotor trial of the same rat performed before injury (intact), **(B)** 1 week (sub-acute SCI) and **(C)** 9 weeks post-injury (chronic SCI) is shown. Above each panel, the % of BWS is indicated and a stick diagram decomposition of hindlimb motion is shown together with color-coded trajectories of hindlimb endpoints. Vectors represent the direction and intensity of the hindlimb endpoint velocity at swing onset. The corresponding sequences of hindlimb oscillations, raw EMG activity of an extensor (MG, medial gastrocnemius) and a flexor (TA, tibialis anterior) muscle and vertical ground reaction forces (vGRF) are shown below. Grey and red bars indicate the duration of stance and drag phases, respectively. For each time point, a polar plot representation illustrates the coordination between the oscillations of left and right hindlimbs (black line, single gait cycle; red arrow, average of all gait cycles). The density plot displays the coordination between the antagonistic muscles TA and MG throughout one locomotor trial. L-shaped patterns reflect perfect reciprocal activation of muscles.

We next aimed at quantifying gait performance pre-injury, and at the sub-acute and chronic stages of SCI. To achieve this, we applied a multi-step statistical procedure based on principal component (PC) analysis. We first conducted detailed kinematic, kinetic, and EMG recordings, which allowed the computation of a large number of variables (n = 147) that provided a comprehensive quantification of gait patterns for each rat and time point. PC analysis creates new variables (PC) that linearly combine the original parameters in order to maximize the amount of explained variance per PC.

Individual gait cycles can be represented in the new denoised space defined by the first three PCs. Gait patterns associated with each experimental time point emerged in distinct spatial locations **(Figure 3.2A).** To visualize these differences, we applied a least square elliptic fitting on each cluster. The distance between data points in the PC space provides a measure of the degree of discrepancy or similarity between the clusters, i.e. gait patterns **(Figure 3.2B).** The dispersion of data points accounts for the variability of gait patterns within each rat and time point **(Figure 3.2B)**. This analysis revealed that gait patterns recorded in the chronic stage significantly differed from ($p < 0.01$), and showed a high gait variability compared to ($p < 0.05$) those observed in the same rats pre-injury and in the sub-acute stage ($n = 9$). PC scores indicate the location of data points and conditions along each individual PC axis **(Figure 3.2C).**

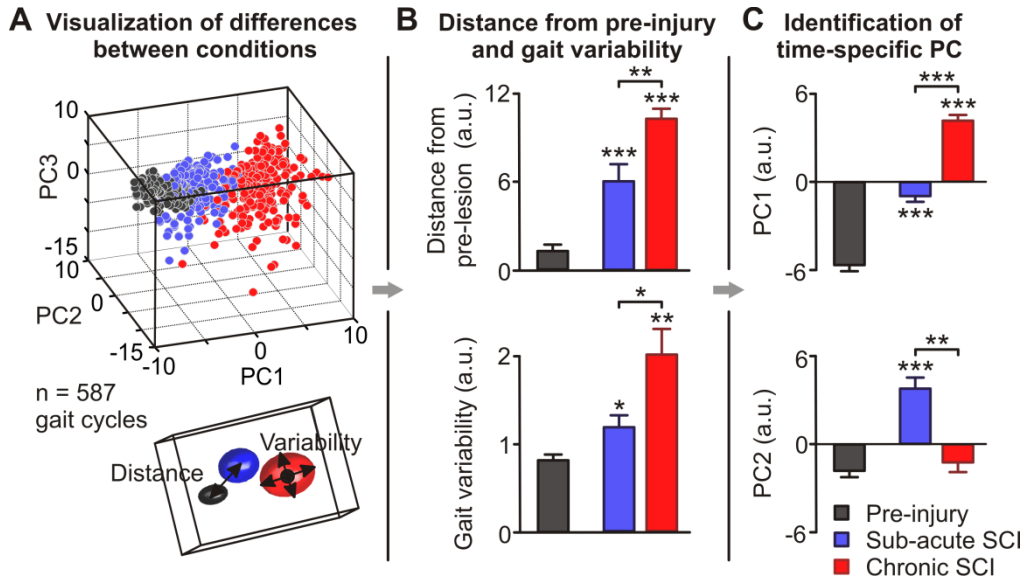

Figure 3.2 Multi-step statistical analysis of gait patterns.
(A) Representation of individual gait cycles in the new denoised space created by PC1-3. Least square elliptic fitting reveals widely separated clusters of data points for each time point. **(B)** Locomotor performances were quantified, for each rat, as the 3D Euclidean distance between the location of gait cycles and the average location of all gait cycles from the same rats pre-lesion (n = 9 rats). Variability of gait cycles was assessed as the dispersion of data points for each rat and time point. **(C)** The scores indicate which experimental time points are differentiated by each PC. *, P < 0.05; **, P < 0.01; ***, P < 0.001. Error bars, s.e.m.

Here, extraction of scores revealed that PC1 captured differences across the time points ($p < 0.001$), while PC2 distinguished the sub-acute stage from the other time points ($p < 0.01$). Next, we computed the factor loadings, which correspond to the correlation between each variable and each PC. We then identified variables with significant factor loading ($|value| > 0.5$, $p < 0.05$), which we regrouped into functional

clusters that we named for clarity **(Figure 3.3A).** To provide a more classical representation of differences between time points, histogram plots were generated for the most prominent variable (highlighted within yellow frames; **Figure 3.3A**) per extracted functional cluster in PC1 **(Figure 3.3B)** and PC2 **(Figure 3.3C)**. This multi-step analysis showed that in the chronic stage of the SCI rats exhibited highly variable gait patterns, a pronounced flexed posture, poor interlimb coordination, altered distal joint control, and enhanced extensor muscle activation during electrochemically-enabled locomotion (PC1 clusters; Figure 3B). Instead, slow movement, low level of weight bearing, and prolonged swing duration characterized gait patterns underlying stepping in the sub-acute stage (PC2 clusters; **Figure 3.3C)**.

Together, these results not only emphasize the dramatic degradation of stepping capacities in the chronic stage of the SCI, but also identify the ensemble of gait features that characterizes the syndromic signature of this neuronal dysfunction. We sought to leverage this detailed evaluation to decipher putative mechanisms underlying these functional changes.

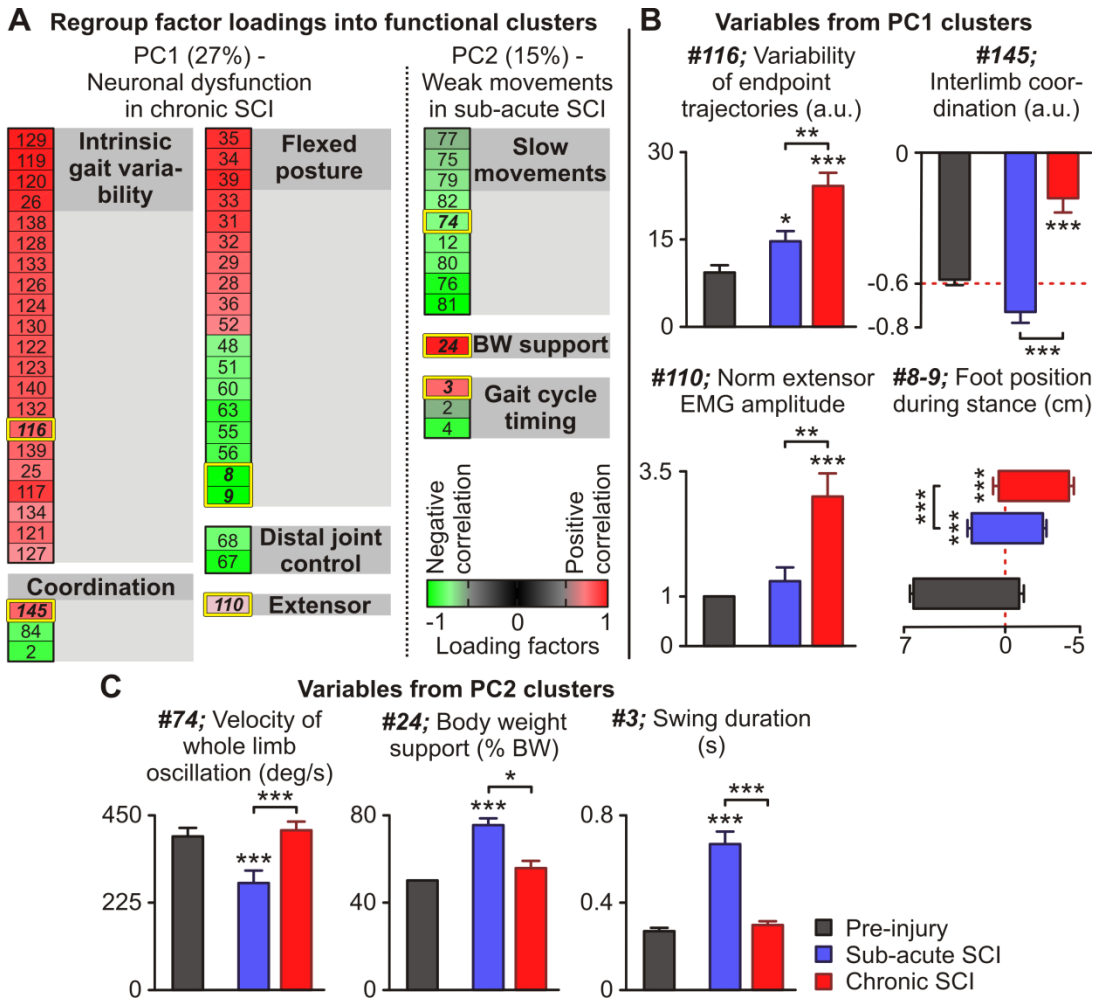

Figure 3.3 Multi-step statistical analysis of gait identified, time-specific features of locomotor patterns after severe SCI.
(A) Extraction of factor loadings, i.e. correlation between gait variables and the first two PCs. Variables with the highest factor loading (|value| > 0.5, $p < 0.05$) were regrouped into functional clusters, which are named for clarity. **(B),(C)** Bar graphs of single variables (highlighted within yellow frames in **(A)** for each extracted functional cluster of **(B)** PC1 and **(C)** PC2 (n = 9 rats). *, $P < 0.05$; **, $P < 0.01$; ***, $P < 0.001$. Error bars, s.e.m.

Staggered hemisection SCI leads to pre-mature exhaustion of locomotor muscle activity

Chronically injured, non-ambulatory SCI patients showed pre-mature exhaustion of leg muscle activity during robotically assisted locomotion (**Figure 3.4C**; adapted from (Dietz *et al.*, 2009)). We tested whether rats with a severe, chronic SCI exhibited a similar decrease in hindlimb muscle activation during electrically enabled stepping **(Figure 3.4A).** At the onset of stepping, the electrical neuroprosthesis promoted coordinated locomotor movements with alternation between powerful bursts of EMG activity in flexor and extensor muscles. The recruitment of hindlimb muscles rapidly declined over time, and

eventually reached amplitudes that were too low to sustain locomotion ($p < 0.05$; **Figure 3.4B)**. Similar exhaustion of locomotor EMG was observed during manually assisted movements in rats (data not shown). These results show that, as observed in humans, rats exhibited premature exhaustion of the overall locomotor muscle output in the chronic stage of a severe SCI.

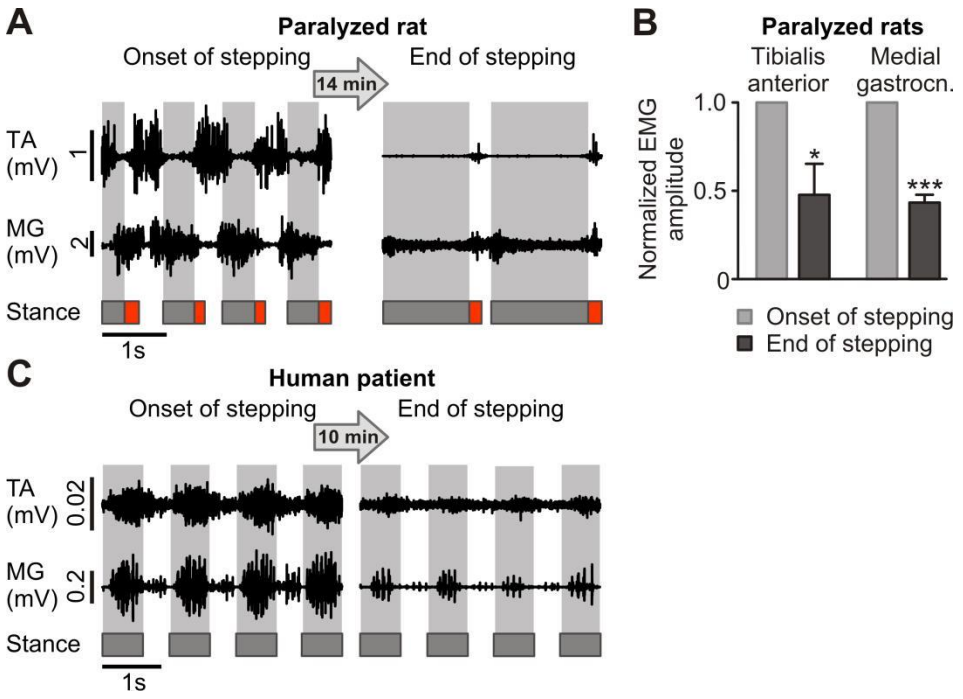

Figure 3.4 Exhaustion of locomotor muscle activity in the chronic stage of SCI.
(A) Evaluation of exhaustion of locomotor muscle activity in rats at the chronic stage of SCI. Rats were positioned bipedally over a moving treadmill belt with 90% BWS at a speed of 9 cm/s. Stepping was enabled with the electrical neuroprosthesis and a representative example of muscle activity is shown at the onset and end of a 14-min continuous stepping bout. **(B)** Bar graphs of the normalized EMG amplitudes recorded at the beginning and end of stepping in rats (n = 4). **(C)** Representative example of EMG activity recorded in a chronically paralyzed human patient during robotically assisted leg movements at a constant speed of 2.0 km/h and 65-75% BWS. EMG activity is shown at the onset of stepping and after 10 min of a continuous bout of locomotion. Adapted from Dietz *et al.*, 2009; Figure 1C**.** *, $P < 0.05$; ***, $P < 0.001$. Error bars, s.e.m.

Staggered hemisection SCI leads to the emergence of abnormal long-latency reflex responses

In severely paralyzed humans, exhaustion of locomotor muscle activity occurred in parallel with the emergence of abnormal, long-latency reflex responses in leg muscles (Dietz *et al.*, 2009). To elicit these reflexes, a train of stimuli was applied to the tibial nerve in upright and unloaded human subjects. In the absence of neurological impairments, the stimulation evoked a short-latency (75–100 ms) reflex response in the ipsilateral TA muscle **(Figure. 3.5A)**. Reflex responses with similar latency but markedly

reduced amplitude were recorded in the sub-acute stage of the injury (2 months post-SCI). Chronic, non-ambulatory SCI patients showed a diminished or nearly absent, early reflex response, and concurrently developed an abnormal, long-latency reflex response (200–300 ms) **(Figure 3.5A)**. The relative amplitude of this long-latency reflex response inversely correlated with locomotor capacities **(Figure 3.5E)**.

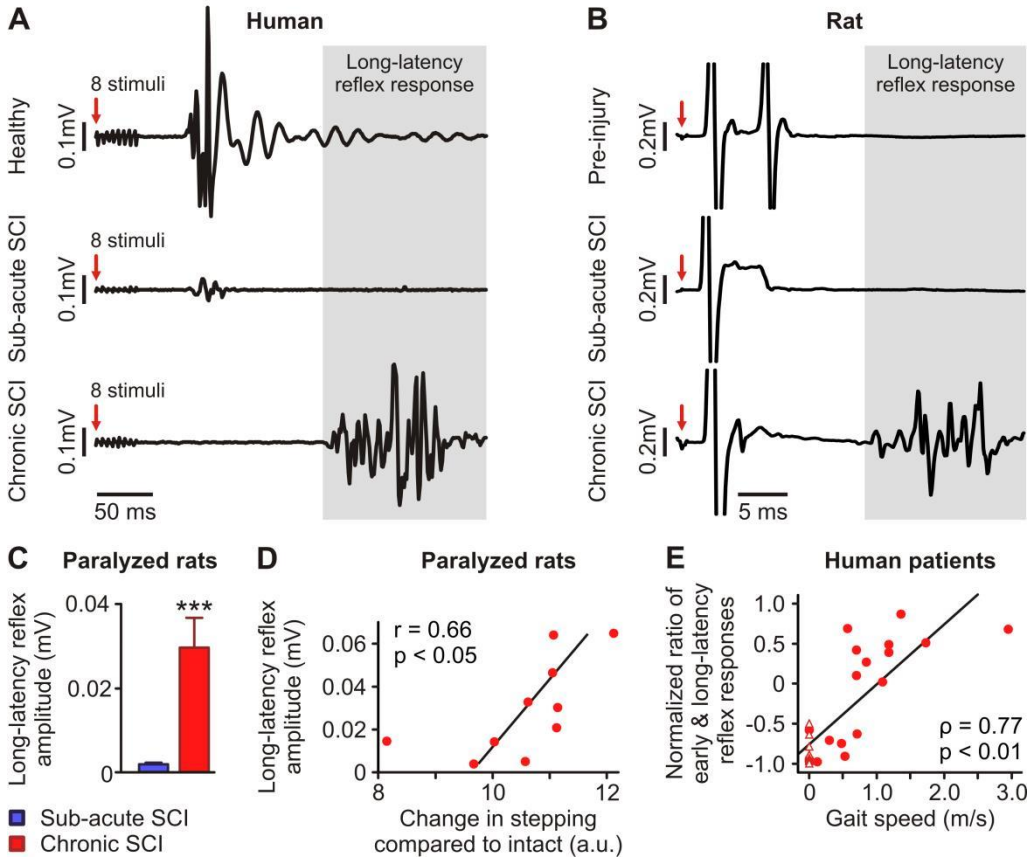

Figure 3.5 Emergence of long-latency reflex responses in the chronic stage of the SCI correlated with deterioration of locomotor capacities.
(A) Representative reflex traces recorded from the TA muscle in response to a train of tibial nerve stimulations in a healthy subject, and a severely paralyzed non-ambulatory patient recorded in both the sub-acute and chronic stage of SCI. Adapted from Dietz *et al.*, 2009; Figure 1. **(B)** Representative reflex traces recorded from the TA muscle in response to a single epidural stimulus at S1 in the same rat pre-lesion, and in the sub-acute and chronic stage of SCI. The shaded area highlights the window for the long-latency reflex responses. **(C)** Bar graph reporting the amplitude of the long-latency reflex response in the sub-acute and chronic stage of SCI in rats (n = 8). **(D)** Correlation between stepping capacities and the amplitude of the long-latency reflex response in chronically paralyzed rats (n = 10). Stepping capacities were quantified as the 3D distance (see **Figure 3.2**) between gait cycles pre-lesion and in the chronic stage of SCI. **(E)** Correlation between the normalized ratio of early and long-latency reflex responses and the walking speed converted from the 10 minute walk test in patients with clinically complete (triangle) and incomplete (circle) SCI. Adapted from Hubli *et al.*, 2012; Figure 1**.** ***, P < 0.001. Error bars, s.e.m. ρ, Spearman's rank correlation coefficient.

We investigated whether similar changes in hindlimb reflex responses occurred in severely paralyzed rats. Before the SCI, electrical stimulation delivered through the S1 epidural electrode in fully awake rats elicited two well-defined reflex responses in the TA muscle **(Figure 3.5B)**, which engaged a monosynaptic and a polysynaptic neural circuit (Gerasimenko *et al.*, 2006). As previously described (Lavrov *et al.*, 2006), the polysynaptic response corresponds to the short latency reflex response evoked in humans. In the sub-acute stage of the SCI, the polysynaptic response was either markedly reduced or completely suppressed **(Figure 3.5B)**. The same rats tested in the chronic stage of the SCI displayed a new, long-latency reflex response in the TA muscle (25–50 ms, $p < 0.001$; **Figure 3.5B-C**). Although epidural electrical stimulation primarily recruits afferent fibers (Courtine *et al.*, 2009c; Musienko *et al.*, 2012), including the tibial nerve, these responses might not be completely equivalent to those observed in humans. As previously described in human patients, however, the amplitude of this abnormal long-latency reflex response inversely correlated with locomotor capacities in rats ($r = 0.66$, $p < 0.05$; **Figure 3.5D**).

Staggered hemisection SCI triggers extensive reorganization within denervated neuronal networks

We surmised that the neuronal dysfunction syndrome, characterized by degradation of stepping capacities, pre-mature EMG exhaustion and abnormal reflex responses, was in part due to abnormal rewiring of the denervated lumbosacral networks. To test this hypothesis, we first assessed putative changes in overall fiber density in spinal segments caudal to the SCI **(Figure 3.6A)**. Evaluation of neurofilament staining at spinal segment L4 revealed a 28% decrease in fiber density in intermediate and ventral laminae in the sub-acute phase compared to intact rats ($p < 0.001$; Figure 6B). After the complete interruption of supraspinal pathways, severed axons show a rapid Wallerian degeneration (Hausmann, 2003) that likely accounted for this pronounced loss of neurofilament in sub-lesional spinal segments. We found a near complete, lamina-specific restoration of neurofilament density in denervated segments of chronically injured rats ($p < 0.01$; **Figure 3.6B-C**).

This result suggested that the SCI led to the formation of new arbors in sub-lesional segments, which we evaluated in more detail with neuronal tract-tracing techniques. We injected the antero- and retrograde neuronal tracer TMR into spinal segments L1-L2 **(Figure 3.6A)**. We first quantified retrogradely labeled neurons at L6 and found a twofold increase in the number of labeled neurons in rats with chronic SCI compared to both intact and sub-acutely lesioned animals ($p < 0.001$; **Figure 3.6D**). We next evaluated the

density of anterogradely labeled fibers projecting to L6. The number of labeled fibers at L6 was significantly reduced in the sub-acute stage ($p < 0.001$), presumably due to the loss of descending fibers. We observed a threefold increase in the density of fibers at L6 in the chronic stage of SCI ($p < 0.001$; **Figure 3.6D-E**). This increase in fiber density reestablished the level of innervation observed in intact rats ($p = 0.96$; **Figure 3.6D**, right).

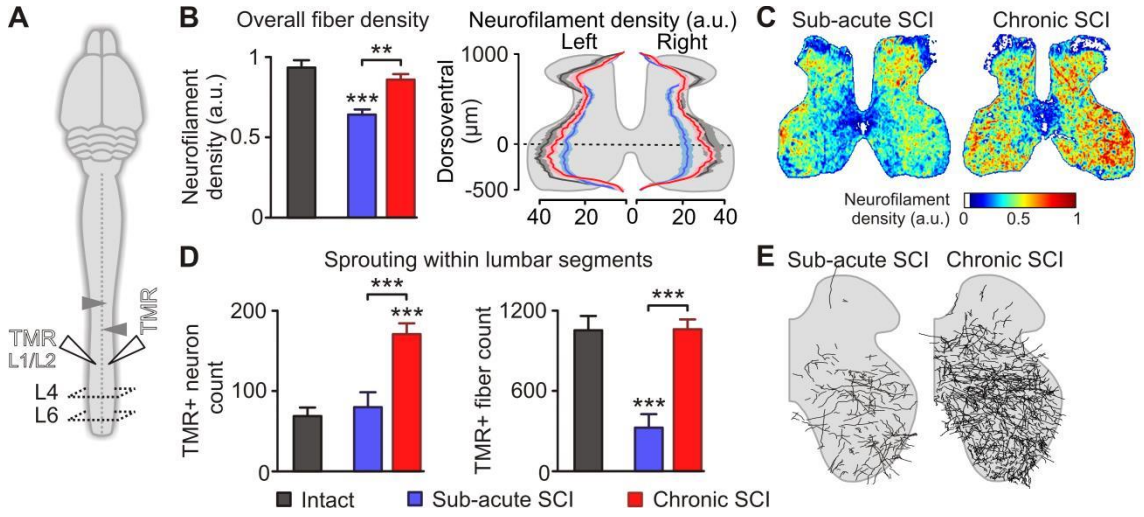

Figure 3.6 Staggered lateral hemisection SCI led to substantial intraspinal reorganization in the denervated lumbosacral segments.
(A) Diagram illustrating anatomical experiments. **(B)** Bar graph and density plot reporting the overall neurofilament density and laminae-specific neurofilament density within the spinal segment L4 for each experimental group (n = 4-5 rats per group). **(C)** Representative heatmaps displaying neurofilament density throughout the spinal cord grey matter. **(D)** Bar graphs reporting the number of retrogradely labeled neurons at L6, and manual fiber counts at L6 after injecting TMR at L1-L2 (n = 5-6 rats per group). **(E)** Single-slice fiber reconstructions of TMR-labeled fiber density in the right L6 hemicord. **, $P < 0.01$; ***, $P < 0.001$. Error bars, s.e.m.

To confirm and expand these findings, we next evaluated changes in the density of synapses associated with intraspinal afferent fibers. Glutamate is the most abundant excitatory neurotransmitter in the spinal cord. The vesicular glutamate transporter 2 (vGlut2) is expressed in the synaptic terminals of various spinally projecting supraspinal neurons and intraspinal neurons. Due to the complete interruption of descending pathways after staggered hemisections, vGlut2 is near-exclusively associated with segmental afferents in injured rats (Oliveira *et al.*, 2003; Todd *et al.*, 2003; Alvarez *et al.*, 2004; Landry *et al.*, 2004). vGlut2 positive fiber endings were primarily found in the superficial dorsal horn and in the intermediate and ventral laminae 7 to 10 **(Figure 3.7B)**. Compared to intact rats, we found a significant decrease in vGlut2 density in spinal segment L4 of rats in the sub-acute stage of the SCI ($p < 0.001$; **Figure 3.7A**). Rats in the chronic stage of SCI exhibited a near complete, lamina-specific restoration of vGlut2

density ($p < 0.01$; **Figure 3.7A-B**). These combined results reveal that a striking, lamina-specific reorganization of intraspinal connectivity and associated synaptic terminals spontaneously takes place in the chronic stage of severe SCI.

Staggered hemisection SCI leads to remodeling of sensory terminals within denervated segments

We sought to investigate whether sensory afferents also undergo remodeling in response to severe SCI. Staining of vesicular glutamate transporter 1 (vGlut1) in the spinal cord mainly identifies the synaptic terminals of corticospinal fibers (Persson *et al.*, 2006), as well as myelinated primary afferents (Oliveira *et al.*, 2003; Todd *et al.*, 2003; Alvarez *et al.*, 2004; Landry *et al.*, 2004), which essentially arise from muscle proprioceptive fibers (Alvarez *et al.*, 2004). Due to the complete interruption of the corticospinal tract after staggered hemisections, vGlut1 staining provides the opportunity to quantify the density of synaptic contacts formed by proprioceptive fibers in denervated spinal segments. vGlut1-positive fiber endings were concentrated in the deep dorsal horn and around the central canal (**Figure 3.7D**), which complemented the distribution pattern of vGlut2-positive synapses. Compared with intact rats, vGlut1 density was significantly reduced in intermediate and ventral laminae in the sub-acute stage of the SCI ($p < 0.01$; **Figure 3.7C**). Rats in the chronic stage of SCI showed a density of myelinated primary afferent terminals that did not differ from that observed in intact rats **(Figure 3.7C)**. The recovery of vGlut1-positive fiber endings occurred in a lamina-specific manner **(Figure 3.7D)**.

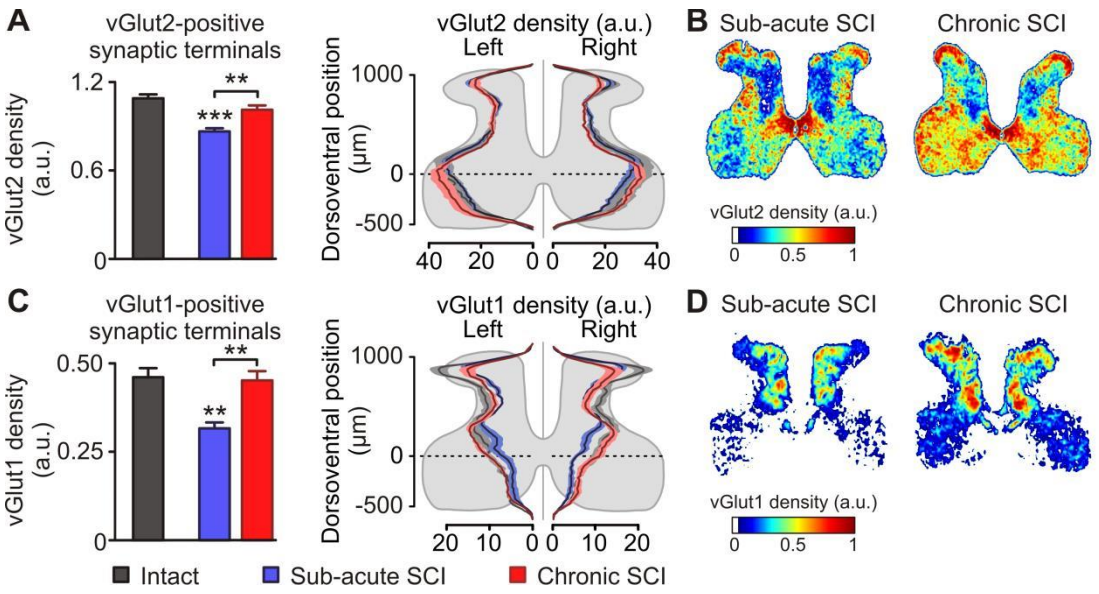

Figure 3.7 The staggered lateral hemisection SCI led to reorganization of sensory afferents in denervated lumbosacral segments.
(A) Bar graph and density plot reporting density of vGlut2-positive synaptic terminals in spinal segment L4 (n = 4-5 rats per group). **(B)** Representative heatmaps of vGlut2-positive synaptic terminals. **(C)** Bar graph and density plot reporting density of vGlut1-positive synaptic terminals in spinal segment L4 (n = 4-5 rats per group). **(D)** Representative heatmaps of vGlut1-positive synaptic terminals. **, P < 0.01; ***, P < 0.001. Error bars, s.e.m.

Rats with chronic SCI show aberrant recruitment of neurons during stepping

We sought to evaluate whether the increased density of fibers and synapses observed in rats with chronic SCI had an impact on the recruitment of sensorimotor circuits during gait execution. To address this question, we studied the expression pattern of the activity-dependent early gene protein c-fos in response to a continuous bout of electrochemically enabled stepping (Ichiyama *et al.*, 2008; Courtine *et al.*, 2009a). Rats in the chronic stage of SCI exhibited a 2-fold increase in the number of c-fos^{on} neurons in motor-related spinal regions (laminae 7 to 10) compared to intact rats ($p < 0.001$; **Figure 3.8A-C**). The number of c-fos^{on} neurons inversely correlated with locomotor capacities ($r = -0.86$, $p < 0.001$; **Figure 3.8B**).

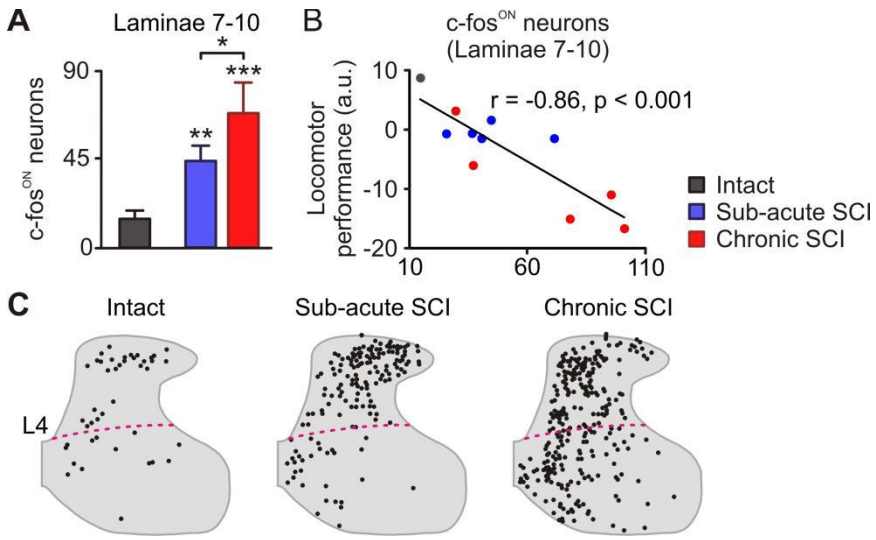

Figure 3.8 Locomotor activity engaged an aberrant neuronal population in the chronic stage of severe SCI.
(A) Bar graph reporting the number of c-fos^{ON} neurons in laminae 7-10 of L4 spinal segment after a bout of 45 min of continuous stepping (n = 5 rats per group). **(B)** Correlation between c-fos^{ON} neuron counts and stepping performance quantified as the sum of PC1 and PC2 for each animal. **(C)** Single-slice reconstructions of c-fos^{ON} neurons in spinal segment L4. Laminae 7-10 are delineated by the dotted line. *, P < 0.05; **, P < 0.01; ***, P < 0.001. Error bars, s.e.m.

Syndromic analysis establishes relationships between functional and neuromorphological changes after severe SCI

We finally aimed at establishing multi-directional correlative relationships between functional, electrophysiological, and neuromorphological alterations in chronically injured rats. For this purpose, we applied a syndromic analysis (Ferguson *et al.*, 2013) to all the computed variables (n = 55) in order to uncover causal links between neuronal dysfunction and compensatory plasticity. The first PC accounted for 32% of the total variance **(Figure 3.9)**. Extraction of PC1 factor loadings revealed that deterioration of stepping capacities, emergence of long-latency reflex responses, and extensor over-activity during electrochemically enabled motor states significantly correlated with injury-induced reorganization of primary afferent and intraspinal axonal systems. This syndromic analysis thus suggested that the aberrant remodeling of lumbosacral circuits significantly contributed to the syndrome of neuronal dysfunction after a severe SCI.

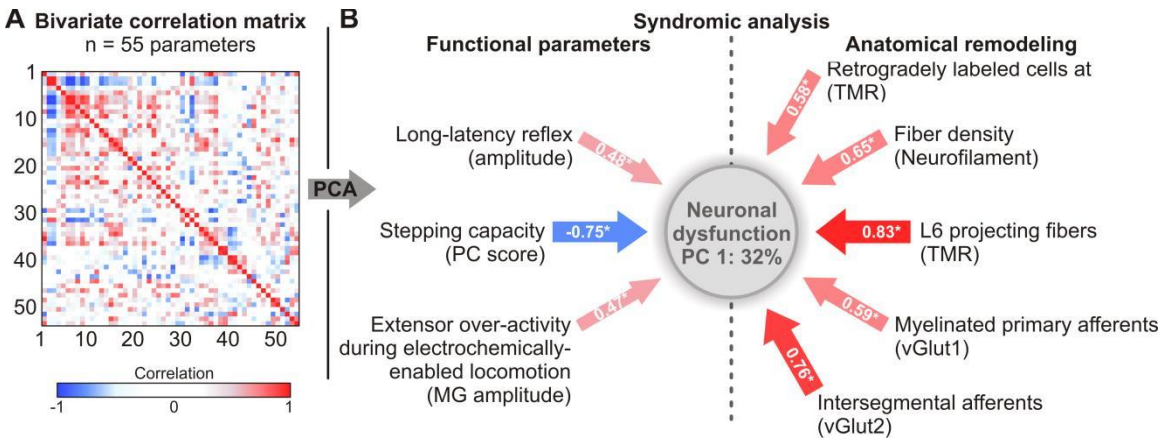

Figure 3.9 Syndromic analysis establishes relationships between functional and neuromorphological changes after severe SCI.

(A) Bivariate correlations were applied to all the functional, electrophysiological and neuromorphological variables (n = 55) for all the rats in the sub-acute and chronic stage of the SCI. **(B)** PCA was performed on the bivariate correlation matrix and stepping capacities significantly correlated with PC1 (32% of explained variance), indicating that PC1 was associated with the development of neuronal dysfunction. Each arrow represents a functional or neuromorphological variable with a high factor loading on PC1. The thickness of each arrow is proportional to the contribution of each represented variable to PC1. Blue and red colors correspond to a decrease or increase in the values of the variables, respectively. For example, this analysis shows that a decrease in stepping capacities (blue) correlates with an increase in the number of L6 projecting fibers (red). Asterisks indicate statistically significant factor loadings (|value| > 0.45).

3.5 Discussion

We show that chronically paralyzed rats and humans exhibited similar changes in locomotor activity and reflex behavior. Using a syndromic analysis (Ferguson *et al.*, 2013) applied on a range of functional, electrophysiological, and neuromorphological assessments, we provide statistical evidence that aberrant remodeling of denervated spinal circuits was in part responsible for the development of neuronal dysfunction in the chronic stage of SCI.

Severely paralyzed rats and humans exhibit similar neuronal dysfunction in the chronic stage of SCI

We aimed at developing an SCI model that shares some of the key pathophysiological and functional features of a severe SCI in humans. Specifically, we sought to create a lesion that induces permanent paralysis, but spares residual bridges of intact neural tissue (Courtine *et al.*, 2008; Murray *et al.*, 2010). We placed a staggered lateral hemisection SCI that met these criteria while providing controlled experimental conditions to assess injury- and intervention-mediated anatomical reorganization (van den Brand *et al.*, 2012). This SCI induced a neuronal dysfunction in the chronic stage of the injury, which contrasted with the progressive recovery of sensorimotor functions that spontaneously occurs after partial SCIs in rodents (Raineteau & Schwab, 2001; Bareyre *et al.*, 2004; Courtine *et al.*, 2008), non-human primates (Courtine *et al.*, 2005; Rosenzweig *et al.*, 2010) and humans (Curt *et al.*, 2008). Neuronal dysfunction in rats was characterized by a premature exhaustion of locomotor muscle activity, which was also observed in chronic, non-ambulatory patients (Dietz & Muller, 2004); and by a dramatic dysfunction of spinal locomotor circuits that we uncovered with the use of an electrochemical neuroprosthesis (Courtine *et al.*, 2009a; Musienko *et al.*, 2012). While the progressive decline of functional capacities has been well documented after a severe SCI (De Leon *et al.*, 1999a; Dietz *et al.*, 2002; Boulenguez *et al.*, 2010) our detailed neurobiomechanical and statistical analyses identified, for the first time, the syndromic signature of deterioration of stepping function in rats. This syndrome included high gait variability, pronounced flexed posture, and undesired co-activation between antagonistic muscles, poor interlimb coordination, altered distal joint control, and increased extensor muscle activity during electrochemically enabled locomotion. Comparable changes in gait pattern characteristics have been reported in humans with SCI (Grasso *et al.*, 2004; Lunenburger *et al.*, 2006; McKay *et al.*, 2011). Here, we hypothesized that the development of neuronal dysfunction is largely due to multifaceted plastic changes that propagate throughout local and long-distance interneuronal circuits after severe SCI.

Severely paralyzed rats and humans exhibit similar changes in reflex behavior in the chronic stage of SCI

We previously documented the emergence of abnormal long-latency reflex responses in ankle flexor muscles following stimulation of the tibial nerve in non-ambulatory individuals with chronic SCI (Dietz *et al.*, 2009). The amplitude of these reflex responses correlated with the development of neuronal dysfunction (Hubli *et al.*, 2012). These long-latency reflex responses resemble an exacerbation of the flexor reflex afferent (FRA) response, which plays an important role in the production of locomotion (Bussel *et al.*, 1989; Nicol *et al.*, 1995). To date, this syndrome has never been observed in experimental animals with SCI (Dietz *et al.*, 2009). Here, we developed a new model of SCI in which we observed the appearance of abnormal long-latency reflex responses in the chronic stage of the injury. As previously observed in humans (Hubli *et al.*, 2012), the amplitude of long-latency reflexes correlated with the development of neuronal dysfunction in SCI rats.

These results highlight remarkable similarities in the functional response of the rodent and human spinal cord after the chronic interruption of supraspinal input. The profound reorganization of sub-lesional reflex circuits suggested that a significant anatomical remodeling took place within denervated neuronal networks in the chronic stage of SCI.

Undirected plasticity of denervated circuits leads to the development of neuronal dysfunction in the chronic stage of SCI

Previous investigations in animal models of SCI documented the progressive upregulation of receptor, synapse and fiber density in spinal circuitries deprived of supraspinal input (Krenz & Weaver, 1998; Kitzman, 2006; Boulenguez *et al.*, 2010; Ichiyama *et al.*, 2011; Kapitza *et al.*, 2012; Tan *et al.*, 2012; Bos *et al.*, 2013). In the present study, we also found a multiplicity of plastic changes in spinal segments caudal to a staggered lateral hemisection SCI. Chronically denervated lumbosacral segments showed sprouting of myelinated primary afferent fibers, increased intraspinal axon density, enhanced bidirectional connectivity between distant spinal segments, and upregulation of the number of glutamatergic synaptic terminals. Using a syndromic analysis (Ferguson *et al.*, 2011; Ferguson *et al.*, 2013), we established mechanistic relationships between this extensive anatomical reorganization, and the alteration of reflex behavior and stepping capacities. These results suggested that injury-induced rewiring of denervated spinal segments formed aberrant sensorimotor circuits that caused abnormal reflex responses and recruited inappropriate combinations of neuronal

networks during gait execution. Complementary experimental results directly supported this conclusion; analysis of stepping-associated c-fos expression patterns revealed that rats with chronic SCI engaged an abnormally high number of spinal neurons to produce locomotor output.

These combined results reveal that the interruption of supraspinal pathways induces a profound rewiring within denervated spinal segments, which can lead to the formation of aberrant sensorimotor circuits in the chronic stage of the injury. We suggest that these newly established connections misdirect neural information in spinal circuits during gait execution, which leads to the syndrome of neuronal dysfunction in paralyzed rats, and probably in non-ambulatory humans with SCI.

Undirected compensatory plasticity is responsible for the detrimental rewiring of lumbosacral circuits after severe SCI

Our results provide overwhelming evidence that a massive reorganization of neural connectivity occurred in denervated spinal segments after severe SCI. At first sight, these extensive and ubiquitous changes appear to be chaotic. However, a closer examination suggested that they follow a common biological principle. Injury-induced anatomical reorganization of denervated neural systems occurred in a lamina-specific manner. Changes in the density of fibers and synapses in each lamina at the chronic stage of the SCI invariably reached the innervation level observed in non-injured rats. These results highlight the systematic effort of denervated neural systems to restore their normal synaptic environment. Along the same line, blockage of synaptic transmission induces a substantial increase in the number of dendritic spines on hippocampal neurons (Kirov & Harris, 1999). This phenomenon, which has been termed homeostatic plasticity (Turrigiano *et al.*, 1998), is interpreted as an attempt to maintain a well-balanced synaptic activity in neuronal networks. After incomplete SCIs that leave residual motor capacities, activity-dependent mechanisms likely contribute to steering plasticity. The associated reconfiguration of the synaptic environment promotes useful remodeling that ameliorates sensorimotor functions (Raineteau & Schwab, 2001; Weidner *et al.*, 2001; Edgerton *et al.*, 2004; Courtine *et al.*, 2008; Rosenzweig *et al.*, 2010). For instance, laminae-specific restoration of serotonergic projections in segments caudal to a moderate SCI has been associated with improved locomotion in rats (Mullner *et al.*, 2008).

In contrast, we show here that after a severe SCI leading to chronic paralysis, the absence of activity leads to a chaotic remodeling of denervated neuronal networks. The resulting undirected compensatory plasticity leads to neuronal dysfunction in the chronic stage of SCI. This potentially detrimental impact of compensatory plasticity has been

described in other neural networks, including the autonomic nervous system such as the pyloric network of the stomatogastric ganglion (Nahar *et al.*, 2012). In the spinal cord, the increased expression of constitutively active 5-HT_{2C} receptor isoforms partially compensated for the depletion of brainstem-derived serotonin after severe SCI (Murray *et al.*, 2010). However, the regained excitability in motoneurons contributed to the development of abnormal reflex responses (Murray *et al.*, 2010). Likewise, the depletion of corticospinal tract associated vGlut1 terminals after a pyramidotomy induced a specific sprouting of vGlut1 proprioceptive afferent fibers, but also in this condition, the synaptic reorganization adversely altered proprioceptive reflex circuits (Tan *et al.*, 2012). Although additional mechanisms such as changes in motoneuron membrane excitability (Lin *et al.*, 2007; Boulenguez *et al.*, 2010) likely contribute to neuronal dysfunction in the chronic stage of SCI, our combined results suggest that undirected compensatory plasticity plays an important role in the emergence of this syndrome.

Directing compensatory plasticity to improve functional recovery after severe SCI

We propose that the myriad of anatomical and functional changes that follow after a severe SCI obeys a common biological principle—compensatory plasticity, which is a powerful mechanism to maintain the stability of neurons, and shape the reconfiguration of circuits and pathways following injury (Turrigiano *et al.*, 1998). However, unless this process is directed with use-dependent cues, compensatory plasticity can lead to an aberrant reorganization of denervated spinal circuits, which contributes to the development of neuronal dysfunction in the chronic stage of SCI.

Spinal cord repair interventions primarily focus on developing strategies to promote regeneration of severed neural pathways. The present findings in rats and humans demonstrate that recovery after severe SCI will also necessitate directing and exploiting compensatory plasticity to preserve and improve the functional capacities of denervated spinal sensorimotor circuits (Dietz, 2010). Electrochemically enabled training is capable of promoting useful remodeling of spinal circuits and functional improvement in severely paralyzed rats (Ichiyama *et al.*, 2008; Courtine *et al.*, 2009a; Ichiyama *et al.*, 2011; van den Brand *et al.*, 2012). Robotically assisted training also shows efficacy to improve both spinal reflex behavior and mobility in individuals with incomplete SCI (Hubli *et al.*, 2012). Future studies will need to investigate how activity-based rehabilitation steers compensatory plasticity of spinal sensorimotor circuits in order to prevent, and potentially reverse, the development of neuronal dysfunction after severe SCI.

4 Versatile robotic interface to evaluate, enable and train locomotion and balance after neuromotor disorders

Original article: “Novel robotic interface to evaluate, enable and train locomotion and balance after neuromotor disorders”

Nadia Dominici[1,2]*, Urs Keller[3]*, Heike Vallery[3,7], Lucia Friedli[1,2], Rubia van den Brand[1,2], Michelle L. Starkey[4,5], Pavel Musienko[1,2,6], Robert Riener[3,5] and Grégoire Courtine[1,2]

Nature Medicine 2012 July; 18(7): 1142-7

1. Neurology Department, University of Zurich, Zurich, Switzerland
2. Center for Neuroprosthetics and Brain Mind Institute, School of Life Science, Swiss Federal Institute of Technology, Lausanne, Switzerland
3. Sensory-Motor Systems Lab, Institute of Robotics and Intelligent Systems, Swiss Federal Institute of Technology, Zurich, Switzerland
4. Brain Research Institute, University of Zurich, Zurich, Switzerland
5. Spinal cord injury Center, Balgrist University Hospital, University of Zurich, Switzerland
6. Pavlov Institute of Physiology, St Petersburg, Russia
7. Department of Biomedical Engineering, Khalifa University, Abu Dhabi, UAE

* These authors contributed equally to this work.

The PhD candidate's contribution: conception and performance of behavioral experiments, performance of surgical procedures

4.1 Abstract

CNS disorders distinctly impair locomotor pattern generation and balance, but technical limitations prevent independent assessment and rehabilitation of these sub-functions. Here, we introduce a versatile robotic interface to evaluate, enable, and train pattern generation and balance independently during natural walking behaviors in rats. In evaluation mode, the robotic interface affords detailed assessments of pattern generation and dynamic equilibrium after spinal cord injury (SCI) and stroke. In enabling mode, the robot acts as a propulsive or postural neuroprosthesis that instantly promotes unexpected locomotor capacities including overground walking after complete SCI, stair climbing following partial SCIs, and precise paw placement shortly after stroke. In training mode, robot-enabled rehabilitation, epidural electrical stimulation and monoamine agonists restore weight-supported locomotion, coordinated steering, and balance in rats with a paralyzing SCI. This new robotic technology and associated concepts have broad implications to assess and return motor functions after CNS disorders, both in animals and in humans.

4.2 Introduction

The gravitational field created by the mass of Earth allows terrestrial mammals to exert force on the external environment to propel the body forward efficiently (Dickinson *et al.*, 2000), but gravity also threatens the maintenance of equilibrium at each step. The organization of locomotor control mechanisms reflects this dichotomy between propulsion and balance (Orlovsky *et al.*, 1999). While motor pattern generation essentially results from interactions between afferent systems and spinal circuitries (Grillner, 2006; Courtine *et al.*, 2009a), the concomitant maintenance of equilibrium heavily relies on brainstem (Macpherson *et al.*, 1997) and forebrain (Drew *et al.*, 2004) motor centers. Consequently, CNS disorders such as spinal cord injury (SCI) and stroke significantly impair the ability to control balance and weight bearing, but leave locomotor pattern generating circuitries largely unaffected (Wirth *et al.*, 2008; Courtine *et al.*, 2009a).

The differential impact of neuromotor disorders on pattern generation and balance emphasizes the necessity to develop novel technologies to dissociate these sub-functions during assessment and rehabilitation of locomotion in subjects with SCI, stroke, or other CNS disorders affecting the control of gait. Conceptually, the designed system should act as a propulsive or postural neuroprosthetic interface that can perturb or assist propulsion, balance, or the combination of both with varying degrees according to the experimental purpose or the specific needs of the patient.

Currently, the primary solution used to compensate for impaired balance and weight-bearing capacities relies on passive supporting systems. Typically, subjects are positioned in a harness that supports part of their body weight against gravity while the limbs are moved backward on a motorized treadmill belt to encourage stepping. However, this approach presents several issues and drawbacks. (i) These support systems fail to simulate a reduced gravitational environment, which is critical for the production of efficient gait in terrestrial mammals (Dickinson *et al.*, 2000). (ii) They only provide support in the vertical direction whereas well-balanced locomotion requires finely tuned trunk movements in virtually every direction(Winter *et al.*, 1993). (iii) Evaluation and training of gait is restricted to stepping on a treadmill (Musselman *et al.*, 2011a); a condition that markedly differs from the rich repertoire of locomotor tasks underlying daily living activities.

Here we introduce a novel multidirectional robotic interface that can continuously and independently perturb or assist propulsion and balance along four degrees of freedom while rats are progressing overground within a large workspace. Using the multifaceted control mode of the robotic interface in various models of SCI and stroke, we document

advanced capacities to evaluate, enable, and train the control of, and interactions between, pattern generation and balance during walking under natural conditions and over a broad spectrum of locomotor behaviors. Our robotic technology and associated biomedical concepts can readily translate into effective neuroprosthetic interfaces and novel neurorehabilitative strategies for humans with various CNS disorders.

4.3 Methods

Design of the robotic interface

We built a large robotic system to provide rats with adjustable trunk support along 4 independent degrees of freedom (DoF). Three actuated linear modules (MSK40, Amsler AG, Feuerthalen, Switzerland) define a Cartesian workspace capable of translating the rat in X, Y, Z directions. The first two axes (**Figure 4.1a**, X and Y), which are used for movements in the horizontal plane, cover an area of 1.2 m^2. The third axis (**Figure 4.1**a, Z) provides the subject with support against gravity, and allows vertical movements over a range of 35 cm. At the extremity of this Cartesian structure, a fourth motor (RE25, Maxon motor AG, Sachseln, Switzerland) actuates rotations (300 deg) in the horizontal plane (**Figure 4.1**a, φ). This serial configuration provides a large workspace in which forces can be applied to the subject while preventing inclinations in both horizontal directions.

We aimed to design a highly flexible robotic system capable of guiding the rats along any desired trajectory, but that can also behave transparent, i.e. allowing the rats to walk freely in the entire workspace. Such transparency requires reducing the interaction forces between the subject and the robot to a minimum. The moved mass of the robot (> 60 kg) is significantly larger than the mass of the rat (< 0.25kg). Consequently, a direct coupling between the robot and the subject would yield substantial interaction forces that will interfere with the natural movements of the rat (Colgate & Hogan, 1989). To decouple the inertia of a massive robotic structure from a substantially lighter interacting subject, Pratt et al. (Pratt *et al.*, 1995b) proposed a solution based on Series Elastic Actuator (SEA). SEAs couple an actuator to a robotic structure via a compliant element that hides the actuator inertia. Moreover, interaction forces and torques can be measured directly by monitoring the deformation of the compliant element.

Here, we extended the concept of SEAs in multiple directions. We conceived a light, low-friction (< 10g), compliant module consisting of a base platform with three protruding legs forming a cage, a spring-suspended platform within this cage, and a Delta structure that constrains the unactuated DoF (i.e. tilting of the rat) (**Supplementary Figure 4.1 and Supplementary Video 1**). The cage is connected to the suspension platform via six linear springs (angle in the horizontal plane, 120deg angle; stiffness, 112 N.m-1 for upper strings, 57 N.m-1 for lower strings, **Supplementary Figure 4.1**). An additional spring pair is attached to the rotating shaft in the center of the platform, providing an elastic torque about the vertical axis. Together, this configuration decouples inertia of the serial module from the suspension platform in the 4 actuated DoFs.

The Delta structure allows to measure the displacements of the suspended platform, and thereby the deflection of the springs along each DoF. Four contact-free magnetic encoders (12 bits) are located in the joints of the Delta structure. The position of the end-effector with respect to the serial robot is calculated by combining information from these angular sensors and a forward kinematic model of the Delta structure (**Supplementary Figure 4.1**). The relative position of the platform encodes the spring lengths, and thereby the interaction forces and torques that are derived from the linear spring characteristics.

The control strategy is implemented in MATLAB/Simulink (**Supplementary Figure 4.1**) and executed in real-time on a desktop PC running xPC target (Sampling rate, 1 kHz). This computer communicates with the motor drives and acquires information coming from the sensors and a Windows computer that runs a user interface for online changes of the robot control parameters.

Animals and Animal Care

All procedures and surgery were approved by the Veterinarian Office Zurich, Switzerland. The experiments were conducted on adult female Lewis rats (~200 g body weight, Centre d'Elevage R. Janvier, France). Animals were housed individually on a 12h light/dark cycle, with access to food and water *ad libitum*.

Surgical Procedures and Post-Surgical Care

All procedures have been described in detail previously (Courtine *et al.*, 2008; Courtine *et al.*, 2009a; Musienko *et al.*, In press). The surgical interventions were performed under general anesthesia and aseptic conditions. The rats underwent two surgical interventions. They first were implanted with bipolar intramuscular EMG electrodes (AS632; Cooner Wire, Chatsworth, CA) into selected hindlimb muscles (Courtine *et al.*, 2009a). For some experiments, electrodes were also secured at the midline of the spinal cord at spinal level L2 and S1 by suturing wires (same as EMG wire) over the dura mater above and below the electrode (Courtine *et al.*, 2009a). The rats were allowed to recover for 2 weeks post-implantation. After completion of pre-lesion behavioral recordings, the rats underwent a second surgical intervention during which they received a SCI or a stroke. SCIs included complete transection of the thoracic (T7) spinal cord (Courtine *et al.*, 2009a), right cervical (C7) lateral hemisection (Courtine *et al.*, 2008), or two lateral hemisections placed on opposite side and at different spinal levels (T7 and T10) (Courtine *et al.*, 2008). Ischemic lesion to the cortex (stroke) was induced by injecting the vasoconstrictor endothelin-1 (ET-1, 0.3 microg microl−1; Sigma-Aldrich) at 14 locations into the left motor cortex (fore- and hindlimb areas). We injected a volume

of 500 nl at a depth of 1.2 mm with a rate of 6 nl s−1. After each injection, we left the needle in place for 3 min before it was carefully removed (Zorner *et al.*, 2010a). The extent and location of the lesions were verified post-mortem.

Locomotor tasks

A total of 7 locomotor tasks were used in the present experiments: bipedal locomotion on a moving treadmill belt (13 cm/s), bipedal walking along a straight runway, quadrupedal walking along a straight runway, lateral perturbation during quadrupedal walking along a straight runway, quadrupedal walking along irregularly-spaced round rungs, quadrupedal stair climbing along regularly-spaced staircases, and quadrupedal steering along a 90deg-curved runway. The characteristics of the tasks and the dimensions and features of the custom-designed runways can be found in **Supplementary Figure 4.2**.

Behavioral training of the rats

The rats were first acclimatized to wear the custom-made jacket for 1-2 weeks while navigating freely along the runways. We then trained the animals daily in 1 or 2 sessions until they crossed the runways with a constant speed. Positive reinforcement (food reward) was used to encourage the rats to perform the requested tasks. Rats were trained on the ladder with a regular arrangement of rungs. For testing, rung sequences were irregular and varied to avoid habituation to a particular rung pattern (Zorner *et al.*, 2010a).

Motor control enabling factors

To encourage locomotion in paralyzed rats, we applied epidural electrical stimulation and a cocktail of monoamine agonists (Musienko *et al.*, In press). Rectangular pulses (0.2 ms duration) were delivered at 40Hz using two constant-current stimulators (AM-Systems, WA, USA) connected to L2 and S1 electrodes. The intensity of stimulation was adjusted (50-200 µA) to obtain optimal facilitation of stepping visually. The rats also received a systemic administration of agonists to $5HT_{1A/7}$ (8-OH-DPAT, 0.05-0.1mg/Kg), $5HT_{2A/C}$ (quipazine, 0.2-0.3 mg/Kg), and SKF-81297 (0.15-0.2 mg/Kg) (Musienko *et al.*, 2011c)

Testing protocols

10 step cycles (treadmill) or 10 trials (runways) were typically recorded for each rat in a given experimental condition. The conditions with and without robot were randomized across rats. The rats wore the body jacket during walking with and without the robot in order to maintain the same testing conditions for both types of recordings. When using

electrical and pharmacological stimulations to facilitate locomotion, stepping was recorded about 10min after drug injection. For testing of spinal rats on the treadmill, a rigid circular (diameter, 0.4 mm) bar was inserted between the rat's limbs to prevent them from crossing.

Neurorehabilitative training

Rats were subjected to 30-min training sessions 5 days per week; starting 12d post-injury. They were trained for 7 weeks. Locomotion was enabled by electrical and pharmacological stimulations. During each training session, the rats practiced quadrupedal locomotion along the horizontal straight runway, along the stairs, and along the 90deg-curved runway. We adjusted the respective duration of each task according to the actual capacities of the animals. For example, rats only performed a few runs along the curve during each training sessions until week 4-5, when they started showing recovery of balance control.

Kinematics, Kinetic, and EMG Recordings

Kinematic. 3-D video recordings (200 Hz) were made using a motion capture system (Vicon, Oxford, UK). 12 infrared T10 cameras were used to track the motion of reflective markers attached bilaterally at the scapula (Scap), iliac crest, greater trochanter, lateral condyle, lateral malleolus, the distal end of the fifth metatarsal (MTP), and the tip of the toe. Nexus (Vicon, Oxford, UK) was used to obtain 3-D coordinates of the markers. The body was modeled as an interconnected chain of rigid segments, and joint angles generated accordingly. The main limb axis termed 'hindlimb' in the figures was defined as the virtual line connecting the greater trochanter to the lateral malleolus.

EMG. EMG signals (2 kHz) were amplified, filtered (10–1000 Hz bandpass), stored, and analyzed off-line to compute the amplitude, duration, and timing of individual bursts (Courtine *et al.*, 2009a). To evaluate temporal coordination between muscles, we generated probability density distributions of normalized EMG amplitudes of agonist and antagonist muscles, as described previously (Courtine *et al.*, 2009a).

Kinetic. Moments and ground reaction forces in the vertical, antero-posterior, and medio-lateral directions were monitored using a biomechanical force-plate (2 kHz, HE6X6, AMTI, USA) located below the treadmill belt or at the middle of the runway (Supplementary Figure 4.2).

Data Analysis

A minimum of 10 step cycles was extracted for both the left and right hindlimbs for each experimental condition and rat. A total of 148 parameters quantifying gait,

kinematics, kinetics, and EMG features were computed for each limb and gait cycle according to methods described in details previously (Courtine *et al.*, 2008; Courtine *et al.*, 2009a; Musienko *et al.*, 2011c). These parameters provide a holistic quantification of locomotor patterns ranging from general features of gait and performance to fine-details of limb motions. The entire list of 148 computed parameters can be found as **Supplementary Table 4.1.**

Statistical analyses

The various experimental conditions were associated with substantial modulations of gait patterns, which were evident in the modifications of a large proportion of the computed parameters. In order to evaluate the more important and reproducible modulation patterns mediated by the different conditions as well as the correlations between the modulated parameters, we implemented a multi-step statistical procedure based on principal component (PC) analysis (Courtine *et al.*, 2009a). The various steps, methods, typical results, and interpretation of the analysis are detailed in Supplementary Figure 4.3. PC analyses were applied on data from all individual gait cycles for all the rats together. Data were analyzed using the correlation method, which adjusts the mean of the data to zero and the standard deviation to 1. This is a conservative procedure that is appropriate for variables that differ in their variance (e.g. kinematic vs. EMG data).

All data are reported as mean values ± S.E.M. Repeated-measures ANOVA's and Student's paired t-test were used to test differences between normally distributed data (Kolmogorov-Smirnov test) from the various experimental conditions. Non-parametric test (Wilcoxon and Kruskall Wallis) were used instead when the distribution was not normal.

4.3 Results

Design and properties of the robotic interface

We developed a multidirectional support system that exploits three advanced robotic principles (**Supplementary Figure 4.1**). (i) We developed a large serial robotic module consisting of three translational axes defining a Cartesian frame (*x*, *y*, *z*), as well as one rotational axis (*φ*, Figure 1a). (ii) A parallel Delta kinematic system prevents tilting, and allows measurement of the rat's position. (iii) To decouple the inertia of the massive robotic structure from the end-effector, we fabricated a suspension system with springs directed in each of the four DoFs of the serial structure (**Figure 4.1a**). This suspension system capitalizes on the high-performance of series elastic actuators for the realization of transparently behaving haptic devices (Pratt *et al.*, 1995a; Vallery *et al.*, 2008). Together, this novel robotic arrangement allows real-time control of body translations (propulsion) and body weight support (BWS) (balance) along four independent DoFs that can be continuously adjusted, i.e. from stiff position control to transparent, zero-force control (**Supplementary Video 1**).

To demonstrate the transparency of the robot, we compared the kinematics and muscle activity underlying locomotion of healthy rats ($n = 7$) walking along a straight runway with and without the robot (**Figure 4.1b** and **Supplementary Figure 4.2**). Despite detailed analyses (**Supplementary Figure 4.3**), we did not detect significant differences between these conditions ($P > 0.3$, **Figure 4.1c**), indicating that the massive robot did not interfere with gait. We confirmed these results during walking on a horizontal ladder ($n = 5$) (**Figure 4.1d**). Even in such challenging conditions, precise paw placement ($p > 0.4$, **Figure 4.1e**) and gait features were virtually unaffected by the robotic interface ($P > 0.3$, **Figure 4.1f**).

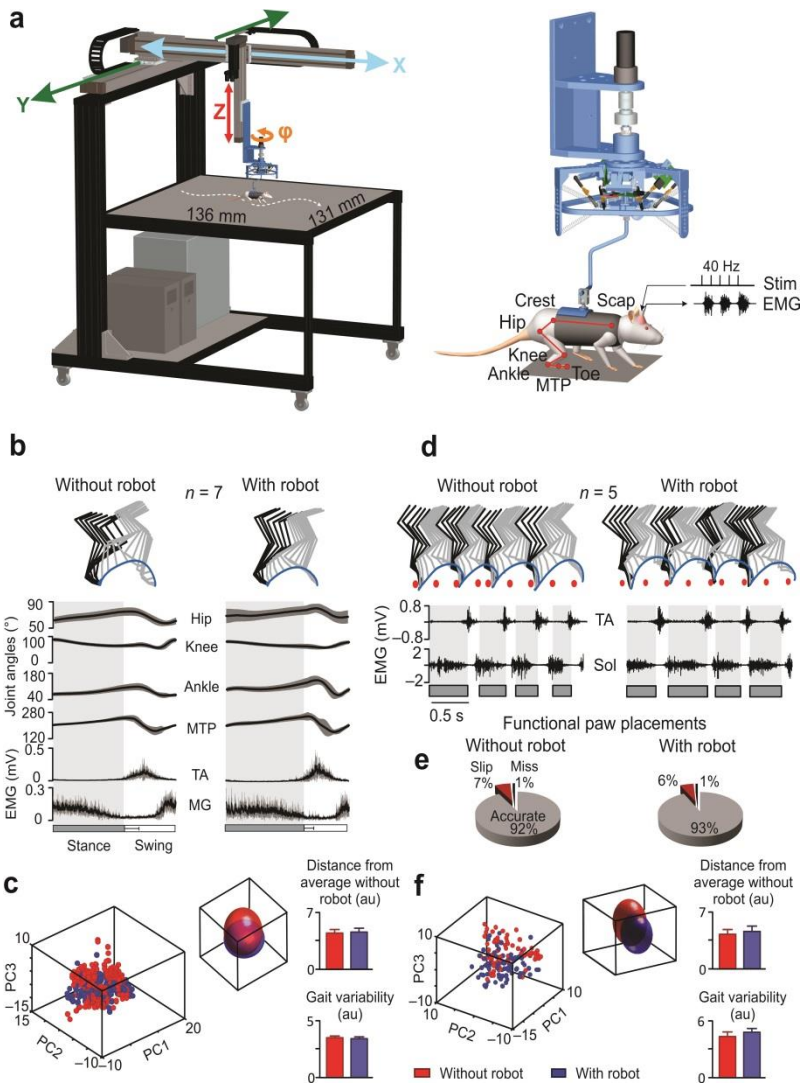

Figure 4.1 Design and transparency of the robotic interface.
a. Large view of the robotic interface (left) and the suspension system (right). The different DoFs are represented with distinct colors. The rat is placed in a skin-like jacket that is attached to a back plate at the trunk level by means of a Velcro strip. Reflective markers (scap, scapula; MTP, metatarsal phalange) are positioned overlying bony landmarks to record whole body kinematics. **b.** Representative stick diagram decomposition of hindlimb motion during stance (dark) and swing (light) together with limb endpoint trajectory during runway locomotion without and with transparent robotic support. The plots show averaged (n = 7 rats, +/- S.E.M.) hindlimb joint angles and rectified EMG activity of medial grastrocnemius (MG) and tibialis anterior (TA) muscles. **c.** Principal component (PC) analysis was applied on all the measured variables (n=144) from all the rats. The gait cycles are represented in the new 3-D space created by the 3 first PCs (explained variance, 39%). Least-squares spheres are traced to emphasize the overlap between gaits performed with and without robot. The bar graphs report the average (n = 7 rats) 3D distance between conditions (relative difference between conditions) as well as 3D dispersion (gait variability) (see **Supplementary Figure 4.3**). **d.** The same representation is shown during locomotion along irregularly spaced rungs (red dots) with and without transparent robotic support. **e.** The circular plots show the percentage of steps that were accurately placed vs. when the paw missed or slipped off the rung. **f.** PC analysis (explained variance, 31%) applied on ladder gait cycles. Error bars, S.E.M.

Evaluation of motor pattern generation and balance (evaluation mode)

We first aimed to document advanced robot-assisted capabilities to assess motor pattern generation and balance. We embodied these control schemes under the term *evaluation mode*.

Most BWS systems rely on passive spring mechanisms, which provide a support against gravity that is proportional to the subject's vertical position. Although special kinematic configurations can achieve position-independent, constant force support (Nessler *et al.*, 2005), these passive systems do not compensate for rapid movements. Our robotic system can apply well-controlled, arbitrary vertical force profiles that emulate a reduced gravitational environment. We exploited this advanced functionality to compare the effect of spring-like vs. constant-force BWS conditions on locomotor pattern generation in rats with complete SCI (n = 5, **Figure 4.2a-c**). To enable stepping, we applied a combination of epidural electrical stimulation and monoamine agonists (Courtine *et al.*, 2009a) (**Figure 4.2a-b**). We tuned the spring-constant to an optimal value for facilitating stepping (Courtine *et al.*, 2009a), and maintained the exact same amount of support during constant-force conditions. Compared to spring-like BWS, the constant-force BWS markedly improved the quality and consistency ($P < 0.01$, **Figure 4.2b-c**) of gait features (**Supplementary Figure 4.4**), and promoted locomotor patterns that converged towards those of healthy rats ($p < 0.01$, **Figure 4.2c** and **Supplementary Video 2**).

The human (Harkema *et al.*, 2011) and rat (Timoszyk *et al.*, 2005; Courtine *et al.*, 2009a) lumbosacral spinal cord can interpret weight-bearing information during stepping. We evaluated whether weight-bearing input also determines gait quality in rats with complete SCI ($n = 4$). Decreasing the level of BWS resulted in graded adjustments in hindlimb kinematics, forces, and muscle activity ($P < 0.01$; **Supplementary Figure 4.5b-e**), which confirmed the ability of lumbosacral circuitries to transform weight-bearing information into specific locomotor patterns (**Supplementary Video 2**). However, we found an inverted U-shaped relationship ($R^2 = 0.87$, **Supplementary Figure 4.5c**) between gait quality and the level of BWS.

These findings emphasize the importance of optimal constant-force support conditions to enable and train locomotion in subjects with gait disorders.

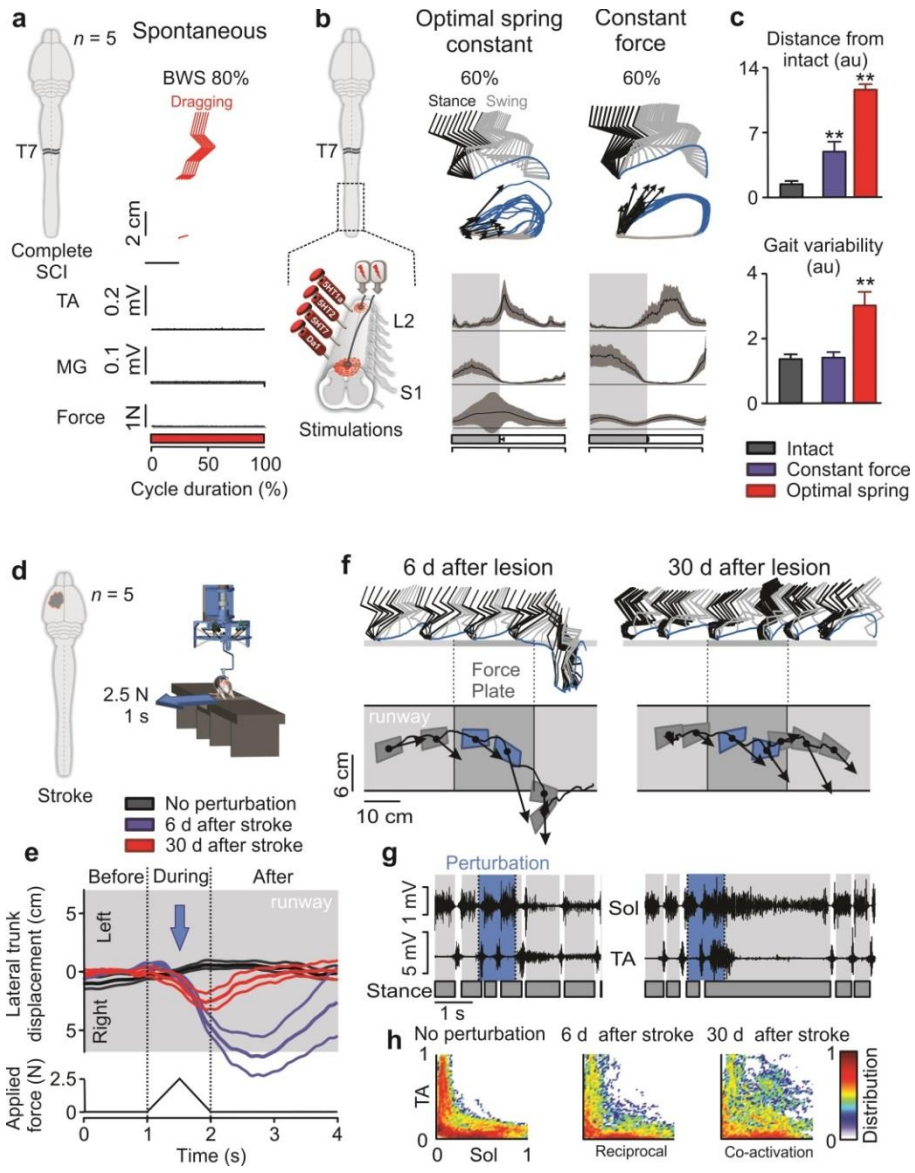

Figure 4.2 The robotic interface affords detailed assessment of pattern generation and balance.
a. Rats received a complete SCI that led to permanent hindlimb paralysis. **b**. Locomotion was enabled by electrical and pharmacological stimulations. Stick diagram decomposition of hindlimb motion with spring-like vs. constant-force BWS is shown together with successive limb endpoint trajectories (n = 10 steps), activity of TA and MG muscles, and vertical ground reaction forces. The vectors indicate the direction and intensity of foot velocity at swing onset. **c.** The bar graphs report the average distance from intact rats as well as gait variability computed through PC analysis. a.u. arbitrary unit. **d.** A brief (1s) force was applied (rightward) during runway locomotion in rats with a left-sided cortical stroke. **e.** Averaged (n = 5 rats) lateral trunk displacements 1s before, during, and 2s after perturbation**. f.** Stick diagram decomposition of hindlimb motion and trunk positioning. Arrows indicate the intensity (velocity) and direction of trunk motion. Blue, during perturbation. **g.** EMG activity of Sol and TA muscles during a representative trial at 6d and 30d post-lesion. **h.** The plots illustrate the coordination (density distribution) between Sol and TA muscles without perturbation and during perturbation at 6d and 30d post-lesion (all trials and rats, scale is the same for all the plots). At 30d post-lesion, rats showed clear co-activation of antagonistic muscles during perturbation to stabilize the body. Error bars, S.E.M. **: significantly different at $p < 0.01$ from all the other non-marked conditions.

A unilateral cortical stroke has limited impact on basic locomotion in rats, but behavioral observations have suggested deficits in balance control (Zorner *et al.*, 2010b). To demonstrate impairment of equilibrium after stroke, we exploited the capacity of the robot to superimpose any force at any time and in any actuated DoF onto the transparent control mode. Specifically, we applied a sudden triangular-shaped force (2.5 N, **Figure 4.2d-e**) in the medio-lateral direction (*y* axis, pushing rightward) for 1s while rats were progressing freely along a straight runway. Shortly after a left-sided stroke (6d), the rats failed to compensate for the perturbation. They displayed ample rightward deviations ($P < 0.002$, **Figure 4.2e-f**) and frequently fell off the runway (56 ± 39%, mean ± S.D.). After one month of recovery, the rats responded to the perturbation with a controlled co-activation of extensor and flexor muscles (**Figure 4.2g-h**), followed by a prolonged activity of contralesional extensor muscles (360 +/- 80%, $p < 0.001$, **Figure 4.2g-h**). This muscle synergy stabilized the trunk and hindlimb (**Figure 4.2e-f**), and produced substantial mediolateral forces ($P < 0.001$, 0.60 ± 0.07N at 6d vs. 1.54 ± 0.18N at 30d post-lesion) that restored the locomotor trajectory (**Supplementary Video 3**).

Robotically enabled motor control after CNS disorders (enabling mode)

We next sought to utilize the robotic interface as a propulsive or postural neuroprosthesis that provides adjustable assistance to propel the body forward and to restore postural orientation and stability. We hypothesized that this so-called *enabling mode* would uncover unexpected locomotor capacities that are dissimulated by impairments in propulsion and/or balance.

Electrical and pharmacological stimulations enable locomotion in rats with complete SCI **(Supplementary Figure 4.6a-b),** but the animals fail to produce the necessary forces to propel their body forward overground. Instead, they display tonic activity in extensor muscles, behaviorally apparent as standing **(Supplementary Figure 4.6c)**. To compensate for the lack of propulsion, we configured the robot to act as a propulsive neuroprosthesis that moved the rats forward (*x* axis, 13 cm/s) while providing constant-force vertical support (60 +/- 10% of BWS). When initiating the robotic sequence, the rats smoothly transitioned from quiet standing to continuous locomotion **(Supplementary Figure 4.6d)**. Rhythmic movements arrested instantly when the propulsive neuroprosthesis stopped translating the rat forward **(Supplementary Video 4)**.

Rats with unilateral cortical stroke display significant impairments in contralesional paw placement when crossing a horizontal ladder (Zorner *et al.*, 2010b) **(Figure 4.3b-d)**. These deficits have been attributed to the loss of visuomotor control, which heavily relies on the damaged motor cortex (Drew *et al.*, 2008). We tested the hypothesis that impaired

equilibrium maintenance **(Figure 4.2d-h)** may also contribute to the alteration of skilled locomotion after a cortical stroke. We configured the robotic interface to act as a postural neuroprosthesis. In this enabling mode, the robot provided a constant-force support in the vertical direction (*z* axis, 27 ± 4 % of BWS) and stiff support in the lateral directions (*y* and rotational axes). The robotic postural neuroprosthesis instantly improved the rats' ability to position their contralesional hindpaw accurately onto the irregularly spaced rungs of the ladder (*P* < *0.002*, **Figure 4.3b-c** and **Supplementary Video 5**). Statistical analyses showed that the robot significantly decreased the number of miss/slip (*P* < *0.01*, **Figure 4.3d**), which correlated with improved postural stability (*P* < *0.01*, **Supplementary Figure 4.7c**).

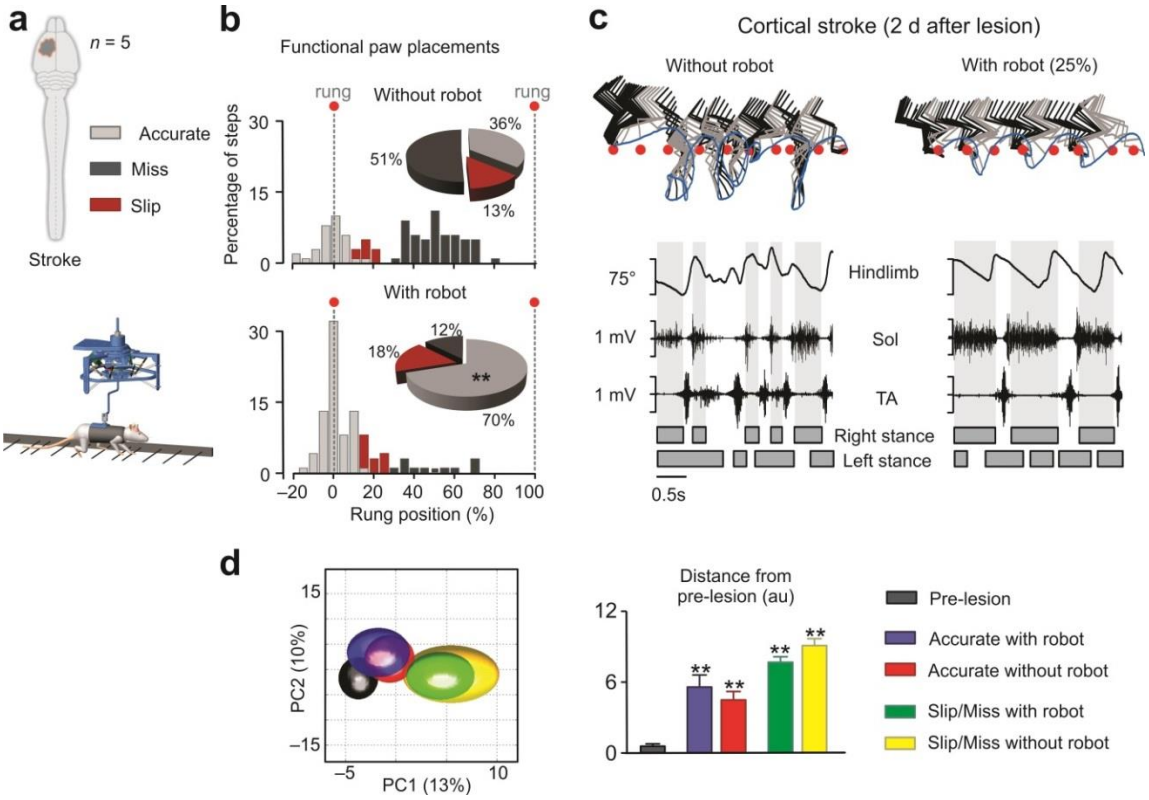

Figure 4.3 The robotic postural neuroprosthesis enables skilled motor control after cortical stroke
a. Rats received a left-sided cortical stroke. They were tested during walking along a ladder with irregularly-spaced rungs. **b.** The relative positioning of the contralesional hindpaw with respect to two successive rung positions (red dots) was evaluated over all the trials from all the rats without and with constant-force robot support. The number of occurrence per 5% bin is reported together with the percentage of accurate, slipped, and missed placements. **c.** Stick diagram decomposition of hindlimb motion during a trial along the ladder with and without robot. Hindlimb oscillations and EMG activity of TA and Sol muscles are shown below. **d.** PC analysis (explained variance, 28%). Accurate steps are dissociated from missed steps to emphasize that the robot increased the percentage of accurate steps, but had no influences on locomotor strategy per se. The bar graph reports the average (n = 5 rats) 3D distance from pre-lesion trials. **: significantly different at p < 0.01 from all the pre-lesion condition.

We next assessed the capacity of the robotic postural neuroprosthesis to enable motor control in rats with a lateral C7 hemisection (*n = 5*). Ten days post-lesion, the rats dragged the ipsilesional hindlimb during locomotion (**Supplementary Figure 4.8a**), especially during climbing on a staircase (**Figure 4.4b**). Without robotic support, they stumbled against, and rarely stepped onto the staircase (**Figure 4.4b,d**). The robotic postural neuroprosthesis instantly enabled coordinated plantar stepping, both during horizontal walking (32 ± 4 % of BWS; **Supplementary Figure 4.8a-b**) and climbing on a staircase (28 ± 3 % of BWS**; Figure 4.4b-c**). The robotic support restored trunk orientation and stability (*P < 0.001*, **Supplementary Figure 4.9b-c**), which correlated with near-normal hindlimb kinematics (**Supplementary Figures 4.8-9**) and accurate positioning of the ipsilesional paw onto the staircase (*P < 0.001,* **Figure 4.4d** and **Supplementary Video 6**).

We then investigated whether the robotic postural neuroprosthesis could enable motor control shortly after a more severe SCI consisting of two lateral hemisections placed on opposite sides and at different spinal levels (T7 and T10, **Figure 4.4e**). This SCI completely interrupted direct supraspinal input, thus leading to permanent hindlimb paralysis (Courtine *et al.*, 2008) (**Figure 4.4e**). To enable locomotion as early as 12 days post-SCI, we applied electrical and pharmacological stimulations. Without robotic support, the rats exhibited rhythmic hindlimb movements, but they failed to perform plantar steps (91 ± 7 % of dragging, **Supplementary Figure 4.8e**) and often fell laterally during walking (**Figure 4.4e**). With the robotic postural neuroprosthesis, all the tested rats (*n = 5*) displayed bilateral weight-bearing plantar steps (**Figure 4.4e** and **Supplementary Video 7**). Despite the interruption of direct supraspinal pathways, the rats immediately regained the ability to accurately position both hindpaws onto the staircase (*P < 0.001*, **Figure 4.4g**). The otherwise paralyzed rats demonstrated gait patterns that were nearly indistinguishable from those of healthy rats, both during horizontal locomotion (**Supplementary Figure 4.8e-h**) and stair climbing (**Figure 4.4e-g**). For both tasks, improvement of hindlimb locomotion correlated with robot-enabled recovery of trunk position and stability (**Supplementary Figures 4.10b-c**).

Together, these findings demonstrate that the *enabling mode* of the robotic interface instantly restored unexpected locomotor capacities across a wide range of natural walking behaviors after moderate to severe neuromotor disorders.

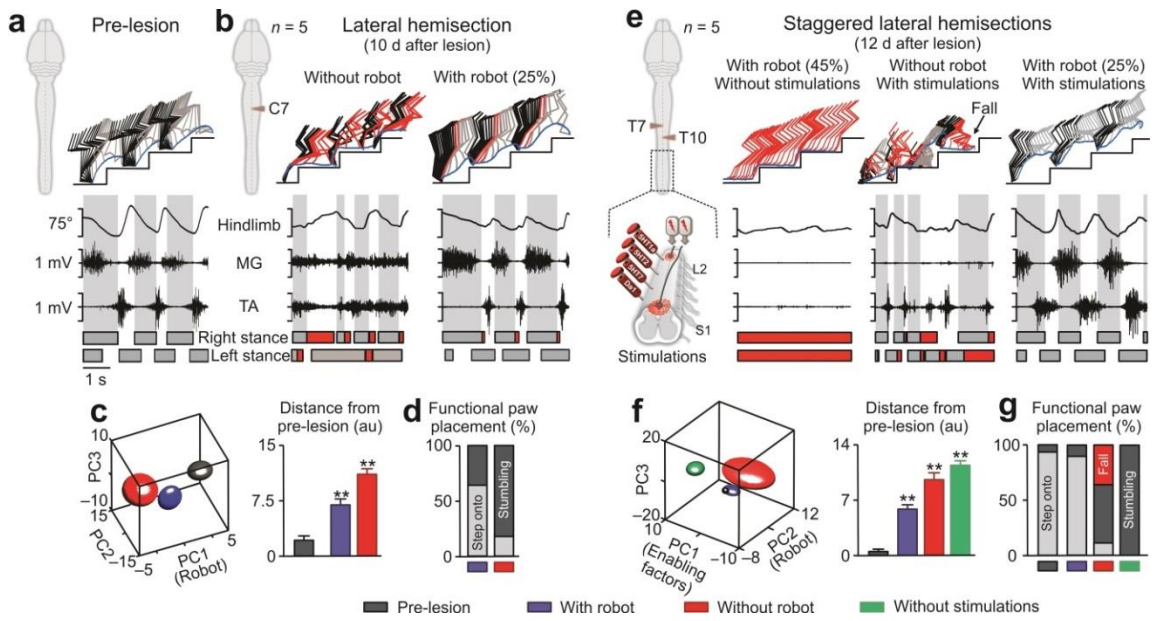

Figure 4.4 The robotic postural neuroprosthesis enables coordinated locomotion on a staircase after moderate and severe SCI

a. Representative stick diagram decomposition of hindlimb motion during climbing on a staircase pre-lesion. The plots show hindlimb oscillations and EMG activity of MG and TA muscles. **b.** Climbing on a staircase without and with constant-force robotic support 10d after a C7 lateral hemisection. **c.** PC analysis was applied on all gaits and rats. **d.** Percentage of steps accurately positioned onto the staircase. **e.** Locomotion on a staircase without and with constant-force robotic support 12d after staggered hemisections. Locomotion is shown without (spontaneous) with electrical and pharmacological stimulations. Data are shown with and without motor control enabling factors (stimulations). **f.** PC analysis. **g.** Percentage of steps accurately positioned onto the staircase. a.u. arbitrary unit. Error bars, S.E.M. **: significantly different at $p < 0.01$ from the pre-lesion condition. The bar links conditions that are statistically different at $p < 0.01$.

Robot-enabled training after a paralyzing SCI (training mode)

Finally, we exploited the *enabling mode* of the robotic interface to enhance functional capacities with repeated practice; a control scheme that we termed *training mode*. We subjected rats ($n = 5$) with staggered hemisection SCIs to 30-min locomotor training sessions every other day for 8 weeks (see Methods). The robotic postural neuroprosthesis provided support against gravity (z axis), but was set transparent in the other directions (x, y, and φ axes, **Supplementary Figure 4.2**). Locomotion was enabled by electrical and pharmacological stimulations. At 9 weeks post-lesion, non-trained rats displayed weight-bearing steps, but they failed to control body inertia and balance during robot-assisted locomotion along a curved runway ($P < 0.001$, **Figure 4.5c-e**). In contrast, trained rats were capable of steering curves (**Figure 4.5c-f**) while maintaining equilibrated trunk movements ($P < 0.001$, **Figure 4.5c,f** and **Supplementary Video 8**).

These results reveal that the *training mode* of the robotic interface significantly improved locomotor capacities in rats with paralyzing SCI.

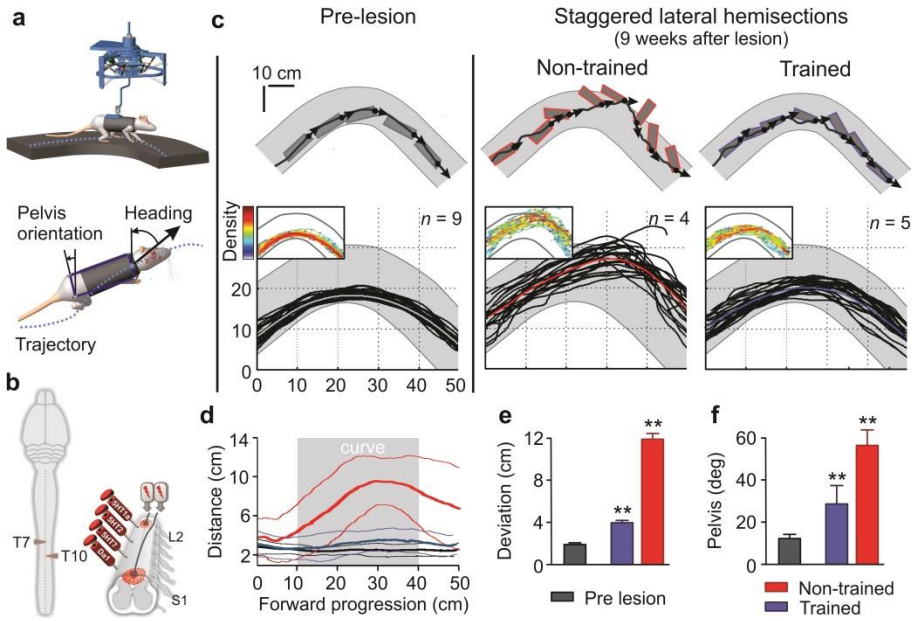

Figure 4.5 Training enabled by the robotic postural neuroprosthesis restores equilibrated steering in rats with a severe SCI.

a. Rats were positioned quadrupedally in the robotic interface, which provided constant force vertical support while behaving transparently in all the other directions. The rats walked along a 90deg-curved runway. Trunk orientation was measured as the angle between the pelvis and the orientation of the upper body velocity vector, termed heading, which also defined the locomotor trajectory. **b.** Locomotion was enabled by electrical and pharmacological stimulations. **c.** Successive positions of the trunk at swing onset, locomotor trajectory, and intensity (velocity) and direction of upper body motion (arrow) during a representative trial performed before the lesion, and at 60 days post-lesion for a non-trained and a trained rat. The lower plots show the superimposed locomotor trajectories extracted from all the trials of all the rats. The density distribution of locomotor trajectories (all trials and rats) is shown in the upper corner of each plot. **d.** Averaged (all rats, +/- S.D.) distance between locomotor trajectories and the optimal trajectory computed from all the pre-lesion trials (n = 9 rats). The shaded area indicates the progression along the curved section of the runway. **e.** The bar graph reports the averaged distance between each locomotor trajectory and the optimal trajectory. **f.** Maximal deviation of the pelvis segment with respect to the heading vector. Error bars, S.E.M. **: significantly different at $p < 0.01$ from all the other non-marked conditions.

4.4 Discussion

We have introduced an advanced robotic interface to evaluate; enable and train motor pattern generation and balance across a variety of natural walking behaviors in rats with neuromotor impairments. To hide the inertia of the massive robotic structure, we developed a multidirectional elastic decoupling system that rendered the robot transparent. This robotic interface effectively solves the main issues associated with existing rodent and human support systems, such as unidirectional trunk support, high inertia, and treadmill-restricted stepping. We validated our methods and concepts in rats with various SCIs and stroke. We expect that similar multidirectional trunk support systems will significantly improve gait rehabilitation in humans with neuromotor disorders.

Robot-assisted evaluation of gait, balance, and their interactions

Evaluation of locomotor function in animals often relies on visual scoring systems (Basso *et al.*, 1996) or single-variable analysis (Zorner *et al.*, 2010b) that not only lack objectivity but also fail to capture the multidimensional correlative structures of locomotor control strategies (Musienko *et al.*, 2011c). Here, we combined robotically assisted evaluation tools with sophisticated neurobiomechanical and statistical analyses. Together, these paradigms provide the means for assessing the control of, and interactions between, gait and balance with refinement and objectivity. Future animal and human studies can exploit these analytical tools to evaluate whether and, to a certain extent, how a given therapeutic intervention can enhance specific features of functional recovery following neuromotor disorders.

Robot-enabled motor control after CNS disorders

When acting as a postural or propulsive neuroprosthesis, the robotic interface instantly enabled unexpected locomotor capacities in rats with SCI or stroke. We systematically found correlations between robotically restored multidirectional trunk balance and improved hindlimb motor control. These immediate functional improvements emphasize the importance of expanding current trunk support systems, which are exclusively unidirectional, to multiple dimensions. Likewise, robotic exoskeletons that provide multidirectional support against gravity enable enhanced upper limb recovery in stroke survivors (Kwakkel *et al.*, 2008) and improved locomotion in humans with partial SCI (Duschau-Wicke *et al.*, 2010). These results demonstrate that the concept of robotically enabled motor control has broad implications to enhance functional recovery after CNS disorders.

Our robotic postural neuroprosthesis not only provided multidirectional trunk support but also restored limb and trunk orientation. In consequence, the flow of stretch- and load-related afferent input from hip and ankle joints, which plays an essential role to coordinate locomotion (Pearson, 2004), came closer to a normal range. We surmise that the recovery of crucial sensory feedback and its task-specific modulation significantly contributed to reestablishing gait control. For example, the robotic postural neuroprosthesis enabled enhanced hip extension during stair climbing compared to horizontal locomotion. This information appeared sufficient to mediate increased step height and accurate paw placement onto the staircase. Similarly, side-dependent modulation of load- and stretch-sensitive receptors from ankle and trunk muscles during curve-walking resulted in the production of asymmetric force patterns that maintained equilibrated steering. These sensorimotor processes were improved with training. Together, these findings confirm and expand current views on the ability of sensory information to act as a source of control for locomotion after the loss of supraspinal influences (Courtine *et al.*, 2009a; Harkema *et al.*, 2011). To this respect, our interface could be equipped with robotic legs attached to the hindlimbs (Nessler *et al.*, 2005) to ensure appropriate task-specific sensory feedback during rehabilitation (Edgerton & Roy, 2009).

Assessment and rehabilitation of humans with neuromotor disorders

There is a mosaic of evidence suggesting that gait rehabilitation should be conducted overground (Wessels *et al.*, 2010), across multiple walking paradigms (Musselman *et al.*, 2011b), with adequate support conditions (Reinkensmeyer *et al.*, 2006; Ada *et al.*, 2010; Wessels *et al.*, 2010), enabling systems (Reinkensmeyer *et al.*, 2006; Kwakkel *et al.*, 2008; Courtine *et al.*, 2009a; Edgerton & Roy, 2009; Harkema *et al.*, 2011), task-specific sensory cues (Courtine *et al.*, 2009a; Harkema *et al.*, 2011), and active patient cooperation (Edgerton & Roy, 2009; Duschau-Wicke *et al.*, 2010), but these concepts remain fragmented. Our versatile propulsive and postural neuroprosthetic interface crystallizes these views into a unified therapeutic tool to evaluate and restore locomotor function after CNS disorders, both in animals and in humans.

5 Restoring voluntary control of locomotion after paralyzing spinal cord injury

Original article:
"Restoring voluntary control of locomotion after paralyzing spinal cord injury"

Rubia van den Brand[1,2,*], Janine Heutschi[1,2,*] , Quentin Barraud[1,2], Jack DiGiovanna[3], Kay Bartholdi[1,2], Michèle Huerlimann[1], Lucia Friedli[1,2], Isabel Vollenweider[1,2], Eduardo Martin Moraud[3], Simone Duis[1,2], Nadia Dominici[1,2], Silvestro Micera[3], Pavel Musienko[1,2], and Grégoire Courtine[1,2]

Science 2012 Jun 1;336(6085):1182-5

1. Neurology Department, University of Zurich, Zurich, Switzerland
2. Center for Neuroprosthetics and Brain Mind Institute, School of Life Sciences, Swiss Federal Institute of Technology (EPFL), Lausanne, Switzerland
3. Center for Neuroprosthetics, School of Engineering, Swiss Federal Institute of Technology (EPFL), Lausanne, Switzerland

* These authors contributed equally to this work

The PhD candidate's contribution: Performance and analysis of behavioral experiments, conception and performance of surgical procedures, preparation of figures

5.1 Abstract

Half of human spinal cord injuries lead to chronic paralysis. Here, we introduce an electrochemical neuroprosthesis and a robotic postural interface designed to encourage supraspinally-mediated movements in rats with paralyzing lesions. Despite the interruption of direct supraspinal pathways, the cortex regained the capacity to transform contextual information into task-specific commands to execute refined locomotion. This recovery relied on the extensive remodeling of cortical projections, including the formation of brainstem and intraspinal relays that restored qualitative control over electrochemically enabled lumbosacral circuitries. Automated treadmill-restricted training, which did not engage cortical neurons, failed to promote translesional plasticity and recovery. By encouraging active participation under functional states, our training paradigm triggered a cortex-dependent recovery that may improve function after similar injuries in humans.

5.2 Introduction

Activity-based interventions exploiting proprioceptive information to enhance spinal motor output during training (Lovely *et al.*, 1986; Barbeau & Rossignol, 1987; Wernig & Muller, 1992) promote plastic changes capable of restoring locomotion after severe though incomplete spinal cord injury (SCI) (Wernig & Muller, 1992; Wernig *et al.*, 1995). A recent case study suggests that, in combination with epidural electrical stimulation of lumbosacral segments, activity-based rehabilitation may also restore supraspinally-mediated movements after motor complete paraplegia (Harkema *et al.*, 2011). We aimed to design a multi-system neuroprosthetic training program that took full advantage of this concept. We hypothesized that after the complete interruption of direct supraspinal input, a robotic postural interface encouraging the brain to actively use the paralyzed hindlimbs during electrochemically enabled motor states (Courtine *et al.*, 2009a) would reestablish supraspinal control of locomotion by promoting extensive and ubiquitous remodeling of spared neuronal circuitries.

5.3 Methods

Animals and behavioral training

Experiments were conducted on adult female Lewis rats (200-220 g body weight) housed individually on a 12-hour light/dark cycle with access to food and water *ad libitum*. All experimental procedures were approved by the Veterinary Office of the Canton of Zurich. Prior to surgery, all the rats (non-trained and trained) were first acclimatized to wearing the custom-made jacket for 1-2 weeks while navigating freely along the runway. The rats were then trained for an additional 1-2 weeks to walk bipedally. All the rats learned this task rapidly. Typically, they produced consistent stepping patterns within 1-2 sessions (**supplementary figure 5.5**). Positive reinforcement (food reward) was used to encourage the rats to perform the requested tasks.

Surgical procedures

All basic surgical procedures and post-operative care for SCI rats have been described in detail previously (Courtine *et al.*, 2008; Courtine *et al.*, 2009a; Musienko *et al.*, 2011c). Briefly, under general anesthesia and aseptic conditions, bipolar EMG electrodes were inserted into hindlimb muscles. Two stimulating electrodes were secured onto the dura at the midline of spinal levels L2 and S1. After pre-lesion recordings, rats received a left T7 lateral over-hemisection and a right lateral hemisection at T10 (Courtine *et al.*, 2008). For the T7 over-hemisection, we aimed at interrupting the dorsal column bilaterally while sparing ventral pathways on the contralateral side (**supplementary figure 5.1**). The completeness of the hemisections was assessed on 30-µm thick longitudinal sections incubated in serum containing anti-GFAP (1:1000, Dako, USA) antibodies. In addition, we confirmed the absence of BDA-labeled corticospinal axons in the dorsal column of the T8 spinal segment in transverse sections.

Multi-system neuroprosthetic training

Ten min prior to training, the rats received a systemic (I.P.) administration of quipazine (5-$HT_{2A/C}$, 0.2 - 0.3 mg/kg), SKF-82197 (D_1, 0.1 - 0.2 mg/kg) and 8-OH-DPAT (5-$HT_{1A/7}$, 0.05 - 0.2 mg/kg). During training, we delivered monopolar electrical stimulation (0.2ms, 100-300µA, 40Hz) through L2 and S1 electrodes. Locomotor training was conducted bipedally on a treadmill (9cm/s) with vertical robotic support, as well as overground with a robotic postural interface (**supplementary figure 5.3**). The content of each training session evolved with the actual capacities of the rats and training objectives, as detailed in **supplementary figure 5.3**. Positive reinforcement was used to

encourage the rats to perform the requested tasks. An additional group of rats was trained with the same frequency and duration, but rehabilitation was restricted to step training on a treadmill. These rats were trained to walk bipedally overground with the robotic postural interface for 2 weeks prior to the lesion. They were also tested in this paradigm at 1 and 9 weeks post-lesion. At the end of the training period, treadmill-trained rats practiced overground locomotion with the robotic postural interface for about 10 min per day during 4-8 sessions to ensure that the specificity of the task was not responsible for their incapacity to initiate and sustain locomotion.

Kinematic, kinetic and EMG recordings and analysis

Bipedal locomotion was recorded on a treadmill (9 cm/s) as well as overground. The different paradigms and their features can be found in **supplementary figure 5.2**. Kinematic (12 cameras, 200 Hz), kinetic (force plate, 2 kHz) and EMG (2 kHz, 10–1000 Hz bandpass) recordings were performed using an integrated motion capture system. Procedures for data collection, data analysis, and computation have been described in detail previously (Courtine *et al.*, 2009a; Musienko *et al.*, 2011c). The complete list of computed gait, kinematic, kinetic and EMG variables is reported in **supplementary table 5.1**. To quantify locomotor performance, we applied a principal component (PC) analysis on all the computed variables (Musienko *et al.*, 2011c). **Supplementary figure 5.5** provides a step-by-step explanation of the procedure and interpretation. We quantified recovery of locomotor function as the distance between gait cycles of intact and injured rats in the 3D space created by PC1-3 (Micera *et al.*, 1999).

Brain stimulation and recordings

A monopolar electrode was implanted epidurally over the left hindlimb motor cortex. A train of stimuli (0.2ms, 10ms pulse length, 300 Hz, 0.5 -1.5 mA) was delivered during bipedal standing in fully awake conditions. Testing was performed without and with electrochemical stimulations. Peak-to-peak amplitude and latency of evoked responses were computed from EMG recordings of the left TA muscle.

Neuronal modulations

At 60-70 days post-injury, a microwire array (16 or 32 channel) was implanted stereotaxically into layer V of the hindlimb area of the left motor cortex (**Figure 5.4**). Recordings were conducted 5-7 days post-surgery. Neural signals were acquired (24.4 kHz) with a neurophysiology workstation synchronized to kinematic recordings. All spike-sorting was performed offline via super-paramagnetic clustering (Quiroga *et al.*, 2004). Clusters were manually tuned based on established principles (Lewicki, 1998) to identify

single units. Modulations were analyzed in single experimental sessions to avoid potential instability confounds. Two recurring behaviors were used to evaluate the significance of neuronal modulations. (i) *Initiation* was defined as swing onset from rest. (ii) *Correction* was defined as beginning of swing phase after irregular gait (**supplementary figure 5.14**). A two-sample Kolmogorov-Smirnov test compared firing rates (estimated in 250ms windows) in successive, one-second periods encompassing initiation and correction to determine whether modulations were significant.

NMDA and Muscimol microinjections

To ablate T8-T9 neurons, we infused NMDA (1% in dH_2O) into 14 sites (depth 1 mm, total volume 3 µl) covering spinal levels T8-T9. Rats were tested 5 days post-lesion, and sacrificed on the following day. The ablation of neurons was verified *post mortem* on tissue sections stained with mouse anti-NeuN (1:500, Chemicon, USA) antibodies. To inactivate the motor cortex, we injected the GABA-agonist muscimol intra-cortically (800nl, 4.5 mg/Kg). Five days prior to experiments, we stereotaxically implanted a catheter (OD: 0.61 mm, ID: 0.28 mm) into the left motor cortex at a depth of 1.5 mm (**Figure 5.4D**). Proper catheter location was verified *post mortem* on tissue sections stained for fluorescent Nissl visualization (Invitrogen, USA).

Tracing and immunohistochemistry

We conducted retrograde tract tracing by infusing Fastblue (2% in 0.1M phosphate buffer and 2% dimethyl sulfoxide) bilaterally into L1-L2 spinal segments (Courtine *et al.*, 2008). A total of 1.2 µl was pressure-injected over 6 sites (depth 1.5 mm). To trace motor cortex axonal projections, we injected the anterograde tracer BDA 10,000 (10% in 0.01M PBS) into the left motor cortex over 6 sites covering the hindlimb area (coordinates centered -1 mm rostrocaudal and -1.75 mm mediolateral to Bregma, depth 1.5 mm). The rats were perfused 18 days later with Ringer's solution containing 100 000 IU/L heparin and 0.25% $NaNO_2$ followed by 4% phosphate buffered paraformaldehyde, pH 7.4 containing 5% sucrose. For cfos experiments, rats were perfused 60 min after cessation of a 45 min bout of continuous locomotion (Courtine *et al.*, 2009a). Locomotion was performed overground for intact and overground-trained rats, and during overground guided locomotion for treadmill-trained and non-trained rats in order to ensure the presence of stepping in all the animals. The brain, brainstem, and spinal cords were dissected, post-fixed overnight, and transferred to 30% phosphate buffered sucrose for cryoprotection. After 4 days, the tissue was embedded and sectioned on a cryostat at a 40-µm thickness.

For immunohistochemistry experiments, sections were incubated in serum containing rabbit anti-cfos (1:2000, Santa Cruz Biotechnologies, USA), anti-GFAP (1:1000, Dako, USA), or anti-5HT (1:5000, Sigma Aldrich, Germany), or mouse anti-synaptophysin (1:1000, Millipore, USA) antibodies. Immunoreactions were visualized with secondary antibodies labeled with Alexa fluor® 488 or 555. BDA-labeled fibers were detected using streptavidin-horseradish peroxidase (1:200) in 0.1M PBS-Triton (1%). Tyramide signal amplification Cyanine 3 was used at a dilution of 1:100 for 1 min.

Neuromorphological evaluations

Fastblue- and cfos-positive neurons were counted using image analysis software on 5 evenly spaced slices separated by 1.2 mm and centered on the T8-T9 junction. Fiber density was measured using 5 confocal image stacks per region per rat acquired with standard imaging settings and analyzed using custom-written scripts according to previously described methods (Carmel *et al.*, 2010). Confocal output images were divided into square regions of interest (ROI), and densities computed within each ROI as the ratio of traced fibers (amount of pixels) per ROI area. Files were color-filtered and binarized by means of an intensity threshold. Threshold values were set empirically and maintained across sections, animals and groups. Comparisons of computerized and manual counting of CST labeling in T8-T9 showed no differences between both methods. Manual fiber counts were conducted on spinal cord sections overlaid with 5 vertical lines. Fibers crossing these lines within the grey matter were marked, and all intersecting fibers on 3 sections per rat were summed to obtain a cumulative count. Both manual and computerized counts were performed blindly. Image acquisition was performed using a laser confocal scanning microscope and the LAS AF interface and stacks were processed offline.

Statistics

All data are reported as mean values ± s.e.m. Statistical evaluations were performed using one- or two-way ANOVA, repeated-measures ANOVA, or non-parametric Wilcoxon tests. The *post hoc* Kruskall-Wallis test was applied when appropriate.

5.4 Results

Adult rats received a left lateral over-hemisection at T7 and a right lateral hemisection at T10. This SCI interrupts all direct supraspinal pathways (**supplementary figure 5.1A-C**), but leaves an intervening gap of intact tissue. The lesion, however, led to a complete loss of hindlimb function, with no sign of recovery over 2 months post-injury (**supplementary figure 5.1D**). Likewise, humans with clinically complete SCI frequently show maintenance of connections through the lesion (Kakulas, 1999). Thus, this experimental lesion reproduces key anatomical and functional features of human SCIs, while providing well-controlled conditions to investigate the mechanisms underlying recovery (Courtine *et al.*, 2008).

To transform lumbosacral circuits from dormant to highly functional states (Musienko *et al.*, 2011a), we applied tonic (40 Hz) epidural electrical stimulation over L2 and S1 spinal segments (Courtine *et al.*, 2009a), and systemically administered a tailored cocktail of $5HT_{1A/7}$, $5HT_{2A/C}$, and D_1 receptor agonists (Musienko *et al.*, 2011c). By increasing the general level of spinal excitability, this electrochemical spinal neuroprosthesis enables sensory information to become a source of control for stepping (Courtine *et al.*, 2009a; Musienko *et al.*, 2011a). This intervention promoted coordinated, although involuntary, bipedal stepping on a treadmill as early as 7 days post-injury (**Figure 5.1C**).

These stepping movements are elicited by the moving treadmill belt (Courtine *et al.*, 2009a), suggesting that the rats would not be capable of voluntarily initiating hindlimb locomotion overground. To verify the absence of supraspinal control, we applied the electrochemical neuroprosthesis, and positioned the same rats bipedally in a robotic postural interface that provided adjustable vertical and lateral trunk support, but did not facilitate locomotion in any direction (**Figure 5.1B** and **supplementary figure 5.2**). All the rats ($n = 27$) failed to initiate hindlimb locomotion overground at 7 days post-injury ($p < 0.001$; **Figure 5.1C**).

We then designed a multi-system neuroprosthetic training program that encompassed two objectives. First, we aimed to improve the functionality of lumbosacral circuits through treadmill-based training enabled by the electrochemical neuroprosthesis (Courtine *et al.*, 2009a). Second, we sought to promote the recovery of supraspinally-mediated movements; we exploited the robotic postural interface not only to enable, but also to force the rats to actively use their paralyzed hindlimbs in order to locomote bipedally towards a target.

Rats (n = 10) were trained daily for 30 min with a combination of both paradigms, starting 7-8 days post-injury (**Supplementary figure 5.3**). The first, effortful voluntary steps emerged after 2-3 weeks of training ($p < 0.01$; **Figure 5.1D**). As voluntary movements recovered, we gradually increased the relative duration of overground training (**Supplementary figure 5.3B**). 5-6 weeks post-injury, all the rats (**Supplementary figure 5.4**) were capable of initiating and sustaining full weight-bearing bipedal locomotion for extended periods of time, but only during electrochemically enabled motor states (**Figure 5.1C-D, Supplementary figure 5.1D** and **Movie S1**). Kinematic analyses (**Supplementary figure 5.5**) revealed that overground-trained rats deployed a similar control strategy as intact animals to produce locomotion (**Figure 5.1A,C** and **Supplementary figure 5.5**). To measure recovery, we adapted the clinically standardized 6-minute walk test (Guyatt *et al.*, 1985) to bipedally stepping rats. Overground-trained animals with a paralyzing SCI covered distances as long as 21 m in 3 min (**Figure 5.1D**).

We next tested whether treadmill-restricted step training under electrochemically-enabled states would also promote the recovery of voluntary locomotion (n = 7 rats). This automated step training failed to reestablish overground locomotion despite repeated testing during 4-8 sessions at 9 weeks post-injury ($p < 0.001$; **Figure 5.1C-D** and **Movie S1**). Moreover, treadmill-trained rats were not capable of sustaining robotically initiated locomotion overground (**Supplementary figure 5.6**).

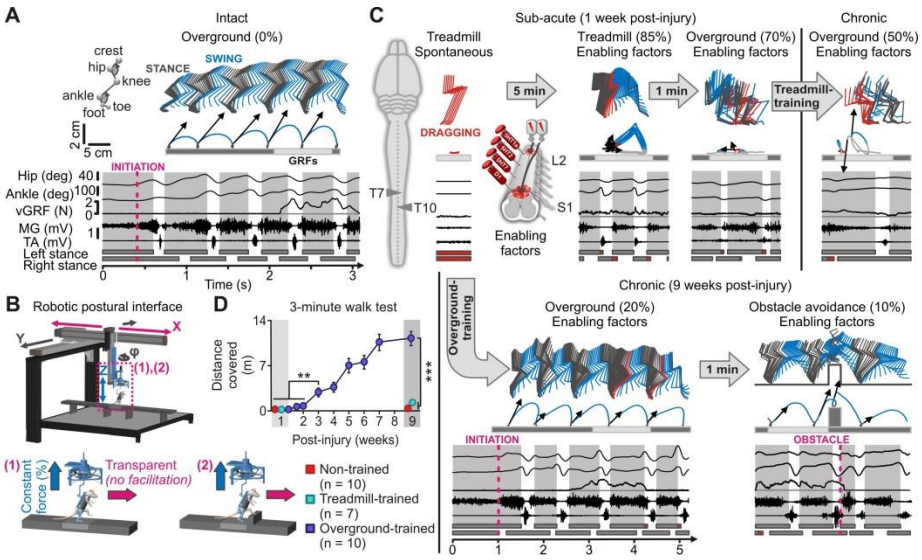

Figure 5.1 Multi-system neuroprosthetic training restores voluntary locomotion after paralyzing SCI.

(A) Left hindlimb kinematics, hindlimb endpoint trajectory and velocity vector, vertical ground reaction forces (vGRF) as well as EMG activity of medial gastrocnemius (MG) and tibialis anterior (TA) muscles during bipedal locomotion in an intact rat. **(B)** Robotic postural interface providing vertical and lateral support, but no facilitation in the forward direction. **(C)** Representative left hindlimb stepping patterns recorded under the various experimental conditions at 1 and 9 weeks post SCI. **(D)** Distance covered in 3 minutes during bipedal locomotion. %, Body weight support. **, P < 0.01. ***, P < 0.001. Error bars, s.e.m.

To further enhance supraspinal contribution, we introduced stairs and obstacles; two conditions requiring voluntarily mediated gait tuning (Drew *et al.*, 2008). After 2-3 additional weeks, overground-trained rats were capable of bipedally sprinting up stairs and avoiding obstacles (**Figure 5.1C, Supplementary figure 5.7** and **Movie S1**). To accomplish these paradigms, the animals displayed a range of task-specific adjustments of hindlimb movements (**Supplementary figure 5.7**).

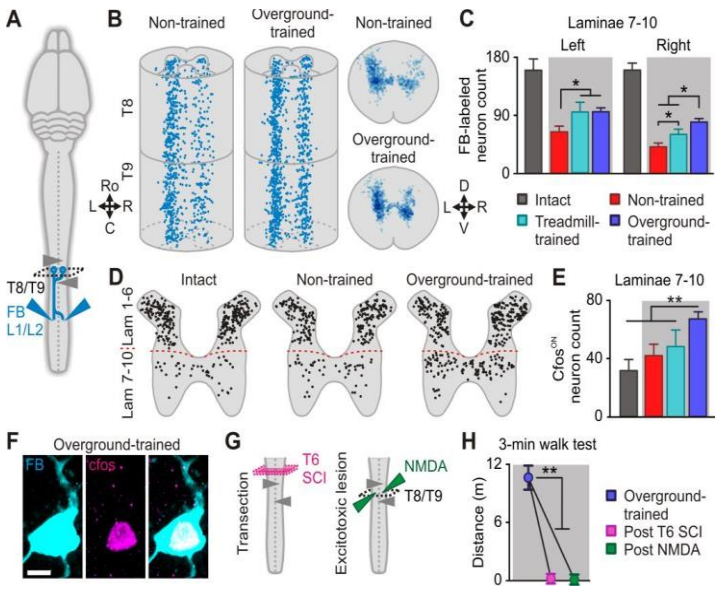

Figure 5.2 Multi-system neuroprosthetic training promotes the formation of intraspinal detours that relay supraspinal information.
(A) Diagram illustrating anatomical experiments. **(B)** Longitudinal and transverse views of 3D reconstructions of Fastblue-labeled (FB) neurons between the lesions. L, left; R, right; Ro, rostral; C, caudal. D, dorsal; V, ventral. **(C)** Counts (n = 6-9 rats per group) of FB-labeled neurons in laminae 7-10 of T8-T9 segments after 45min of continuous locomotion. **(D)** Cfos expression patterns in T8-T9 segments. **(E)** Counts (n = 5-7 rats per group) of $cfos^{ON}$ neurons in laminae 7-10 after continuous locomotion. **(F)** Co-localization of FB and cfos. Scale bar, 10 µm. **(G)** Overground-trained rats received a complete T6 SCI (n = 2) or T8-T9 NMDA microinjections (n = 3). **(H)** Distance covered in 3 minutes before and after the lesions. **, P < 0.01. Error bars, s.e.m.

Anatomical examinations highlighted an extensive remodeling of supraspinal and intraspinal projections in rats that regained voluntary locomotion. We first conducted retrograde tract tracing from L1-L2 locomotor centers (**Figure 5.2A**). We found a significant increase ($p < 0.01$; **Figure 5.2B-C**) in the number of labeled neurons in intermediate and ventral laminae of T8-T9 segments in both overground-trained and treadmill-trained rats compared to non-trained animals. Analysis of the activity-dependent marker cfos after continuous overground locomotion confirmed that the labeled neurons were active during walking (**Figure 5.2F**). The number of $cfos^{on}$ nuclei in the regions rich in neurons retrogradely labeled from L1-L2 locomotor centers was larger in overground-trained rats compared to all the other groups ($p < 0.05$; **Figure 5.2D-E**). Thoracic neurons may thus play a pivotal role in restoring voluntary locomotion (Bareyre *et al.*, 2004; Courtine *et al.*, 2008; Cowley *et al.*, 2008). To address this hypothesis, we ablated T8-T9 neurons by infusing the axon-sparing excitotoxin N-methyl-D-aspartic acid (NMDA) (Courtine *et al.*, 2008) (**Figure 5.2G** and **Supplementary figure 5.8**). Infusion of NMDA

abolished the regained voluntary locomotion ($p < 0.01$; **Figure 5.2H** and **Movie S2**), despite uncompromised functionality of lumbosacral circuits (**Supplementary figure 5.8**). Likewise, overground-trained rats lost voluntary control of locomotion after the complete interruption of supraspinal input to T8-T9 neurons ($p < 0.01$; **Figure 5.2G-H**).

We labeled projections from the left hindlimb motor cortex with injections of biotinylated dextran amine (BDA) (**Figure 5.3A**). The bilateral interruption of the dorsal column at the T7 over-hemisection only spared a few (1-2%) (Brosamle & Schwab, 1997) corticospinal tract (CST) axons in the right dorsolateral funiculus (**Supplementary figure 5.9E**). Consequently, non-trained rats showed scarce CST labeling in T8-T9 segments (**Figure 5.3B-C** and fig. **Supplementary figure 5.9E**). Treadmill-restricted training did not promote significant changes in the density of thoracic CST projections (**Figure 5.3B-C** and **Supplementary figure 5.9E**). In contrast, we found a reconstitution of 45 ± 7% of pre-lesion bilateral fiber density in overground-trained rats (**Figure 5.3B-D**). These CST axons exclusively branched from the right dorsolateral funiculus (**Figure 5.3D**), and profusely innervated the right, and more unexpectedly, the left gray matter of T8-T9 segments (**Supplementary figure 5.9F**) (Rosenzweig *et al.*, 2010). We detected multiple CST fibers extending from the gray matter at the T7 lesion site into the right dorsolateral funiculus (**Figure 5.3E-F**). These ectopic fibers, suggestive of regenerative sprouting (Steward *et al.*, 2003), led to a near two-fold increase in the CST axon density of the T8-T9 dorsolateral funiculus ($p < 0.001$, **Supplementary figure 5.9G**). Thoracic CST fibers bypassed the T7 over-hemisection through the right dorsolateral funiculus, branched into the gray matter, and re-crossed the midline (**Figure 5.3E**). These fibers developed large axonal structures with bouton-like swellings suggestive of sprouting in terminal arbors (**Supplementary figure 5.9F**). Confocal microscopy confirmed that thoracic CST fibers bore synaptic elements because they colocalized with synaptophysin (**Figure 5.3G**). These fibers established contacts with relay neurons retrogradely labeled from L1-L2 locomotor centers (**Figure 5.3G**).

Remodeling of motor cortex axonal projections was not restricted to the spared tissue bridge. Quantification of CST fibers at T4-T5, above the injury, revealed a significant bilateral increase of axon density in overground-trained compared to non-trained, treadmill-trained, and intact rats ($p < 0.01$; **Supplementary figure 5.9A-D**). We found a near fourfold increase in the density of cortical projections in various brainstem motor areas (**Figure 5.3H** and **Supplementary figure 5.10**) including the left and right vestibular nuclei ($p < 0.01$), the entire reticular formation ($p < 0.001$), and parapyramidal regions ($p < 0.01$). These areas contain reticulospinal neurons and spinally projecting serotonergic (5HT) neurons (**Supplementary figure 5.11C**) that both contribute to

initiating and sustaining locomotion (Liu & Jordan, 2005; Hagglund *et al.*, 2010). Descending 5HT fibers might thus reorganize with training. We found a nearly complete, lamina-specific restoration of T8-T9 serotonergic innervation in overground-trained rats, which contrasted with the depletion of 5HT fibers in non-trained and treadmill-trained animals ($p < 0.05$, **Supplementary figure 5.11**).

Collectively, these analyses demonstrate that automated treadmill-restricted training failed to mediate anatomical changes in descending pathways, whereas active training under highly functional states promoted multi-level plasticity in cortex- and brainstem-derived axonal systems.

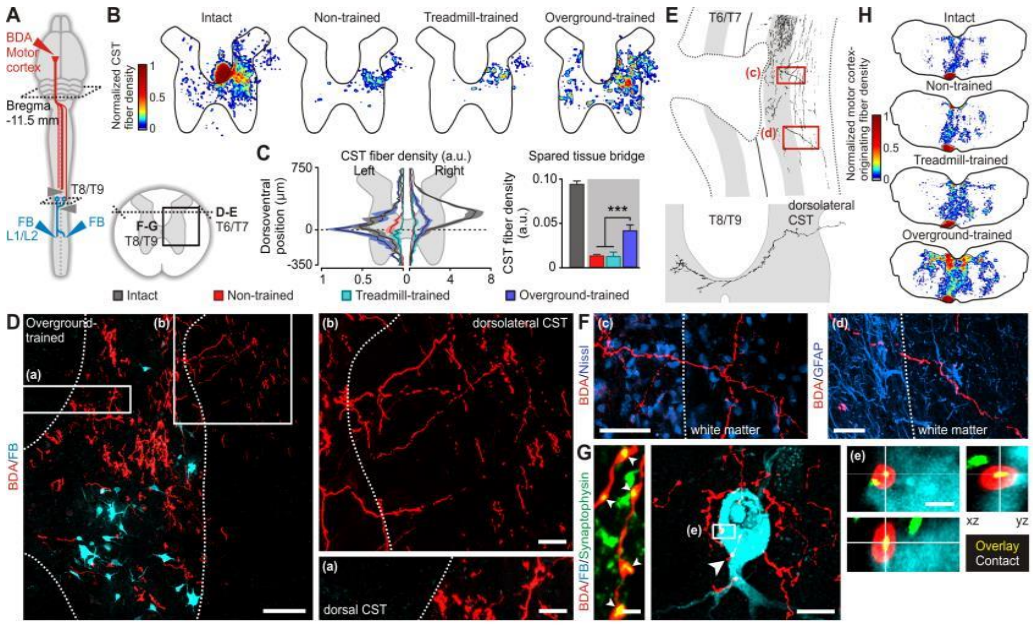

Figure 5.3 Multi-system neuroprosthetic training promotes extensive remodeling of motor cortex projections.
(A) Diagram illustrating anatomical experiments and analyzed regions. **(B)** Heat maps and **(C)** graphs (n = 5 rats per group) showing bilateral CST axon density in T8-T9 segments. **(D)** Confocal overview of the right T8-T9 hemicord of an overground-trained rat. Scale bar, 100 µm; inset (a, b), 30 µm. **(E)** 3D CST fiber reconstruction along the longitudinal (top) and transverse (bottom) plane. **(F)** Confocal images of insets shown in **(E)**. Scale bar, 50 µm. **(G)** Co-localization of CST fibers with synaptophysin (arrows), and close appositions (inset and arrow) with a FB-labeled neuron. Scale bar, 2 µm; overview neuron, 10 µm. **(H)** Heat maps showing density of cortical projections in the brainstem (bregma -11.5mm). ***, $P < 0.001$. Error bars, s.e.m.

Contrary to primates, the rodent motor cortex is not essential to produce locomotion (Courtine *et al.*, 2007a). Consequently, we sought to demonstrate that training-induced remodeling of motor cortex projections did contribute to controlling voluntary locomotion. First, we implanted stimulating epidural electrodes over the left motor cortex to verify that

the reorganization of neuronal pathways reestablished connectivity across the lesion. Before the SCI, applying a train of low intensity (0.7-1.5 mA) electrical stimuli evoked large responses in the left tibialis anterior muscle (**Figure 5.4A**). The SCI permanently abolished these responses in non-trained rats ($p < 0.001$; **Figure 5.4A**). In contrast, overground-trained rats regained responses below the lesion, averaging about 10% of their pre-lesion amplitude ($p < 0.001$; **Figure 5.4B**).

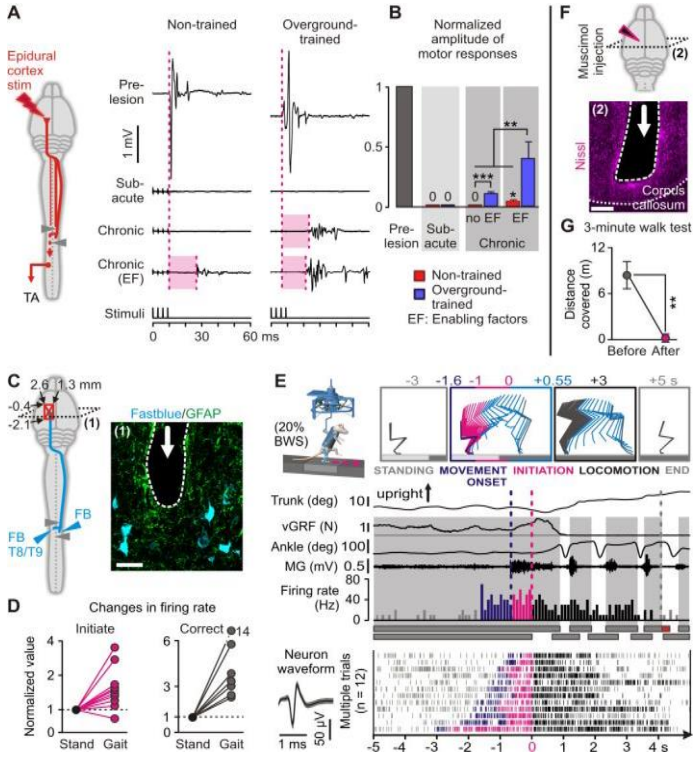

Figure 5.4 Overground-trained rats regained cortical control of hindlimb locomotion.
(A) Responses evoked by a train of epidural motor cortex stimulations in the left TA muscle in a non-trained and overground-trained rat. **(B)** Mean (n = 5 rats per group) amplitude of responses. **(C)** Diagram and GFAP staining (1) illustrating microwire array localization. Scale bar, 50 µm. **(D)** Change in firing rate for significantly modulated neurons during initiation and correction compared to standing. **(E)** Trunk vertical position, left ankle joint angle, EMG activity of left MG muscle, vGRFs, and modulation of a motor cortex neuron during one trial. Raster of the same neuron for multiple trials. Movement onset and initiation are defined as hip extension and foot clearance, respectively. The color-coding indicates the period during which firing rate significantly increased before these events. **(F)** Diagram and Nissl staining (2) showing catheter location for muscimol microinjection. Scale bar, 300 µm. **(G)** Distance covered in 3 minutes before and after muscimol injection. **, $P < 0.01$. ***, $P < 0.001$. Error bars, s.e.m

These responses were delayed by 12 ± 3 ms ($p < 0.01$; **Figure 5.4A**), suggesting that a larger number of synaptic relays was necessary to convey the supraspinal volley to hindlimb motor pools. The amplitude of responses substantially increased during

electrochemically enabled motor states ($p < 0.01$; **Figure 5.4A-B**), indicating enhanced transmission of the supraspinal command (Cowley *et al.*, 2008). Second, we implanted a microwire array in the vicinity of CST neurons projecting to T8-T9 segments (**Figure 5.4C**), and recorded neuronal modulations during voluntary locomotion in overground-trained rats ($n = 3$). We found a variety of neurons ($n = 17/24$ neurons) whose modulation patterns significantly ($p < 0.05$; **Figure 5.4D**) correlated with gait initiation, sustained locomotion, and corrective movements (**Supplementary figure 5.12** and **Movie S3**). A substantial number of motor cortex neurons (36%) exhibited a sharp increase in firing rate before any overt movement or locomotor-related muscle activity had occurred (**Figure 5.4E**). Instead, the firing rate of motor cortex neurons significantly decreased during involuntary locomotion compared to quiet standing ($p < 0.05$, **Supplementary figure 5.13A-C**). Third, we inactivated the left motor cortex with a microinjection of the GABA agonist Muscimol (**Figure 5.4F**). Muscimol immediately suppressed voluntary hindlimb locomotion ($p < 0.01$; **Figure 5.4G** and **Movie S3**), despite uncompromised functionality of lumbosacral circuits (**Supplementary figure 5.14**).

5.5 Discussion

Thus far, functional restoration after SCI has been interpreted as the need to promote long-distance regeneration of severed fibers to their original targets (Alto *et al.*, 2009; Sun *et al.*, 2011). Undoubtedly, neuroregeneration will be essential following near-complete SCI. However, a more immediate approach might capitalize on the remarkable capacity of spared neuronal systems to reorganize through use-dependent mechanisms (Wernig & Muller, 1992; Edgerton *et al.*, 2008; Harkema *et al.*, 2011). Here, we established training conditions that not only enabled but also forced the brain to construct a multiplicity of *de novo* brainstem and intraspinal relays to regain quantitative and qualitative access to electrochemically enabled lumbosacral circuitries. There is growing evidence that active training with appropriate sensory cues is markedly superior to passive, robot-guided rehabilitation to improve stepping capacities in humans (Wernig & Muller, 1992; Wernig, 2005; Wirz *et al.*, 2005; Cai *et al.*, 2006b; Edgerton *et al.*, 2008; Harkema *et al.*, 2011). Likewise, automated treadmill-restricted training, which did not engage cortical neurons, promoted sub-lesional plasticity, but failed to promote remodeling of descending pathways. Treadmill-trained rats did not regain supraspinally-mediated locomotion. Instead, our new training paradigm encouraged active rat participation, and triggered a cortex-dependent, activity-based process that restored voluntary control over sophisticated locomotor movements after a SCI leading to chronic paralysis. These results confirm the capacity of intraspinal circuits to bypass lesions (Bareyre *et al.*, 2004; Courtine *et al.*, 2008), and expand their therapeutic potential to the restoration of function after paralyzing SCI. The ability of training under highly functional states to promote this extensive plasticity and recovery may lead to novel interventions capable of improving function in humans with a range of neuromotor disorders (Fuentes *et al.*, 2009; Musienko *et al.*, 2009; Harkema *et al.*, 2011).

6 Reticular formation mediates motor function recovery after severe spinal cord contusion

Lucia Friedli[1] *, Janine Beauparlant[1] *, Cristina Martinez Gonzalez[1], Jean Laurens[1] & Grégoire Courtine[1]

Manuscript in preparation.

1. Center for Neuroprosthetics and Brain Mind Institute, School of Life Science, Swiss Federal Institute of Technology Lausanne (EPFL), Lausanne, Switzerland

* These authors contributed equally to this work.

6.1 Abstract

Neuroprosthetic rehabilitation combining electrochemical neuromodulation of spinal circuits and robot-assisted training re-establishes supraspinal control of locomotion after staggered spinal cord hemisections. Here, we evaluated the capacity of neuroprosthetic rehabilitation to restore motor function after a more clinically relevant spinal cord injury (SCI). Adult rats received a severe mid-thoracic contusion that spared less than 10% of descending fibers. After two months of training, all rats were able to walk overground while supporting their entire body weight under electrochemical stimulations. Approximately half of the trained animals displayed weight-bearing leg movements, and were capable of swimming continuously in the complete absence of any stimulation. In contrast, non-trained rats failed to recover spontaneous hindlimb motions during swimming and stepping tasks. Recovery of supraspinally driven locomotion was associated with reorganization in cortical and medullary descending with a special emphasis on the reticulospinal tract. We used deep brain stimulation in the mesencephalic locomotor region to indirectly activate and virus-induced specific suppression to inactivate the spared reticulospinal tract thus demonstrating its crucial role in mediating locomotor recovery after severe contusion SCI. Further, we exploited the potential and limitations of neuroprosthetic rehabilitation by applying the training paradigm in the chronic state of SCI. Delayed training induced diminished but highly significant recovery of locomotor functions. Our results confirm the ability of neuroprosthetic rehabilitation to re-establish supraspinal control of leg movement after a severe SCI, and expand its therapeutic potential to more clinically relevant lesions, settings, and outcomes. We further provide insights into the mechanisms of recovery after severe, clinically relevant contusion SCI. Our findings also illustrate the potential limitation of neuroprosthetic rehabilitation, thus providing a useful framework to translate this intervention into medical practices to improve motor recovery after spinal cord injury.

6.2 Introduction

Spinal cord injury (SCI) leads to a range of disabilities, including locomotor impairments that seriously diminish the patients' quality of life (Anderson, 2004). In the majority of cases, the neuronal networks that coordinate leg movements are located below the injury. Due to the interruption of supraspinal signals, these networks are in a non-functional state. Over the past decade, spinal neuromodulation therapies including electrochemical stimulation of the spinal cord have been shown to restore stepping functions after complete SCI (Fong *et al.*, 2005; Courtine *et al.*, 2009a; Musienko *et al.*, 2009; Musienko *et al.*, 2011c). These paradigms are using the intact yet dormant neuronal machinery below the SCI to enable coordinated yet automated motor control after SCI. In order to restore supraspinal control of movement intact tissue bridging the SCI is needed. Van den Brand et al. showed that robot-assisted rehabilitation, enabled by spinal neuromodulation, restored supraspinal control of locomotion in paralyzed rats (van den Brand *et al.*, 2012). However, the advanced motor control capacities only occurred in the presence of robot assistance and electrochemical neuromodulation, which limits the clinical relevance of neuroprosthetic rehabilitation. Furthermore, the model of staggered lateral hemisection SCI enables a mechanistic understanding of use-dependent plasticity under well-controlled and reproducible experimental conditions, yet human SCIs are poorly modeled with cut injuries (Courtine *et al.*, 2007a). The majority of human traumas are associated with lasting spinal cord compression, which induces secondary damage including the formation of cavities, demyelination of surrounding fibers, and inflammatory responses that alter the conductive properties of spared fibers (Schwab *et al.*, 2006; James *et al.*, 2011). However, even in individuals with motor complete paralysis a substantial number of residual fibers are spared, and still connect supraspinal centers with spinal locomotor networks located below the injury site (Kakulas, 1999; Norenberg *et al.*, 2004). Force-controlled contusion SCIs provide a more accurate model of this type of functional and anatomical outcome in experimental animals (Metz *et al.*, 2000; Scheff *et al.*, 2003). Experimental contusion SCIs typically spare ventral and ventrolateral white matter tracts as the impact is applied dorsally to the spinal cord. In consequence, the reticulospinal tract that runs in the dorsolateral and the ventrolateral funiculus (Zemlan *et al.*, 1984; Martin *et al.*, 1985) is partially spared. Reticular neurons receive among other cortical, mesencephalic (Steeves & Jordan, 1980) and cerebellar (Mori *et al.*, 1996) input and play an important role in the control of posture and locomotion (Mori *et al.*, 1996; Brustein & Rossignol, 1998; Jordan, 1998). After partial SCI, anatomical studies demonstrated that reticulospinal projections sprout and rewire

spontaneously (Ballermann & Fouad, 2006; Weishaupt *et al.*, 2013) and thereby account for functional recovery. Furthermore, Schucht et al. showed that only a small unilateral portion of ventrolateral tract is sufficient for spontaneous locomotor recovery after partial SCI whereas similar sparing of the dorsal spinal cord resulted in complete paraplegia (Brustein & Rossignol, 1998; Schucht *et al.*, 2002).

Here, we aimed to evaluate the impact of neuroprosthetic training on stepping and general leg functions in the presence and absence of electrochemical neuromodulation and robotic support in rats with acute and chronic severe spinal cord contusion. We hypothesize that neuroprosthetic rehabilitation restores voluntary control over the hindlimbs after severe contusion SCI and that this recovery is sustained in the absence of electrochemical neuromodulation only in acute trained rats. Lastly, we hypothesized that the mechanisms underlying recovery of voluntary hindlimb stepping are mediated primarily through spared bulbospinal projections.

The results of this study further characterize neuroprosthetic rehabilitation and stress the importance of spared brainstem projections as a substrate for recovery and hence as a target for therapeutic interventions after contusion SCI. Together these findings raise awareness towards key issues concerning clinical translation of neuroprosthetic training for human SCI, and other motor deficit causing conditions.

6.3 Methods

Experimental setup

Experiments were conducted on adult female Lewis rats (~220 g body weight). Animals were housed individually on a 12 h light/dark cycle, with access to food and water ad libitum. All animals were handled daily for at least two weeks prior to the first surgeries. Animal care, including manual bladder voiding, was performed twice daily for 3 weeks and once daily for the remaining post-injury period. All procedures and surgeries were approved by the Veterinary Office of the canton of Vaud in Switzerland.

Surgical procedures and post-surgical care

All surgical procedures used have been described previously (Courtine *et al.*, 2009a; Musienko *et al.*, 2011c). Under aseptic conditions and general anesthesia, a partial laminectomy was made at the mid-thoracic level (T9 vertebra) and a 250 kdyn (1 dyn = 10 µN) contusion injury was applied using a force-controlled spinal impactor (IH-0400 Impactor, Precision Systems and Instrumentation LLC, USA). For the acute trained and non-trained groups, a partial laminectomy was simultaneously performed over spinal segments L2 and S1. Stimulating electrodes were created by removing a small part (~400 µm notch) of insulation from Teflon-coated stainless steel wires (AS632, Cooner Wire, USA), which were subsequently secured at the midline overlying spinal level L2 and S1 by suturing the wires to the dura. A common ground wire (~1 cm of teflon removed at the distal end) was inserted subcutaneously over the right shoulder. Bipolar intramuscular EMG electrodes, using the same wire type, were inserted bilaterally in the medial gastrocnemius (MG) and tibialis anterior (TA) muscles (**Supplementary figure 6.2c**). All electrode wires were connected to a percutaneous amphenol connector (Omnetics Connector Corporation, USA) fixed to the skull of the rat. While the acute trained and non-trained groups were lesioned and implanted with electrodes in the same surgery, chronic trained and non-trained groups underwent two individual surgeries separated by 2 months. Analgesia (buprenorphine Temgesic®, ESSEX Chemie AG, Switzerland, 0.01-0.05 mg per kg, s.c.) and antibiotics (Baytril® 2,5%, Bayer Health Care AG, Germany, 5-10 mg per kg, s.c.) were provided for 3 and 5 days post-surgery, respectively. Lesion severity was verified post mortem by three-dimensional reconstruction of each individual injury (Neurolucida, MBF Bioscience, USA).

Neuroprosthetic rehabilitation procedures

Rats were randomly divided into 4 groups; two non-trained groups (9 weeks survival and 17 weeks survival each n = 8), an acute training group that was trained using

electrochemical neuromodulation (trained; n = 8) and a delayed training group (trained delayed; n = 8). Both trained groups underwent multi-system neurorehabilitation over 2 months on 6 days per week and for 25 minutes per day (**Supplementary figure 6.2d**). Five minutes prior to training, the rats received a systemic (i.p.) administration of quipazine (5-HT2A/C, 0.2 - 0.3 mg/kg) and 8-OH-DPAT (5-HT1A/7, 0.05 - 0.2 mg/kg). During training, we delivered monopolar electrical stimulation (0.2ms, 100-300μA, 40Hz) through L2 and S1 electrodes. Locomotor training was conducted bipedally on a treadmill (11 cm/s; Robomedica, USA) with vertical robotic support, as well as overground with a robotic postural interface (Dominici *et al.*, 2012a). The content of each training session evolved with the actual capacities of the rats and training objectives (van den Brand *et al.*, 2012). Positive reinforcement was used to encourage the rats to perform the requested tasks (**Supplementary figure 6.1**).

Kinematic, kinetic and EMG recordings

Bipedal locomotion was recorded on a treadmill (11 cm/s) as well as overground in the robotic interface. Swimming was recorded in a custom-made swimming pool (dimensions; length 150 cm, width 13 cm, height 40 cm, water depth 24 cm). Rats of acute groups participated in two sets of behavioral evaluations 1 week and 9 weeks post-injury. The two chronic groups (delayed trained and non-trained) were recorded 9 weeks and 17 weeks after SCI (**Supplementary figure 6.2a,d**). For both locomotion and swimming, all the rats were evaluated in three experimental conditions independent of their training paradigm: with the full electrochemical neuroprosthesis, with only electrical stimulations, and without electrical or pharmacological stimulations. To ensure that the specificity of the task was not responsible for their incapacity to initiate and sustain locomotion, non-trained rats practiced overground locomotion with the robotic postural interface for about 10 min per day during 8-10 sessions before behavioral recordings. All the trained and non-trained rats equally practiced the swimming task over 1 week prior to recordings in order to gain orientation in the swimming pool.

Kinematic, kinetic and EMG analyses

All procedures used have been detailed previously (Courtine *et al.*, 2009a; Musienko *et al.*, 2011c; van den Brand *et al.*, 2012). Kinematics of hindlimb stepping were captured by the high speed motion capture system Vicon (Vicon Motion Systems, UK), consisting of 12 infrared cameras (T10, 200 Hz). Reflective markers were attached bilaterally at the iliac crest, the greater trochanter (hip joint), the lateral condyle (knee joint), the lateral malleolus (ankle), the distal end of the fifth metatarsophalangeal (MTP) joint and the tip of the fourth toe. The body was modeled as an interconnected chain of rigid segments, and

joint angles were generated accordingly. Vertical ground reaction forces (vGRF) were recorded using a biomechanical force plate (2 kHz; HE6X6, AMTI, USA) located below the treadmill belt. Electromyographic (EMG) signals (2 kHz) were amplified, filtered (10-1000 Hz bandpass), stored and analyzed offline to compute the amplitude, duration and timing of individual bursts. For both the left and right hindlimbs, 15 successive step cycles were extracted over several sequences of stepping on the runway for each rat under each condition. A 20-second interval was used when no or very minimal stepping movements were observed. For characterization of locomotion, a total of 155 parameters quantifying gait, kinematics, kinetics, and EMG features were computed for each limb and gait cycle according to methods described in detail previously (Courtine *et al.*, 2008; Courtine *et al.*, 2009a; Musienko *et al.*, 2011c; van den Brand *et al.*, 2012).

Hindlimb kinematics during swimming were captured by two Basler cameras (100 Hz; Basler Vision Technologies, Germany). Black dots were drawn on the shaved skin over the iliac crest, the greater trochanter (hip joint), the lateral condyle (knee joint), the lateral malleolus (ankle), the distal end of the fifth metatarsophalangeal (MTP) joint and the tip of the fourth toe. For analysis, hindlimb movements were reconstructed as a single segment connecting the iliac crest and the MTP. Kinematracer (Kissei Comtec Co., Japan) motion tracking software was used to obtain 2-D coordinates of joint positions for offline analysis of interlimb coordination. EMG signals were analyzed and computed identically to the previously described analysis of locomotion (**Supplementary figure 6.2a**).

Principal component analysis

To evaluate the characteristics underlying stepping for the different experimental conditions, we implemented a multi-step statistical procedure based on principal component (PC) analysis (Courtine *et al.*, 2009a; Musienko *et al.*, 2011c; Dominici *et al.*, 2012a). The various steps, methods, typical results, and interpretation of the analysis are detailed in Figure 6.3. PC analyses were applied on data from all individual gait cycles or swim strokes for all the rats together. Data were analyzed using the correlation method, which adjusts the mean of the data to 0 and the SD to 1. This method of normalization allows the comparison of variables with disparate values (large vs small values) as well as different variances. We quantified recovery of motor function as the distance between gait cycles or swim strokes of intact and injured rats in the new space created by the first 2 to 3 PCs (Micera *et al.*, 1999; van den Brand *et al.*, 2012).

Electrophysiological experiments

A monopolar electrode was implanted for deep brain stimulation (DBS) of the mesencephalic locomotor region (MLR). Electrodes consisted of 24-gauge stainless steel guiding tubes carrying four 41 AWG teflon coated stainless steel wires (793200, AM Systems, USA). Wires were crimped to a custom-made circular nano connector (Omnetics Connector Corporation, USA) on one side. The other end was bent 90°, fixed with biocompatible glue and cut transversally to expose 4 conductive electrode sites. Two extra wires were attached to the guiding tube as reference electrodes (~1 cm of teflon removed at the end). Implantation coordinates were -7.6 mm to -7.8 mm from Bregma and 2 mm from the longitudinal midline at a depth of approximately 5.7 mm to 6.7 mm. A train of stimuli (1 - 3s train length, 0.2 ms, 40 Hz, 0.15 mA) was delivered to trigger bipedal locomotion supported by the robotic postural interface.

Virus-mediated shutdown experiments

We specifically and reversibly inactivated reticulospinal projections to lumbar L1/L2 segments using a virus construct established and supplied by Tadashi Isa's laboratory at the National Institute for Physiological Sciences in Myodaiji, Japan (Kinoshita *et al.*, 2012). HiRet-TRE-EGFP.eTeNT was described as a highly efficient retrograde gene transfer (HiRet) lentiviral vector carrying enhanced tetanus neurotoxin light chain (eTeNT) and the enhanced GFP (EGFP) downstream of the tetracycline-responsive element (TRE) (Kinoshita *et al.*, 2012). We placed 4 injections of 250 nl HiRet-TRE-EGFP.eTeNT per hemicord in the spinal segments L1/L2. Injection sites were at 800 µm distance from the midline and rostrocaudally separated by 1 mm. Injection depth was 1.5 mm. In a second surgery, separated by 14 days, animals received injections of AAV2-CMV-rtTAV16 bilaterally in the reticular formation. AAV2-CMV-rtTAV16 is an adeno-associated virus serotype 2 (AAV2) vector carrying the Tet-on sequence, a variant of the reverse tetracycline transactivator (rtTAV16) under the control of the cytomegalovirus (CMV) promoter (Kinoshita *et al.*, 2012). Injection coordinates and volumes delivered were identical to the AAV1-CMV-GFP injections used to label the reticulospinal tract and described below. 7 days after the injections, the oral administration of doxycycline was initiated to induce the expression of eTeNT (Kinoshita *et al.*, 2012). Trained animals (n = 3) were tested for overground locomotion enabled with electrochemical stimulations before doxycycline administration (baseline), during doxycycline administration (3 to 4 days after initiation) and after doxycycline washout.

Tracing procedures

Under general anesthesia, two craniotomies were performed over the left motor cortex and bilaterally over the brainstem medulla oblongata. Animals of acute trained and non-trained groups were injected with BDA 10,000 (10 % in 0.01M PBS) into the left motor cortex over 6 sites covering the hindlimb area (coordinates centered -1 mm rostrocaudal and -1.75 mm mediolateral to Bregma, depth 1.5 mm). In the same surgery, an adeno-associated virus serotype 1 (AAV1) expressing green fluorescent protein (GFP) under the cytomegalovirus (CMV) promoter (AAV1-CMV-GFP, generously supplied by Patrick Aebischer's Neurodegenerative Disease Laboratory, EPFL, Lausanne, Switzerland) was injected in the gigantocellular reticular nucleus of the brainstem. Three injections of 300 nl each were made on both sides at -11, -11.5 and -12 mm longitudinal distance from Bregma and 8 mm below the surface of the cerebellum (**Supplementary figure 6.2.b**).

After a survival time of 21 days, all animals were deeply anesthetized by an i.p. injection of 0.5 ml Pentobarbital-Na (50 mg/mL) and transcardially perfused with approximately 80 ml Ringer's solution containing 100'000 IU/L heparin (Liquemin, Roche, Switzerland) and 0.25 % $NaNO_2$ followed by 300 ml of cold 4 % phosphate buffered paraformaldehyde (pH 7.4) containing 5 % sucrose. The brain and spinal cord were removed and postfixed in the same fixative before they were transferred to 30 % sucrose in phosphate buffer (PB) for cryoprotection. The tissue was embedded in Tissue Tek O.C.T (Sakura Finetek Europe B.V., The Netherlands), frozen at -40°C, and cut to a thickness of 40 µm.

Immunohistochemistry

For immunohistochemistry experiments, sections used for 5HT staining were pretreated with 0.03 % H_2O_2. Mounted or free-floating sections were washed 3 times in 0.1M phosphate buffered saline (PBS) and blocked in 5 % (5HT, NeuN) or 10 % (GFAP, GFP) normal goat serum containing 0.3 % Triton. Sections were then incubated in primary antibody diluted in the blocking solution overnight at 4°C (GFAP, NeuN,) or room temperature (GFP, 5HT). Primary antibodies used were rabbit anti-GFAP (1:1000, Dako, USA) or anti-5HT (1:5000, Sigma Aldrich, Germany), or mouse anti-NeuN (1:300, Chemicon, Millipore Corporation, USA) and chicken anti-GFP (1:500, Life Technologies, USA), respectively. Sections were again washed 3 times in 0.1M PBS and incubated with the appropriate secondary antibody (Alexa fluor® 488 or Alexa fluor® 555; Molecular Probes, Life Technologies, USA) in blocking solution. The following concentrations were used: 5HT 1:400, GFAP 1:400, GFP 1:200, NeuN 1:300. Tyramide System Amplification

(TSA)-Cyanine 3 kit (PerkinElmer, USA) was used to visualize BDA-labeled fibers. Sections were first washed and endogenous peroxidase activity was quenched by 30 min incubation in 0.1 % H_2O_2. After overnight incubation at 4°C with streptavidin-horseradish peroxidase (1:200) in 0.1M PBS-Triton (1 %), sections were again washed and incubated in TSA Cyanine 3 for 45 sec (1:100, spinal cord sections) or 3 min (1:200, brainstem sections), respectively. NeuroTrace™ (Life Technologies, USA) was used as a Nissl counterstain at a dilution of 1:50 in 0.1M PBS. Slides were finally washed, air-dried and coverslipped with Mowiol.

Neuromorphological evaluations

Fiber density (BDA, GFP, 5HT) was measured using 3 confocal image stacks per region per rat acquired with standard imaging settings and analyzed using custom-written Matlab (MathWorks, USA) scripts according to previously described methods (Carmel *et al.*, 2010; van den Brand *et al.*, 2012). Confocal output images were binarized by means of an intensity threshold and divided into square regions of interest (ROI). Densities were computed within each ROI as the ratio of traced fibers (number of pixels) per ROI area. Axon length was calculated using the same Matlab scripts applied on skeletonized confocal image stacks. Image acquisition was performed using a Leica TCS SPE or SP5 laser confocal scanning microscope and the LAS AF interface (Leica Microsystems, Germany) and stacks were processed offline using the Imaris software (Bitplane, USA) and Image J (National Institute of Health (NIH), USA). Axon caliber was computed as the ratio between axon density and axon length.

Statistical procedures

All data are reported as mean values ± s.e.m. Statistical evaluations were performed using one-way ANOVA for neuromorphological evaluations, and one- or two-way repeated-measures ANOVA for functional assessments (Prism, GraphPad Software, USA). The post hoc Fisher LSD test was applied when appropriate. The significance level was set as $|R \text{ value}| > 0.45$ and $p < 0.05$, respectively.

6.4 Results

Severe contusion SCI leads to limited but variable white matter sparing

We applied a 250 kdyn (255.5 ± 1.3 kdyn) force-controlled contusion SCI over thoracic levels 9-10 spinal segments. Lesions from all the rats were reconstructed in 3-D *post mortem* and no differences were found between groups ($p > 0.05$ for all analyses, **Figure 6.1a,b**). Tissue sparing was limited to a small rim (8.5 ± 0.65 % of healthy cross-sectional tissue) of white matter along the ventral and lateral spinal cord (**Figure 6.1c-d**).

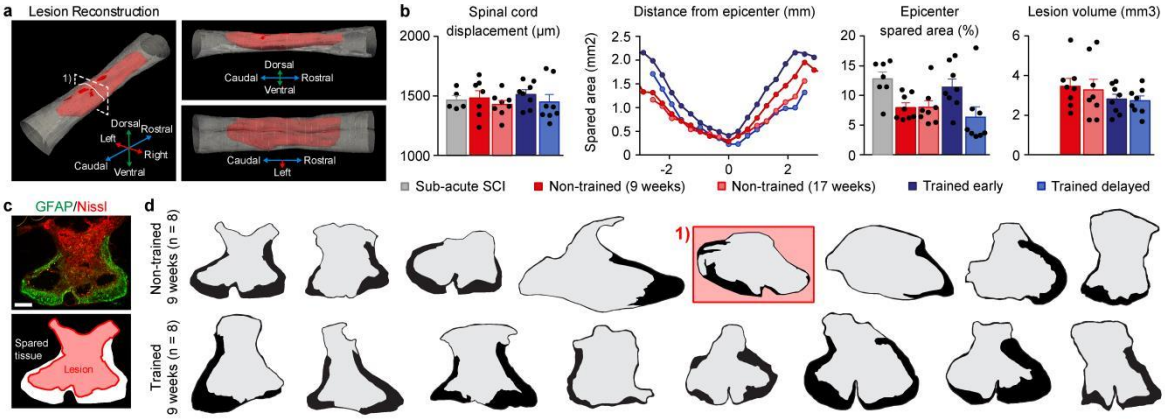

Figure 6.1 Severe contusion SCI leads to limited but variable white matter sparing.
(a) 3D reconstruction of a contusion injury (highlighted within square in **(d)**). **(b)** 2D and 3D evaluation of contusion injuries based on surgery outcome and histology across all chronic SCI groups. **(c)** Epifluorescent images showing the injury epicenter and a 2D contour tracing. Scale bar, 500µm. **(d)** 2D contour tracing of injury epicenters of all non-trained and trained SCI animals at 9 weeks post-injury. Error bars, s.e.m.

Severe contusion SCI leads to permanent locomotor impairments

We first characterized spontaneous locomotor recovery following severe contusion SCI in non-trained rats. Seven days after severe contusion SCI, all animals (n = 16) showed flaccid paralysis of the hindlimbs without muscle activation when mounted over a moving treadmill belt (data not shown). Within 5 minutes, the same rats performed coordinated and alternating stepping patterns under the influence of electrochemical neuromodulation. However, none of the rats was able to voluntarily initiate locomotion overground when supported by the neuroprosthetic postural interface (data not shown). After 2 months without neurorehabilitative interventions, 53 % of non-trained rats recovered voluntary extension in the absence of propulsive capacities while 35 % regained a variable degree of forward propulsion in the presence of the electrochemical

neuroprosthesis (n = 8; **Figure 6.2c** and **6.2e,f**). Little or no stepping behavior was observed both with only electrical stimulations and spontaneously (without neuromodulation strategies) (data not shown).

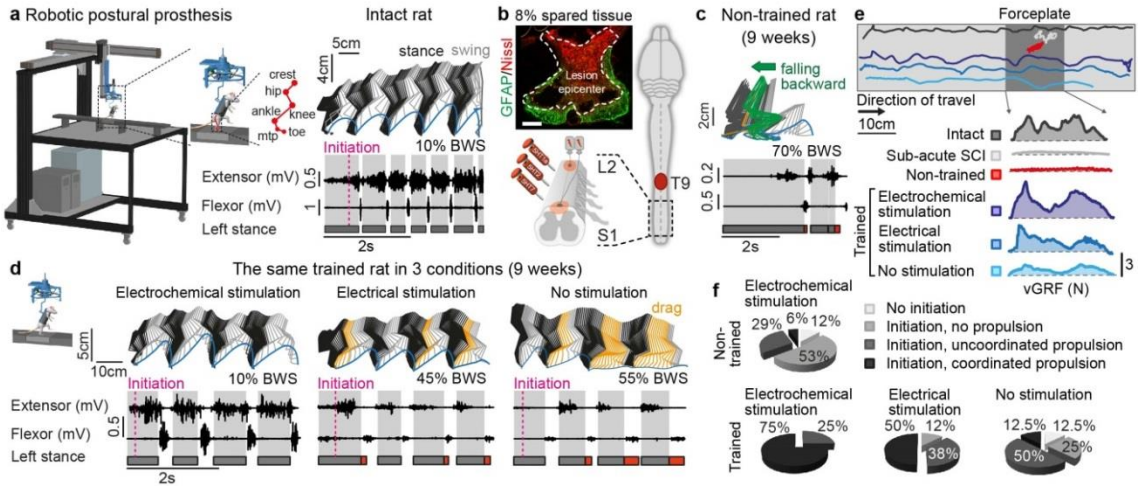

Figure 6.2 Neuroprosthetic rehabilitation restores voluntary locomotion after severe contusion SCI.
(a) Bipedal overground stepping using the postural robotic prosthesis developed earlier (Dominici *et al.*, 2012a), left hindlimb kinematics with endpoint trajectory and EMG activity of medial gastrocnemius (MG, extensor) and tibialis anterior (TA, flexor) muscles during bipedal locomotion in a intact rat. Grey bars indicate the duration of stance phases. **(b)** A representative picture of a coronal section of a lesion epicenter stained for GFAP and Nissle substance and a scheme illustrating the electrochemical prosthesis **(c)** Left hindlimb kinematic and EMG activity analogous to the representation of the healthy rat kinematic and muscle activity in **(a)** where red bars and sticks represent drag phases. **(d)** The same trained rat during bipedal locomotion under three different experimental recording conditions; with electrochemical stimulation (left), with electrical stimulation (middle) and without stimulation (right). **(e)** Representative traces of forward motion and vertical ground reaction forces (vGRF) recorded under the various experimental conditions at 1 and 9 weeks post SCI. **(f)** Proportional group performance of non-trained (electrochemical stimulation) and trained (electrochemical stimulation, electrical stimulation, no stimulation) rats. BWS, body weight support. mtp, metatarsophalangeal joint. vGRF, vertical ground reaction force.

In order to quantify in detail gait of all the animals, we applied a principal component analysis (PCA) over 129 gait variables and analyzed the data distribution within the newly generated principal component (PC) space defined by the first and second PC. Each data point represents one animal. PC scores indicate the location of data points and experimental groups along each individual PC axis. Extraction of scores suggested that PC1 captured recovery of locomotion over time and following neuroprosthetic rehabilitation ($p < 0.001$). Severe contusion SCI lead to limited spontaneous recovery ($p < 0.001$; **Figure 6.3a,b**) characterized by increased weight-bearing ($p < 0.001$) and increased maximal endpoint velocity ($p < 0.01$). A lack of coordination, endpoint control

and timed muscle activation, nevertheless, resulted in an incapability to initiate and sustain locomotion in the robotic interface in non-trained rats (**Figure 6.3c)**.

Neuroprosthetic rehabilitation restores voluntary locomotion after severe contusion SCI

In stark contrast to the limited spontaneous recovery, all trained animals regained coordinated overground locomotion when supplied with the electrochemical neuroprosthesis (n = 8; **Figure 6.2d-f**). PCA revealed a strong overall resemblance of voluntary locomotion after SCI with healthy gait based on PC1 score ($p = 0.26$; **Figure 6.3a,b**). Recovery of overground locomotion was characterized by an increased weight-bearing capacity, ameliorated gait timing, i.e. normal cycle duration, increased range of motion of proximal and distal joints, decreased gait variability, re-established inter- and intralimb coordination, higher movement speeds and well-timed muscle activities (**Figure 6.3c,d**). Thus, neuroprosthetic rehabilitation is capable of restoring highly coordinated overground locomotion when applied acutely after a clinically relevant, severe contusion SCI.

Further we assessed whether the electrochemical neuroprosthesis will always be needed for the performance of sustained locomotion, we additionally tested the trained rats both with only electrical stimulations and without any stimulations. Indeed, 88% of trained rats showed voluntary propulsive capacities in the absence of pharmacological stimulation and, most strikingly, more than 50% were able to sustain voluntary walking in the absence of neuromodulation strategies (**Figure 6.2d-f**). Despite impressive locomotor capacities, detailed analysis revealed that endpoint velocity was altered ($p < 0.05$) along with decreased weight-bearing capacities and slower movement velocity (both $p < 0.05$; **Figure 6.3d**). Notably, interlimb coordination ($p < 0.01$) and gait cycle duration ($p < 0.05$) were significantly affected only in the complete absence of stimulations but not in the presence of electrical stimulation (**Figure 6.3c**). Variability of endpoint trajectory as well as proximal range of motion (i.e. hip angle) remained at the level of healthy performance irrespective of neuromodulation strategies ($p > 0.05$; **Figure 6.3.c**). These results constitute the first demonstration of a restoration of voluntary overground locomotion without the aid of electrical or pharmacological neuromodulation after severe SCI.

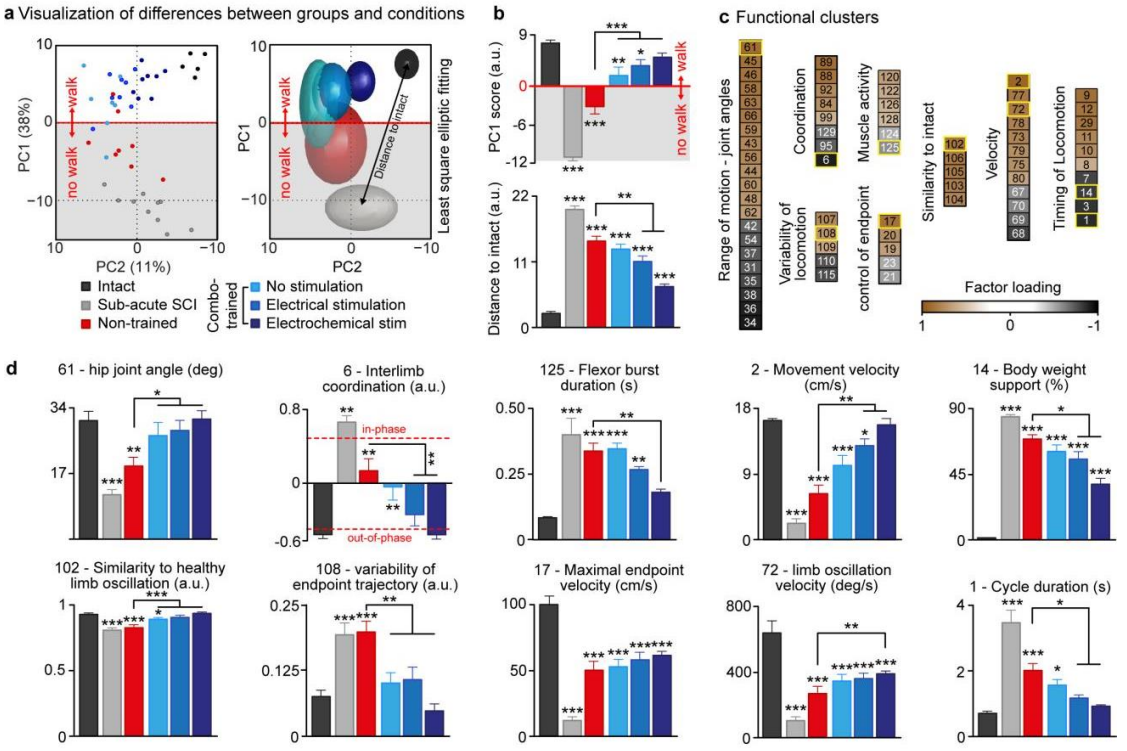

Figure 6.3 Multi-step statistical analysis of locomotor patterns across groups.
(a) Representation of individual animals in the new denoised space created by PC1-2. Least square elliptic fitting reveals separated clusters of data points for each time point and recording condition. **(b)** PC scores indicate which experimental time points and recording conditions are differentiated by each PC. Locomotor performances were quantified as the 2D Euclidean distance between the location of an individual animal and the average location of intact rats. **(c)** Extraction of factor loadings, i.e. correlation between gait variables and the first principle component analysis are regrouped into functional clusters which are named for clarity. Detailed list of parameters is available in **supplementary table 6.1**. A bar graph of variables for each cluster is represented in **(d)**. * $p < 0.05$; ** $p < 0.01$; *** $p < 0.001$. Error bars, s.e.m. a.u., arbitrary unit.

Neuroprosthetic rehabilitation restores swimming after severe contusion SCI

Next we investigated whether the robotic support was required for the performance of voluntary hindlimb movements. We minimized the influence of weight-bearing information and feedback by introducing swimming as a task. To reveal supraspinal control capacities, all rats were tested in the absence of neuromodulation strategies. Intact rats showed coordinated swimming characterized by out-of-phase strokes of hindlimbs and alternating activation of antagonistic muscles (**Figure 6.4a**; left panel). Non-trained rats used the forelimbs to compensate for weak or absent hindlimb movements as they essentially dragged their motionless hindlimbs through the water (**Figure 6.4a**; middle panel); hindlimb muscles exhibited infrequent and uncoordinated bursts of activity, which lead to co-contraction of antagonist muscles (**Figure 6.4b,c**). In

contrast, trained rats displayed strong alternating activity of extensor and flexor muscles (**Figure 6.4a,b**) resulting in limb oscillations and trajectories that were similar to healthy rats (**Figure 6.4a**; right panel). Swimming strokes of trained rats were faster, covered a larger range of motion and showed less variability than those observed in non-trained rats ($p < 0.05$; **Figure 6.4c**). Periods of co-contraction of antagonist muscles were significantly more frequent in non-trained compared to trained rats ($p < 0.01$). Co-contraction values were statistically not different from those of intact rats ($p = 0.23$; **Figure 6.4b,c**). Despite the impressive capacity to swim, trained rats did not recover interlimb coordination ($p < 0.001$; **Figure 6.4c**), which resulted in alternating sequences of out-of-phase and in-phase movements (**Figure 6.4b**). In summary, we conclude that neuroprosthetic rehabilitation enabled trained rats to regain the capacity to perform functional hindlimb movements in the absence of robotic support and electrochemical stimulations in an untrained task.

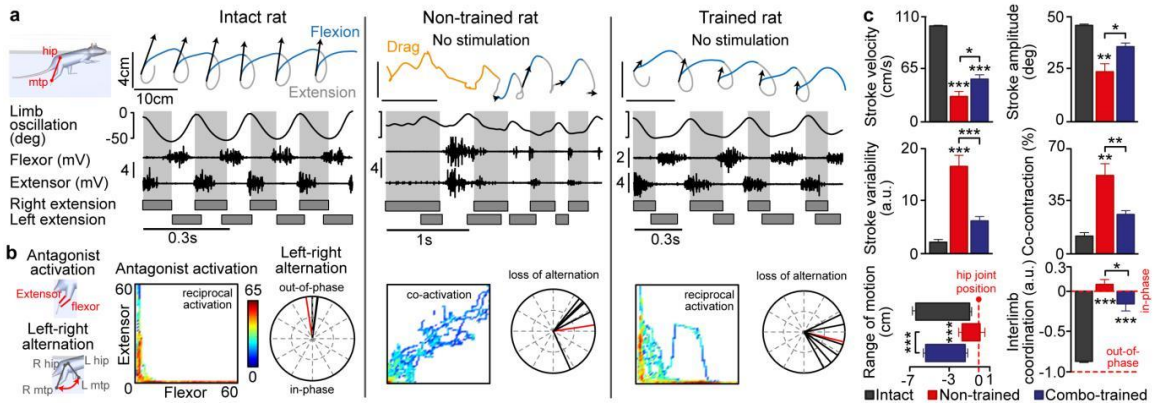

Figure 6.4 Neuroprosthetic rehabilitation restores swimming movements after severe contusion SCI.

(a) Right hindlimb endpoint trajectory, limb oscillation and EMG activity of extensor (medial gastrocnemius) and flexor (tibialis anterior) muscles during spontaneous swimming in an intact (left), non-trained (middle) and trained (right) SCI rat. **(b)** Density plots (left column) display the coordination between the antagonistic muscles throughout one locomotor trial (6-10 strokes). L-shaped patterns reflect reciprocal activation of muscles. Polar plot representations (right column) illustrate the coordination between the oscillations of left and right hindlimbs (black line, single gait cycle; red line, average of all gait cycles). **(c)** Bar graphs of a subset of variables showing a high correlation with PC1 (|R value| > 0.5). * $p < 0.05$; ** $p < 0.01$; ***, $p < 0.001$. Error bars, s.e.m. a.u., arbitrary unit. mtp, metatarsophalangeal joint.

Neuroprosthetic rehabilitation leads to sprouting of spared descending brainstem systems

We hypothesized that recovery of voluntary hindlimb movements was mediated through spared descending brainstem projections. We visualized projections of the gigantocellular reticular formation by injection of an adeno-associated virus serotype 1 (AAV1) expressing green fluorescent protein (GFP) under the cytomegalovirus (CMV) promoter (AAV1-CMV-GFP). The reticulospinal tract descends in the lateral and ventral aspects of the spinal cord white matter. Therefore, reticulospinal projections are largely spared by severe contusion injuries, providing an optimal substrate for activity-dependent reorganization to re-establish supraspinal control of leg movements. We evaluated AAV1-expressing fiber density in T7 spinal segments above the SCI and in T12/T13 and L4 spinal segments below the SCI with respect to the Rexed laminae (Molander *et al.*, 1984) (**Figure 6.5a**). Above the SCI, we found an overall increase in AAV1 fiber density in both, in trained and non-trained rats ($p < 0.05$, **Figure 6.5b**). Below the injury at T12/13 spinal segment, trained rats showed an increased AAV1 fiber density in both dorsal (laminae 1 to 6) and intermediate (lamina 7 and 10) spinal areas compared to non-trained rats ($p < 0.05$; **Figure 6.5c,d**), which surpassed intact innervation levels in some rats (**Figure 6.5d,e**). Reticulospinal axonal reorganization was primarily directed towards the intermediate laminae that are responsible for sensorimotor processing, while the motor-associated laminae 8 and 9 remained unaffected at T12/T13 ($p = 0.77$; **Figure 6.5c**). Similar to results in the lower thoracic spinal cord, we found increased AAV1 fiber density in lumbar spinal segment L4 in trained compared to those of non-trained rats ($p < 0.05$, **Figure 6.5f**). Spared reticulospinal axons thus reorganize with neuroprosthetic rehabilitation to strengthen connectivity with the segments below the lesion, in particular by reinforcing innervation of the intermediate thoracic and ventral lumbar laminae.

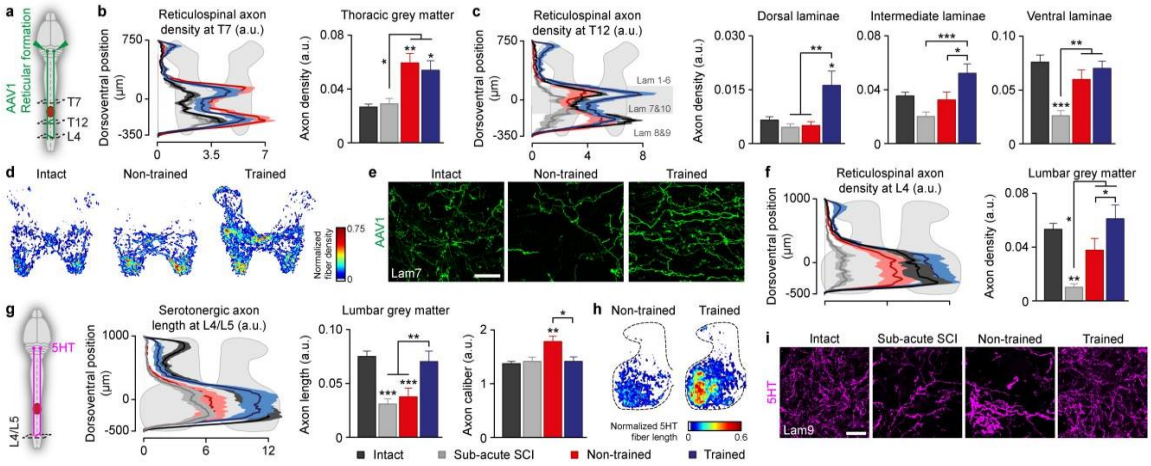

Figure 6.5 Neuroprosthetic rehabilitation leads to sprouting of spared bulbospinal projections. **(a)** Diagram illustrating anatomical experiment. **(b)** Dorsoventral density plot and bar graphs reporting axon density of AAV1-labeled reticulospinal fibers within the spinal segment T7. **(c)** Dorsoventral density plot and bar graphs reporting lamina-specific axon density of AAV1-labeled reticulospinal fibers within the spinal segment T12 for each group. **(d)** Representative heatmaps of AAV1-labeled reticulospinal fibers. **(e)** Representative images of AAV1-labeled axon density in lamina 7. **(f)** Dorsoventral density plot and bar graphs reporting axon density of AAV1-labeled reticulospinal fibers within the spinal segment L4. **(g)** Diagram illustrating anatomical experiment. Dorsoventral density plot and bar graphs reporting the overall serotonergic axon length and caliber within the spinal segments L4/L5 for each group. **(h)** representative heatmaps of serotonergic fiber density. **(i))** Representative images of 5HT axon density in lamina 9. Scale bar, 25µm. Scale bar, 25µm. * $p < 0.05$; ** $p < 0.01$; *** $p < 0.001$. Error bars, s.e.m. a.u., arbitrary unit. Lam, lamina.

Serotonergic (5HT) neurons are located in the raphe nucleus and contribute to initiating and sustaining locomotion (Liu & Jordan, 2005; Hagglund *et al.*, 2010; van den Brand *et al.*, 2012). Their projections descend in the dorsolateral aspects of the spinal cord white matter and are thus partially spared by severe contusion injuries. Evaluation of 5HT staining at lumbar spinal segments L4/L5 revealed significantly decreased axon length sub-acutely and chronically after injury ($p < 0.001$), but restored 5HT axon length in trained animals (**Figure 6.5g**). Reduction of overall 5HT axon caliber, characterized by a shift towards thin D-type fibers (Kosofsky & Molliver, 1987), was previously associated with a treatment effect for spinal cord injury (Mullner *et al.*, 2008). Here, we found that compared to healthy baseline, overall 5HT axon caliber was increased in non-trained animals ($p < 0.01$), whereas healthy rats levels were re-established after neuroprosthetic training (**Figure 6.5g**). Hence, neuroprosthetic rehabilitation lead to sprouting of spared raphespinal fibers in parallel with a reduction of 5HT axon caliber in lumbar segments below a severe contusion SCI.

Spontaneous remodeling of motor cortex projections in the presence of spared descending brainstem tracts

Motor cortex axons project to various brainstem motor areas, including both the parapyramidal region and the gigantocellular reticular formation (**Figure 6.6a**). We found an increased density of cortical axonal projections in the medial reticular formation for both non-trained and trained rats compared to intact and sub-acute SCI animals ($p < 0.05$; **Figure 6.6c,d**). In the presence of spared descending brainstem projections, corticoreticular remodeling hence occurred spontaneously and independent of neuroprosthetic rehabilitation ($p = 0.82$). Analysis of corticospinal axon density in the mid-thoracic spinal cord above the SCI revealed an axonal density similar to healthy baseline (**Figure 6.6b**).

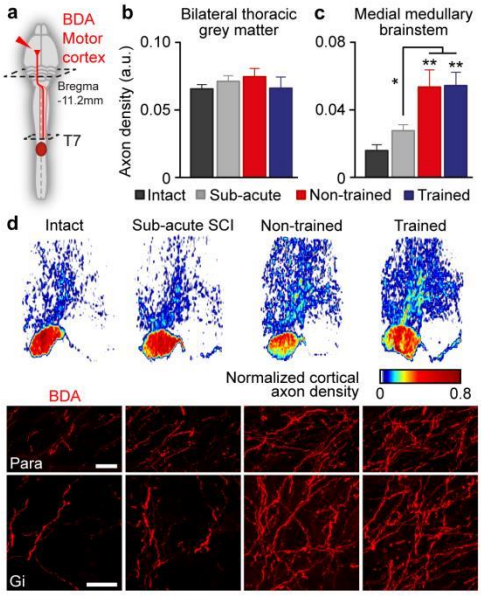

Figure 6.6 Spontaneous remodeling of motor cortex projections.
(a) Diagram illustrating anatomical experiment. **(b)** corticospinal axon density at T7 spinal level. **(c)** . Bar graphs reporting the cortical axon density in the medial reticular formation of the brainstem for all groups. **(d)** Representative heatmaps of the cortical axon density and confocal images. Scale bar, 25µm. *, $P < 0.05$; **, $P < 0.01$; Error bars, s.e.m. a.u., arbitrary unit; Para, paramydal region; Gi, gigantocellular reticular formation; CST, corticospinal tract.

Re-connecting supraspinal with lumbar locomotor centers

We thus investigated several descending fiber systems on various supraspinal and intraspinal levels including the formation of detour circuits (**Figure 6.7a**). Motor cortex axons branched into the medial medullary brainstem and formed excitatory close

appositions with AAV1-infected reticular formation neurons (**Figure 6.7b**). Reticulospinal projections, in turn, showed sprouting above the injury at T7 (**Figure 6.7c**) despite the absence of spared Fastblue-labeled propriospinal neurons (data not shown). Below the injury, spared reticulospinal fibers underwent extensive reorganization including the formation of excitatory contacts with propriospinal neurons projecting to the lumbar locomotor centers (**Figure 6.7d**). Spared reticulospinal and raphespinal projections additionally projected directly contacted presumable hindlimb motoneurons (**Figure 6.7d** right panel).

This suggests that supraspinal commands reach locomotor centers through direct spared brainstem projections that bypass the lesion and form relays to propriospinal neurons projecting to the lumbar spinal cord (**Figure 6.7b,d**). These connections get strengthened by neuroprosthetic rehabilitation through sprouting mechanisms of the spared descending bulbospinal fibers below the SCI (**Figure 6.5c-i**).

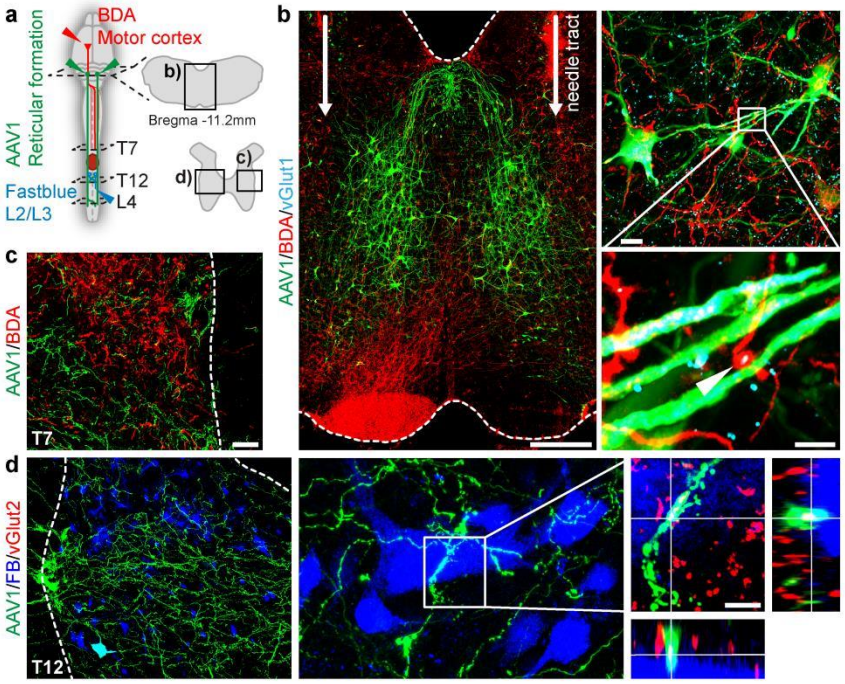

Figure 6.7 neuroprosthetic rehabilitation re-establishes connection between cortex, brainstem and lumbar locomotor circuits.
(a) Diagram illustrating anatomical experiment and analyzed areas. **(b)** Confocal overview of a coronal section at the medullary brainstem at the injection site of AAV1 tracer in a trained rat (left) and an inset displaying close apposition of motor cortex projections to GFP tagged reticulospinal fibers with glutamatergic synapses. Scale bars, 500µm (left), 20µm (top right), 5µm (right lower). **(c)** Representative confocal images of a coronal T7 section showing corticospinal and reticulospinal projections in the intermediate laminae. Scale bars, 50µm **(d)** Representative confocal image of a coronal T12 section. AAV1 traced reticulospinal fibers make connection to intraspinal neurons projecting to the lumbar spinal cord and form glutamatergic synapses. Scale bars, 5µm.

Indirect activation and specific inactivation of the reticulospinal tract

To show a relationship between neuronal drive originating from the reticular formation and restored functional capacities we activated and transiently suppressed reticulospinal projections to lumbosacral locomotor circuits of trained rats. For suppression of reticulospinal neurons, rats were stereotaxically injected with the retrograde virus HiRet-TRE-EGFP.eTeNT bilaterally in L1/L2 spinal segments followed by injections of AAV2-CMV-rtTAV16 in the reticular formation of the medulla oblongata (**Figure 6.8a**). Two weeks after the tracers were injected, the oral administration of doxycycline was initiated to induce the expression of the tetanus neurotoxin (Kinoshita *et al.*, 2012). At baseline, all animals showed voluntary initiation and coordinated bipedal locomotion in the robotic interface (**Figure 6.8b**, left panel). 3 to 4 days after doxycycline administration, trained rats displayed severe deficits in overground gait performance ranging from lack of propulsion, significantly reduced step height, variable foot trajectory and increased cycle duration to complete loss of initiation ($p < 0.01$, **Figure 6.8b,d**). Baseline locomotor capacities were recovered after doxycycline washout, evidenced in similar gait pattern in the two-dimensional representation of the PCA (**Figure 6.8b,c**). Expression of enhanced tetanus neurotoxin (eTeNT) upon doxycycline administration will be confirmed histologically *post mortem*.

Reticulospinal neurons were indirectly activated by deep brain stimulation (DBS) of the mesencephalic locomotor region (MLR). Half a century ago, classical electrophysiological studies first revealed the locomotion-inducing effects upon stimulation of the region at the junction between midbrain and hindbrain (for a review see (Ryczko & Dubuc, 2013)). MLR neurons project extensively to both the medial reticular formation and the raphe nuclei of the medulla oblongata (Edwards, 1975; Steeves & Jordan, 1984; Garcia-Rill & Skinner, 1987b). We hypothesized that MLR DBS leads to immediate and progressively more efficient activation of bipedal overground locomotion in trained animals, thus reflecting bulbospinal fiber reorganization. In order to facilitate activation of lumbosacral locomotor circuitries, all experiments with MLR DBS were performed in conjunction with electrochemical neuromodulation (**Figure 6.8a**). Sub-acutely after the injury (1 week), DBS MLR did not induce bipedal locomotion in any of the tested rats (**Supplementary figure 6.2a**). However, we found that coincidence with first voluntary bipedal stepping capacities, MLR DBS triggered initiation of locomotion (**Supplementary figure 6.2b**). Chronically after the SCI, we found reliable initiation of bipedal overground locomotion 3.03 seconds (s.e.m. 0.34) after MLR DBS onset (**Figure 6.8e**). However, detailed analysis of MLR DBS induced and voluntarily performed stepping, revealed characteristic differences of gait patterns, based on shifts in PC2

scores (**Figure 6.8c**). We found that rats were stepping significantly faster, had a faster hip angle velocity and increased extension in the hip joint ($p < 0.05$). Increased speed was accompanied with shorter stance phase when stepping was induced by MLR DBS compared to voluntary initiation ($p < 0.05$; **Figure 6.8d**). In spite of changes in gait pattern, the results of these experiments confirm that bipedal locomotion in the robotic interface is triggered supraspinally, either voluntarily by the rat or enforced by MLR DBS.

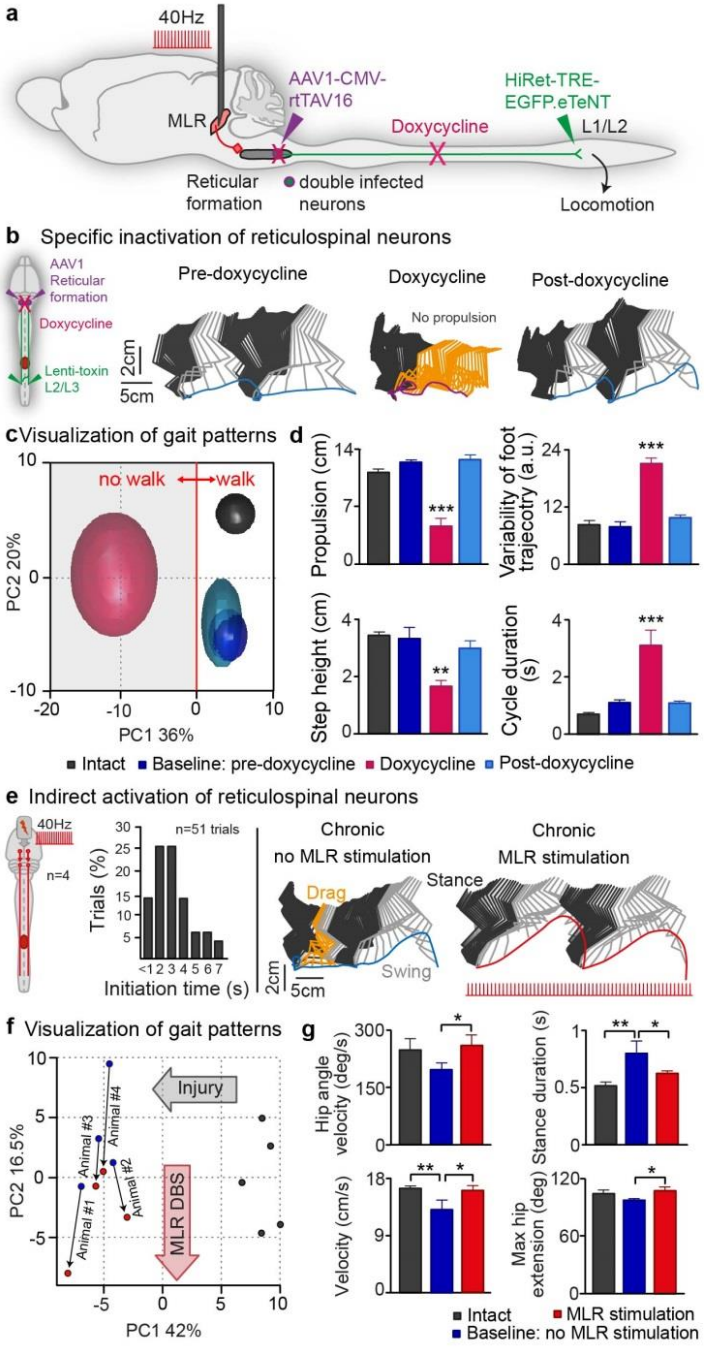

Figure 6.8 The crucial role of the reticulospinal system for performing bipedal overground locomotion
(a) Diagram illustrating DBS and virus-mediated silencing techniques. **(b)** Stick figures displaying behavior before (baseline, left), with (middle) and after (washout, right) of doxycycline application. **(c)** Representation of individual animals in the denoised space created by PC1-2. **(d)** Barplots of kinematic paramters displaying different locomotion before (baseline), with, and after (washout) doxycycline application. **(e)** Indirect activation of the reticular formation. Barplot displaying initiation time of locomotion from MLR DBS onset on (left) and stick figures illustrating behavior evoked by DBS in the MLR compared to volitional bipedal locomotion. **(f)** Representation of individual animals in the denoised space created by PC1-2. **(g)** Barplots of kinematic paramters displaying different locomotion when triggered with MLR DBS or walking volitionally. * $p < 0.05$; ** $p < 0.01$; *** $p < 0.001$. Error bars, s.e.m. a.u., arbitrary unit.

Delayed onset of neuroprosthetic training restores voluntary locomotor

We evaluated the potential and limits of neuroprosthetic rehabilitation in a clinically more relevant setting by delaying the training onset of rehabilitation to the chronic stage (2 months post SCI), after which we did not find any further spontaneous recovery ($p > 0.05$ for all comparisons between non-trained groups at 2 and 4 months post-SCI, **Figure 6.9e**). Strikingly, rats that started training in the chronic state recovered overground locomotor abilities including voluntary gait initiation and forward propulsion. Parameters summarized in the functional clusters gait timing, variability of gait and similarity to intact, reveal a similar recovery in delay trained compared to those of early trained rats. As an example, we found a similar cycle duration and variability of foot trajectory in delay and early trained rats (**Figure 6.9d,e**). However, gait patterns represented in the two-dimensional space of the PCA suggests diminished performance in delay trained rats. Further we found significantly decreased PC1 scores in delay compared to early trained and intact rats ($p < 0.05$; **Figure 6.9b,c**). Difference in gait patters between early and delay trained rats are parameters accounting for robust gait as well as for hip control. For instance, delay trained rats displayed reduced movement velocity and reduced hip extension ($p < 0.01$; **Figure 6.9d,e**). Furthermore, none of the delay trained rats recovered voluntary motor functions in the absence of neuromodulation strategies (data not shown). To the best of our knowledge, these data show for the first time an effective intervention to counteract locomotor deficits after a chronic SCI. This provides a useful framework to translate neuroprosthetic rehabilitation into medical practices, yet they also illustrate the limitation of this intervention to improve motor recovery after severe SCI.

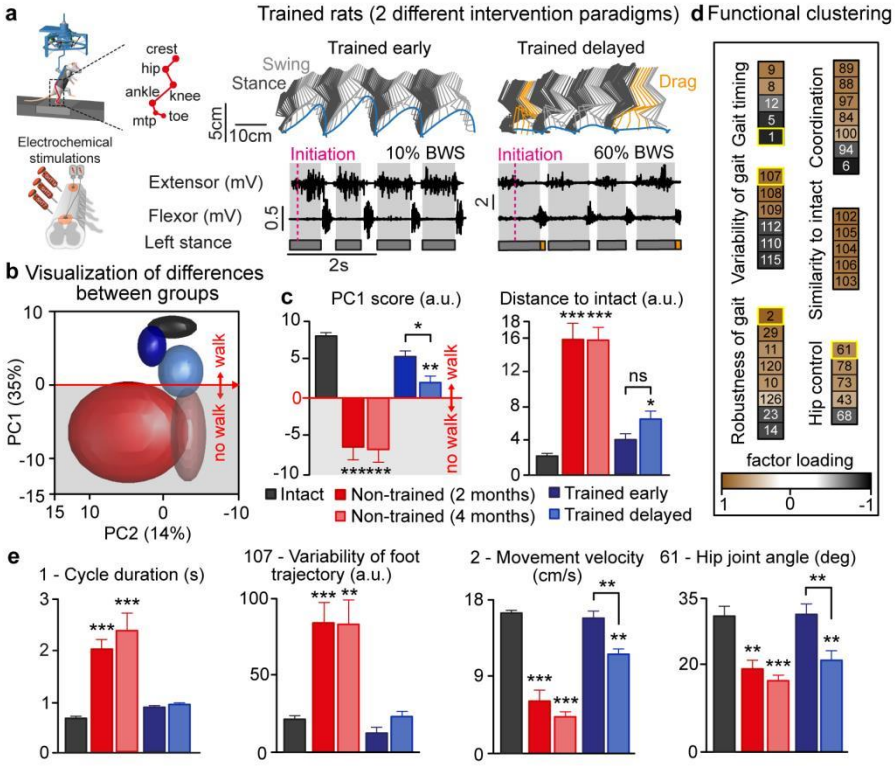

Figure 6.9 Delayed training onset of neuroprosthetic rehabilitation restore voluntary locomotor capacities to a lesser extent.

(a) Representative trials of bipedal locomotion from an early trained (left) and delay trained (right) SCI rat. Conventions are the same as **Figure 6.4**. **(b)** Representation of individual animals in the new space created by PC1-2, which reveals separated clusters of data points for each condition. **(c)** PC scores indicate which experimental time points are differentiated by each PC. Locomotor performances were quantified as the 2D euclidean distance between the location of an individual animal and the average location of intact rats. **(d)** Extraction of factor loadings, i.e. correlation between gait variables and the first principle component analysis (|R value| > 0.5) are regrouped into functional clusters which are named for clarity. Detailed list of parameters is available in **supplementary table 6.1 (e)** Bar graphs of a subset of variables. *, P < 0.05; **, P < 0.01; ***, P < 0.001. a.u., arbitrary unit. BWS, bodyweight support. mtp, metatarsophalangeal joint, BWS bodyweight support.

6.5 Discussion

We show that neuroprosthetic rehabilitation leads to recovery of supraspinally controlled hindlimb movements in rats with acute and chronic contusion SCI. Recovery of motor function was accompanied by spontaneous and use-dependent reorganization in descending bulbospinal axonal projections. We further provide evidence that mesencephalic and medullary locomotor-related brainstem regions play a crucial role in the recovery and control of overground stepping after severe contusion SCI.

Potential and limitations of neuroprosthetic rehabilitation after severe contusion SCI

We exploited the potential of neuroprosthetic rehabilitation to improve locomotor recovery after severe contusion SCI by introducing variations in training paradigms and recording conditions. Only contused rats that were trained early after SCI recovered spontaneous voluntary locomotion overground in some cases, delay trained rats remained dependent on the influence of electrochemical stimulations. Under this condition, delay trained rats displayed highly consistent locomotion, yet it was marked by reduced strength, velocity and control of proximal joints. Despite the absence of pronounced degradation of function (Beauparlant *et al.*, 2013) after contusion SCI, this result suggests that chronic SCI rats were restrained by a reduced capacity of the neuromuscular system. Nevertheless both supraspinal and intraspinal neuronal circuits were capable of learning upon repetitive activation even after a long period of inactivity.

We further investigated the influence of electrical and pharmacological neuromodulation on regained locomotion in early trained rats. Gait performance was most similar to healthy locomotion when enabled with the combination of electrical and pharmacological stimulations. When withdrawing first pharmacological neuromodulation followed by omission of all stimulations, we observed progressive changes for many aspects of locomotion, e.g. generated ground reaction forces and movement velocity. Gait features demanding enhanced motor control such as interlimb coordination were particularly affected by a lack of neuromodulation interventions. Interestingly, interlimb coordination was re-established in overground locomotion but remained severely disturbed in the absence of load information during swimming (Gruner & Altman, 1980), with (data not shown) and without stimulations. Most importantly, however, early trained rats with severe contusion SCI regained supraspinally controlled hindlimb movements in the absence of any stimulation, both during overground locomotion and during swimming.

Use-dependent plasticity in the presence of spared direct supraspinal projections

Use-dependent plasticity induced significant reorganization of spared descending brainstem pathways. The concept of spared tracts sprouting to reconnect denervated spinal circuits with supraspinal sources is well established following lateral hemisection SCI in rodents (Raineteau & Schwab, 2001; Bareyre *et al.*, 2004; Ballermann & Fouad, 2006; Courtine *et al.*, 2008; Weishaupt *et al.*, 2013; Zorner *et al.*, 2014a) and primates (Rosenzweig *et al.*, 2010). In contrast, axon reorganization in the presence of a small number of remaining bilateral projections after severe contusion SCI has rarely been assessed. Previous findings, however, suggested that voluntary exercise induced 5HT fiber growth after a moderate contusion SCI in mice (Engesser-Cesar *et al.*, 2007). Similarly, other studies demonstrated sprouting of bulbospinal projections using a moderate contusion SCI and neuroregenerative treatments (Hellal *et al.*, 2011; Bartus *et al.*, 2014) or immunomodulatory (Iannotti *et al.*, 2011) treatments, respectively. Here, we found that both raphespinal and reticulospinal pathways showed minimal spontaneous sprouting but underwent substantial lamina-specific reorganization with neuroprosthetic rehabilitation. Overall serotonergic axon length was re-established to healthy innervation levels and axon caliber remained unchanged in trained rats, similar to previously described treatment effects (Mullner *et al.*, 2008). Reticulospinal fiber density surpassed baseline measures in intermediate spinal laminae after neuroprosthetic rehabilitation. As expected motor-related ventral laminae, in turn, remained unaffected in thoracic segments below the contusion SCI. Neuroprosthetic training thus induced extensive yet targeted sprouting of spared descending brainstem pathways.

The medial medullary brainstem as a mediator of locomotor recovery after severe contusion SCI

Motor cortex connections to descending projection systems in the medulla oblongata were also reinforced after a severe contusion SCI, both spontaneously and with training. These findings contrast with the complete lack of spontaneous motor cortex plasticity after a staggered hemisection SCI interrupting all direct supraspinal access to lumbosacral spinal segments (van den Brand *et al.*, 2012). In contrast to a staggered hemisection SCI, spontaneous reorganization in the brainstem is of potential functional significance when even a few descending projections are spared by the contusion injury. Locomotor-related brainstem nuclei may serve as relay centers for the cortical command signal; here in particular due to the complete interruption of the corticospinal tract at the level of the contusion SCI and several spinal segments rostral and caudal to the SCI (data not shown). Complementary mechanistic experiments directly supported this

conclusion: specific and transient silencing (Kinoshita *et al.*, 2012) of reticulospinal pathways projecting to lumbar segments caused severe deficits in initiation and coordination of overground locomotion in trained rats. Previous studies have emphasized the crucial contribution of the medullary reticular formation to initiation and control of locomotion in the healthy state (Garcia-Rill & Skinner, 1987a; Noga *et al.*, 1988; Matsuyama *et al.*, 2004; Grillner *et al.*, 2008; Hagglund *et al.*, 2010) and after lateral hemisection (Ballermann & Fouad, 2006; Zorner *et al.*, 2014b). To the best of our knowledge, we here provide the first direct demonstration of its functional role in the recovery of supraspinal control of locomotion after a severe SCI.

The gigantocellular nucleus of the reticular formation receives abundant bilateral input from the mesencephalic locomotor region (MLR) (Steeves & Jordan, 1984; Garcia-Rill *et al.*, 1986; Garcia-Rill & Skinner, 1987b; Zorner *et al.*, 2014a). The locomotion-inducing effects of MLR stimulation were revealed more than half a century ago by classical electrophysiological studies (Shik *et al.*, 1969; Ryczko & Dubuc, 2013). Furthermore, DBS of the MLR was recently suggested as a therapeutic intervention to improve locomotor functions after chronic severe SCI (Bachmann *et al.*, 2013). We found that MLR DBS did not induce bipedal overground locomotion in the sub-acute stage of severe SCI, i.e. when rats were not able to voluntarily initiate gait. After several weeks of neuroprosthetic rehabilitation, trained rats simultaneously recovered bipedal overground locomotion either triggered voluntarily or forcefully evoked by MLR DBS. Importantly, MLR DBS was only effective once voluntary gait initiation recovered. After 2 months of neuroprosthetic training, MLR DBS was most effective and lead to increased stepping strength, increased walking speed, extension and step height. These findings imply both that bipedal locomotion in the robotic interface was supraspinally controlled, and that propagation of the MLR-evoked command signal relied on remodeling of descending systems to bypass the injury. In conclusion, we demonstrate that stimulation of the MLR activates regained voluntary locomotion after severe contusion SCI.

Implications for the clinical translation of neuroprosthetic rehabilitation

Electrical epidural stimulation of the injured spinal cord was successfully implemented in four patients with chronic motor-complete SCI. Voluntary movement occurred immediately upon electrical stimulation despite chronic paralysis in three individuals (Angeli *et al.*, 2014a). Moreover, electrical stimulation was used during training sessions over 7 months in one patient and led to recovery of full weight bearing standing and some voluntary leg movements in the presence of stimulation (Harkema *et al.*, 2011). Neuroprosthetic rehabilitation enabled by electrochemical neuromodulation re-

established voluntary locomotion and swimming the absence of any stimulation. This carry-over effect provides evidence that voluntary movements of paralyzed limbs may be achieved outside laboratory settings for spinal cord injured individuals in the future. Considering the complex and multi-faceted nature of human spinal cord trauma, it is unlikely that patients will have immediate access to neuroprosthetic interventions in the near future. We hence additionally demonstrate the powerful potential of neuroprosthetic rehabilitation applied in the chronic state of a severe SCI, i.e. several months post-injury.

These combined results confirm the ability of neuroprosthetic rehabilitation to re-establish supraspinal control of leg movement after a severe SCI, and expand its therapeutic potential to more clinically relevant lesions, settings, and outcomes. Our findings strongly suggest robot-assisted active training enabled by neuromodulation therapies as a suitable intervention to improve function after severe SCI in humans and as a prime candidate to reach clinical fruition on the fastest track possible.

7 Reorganization of corticospinal function increases recovery after lateralized spinal cord injury

Lucia Friedli[1], Ephron S. Rosenzweig[2], Quentin Barraud[1], Martin Schubert[3], Nadia Dominici[1], Lea Awai[3], Jessica L. Nielson[4], Pavel Musienko[1], Yvette Nout-Lomas[5], Hui Zhong[6], Sharon Zdunowski[6], Roland R. Roy[6], EMSCI Study Group[7], Sarah C. Strand[8], Leif A. Havton[9], Michael S. Beattie[10], Jacqueline C. Bresnahan[10], Adam R. Ferguson[4], V. Reggie Edgerton[6], Armin Curt[3], Mark H. Tuszynski[2], & Grégoire Courtine[1]

Manuscript submitted.

1. Center for Neuroprosthetics and Brain Mind Institute, School of Life Science, Swiss Federal Institute of Technology Lausanne (EPFL), Lausanne, Switzerland
2. Department of Neurosciences, University of California San Diego (UCSD), La Jolla, California, USA.
3. Spinal Cord Injury Center, Balgrist University Hospital, University of Zurich, Zurich, Switzerland.
4. Department of Neurosurgery, University of California San Francisco (UCSF), San Francisco, California, USA.
5. College of Veterinary Medicine and Biomedical Sciences, Colorado State University, Fort Collins, Colorado, USA.
6. Department of Integrative Biology and Physiology and Brain Research Center, University of California Los Angeles (UCLA), Los Angeles, California, USA.
7. European Multicenter Study about Spinal Cord Injury (EMSCI) study group.
8. California National Primate Research Center, University of California Davis (UCD), Davis, California, USA.
9. Department of Anesthesiology and Perioperative Care, University of California Irvine (UCI), Irvine, California, USA.
10. Brain and Spinal Injury Center, University of California San Francisco (UCSF), San Francisco, California, USA.

7.1 Summary

Background

Clinical observations suggest that functional recovery increases with the laterality of spinal cord injury (SCI). However, relationships between SCI laterality and recovery have never been established experimentally, and the underlying mechanisms remain unclear.

Methods

We studied relationships between functional recovery and SCI laterality in more than 400 quadriplegic patients. To monitor corticospinal tract reorganization, we applied transcranial magnetic stimulation over the motor cortex. We then modeled the most extreme lateralized SCI, termed Brown-Séquard syndrome, in cohorts of monkeys and rats using a lateral cervical hemisection. Kinematic and electromyographic analyses were conducted during locomotion and skilled hand manipulation to investigate recovery in animal models compared to Brown-Séquard patients. Bilateral corticospinal projections were examined in animal models, while motor cortex stimulation was performed both in animal models and Brown-Séquard patients.

Findings

Functional gains and recovery of muscle responses following motor cortex stimulation significantly increased with SCI laterality in quadriplegic patients. Hemisected monkeys and Brown-Séquard patients showed greater recovery than hemisected rats, both for locomotion and hand function. In hemisected monkeys, the spared dorsolateral column comprised corticospinal axons originating from left and right motor cortex. These axons exhibited a substantial growth across the spinal cord midline below the hemisection, and extensive sprouting into spinal territories containing deprived hand motoneurons. Due to their course in the dorsal column, corticospinal axons were permanently interrupted in hemisected rats. Multivariate analyses established correlations between corticospinal tract reorganization and functional recovery in humans and monkeys, but not in rats.

Interpretation

Emergence of spinal cord decussating corticospinal fibers and bilateral motor cortex projections during mammalian evolution supports greater recovery after lateralized SCI in monkeys and humans, but not in rats. Novel experimental models and dedicated therapeutic strategies are necessary to take advantage of this powerful neuronal substrate for recovery after SCI.

7.2 Introduction

Despite the regenerative failure of severed axons after spinal cord injury (SCI) (Ramon y Cajal, 1928; Aguayo *et al.*, 1991), partial lesions of the human spinal cord are associated with various degrees of spontaneous improvement in the control of arm and leg movements during the first months after injury (Levi *et al.*, 1996; Curt *et al.*, 2008). Clinical observations have suggested that the level of motor control asymmetry in the sub-acute phase of SCI influences the extent of functional recovery at chronic time-points (Brown-Sequard, 1868; Little & Halar, 1985; Roth *et al.*, 1991; Dlouhy *et al.*, 2013). Patients with the most asymmetrical deficits, which are largely determined by the laterality of spinal cord damage, generally exhibit greater functional gains compared to patients with more symmetrical deficits. However, direct relationships between the laterality of spinal cord damage and functional recovery have never been established experimentally in humans.

To address this issue conclusively, we compared the recovery profile of more than 400 quadriplegic individuals who suffered spinal cord damage covering the entire range of SCI laterality, from perfectly symmetrical deficits to impairments restricted to one side of the body. We show that spontaneous restoration of function gradually increases with the degree of asymmetry in early motor deficits.

We next studied the mechanisms underlying the superior recovery of function after lateralized spinal cord damage. Anatomically, the most salient feature of such injuries is the preservation of the main corticospinal tract on one side of the body. This component of the corticospinal tract runs in the dorsolateral column, and contains axons originating from both the left and right motor cortex (Rosenzweig *et al.*, 2009). A substantial number of these corticospinal axons decussate along the spinal cord midline below injury, providing an anatomical substrate for recovery (Rosenzweig *et al.*, 2010; Zaaimi *et al.*, 2012). We hypothesized that this peculiar architecture of the primate corticospinal system, together with the essential contribution of these inputs to motor control in humans (Lemon, 2008), are largely responsible for the greater recovery of function after lateralized spinal cord damage.

To test this hypothesis, we performed two comprehensive series of experiments in human patients and animal models. First, we monitored the reorganization of corticospinal tract function in quadriplegic patients using transcranial magnetic stimulation of the motor cortex. We predicted that patients with lateralized SCI would regain superior access to muscles below the lesion compared to patients with more symmetrical SCI.

Second, we modeled a lateralized SCI in experimental animals to study anatomical remodeling of corticospinal projections in conjunction with electrophysiological and functional assessments. Our aim was to establish translational syndromic structures (Ferguson *et al.*, 2013) between anatomical, electrophysiological, and functional metrics across animal models and human patients. To circumvent the issue of heterogeneous and uncharacterized damage in patients, we selected the most extreme type of lateralized SCI that produces a distinguishable functional deficit termed Brown-Séquard syndrome (Brown-Sequard, 1868). This rare medical condition results from a lateral hemisection SCI, and is clinically characterized by the complete loss of motor function on the ipsilesional side and deficits in pain and temperature sensation on the contralesional side (Brown-Sequard, 1868).

Lateral spinal cord hemisections accurately mimic Brown-Séquard syndrome in experimental animals (Courtine *et al.*, 2008; Rosenzweig *et al.*, 2010; Filli *et al.*, 2011). Here, we modeled a Brown-Séquard syndrome in both rhesus monkeys and rats. Contrary to humans and non-human primates, the rodent motor cortex near-exclusively projects to the contralateral side through the dorsal column. Consequently, a lateral hemisection SCI almost completely interrupts corticospinal input to the injured side. We hypothesized that corticospinal tract remodeling below a hemisection SCI would correlate with functional recovery in monkeys, but not in rats. This prediction implied that, contrary to the general consensus, hemisected rats would show less recovery than hemisected monkeys and Brown-Séquard patients, especially for motor functions heavily relying on corticospinal function.

7.3 Methods

Experimental animal models and human subjects

EMSCI database. Recovery of upper and lower limb function were analyzed in a total of 437 individuals who suffered a cervical SCI. All individuals were included in the EMSCI database (www.emsci.org). For each subject, we computed a laterality index that quantified the extent of asymmetry in functional deficits at 2 weeks post-SCI. This index was derived from the international standards for neurological classification of spinal cord injury (ISNCSCI), which combine both sensory (pinprick) and motoric (motor score) evaluations. Pinprick scores, which primarily evaluate the integrity of the spinally decussating spinothalamic tract, contributed to the contralateral sensory score. Motor scores were calculated, for each limb and side, as the combined ASIA motor scores of all the segments below the lesion. The segments C2 to T1 contributed to upper limb motor scores, while segments T2 and below contributed to lower limb motor scores. Sensory and motor scores were summed to generate a sensorimotor score for each limb and side. The laterality index was computed as the difference between left and right sensorimotor scores divided by their sum. Consequently, a value equals to 0 would correspond to perfectly symmetrical deficits. Instead, a value equals to 1 would corresponds to a pure Brown-Séquard syndrome. Functional recovery was computed as the relative increase in sensorimotor scores for each limb and side at 6 or 12 months compared to evaluations carried out at 2 weeks post-SCI.

Human subjects. We monitored recovery of motor functions in five patients who presented distinct lateralized sensorimotor deficits classified as Brown-Séquard syndrome. Five patients, three males and two females, met this criterion. Two of the male patients suffered traumatic SCIs at the C5 and C4 level that led to complete paralysis on one side of the body (**Figure 7.3a**). The third male patients suffered traumatic SCI at C6, but asymmetrical deficits were restricted to the legs. The two additional patients had experienced an ischemic injury at thoracic level Th5, and a disc prolapse at Th8, which led to laterality index of 0.65 and 0.50, respectively. These two patients had deficits restricted to the legs. The patients had not suffered from any other neurological disorder or pre-existing gait impairment. All patients followed a conventional SCI rehabilitation program. Recovery of complex motor functions was compared to the same recordings performed in a total of 33 healthy human subjects. The Swiss federal ethics committee approved all aspects of the study. All participants provided written informed consent.

Monkeys. A total of 16 male rhesus monkeys (Macaca mulatta) aged 5 -18 years (mean 9.6 ± 4.1 years) were studied. No effects of age were observed on any of the

variables reported herein. Four out of the 9 monkeys studied for functional evaluations were included in previous reports (Rosenzweig *et al.*, 2010; Nout *et al.*, 2012a; Nout *et al.*, 2012b) and have undergone new analyses that are the subject of the present study. Two monkeys could not be tested on the treadmill after the lesion. All surgical and experimental procedures in these experiments were carried out using the principles outlined by Laboratory Animal Care (National Institutes of Health Publication 85-23, revised 1985) and were approved by the Institutional Animal Care and Use Committee (IACUC) and the council on Accreditation of the Association for Assessment and Accreditation of Laboratory Animal Care (AAALAC).

Rats. A total of 30 female adult rats (Lewis) were studied (~220 g body weight). Animals were housed individually on a 12 h light/dark cycle, with access to food and water *ad libitum*. Temperature (22 ± 1 °C) and humidity (40 - 60 %) in the animal facilities were maintained constant in accordance to Swiss regulations for animal housing. The Veterinarian Office of the Cantons of Zurich and Vaud, Switzerland approved all aspects of the study.

Rehabilitation after SCI. Human patients followed a conventional rehabilitation program. Both rats and monkeys were trained to step on a treadmill and to retrieve objects with their hand 3 times per week for 20 minutes per task.

Experimental surgical procedures

EMG Electrodes. All surgical procedures used have been described previously (Courtine *et al.*, 2009a; Rosenzweig *et al.*, 2010; Musienko *et al.*, 2011c). Under aseptic conditions and general anesthesia (1-2.5% Attane Isoflurane, Piramal Healthcare Limited, Mumbai, India), both rats and monkeys received bipolar intramuscular EMG electrodes (AS632, Cooner Wire, Chatsworth, CA, USA) into selected hindlimb and forelimb muscles. The electrodes were connected to a head-mounted connector in rats, and an implanted recording system in monkeys (Konigsberg Instruments, Pasadena, CA, USA). In subsets of rats and monkeys, the following muscles were implanted: soleus and tibialis anterior for both hindlimbs; the biceps brachii, triceps brachii, extensor digitorum communis and flexor digitorum profundis of the ipsilesional forelimb. The ipsilesional pollicis brevis profundus also was implanted in monkeys. The proper location of EMG electrodes was verified post-mortem. Analgesia and antibiotics were provided post-surgically under monitoring of certified veterinaries.

Cortical electrodes. A subset of rats (n = 8) was implanted with an epidural monopolar electrode over the hindlimb area of the contralesional motor cortex to deliver

stimulation. A reference electrode was positioned near the shoulder girdle (van den Brand *et al.*, 2012).

Lesion. After completion of pre-injury behavioral recordings, a second surgery was performed. A partial laminectomy followed by a lateral hemisection of the spinal cord was made at the C7 spinal segment. In both rats and monkeys, a surgical micro-knife was mounted on a stereotaxic arm, positioned at the spinal midline and midway between the C5 and C6 dorsal laminae. This rostrocaudal position corresponds to the C7 spinal cord segment, as previously described(Rosenzweig *et al.*, 2010). A micro-scissor was used several times to cut all the entire grey and white matters lateral to the inserted micro-knife. Two monkeys received the lateral hemisection using the same technique but at T10 spinal segment. For all the experimental subjects, the segment containing the lesion was reconstructed using continuous series of Nissl stained sections. The lesion area was delimited for each section, and the area of maximum damage projected into a plane to obtain a reconstruction of the lesion extent (**Supplementary Figure 1d,e**).

Behavioral testing tasks

Locomotion. Rats, monkeys, and humans were tested on a motorized treadmill over a range of speeds. A Plexiglas enclosure was used to maintain the rats and monkeys in position while enabling kinematics recordings of the stepping performance. Food reward was used for positive reinforcement. The more comfortable speed to obtain consistent stepping patterns over the entire course of the recovery was selected for further analysis. This corresponded to 9 cm/s in rats, 0.47 m/s in monkeys, and 4 km/h in humans. A total of 10 consecutive steps were recorded and extracted for further analysis. To evaluate skilled locomotion, rats (n=9) and human subjects (n=5 patients; n=4 healthy control subjects) were instructed to walk along a horizontal ladder with evenly spaced rungs. Ten successive trials along the ladder were performed.

Hand function. To examine manual dexterity, a skilled motor task thought to reflect the functional integrity of corticospinal projections to the hand musculature was used. Rats and monkeys were trained over several subsequent sessions to retrieve food rewards from a stick until they reached a stable performance. Monkeys and human subjects were instructed to retrieve a grape, while the rats were presented with a 2 mm piece of chocolate. Monkeys and human subjects were seated. Rats were standing quadrupedally. The subjects were requested to perform 10 trials, and the number of successful food retrievals was recorded for each session.

Time-points. Both rats and monkeys were recorded prior to the lesion, and at regular intervals post-lesion until 2 or 6 months post-injury, respectively. At this stage,

both rats and monkeys had reached a plateau, i.e., when no or limited improvements occur (Courtine *et al.*, 2008; Rosenzweig *et al.*, 2010). To compare rats, monkeys, and humans at comparable time-points, we focused the analysis on three salient time-points: pre-lesion, early, and chronic. Early corresponded to the time when the subjects could locomote on the treadmill despite paralysis of the ipsilesional limbs, and could reach the food reward with the ipsilesional limb, but failed to retrieve the item. In humans, recordings at chronic time-points were obtained between 8 and 12 months post-SCI.

Data acquisition and analysis

Kinematics and electromyographic recordings. Bilateral leg or unilateral arm kinematics were recorded using 12 infrared motion capture cameras (200 Hz; Vicon) in rats and humans, and 4 TV cameras (100 Hz, Basler Vision Technologies) for monkeys. Reflective markers were attached to the shaved skin of rats and humans overlying leg or arm landmarks for locomotion and hand function assessment, respectively. Reflective painting was used for monkeys. The landmarks for the legs were the iliac crest, greater trochanter, knee joint, malleolus, fifth metatarsal, and outside tip of the fifth or fourth digit. The landmarks for the arm were the anterior border of the scapula, head of the humerus, elbow joint, distal head of the ulna, metacarpo-phalangeal joint, and outside tip of the third digit. The body was modeled as an interconnected chain of rigid segments, and joint angles generated accordingly. In humans, bipolar surface electrodes (one cm diameter, electrode separation of one cm) connected to a wireless transmitter (Myon) were placed over leg (medial gastrocnemius, soleus, tibialis anterior) and arm (biceps brachii, triceps brachii, extensor digitorum communis and flexor digitorum superficialis) during locomotor and hand function assessments, respectively. A ground electrode was placed on the wrist. In all the species, signals were sampled at 2 kHz, amplified, band-pass filtered (10-1000 Hz), stored, and synchronized on-line (Vicon Nexus) or off-line (SIMI) for kinematics analysis.

Electrophysiological recordings. In rats, access of the motor cortex to leg motoneurons was tested under fully awake conditions while the animals were suspended in a harness. Five trains of stimuli (0.2 ms, 10 ms pulse length, 300 Hz, 0.5-1.5 mA) and 5 single pulses (0.2 ms, 0.5-1.5 mA) were delivered through the chronically implanted cortical electrode. The same rats were tested prior to the lesion and weekly after the lesion for 2 months. Stimulation bouts were separated by 90 sec. In humans, transcranial magnetic stimulation (TMS) was applied over the leg area of the motor cortex. The coil was positioned over the location eliciting the largest possible responses in the leg muscles, which corresponded to Cz(Schubert *et al.*, 1997). After establishing the

positioning of the coil, a recruitment curve was performed until reaching 100% of the output. In both rats and humans, peak-to-peak amplitude and latency of evoked responses were computed from EMG recordings from the left and right tibialis anterior muscles.

Gait data analysis. A minimum of 10 step cycles was extracted from a continuous bout of stepping on the treadmill for each experimental condition and subject. A total of 99 parameters quantifying gait and kinematics features were computed for each limb and gait cycle according to methods described in detail previously (Courtine *et al.*, 2008; Courtine *et al.*, 2009a; Musienko *et al.*, 2011c; Dominici *et al.*, 2012b). These parameters provide a comprehensive quantification of gait pattern characteristics ranging from general features of locomotion to fine details of individual limb motion. The 103 computed parameters are listed in **Supplementary Table 7.1**. For the ladder, 20 step cycles were extracted for analysis. Additional parameters related to the positioning of the foot with respect to the successive rungs of the ladder were calculated to assess the precision of foot placement during gait (Dominici *et al.*, 2012b). A PC analysis was applied on all computed parameters with two objectives: (i) assess the degree of locomotor recovery compared to pre-lesion or healthy subjects (Dominici *et al.*, 2012b), and (ii) extract, for each limb and species, the most relevant parameters to account for lesion-induced changes in ipsilesional and contralesional leg movements (Beauparlant *et al.*, 2013). For each species, all computed parameters were centered and reduced to obtain dimensionless values ranging from -1 to 1. PC analysis was applied on the normalized parameters for each species and for all species combined. Averaged scores for each limb and conditions were extracted and the relative degree of functional recovery was measured as the 3-D distance between pre- and post-lesion (early and chronic) data points in the space created by PC1-3 (Dominici *et al.*, 2012b). Parameters with high factor loadings (|value| > 0.5) on PC1 and PC2 were extracted and regrouped into functional clusters (Beauparlant *et al.*, 2013).

Hand function data analysis. For each species and time-points, kinematics and EMG data were extracted from 5 representative reaching movements. The trajectory of the hand was segregated into the different phases of the movement: start, reach, grasp, retrieval, and end. To compute the consistency of limb endpoint trajectories, we applied a PC analysis on the 3-D coordinates of the hand marker during the reach phases of all trials. The consistency of limb endpoint trajectories was calculated as the percent of variance explained by the first PC. The degree of co-contraction between proximal and distal pairs of antagonist muscles was measured as the percentage of overlapping area between two EMG traces (Winter, 1990). EMG signals were rectified and filtered with a

4th order zero-phase shift Butterworth filter with a cut-off frequency of 30 Hz. The co-contraction Index between pairs of antagonist muscles (EMG1, EMG2) during reaching and grasping was computed as follows:

$$\text{Co} - \text{contraction Index} = 2 * \frac{\int \min[\text{EMG1(t)}, \text{EMG2(t)}]\,\text{dt}}{\int \text{EMG1(t)dt} + \int \text{EMG2(t)dt}}$$

Where EMG1 and EMG2 are the EMG activity of flexor and extensor muscles normalized to the maximum value observed during the movement, while min denotes the minimum between the activity of both muscles at time t.

Anatomical procedures

Tracing. Rats and monkeys underwent anterograde tracing of corticospinal projections from both left and right motor cortexes using tracers. All animals were anesthetized deeply as reported above. In monkeys biotinylated dextran amine (BDA; 10% solution in H_20; 10,000 molecular weight; 150nl/site; Molecular Probes) was injected into 127 sites spanning the arm, trunk, and leg regions of the right motor cortex. Dextran-conjugated Alexa488 (D-A488) was injected using the same methods into the corresponding coordinates in the left motor cortex. The two monkeys with thoracic hemisection also received unilateral infusion of the retrograde tract tracing Fastblue (2% in 0.1M phosphate buffer and 2% dimethyl sulfoxide, EMS-CHEMIE, Germany) into L2-L3 spinal segments. A total of 2.1 µl was pressure-injected over 7 sites (depth, 4.0 mm; space between injections, 1mm). Seven weeks later, monkeys were anesthetized deeply and perfused transcardially with a 4% solution of paraformaldehyde. For rats, BDA (10% solution in H_20; 10,000 molecular weight; 500nl /site) was injected into 10 sites spanning the forelimb, trunk, and hindlimb regions of the right or left motor cortex. Three weeks later, rats were anesthetized by an intraperitoneal injection of 0.5 ml sodium pentobarbital (50 mg/mL) and perfused transcardially with approximately 80 ml Ringer's solution containing 100'000 IU/L heparin (Roche) and 0.25% $NaNO_2$ followed by 300 ml of cold 4% phosphate buffered paraformaldehyde, pH 7.4, containing 5% sucrose. Our standard protocols were used to detect traced corticospinal fibers and 5-HT fibers using goat anti-5-HT antibodies for monkeys (Immunostar; 1:10,000 in TBS-X) and rabbit anti-5-HT antibodies for rats (Sigma Aldrich; 1:5000 in blocking solution containing 4% NGS) (van den Brand *et al.*, 2012). When appropriate, traced corticospinal fibers were co-labeled with the synaptic protein synaptophysin using mouse anti-synaptophysin antibodies (Millipore; 1:1000 in blocking solution containing 4% NGS) or the vesicular transporter of glutamate (vGlut1) using guinea pig anti-vGlut1 antibodies (Millipore; 1:2000 in blocking solution containing 2% NGS).

Tissue processing. The spinal cord dura was removed and the spinal cord was cut in the transverse plane into blocks, using the nerve roots as a guide for the spinal levels. The block containing the lesion was sectioned in the horizontal plane on a freezing microtome or a cryostat set at 30 µm intervals. Analogous blocks were obtained from the intact animals. Blocks containing segments C3-C6 and C8-T2 were sectioned in the transverse plane on a freezing microtome or a cryostat set at 40 µm. Cut tissue sections were stored at -20°C for monkeys and at 4°C for rats in cryoprotectant (25% glycerin, 30% ethylene glycol in 0.5 M phosphate buffer). Lesion extent was assessed using a 30-µm-thick horizontal section stained for Nissl substance. Transverse sections from the tissue blocks immediately rostral and caudal to the lesion block (segments C3-C4 and C8-T1) were selected for analysis of corticospinal tract and 5-HT fiber density. Our standard protocols were used to detect traced corticospinal fibers (Rosenzweig *et al.*, 2010; van den Brand *et al.*, 2012) and 5-HT fibers using goat anti-5-HT antibodies for monkeys (Immunostar; 1:10,000 in TBS-X) and rabbit anti-5-HT antibodies for rats (Sigma Aldrich; 1:5000 in blocking solution containing 4% NGS).

Quantification. Image capture and manipulation were performed as described previously (Rosenzweig *et al.*, 2010; van den Brand *et al.*, 2012). For corticospinal fiber density quantification each of 3 sections for monkeys and 5 sections for rats were randomly selected per animal. The fiber density of the gray matter were obtained using confocal stacks per animal acquired with standard imaging settings and analyzed using custom-written Matlab (MathWorks) scripts according to previously described methods (van den Brand *et al.*, 2012). Additionally, the number of labeled axons crossing the spinal cord midline was counted manually in each section used for the fiber density analysis. For 5-HT quantification of monkey sections, Stereo Investigator was used to outline lateral motor pools under low magnification and generate optical fractionator sampling sites. With a 100x objective, intersections of 5-HT-labeled axons with the inclusion lines of these sampling sites were marked. For rats, the same regions were quantified using the same methods as described for corticospinal tract axons. Serial reconstructions of some CST axons were performed as described previously for both monkey and rat sections below the level of injury (Rosenzweig *et al.*, 2010; van den Brand *et al.*, 2012). All the evaluations were performed by an investigator who was blind to experimental conditions.

Syndromic analysis

To evaluate the effect of species on the integrated syndromic outcome after SCI (Ferguson *et al.*, 2013), we harnessed non-linear principal components analysis (NLPCA). This method uses a combination of optimal scaling and variance-maximization procedures to detect coherent patterns in data involving linear or non-linear relationships (Linting *et al.*, 2007). We performed separate NLPCA extractions for rat-monkey and rat-human data using variable subsets that allowed direct cross-species comparisons. Datasets from kinematics, food-retrieval success, and anatomical measures were manually curated and combined into a single large dataset for monkeys and rats. Treadmill and ladder locomotion kinematics and neurophysiological measures were combined from human and rat data. Bivariate correlation matrices were created for each combination of outcomes. Syndromic analysis was performed in SPSS Categories v.1.9, to generate syndromic variables (PC1-2) specific to either rat-monkey or rat-human comparisons. PC1 is the shared variance (%) of all measures as they move together in a multivariate space, with each measure loading (weighted arrows) onto PC1 based on their respective correlation to the entire syndrome (PC1, **Figure 7.6c,d**).

Statistics analysis

All data are reported as mean values ± s.e.m. Statistical evaluations were performed using one-way ANOVA for neuromorphological evaluations, one-way repeated-measures ANOVA for functional assessments, and unpaired two-tailed t-tests for syndromic analysis. Tukey's post-hoc test was applied when appropriate.

7.4 Results

Functional recovery correlates with SCI laterality

We implemented the international standards for neurological classification of spinal cord injury (ISNCSCI) to conduct a repeated prospective assessment of functional recovery during 1 year after an incomplete (ASIA-C or above) cervical SCI in 437 patients **(Figure 7.1**). To determine the relative degree of SCI laterality, we computed a laterality index based on the relative difference between left and right sensorimotor scores evaluated at 2 weeks after SCI (See Methods). The laterality index ranged from 0 (symmetric injury equally affecting both sides of the body) to 1 (asymmetric injury affecting one side of the body). More than 80% of analyzed patients reached laterality values below 0.4 (**Figure 7.1B**), indicating bilateral and symmetrical functional impairment. Only 4 out of the 437 studied patients presented clinically a pure Brown-Séquard syndrome with predominant unilateral motor deficits and crossed spinothalamic impairment (**Figure 7.1B**). Magnetic resonance imaging in these patients revealed white matter sparing restricted to one side of the spinal cord, as expected based on functional deficits (**Figure 7.1A** and **Supplementary Figure 7.1F**).

To assess whether SCI laterality influenced recovery, we computed the relative gains in left and right motor scores between early (2 weeks) and chronic (6 to 12 months) time-points after injury. We found that improvements of motor function gradually increased with SCI laterality ($p < 0.0001$; **Figure 7.1C**). Patients with a laterality index above 0.6 ($n = 21$, 5.8%), who were clinically classified with a Brown-Séquard syndrome, regained extensive bilateral motor capacities. These results demonstrate that functional recovery increases with SCI laterality.

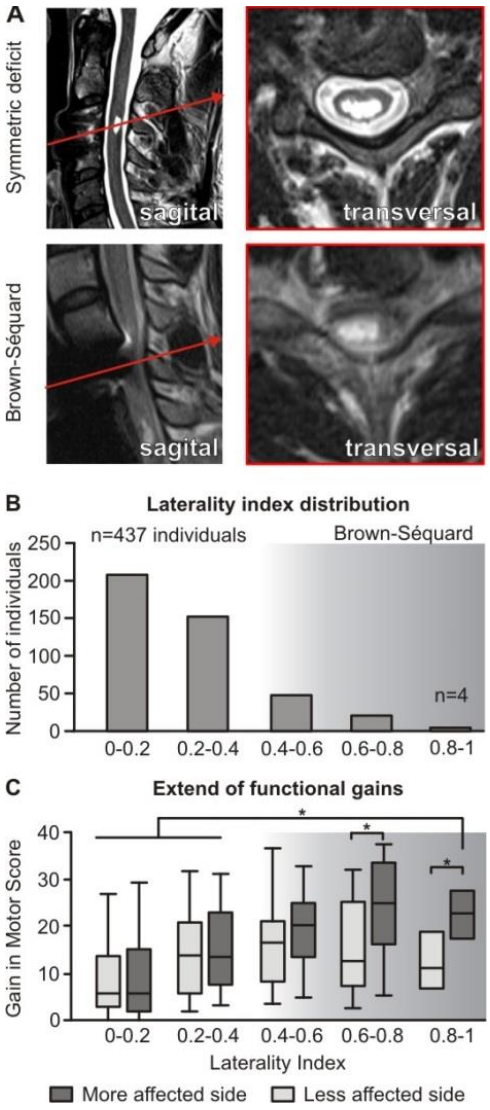

Figure 7.1 Functional recovery correlates with SCI laterality in humans.
(A) MRI picture representing a symmetrical and a lateralized SCI. **(B)** SCI Laterality was defined as the relative difference between motor scores (ASIA) of the left and right sides, termed laterality index. The histogram plot reports the distribution of this laterality index across a population of 437 individuals with a cervical SCI (EM-SCI platform). The shaded area indicates individuals clinically classified with a Brown-Séquard syndrome. **(C)** Histogram plots reporting, for each range of laterality index, the mean gain in upper and lower motor scores in the chronic compared to sub-acute stage of SCI. The horizontal bars report the median. The upper and lower bars correspond to the 75% and 25% percentile of data, while the error bars correspond to the 90% and 10% percentile of the data. * indicates significant differences at $p < 0.05$ compared to non-marked conditions.

Recovery of cortical access to motor pools below lesion increases with SCI laterality

We monitored the recovery of motor responses in ankle flexor muscles following transcranial magnetic stimulation applied over the motor cortex in 34 quadriplegic

patients (**Figure 7.2A**). For patients with symmetric functional deficits, gains in motor response amplitude at chronic time-points were generally proportional to the amplitude of responses measured at early time-points (**Figure 7.2C**). Brown-Séquard patients with laterality index superior to 0.6 displayed a near complete suppression of motor responses in ankle flexor muscle of the more affected side at early time-points (**Figure 7.2B**). Substantial motor responses progressively reappeared in these muscles during recovery, which correlated with significantly larger relative gains in motor response amplitude compared to patients with more symmetrical lesion at chronic time-points ($p < 0.05$, **Figure 7.2B,C**). The latency of motor responses was significantly prolonged on the more affected side (21.35 +/- 0.12 ms) compared to the less affected side (15.7 +/- 0.84 ms, $p<0.05$, **Figure 7.2D**). No significant differences were found in the latencies of motor responses from left and right muscles in patients with more symmetrical spinal cord damage.

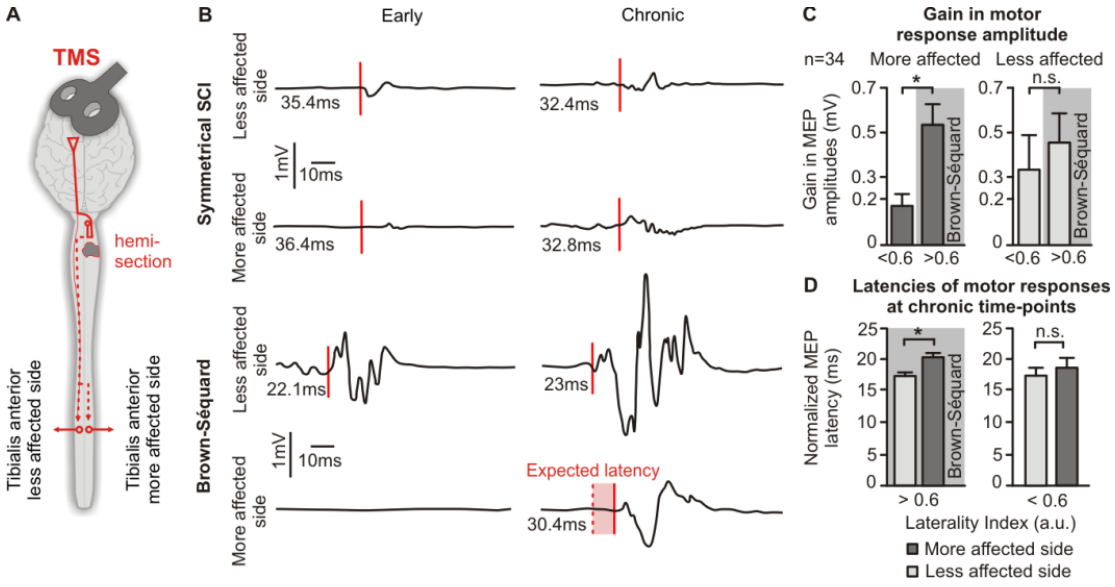

Figure 7.2 Recovery of motor responses in leg muscles following motor cortex stimulation
(A) Schematic overview of experiments recording motor responses in the left and right tibialis anterior in response to transcranial magnetic stimulation applied to the motor cortex. **(B)** Representative traces of motor responses from left and right tibialis anterior obtained at early and chronic time points after SCI for a patient with a symmetrical SCI and a Brown-Séquard-Syndrome. **(C)** Histogram plots reporting mean gains in the amplitude of motor responses on the more and the less affected leg in patients with high and low lateralized SCI. **(D)** Bar plots reporting the mean values of motor response latency at chronic time-points on the more affected compared to the less affected side for both high and low laterality patients. * denote conditions that were significantly different at $p < 0.05$. Error bars, s.e.m.

Clinical cases and animal models of Brown-Séquard syndrome

The extensive recovery of motor responses in leg muscles in Brown-Séquard patients suggested that corticospinal tract reorganization contributes to superior recovery after lateralized SCI. To test this hypothesis, we placed a C7 lateral hemisection SCI in rhesus monkeys and rats. This lesion replicates a Brown-Séquard syndrome in animal models (Rosenzweig *et al.*, 2010; Filli *et al.*, 2011). We performed standardized kinematic and muscle activity recordings to study the recovery profile of animal models compared to 5 patients with a thoracic or cervical Brown-Séquard syndrome. All the patients showed distinct unilateral motor impairments in segments below the lesion at early time-points (**Supplementary Figure 7.1A**).

Greater recovery of locomotor function in monkeys and humans compared to rats

At early time-points, hemisected rats and monkeys essentially dragged their ipsilesional leg on the treadmill (**Figure 7.3A,B**). Because hemiplegic patients could not step independently, we utilized the gait orthosis Lokomat to rhythmically move the left and right legs along pre-defined foot trajectories (**Figure 7.3C**). Despite stepping-like movements, ipsilesional ankle muscles remained quiescent while contralesional muscles displayed robust and alternating bursts of activity (**Figure 7.3A-C**). At chronic time-points, all the studied subjects regained plantar steps on the ipsilesional leg (**Figure 7.3A-C**). However, specific features of locomotion remained clearly impaired. To quantify these residual deficits, we computed a larger number of variables providing objective measurements of bilateral gait features (Courtine *et al.*, 2009b) (n = 101, **Supplementary Table 7.1**), and submitted all the variables to a principal component (PC) analysis (Dominici *et al.*, 2012b). We found that a Brown-Séquard syndrome alters the same variables in rats, monkeys, and humans (**Supplementary Figure 7.2A-C**). However, rats retained significantly more pronounced deficits at chronic time-points compared to monkeys and humans ($p<0.05$ for most comparisons with monkeys and humans, **Supplementary Figure 7.3D**). For example, all the studied species exhibited a significantly longer swing phase duration on the ipsilesional leg compared to the contralesional leg ($p < 0.05$, **Supplementary Figure 7.3D**, top). Prolonged swing duration is well-documented in hemi-paretic patients with unilateral SCI (Courtine *et al.*, 2005) or stroke (Chen *et al.*, 2005). However, this asymmetry was markedly superior in rats (36%, $p <0.001$) compared to monkeys (25%, $p < 0.05$), and even more compared to patients (4%, $p <0.05$).

To directly compare gait recovery between rats, monkeys, and humans, we normalized all the computed variables to intact values for each species, and applied a PC

analysis on all the normalized datasets simultaneously (**Figure 7.3D**). Gait clusters related to chronic time-points occupied significantly more distant locations to intact gait clusters in rats compared to both monkeys and humans ($p < 0.05$, **Figure 7.3E**). This analysis demonstrates that monkeys and humans show a greater recovery of gait compared to rats after a Brown-Séquard syndrome.

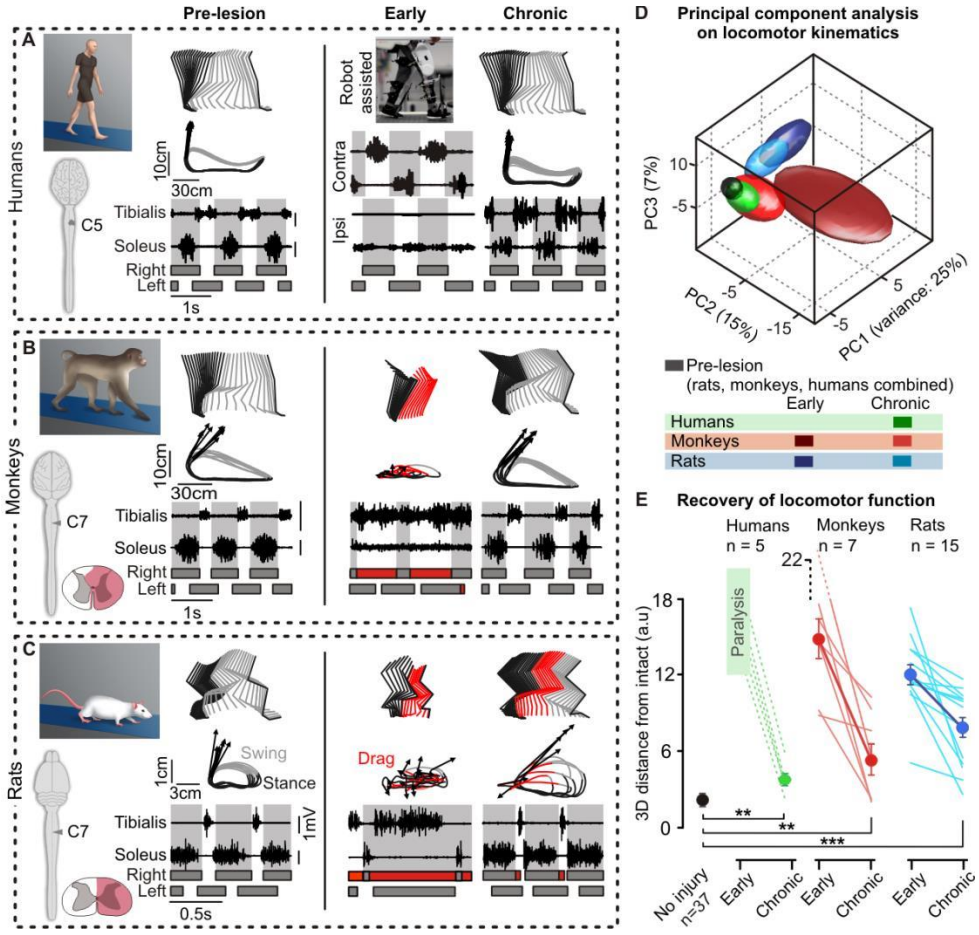

Figure 7.3 Patients and monkeys show greater recovery of locomotion compared to rats.
(A-B) Stick diagram decomposition of lower limb motion during stance (black) and swing (blue) together with successive limb endpoint trajectories during locomotion on a treadmill. The vectors indicate the direction and amplitude of foot acceleration at swing onset. The EMG activity recorded from the soleus and tibialis anterior muscles is shown at the bottom. The shared areas indicate the duration of the stance phases. Representative data are shown for human patients (**A**), monkeys (**B**), and rats (**C)** before the injury (or healthy), and at early and chronic time-points post-SCI. To monitor bilateral EMG activity in hemiplegic patients at early time-points, we used the gait orthosis *Lokomat* that moved both legs in a rhythmic and alternated fashion. (**D)** PC analysis was applied on dimensionless variables (n = 101) characterizing locomotor kinematics of rats, monkeys, and humans. Least-squares spheres are traced to identify gait clusters, and thus emphasize time- and species-dependent gait recovery. (**E)** Individual (lines) and averaged (+/- s.e.m.) 3D distances between non-injured gait clusters, and those measured at the early and late time-points (a.u., arbitrary units). **, *** denote conditions that were significantly different at $p < 0.01$ and $p < 0.001$, respectively. Error bars, s.e.m.

Difference in gait recovery was even more striking during more challenging conditions such as traversing a horizontal ladder. The five Brown-Séquard patients executed this task with 100% success without prior practice (**Supplementary Figure 7.3A**). In contrast, rats failed to position their ipsilesional hindpaw onto the regularly spaced rungs of the ladder ($p < 0.0001$, **Supplementary Figure 7.3B**). Brown-Séquard patients performed well on the horizontal ladder despite the use of distinct gait strategies compared to healthy subjects ($p < 0.05$, **Supplementary Figure 7.2C,D**). Monkeys were not tested on this task.

Extensive recovery of hand function in monkeys and humans, but not in rats

Non-injured rats, monkeys, and humans employed similar motor control strategies to retrieve food items with the hand. All the subjects activated extensor digit muscles to open the hand during reaching, and flexor digit muscles to close the hand during retrieval (**Figure 7.4 and Supplementary Figure 7.4**).

Patients with a cervical Brown-Séquard syndrome, who had completely lost ipsilesional hand function at early-time points, performed this task with 100% success (**Figure 7.4A**). In both monkeys and rats, the hemisection resulted in loss of detectable function and muscle activity in the ipsilesional hand immediately post-injury ($p < 0.001$, **Figure 7.4B-C**). Over time, hemisected monkeys regained the capacity to recruit extensor and flexor digit muscles reciprocally ($p < 0.01$, **Figure 7.4B** and **Supplementary Figure 7.4E,H**), which paralleled extensive recovery of object retrieval ($p < 0.01$, **Figure 7.4E**). The improved performance in monkeys was often accompanied by a change in reward retrieval strategy, including grasping between the fingers and the palm of the hand in a subset of monkeys (Nout *et al.*, 2012b). In contrast, all the hemisected rats permanently lost the ability to retrieve any item with the hand (**Figure 7.4A,D**). Rats produced highly variable hand trajectories ($p < 0.01$) and disorganized muscle activation patterns of muscles ($p < 0.01$, **Figure 7.4A** and **Supplementary Figure 7.4D,G**).

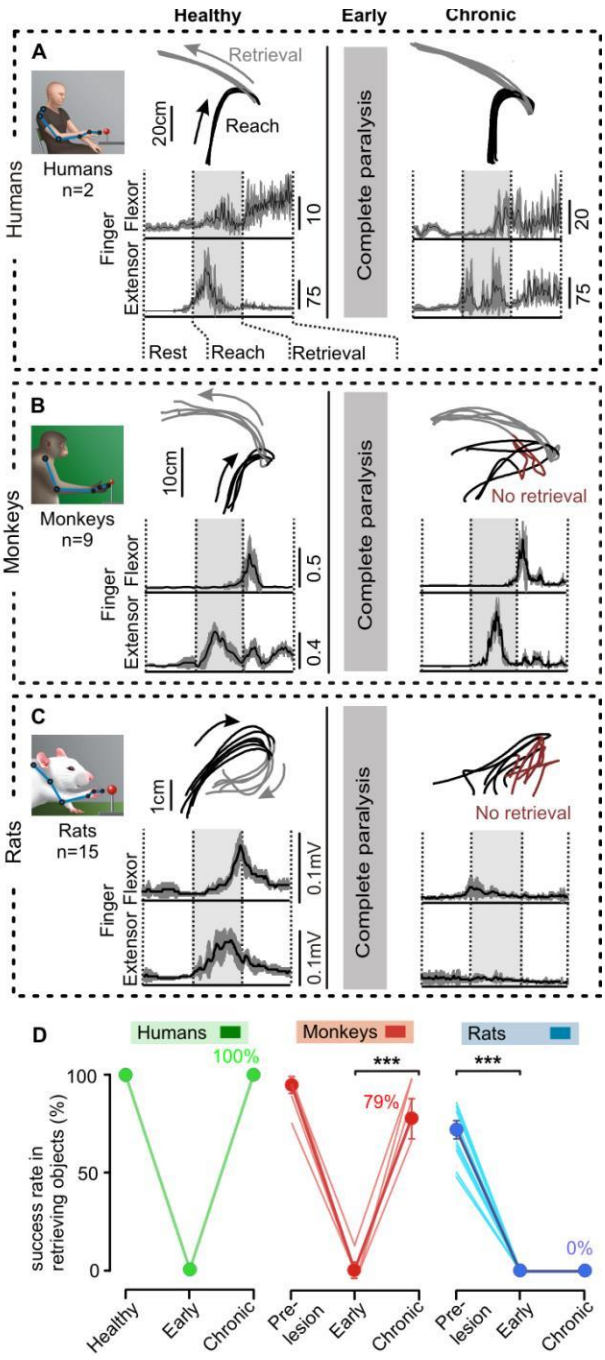

Figure 7.4 Monkeys and humans show greater recovery of hand function compared to rats. (A-C) Limb endpoint trajectories of upper limb motion during reach (black) and retrieval (grey). Failure of item retrieval are displayed in dark red, seen post-SCI in rats and monkeys but not in human patients. The averaged (+/- s.e.m.) EMG activity recorded from the extensor digitorum communis and flexor digitorum muscles is shown during successive retrievals before the injury (or healthy) and chronic time-points post-SCI in human patients **(A)**, monkeys **(B)**, and rats **(C)**. **(D)** Mean success in hand use reported as a percent of successful food retrieval trials (+/- s.e.m.) in humans, monkeys and rats. ** denote conditions that were significantly different at $p < 0.01$. Error bars, s.e.m.

Extensive corticospinal tract reorganization below injury in monkeys, but not in rats

We next investigated reorganization of axonal projections from the corticospinal tracts in both animal models. Corticospinal fibers were labeled with stereotaxic injections of anterograde tracers in the left and right motor cortex (**Figure 7.5A, B**). We compared corticospinal projection patterns in rats and monkeys sacrificed at early (n = 8 rats and 3 monkeys) or chronic (n = 7 rats and 9 monkeys) time-points after SCI.

As observed in humans, intact monkeys showed extensive bilateral axonal projections from motor cortex to cervical spinal segments (Rosenzweig *et al.*, 2009) (**Supplementary Figure 7.1B**). The majority of corticospinal tract fibers projected through the dorsolateral columns. Consequently, the lateral hemisection spared a substantial number of corticospinal axons originating from both the left and right motor cortex (**Figure 7.5C**). In rats, the vast majority of corticospinal fibers decussated at the level of pyramids, extended rostrocaudally in the dorsal column (**Supplementary Figure 7.1C**), and projected contralaterally in the dorsal and intermediate laminae of spinal segments (**Figure 7.5D**). Therefore, the lateral hemisection interrupted nearly all the axonal projections from the contralesional motor cortex (**Figure 7.5D**).

We first analyzed the projection patterns of corticospinal fibers originating from the motor cortex contralateral to the hemisection. Monkeys exhibited a significant increase in the number of corticospinal axons decussating the spinal cord midline below the lesion at chronic compared to early time-points ($p < 0.05$, **Figure 7.5G**), which was not present in hemisected rats (**Figure 7.5H**). These axons displayed increased density in the ventral horn of spinal segments containing deprived motor pools innervating hand muscles ($p < 0.05$, **Figure 7.5C,G**). This sprouting reconstituted a large proportion of intact corticospinal fiber density in hemisected monkeys, which contrasted with the near complete depletion observed in hemisected rats ($p < 0.0001$, **Figure 7.5D,H**).

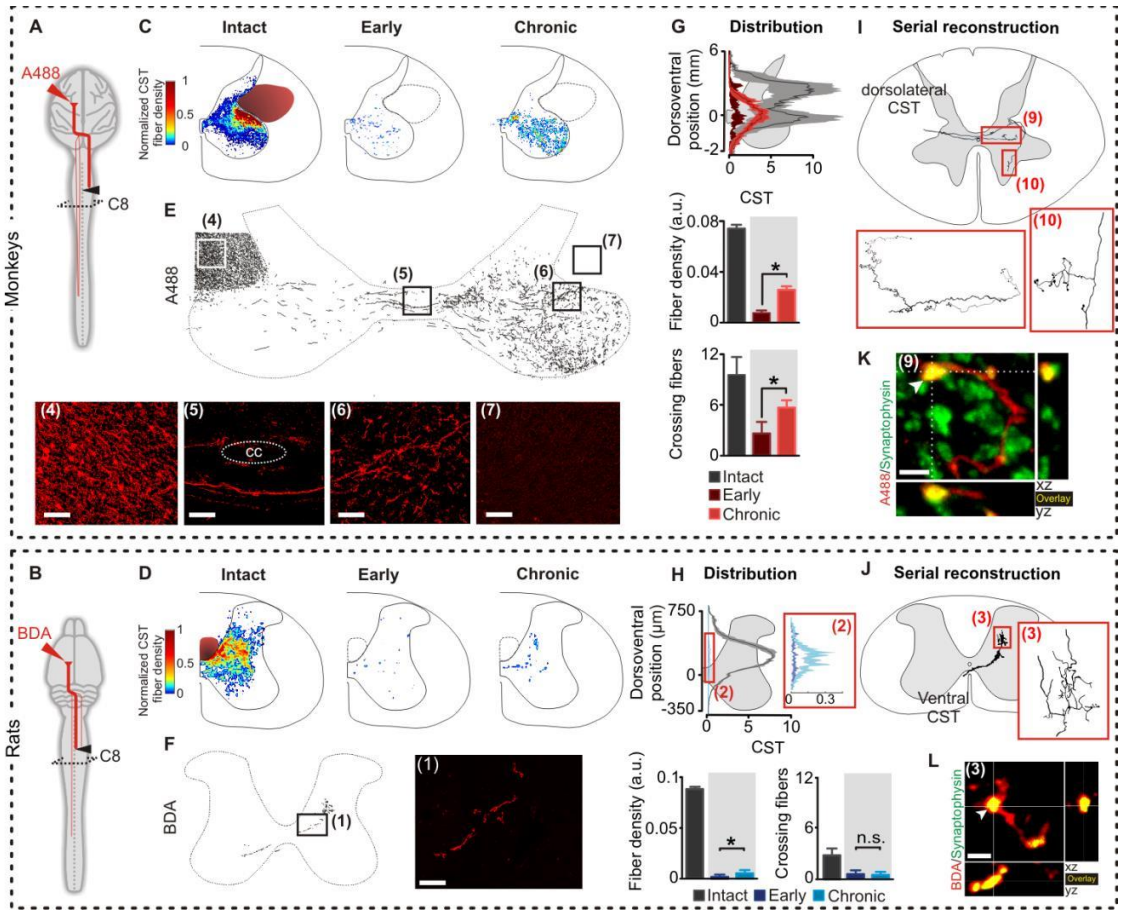

Figure 7.5 Monkeys show greater reorganization of corticospinal tract fibers compared to rats. **(A, B)** Diagram illustrating anatomical experiments and analyzed regions in monkeys and rats. **(C,D)** Heat maps and (**E, F**) representative photographs and reconstruction taken from highlighted areas, showing compensatory sprouting of spared corticospinal axons in sub-lesional segments (CC, central canal). Scale bar, 100 µm for monkeys and 40 µm (insets: 10 µm) for rats. **(G, H)** Fiber density distribution and histogram plots showing ipsilesional corticospinal axon density at C8, below the hemisection, in intact animals, and at early and chronic time-points post-SCI (a.u., arbitrary units), and histogram plots reporting the averaged number of corticospinal fibers crossing the spinal cord mid-line per analyzed C8 section. **(I,J)** Serial reconstruction of a single corticospinal axon, including detailed insets. Corticospinal fibers originated from the left contralesional dorsolateral columns in monkeys, and from the left contralesional ventral corticospinal in rats. In both species, corticospinal fibers crossed the spinal cord midline below the hemisection, but the number of fibers was substantially larger in monkeys than rats, as illustrated in the photographs. **(K, L)** Representative photographs showing 3D co-localization of D-A488 and synaptophysin in monkeys and BDA and synaptophysin in rats, which demonstrate the presence of synaptic terminals onto corticospinal fibers below hemisection. Scale bar, 2 µm and 4 µm for monkeys and rats, respectively. *, denote significant difference at $p < 0.05$. Error bars, s.e.m.

Serial fiber reconstructions revealed that axonal projections detected below the hemisection arose from the contralateral side. Specifically, corticospinal fibers originated from the dorsolateral column in monkeys (**Figure 7.5I**), and the ventral component of the corticospinal tract in rats (Weidner *et al.*, 2001) (**Figure 7.5J**). These corticospinal axons established synapses, as they co-localized with synaptophysin (**Figure 7.5K,L**). In

hemisected monkeys, spinal cord midline crossing corticospinal fibers established synaptic contacts with descending projection neurons connected with lumbar segments (**Supplementary Figure 7.5**). Analysis of corticospinal axon density at C5-C6, above the lesion, also revealed an increased density at chronic compared to early time-points in rats and monkeys ($p<0.05$ in rats; $p=0.10$ in monkeys; **Supplementary Figure 7.6**).

We next analyzed the projection pattern of corticospinal fibers originating from the motor cortex ipsilateral to the hemisection (**Supplementary Figure 7.7**). In both rats and monkeys, axons originating from the right motor cortex decussated at the level of pyramids, and then re-crossed the spinal cord midline below the hemisection. We found that these fibers exhibited significantly increased density in deprived segments for animals sacrificed at chronic compared to early time-points ($p < 0.05$, **Supplementary Figure 7.7**). Importantly, remodeling of spared axons did not occur in all descending projection neurons: the density or distribution of serotonergic axons in cervical segments caudal to the hemisection did not change in either rats or monkeys (**Supplementary Figure 7.8**). These anatomical evaluations reveal that both rats and monkeys exhibit multi-level reorganization of bilateral corticospinal projections after hemisection, but only monkeys show growth of corticospinal fibers across the spinal cord midline, and extensive sprouting of these fibers into deprived spinal segments below the hemisection.

Recovery of cortical access to leg motor pools in humans, but not in rats

The limited plasticity of corticospinal fibers below the hemisection suggested that, contrary to humans (**Figure 7.2**), rats would not regain motor responses in leg muscles following motor cortex stimulation. To test this hypothesis, we delivered electrical stimulations in awake rats through a chronically implanted electrode over the motor cortex (van den Brand *et al.*, 2012). In intact rats, the stimulation evoked bilateral motor responses in ankle flexor muscles with reproducible latencies (**Supplementary Figure 7.9**). As predicted, the hemisection completely and permanently suppressed motor responses in ankle flexor muscles ipsilateral to the lesion ($p<0.001$, **Supplementary Figure 7.9C**).

Corticospinal tract reorganization augments functional recovery

We finally conducted an integrated syndromic assessment using non-linear principal components analysis (Linting *et al.*, 2007) (NLPCA) to explore relationships between anatomical and functional variables (Ferguson *et al.*, 2013). We performed separate NLPCA extractions for rat-monkey and rat-human data using subsets of variables that were collected in both species, allowing direct cross-species comparisons (**Figure 7.6**). We extracted factor loadings on PC1 and PC2, which explained a large amount of

variance (**Figure 7.6B**). In all the studied species, the degree of reorganization from left and right motor cortex axonal projections and electrophysiological properties of corticospinal tract significantly correlated with increased recovery of locomotion, and even more extensively, hand function (**Figure 7.6B**). However, analysis of individual PC scores revealed that this mechanism of recovery was remarkably more efficient in monkeys ($p<0.001$, **Figure 7.6C**) and humans ($p<0.05$, **Figure 7.6C**) compared to rats.

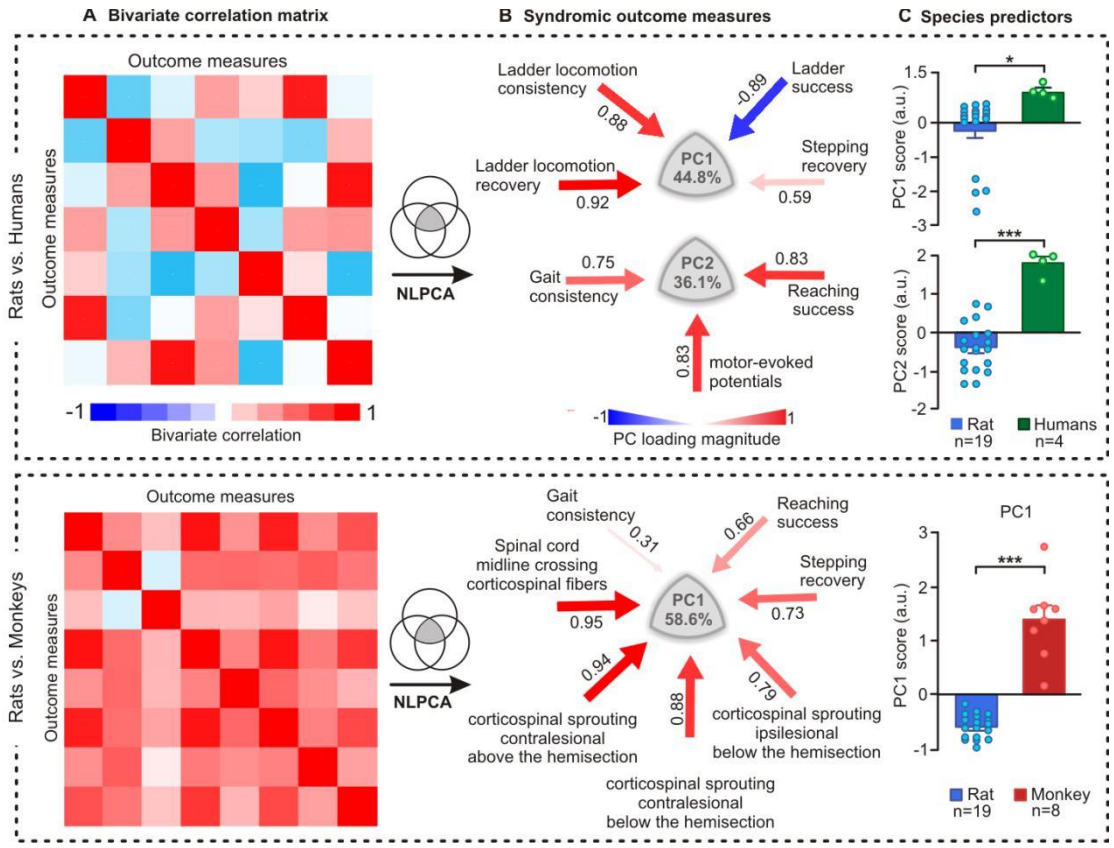

Figure 7.6 Syndromic analysis establishing relationships between reorganization of corticospinal tract function and functional recovery.

(A) Bivariate correlation matrix showing robust correlations between the subset of parameters show in (**B**). **(B)** A categorical PCA was applied on all the parameters measured in rats and humans, and in rats and monkeys. PC1 and PC2 accounted for a large amount of variance, which is reported in the respective panel. Color- and size-coded arrows indicate the direction (red, positive correlation) and amplitude of factor loadings of the represented anatomical, electrophysiological, and functional parameters. Ipsilesional and contralesional refer to the origin of the corticospinal tract. Correlation coefficients are also reported. The rat vs. human analysis revealed robust correlations between the recovery of motor cortex access to motoneurons innervating leg muscles, and recovery of basic locomotion and reaching, both in rats and humans. The rat vs. monkey analysis indicated that the degree of multi-level remodeling of the left and right corticospinal tract significantly correlated with the extent of recovery of locomotion and hand function, both in rats and monkeys. **(C)** Histogram plots reporting the mean (+ s.e.m.) values of scores on PC1 for both analyses and additionally PC2 for the human vs. rat analysis. Each dot represents individual data. Both analyses revealed a significant enhancement in recovery in both monkeys and humans, compared to rats. **, *** denotes significant differences between the studied species ($p<0.01$, $p<0.001$). Error bars, s.e.m.

7.5 Discussion

The development of the corticospinal tract during mammalian evolution has enabled higher primates to perform incrementally more complex motor tasks (Lemon & Griffiths, 2005). Three salient features characterize the adaptions of the corticospinal tract during primate evolution. First, the rapidly increasing number of axons encouraged a migration of the corticospinal tract from the dorsal column to dorsolateral funiculi (Kuypers, 1964). Second, the pattern of corticospinal projections became increasingly bilateral, with a substantial number of axons decussating extensively across the spinal cord midline (Rosenzweig *et al.*, 2009). Third, the appearance of direct cortical projections onto motor neurons correlated with the emergence of precision grip between the thumb and the index fingers (Lemon, 2008; Kinoshita *et al.*, 2012). Our results demonstrate that these evolutionary adaptations in the architecture and properties of the primate corticospinal tract provide significant advantages for recovery after SCI (Oudega & Perez, 2012), especially after lateralized injuries.

We first established that spontaneous recovery of function increases with the laterality of spinal cord damage in quadriplegic patients. Clinical observations have documented extensive functional recovery in patients with Brown-Séquard syndrome (Brown-Sequard, 1868; Little & Halar, 1985; Roth *et al.*, 1991; Dlouhy *et al.*, 2013), but correlations between laterality of spinal cord damage and recovery had never been demonstrated experimentally. Extensive functional gains in patients with lateralized motor deficits correlated with a significant recovery of motor cortex access to deprived motor neurons below the injury. We thus reasoned that lateralized spinal cord damage triggers a specific reorganization of corticospinal tract function that mediates superior recovery after lateralized compared to symmetrical lesion. To address this hypothesis, we modeled this type of injuries in rhesus monkeys and rats, whose corticospinal tract organization differs dramatically.

The architecture of corticospinal tract axonal projections is similar in monkeys and humans. Accordingly, hemisected monkeys followed the same recovery profile as patients with Brown-Séquard syndrome, which contrasted with the poor recovery of skilled leg and hand functions in hemisected rats. We found that a substantial number of corticospinal tract fibers originating from the contralesional motor cortex are spared after a lateral hemisection SCI in monkeys, as previously reported (Rosenzweig *et al.*, 2010) and presumably similar to Brown-Séquard patients (Lemon & Griffiths, 2005). Here, we detected a substantial growth of spared corticospinal fibers across the spinal cord midline below the hemisection in monkeys, and an extensive sprouting into spinal territories

containing deprived hand motor neurons. Moreover, these corticospinal fibers established close appositions with descending projection neurons that are directly connected to lumbar segments. In contrast, due to their course in the dorsal column corticospinal axons originating from the contralesional motor cortex were near completely interrupted in hemisected rats.

We propose that, after a lateral hemisection, spared corticospinal fibers established detour circuits that formed a functional bridge across the hemisection. These fibers contacts spinal circuits directly involved in hand control, and descending projection neurons connected with lumbar motor circuits. This type of intraspinal relays have been shown to play a pivotal role to restore motor functions after partial SCI in rodent models (Bareyre *et al.*, 2004; Jankowska & Edgley, 2006; Courtine *et al.*, 2008; van den Brand *et al.*, 2012). Recovery of motor cortex access to deprived leg motor neurons in patients with lateralized spinal cord damage is consistent with this interpretation. In particular, the significant increase in the latency of motor responses on the more affected side was coherent with the formation of alternative relay circuits that convey the cortical command to leg motor neurons. Post-mortem anatomical analyses (Fishman, 1987), MRI investigation (Freund *et al.*, 2013), and electrophysiological recordings (Curt *et al.*, 1998; Thomas & Gorassini, 2005) provided indirect evidence suggesting that sprouting of spared corticospinal fibers contributes to functional recovery after SCI in humans. In the present study, we performed multivariate analyses that established correlations between corticospinal tract reorganization and functional recovery in humans, monkeys, and rats. These results indicate that, as previously proposed (Rosenzweig *et al.*, 2010; Oudega & Perez, 2012) but not tested directly across multiple species, corticospinal tract reorganization is a fundamental mechanism of recovery after SCI in mammals. However, due to the bilateral projection patterns of corticospinal axons in higher mammals, and probably, the more advanced contribution of these inputs to motor control (Lemon & Griffiths, 2005; Nishimura *et al.*, 2007), monkeys and humans show greater functional recovery than rats after a lateral hemisection of the spinal cord—and potentially after other types of incomplete SCIs.

Other descending tracts appear more resistant to anatomical reorganization post-SCI(Courtine *et al.*, 2008), especially in cervical segments (Courtine *et al.*, 2008; Filli *et al.*, 2011). We did not observe remodeling of serotonergic pathways in cervical segments of both rats and monkeys, which contrasted with the robust reorganization of serotonergic fibers observed in the brain (Hawthorne *et al.*, 2011) and in thoracic segments (Mullner *et al.*, 2008) after injury. These results highlight a surprisingly high degree of specific

sprouting and growth of spared corticospinal tract axons into segments below a SCI in higher mammals (Steward *et al.*, 2008).

These findings emphasize the importance of developing therapeutic interventions targeting regeneration and sprouting of the corticospinal tract in humans (Liu *et al.*, 2010; Rosenzweig *et al.*, 2010; Oudega & Perez, 2012), and neurorehabilitation procedures to enhance the contribution of motor cortex to recovery (Nishimura *et al.*, 2007; van den Brand *et al.*, 2012). New rodent pre-clinical models are necessary to investigate the predictive value of primate-specific treatments on remodeling of spared corticospinal fibers below the injury. Dramatic differences between rodents and primates also highlight the value of continuing the development of non-human primate models for translational SCI research (Courtine *et al.*, 2007a; Nout *et al.*, 2012b).

8 Integration and future approaches in spinal cord medicine

This thesis provides insights into neuroprosthetic neurorehabilitation approaches and translational mechanisms after SCI. I first describe the development of a severe yet incomplete SCI model in rats, which experimentally mimics behavioral and neurophysiological properties of severe SCI in human patients (ASIA A and B). Next, I describe the development of a novel versatile robotic postural prosthesis that allows the training, evaluation and enabling of locomotion after neuromotor disorders. In a third step, I describe neuroprosthetic training which includes bipedal overground step training enabled by the robotic postural prosthesis and previously developed electrochemical stimulation (Musienko *et al.*, 2011c) after staggered hemiesction SCI. Neuroprosthetic training restored not only voluntary overground locomotion, trained rats were also able to climb stairs or pass successfully obstacles. This notable recovery relied on extensive remodeling of motor cortex axonal projections, which included the formation of relays to propriospinal neurons that bypass the SCI. Despite exceptional functional recovery, the qualitative control over the hindlimbs was limited to electrochemically enabled state. The application of neuroprosthetic training in a less severe yet more clinically relevant setting shows the reconstitution of both electrochemically enabled locomotion and more striking the recovery of spontaneous overground stepping after a severe contusion SCI. Anatomical evaluations of descending brainstem-derived projections revealed multi-level reorganization of the spared reticulospinal system and reorganization of interrupted cortical projections in the brainstem. Together these results illustrate the development, significance and necessity of active electrochemically enabled overground step training to induce functional recovery after severe SCI in rats. Last, I discuss recovery mechanisms after cervical hemisection in rats, non-human primates and human patients with a lateralized SCI. Although all species seem to share a similar recovery mechanism, we found diminished recovery in rats compared to non-human primates and humans patients. Our findings show that the unique architecture of the primate corticospinal tract provides an important substrate for recovery after such SCI. This important substrate accounts for superior recovery in primates compared to rats and should be considered in primate's specific therapeutic interventions.

8.1 Neuroposthetic training after SCI

A century of research on neuronal organization in the spinal cord revealed neuronal circuits and networks that interact with specific sensory information and are responsible for locomotion in vertebrates (Sherrington, 1910b; Grillner & Zangger, 1979) and invertebrates (Grillner *et al.*, 1976). These lumbosacral circuits, also referred to as central pattern generators (CPG), are able to produce stepping-like neuronal activity and even locomotor output in the complete absence of supraspinal input in mammals (Lovely *et al.*, 1986; Barbeau & Rossignol, 1987) and man (Dietz, 1992; Dietz & Harkema, 2004). Experiments in animals showed that regular step training induced use-dependent plasticity which modifies motor function of lumbosacral circuits after spinalization in cats (Barbeau & Rossignol, 1987; de Leon *et al.*, 1998b). Furthermore, use-dependent plasticity and training effects are highly task-specific, thus training of walking leads to improved walking function but not standing (De Leon *et al.*, 1998a; de Leon *et al.*, 1999b). These unique properties of the spinal cord were exploited for rehabilitation purpose by the use of task-specific activity-based training following SCI in human patients. Activity-based therapies have been shown to be efficient in restoring function after incomplete SCI (Wernig & Muller, 1992; Wernig *et al.*, 1995; Behrman & Harkema, 2000; Dietz & Harkema, 2004), subjects with motor complete SCI, however, could not profit essentially from locomotor training. In contrast, individuals with a motor complete SCI show functional degradation over time which are accompanied with aberrant spinal circuits formation (Dietz & Muller, 2004; Lunenburger *et al.*, 2006; Dietz *et al.*, 2009). Therefore, there is a critical necessity to improve neurorehabilitation for patients suffering from severe SCI. Staggered hemisection mimics comprehensively such severe, yet incomplete SCIs in an experimental context and provides, thus, an important and powerful instrument for studying both, spontaneous and use-dependent plasticity following severe SCI in rats.

Like humans and in contrast to cats, rats fail to recover weight-bearing locomotion after complete SCI, even after extensive step training. A decade of research on the excitation of dormant spinal cord state revealed that electrochemical stimulation of the spinal cord is able to produce as early as one week post SCI a well-controlled locomotor pattern following complete transection in rats (Courtine *et al.*, 2009c; Musienko *et al.*, 2011c). In combination with step training, this intervention led to the restoration of full-weight bearing bipedal stepping on a treadmill. However, this outstanding stepping capacity did not transfer into voluntary stepping overground. Hebbian plasticity predicts that the outcome of rehabilitation depends on the trained task. Therefore, to induce

recovery of voluntary overground stepping, this task need to be integrated in a rehabilitative training program. The robotic postural prosthesis that was introduced in this thesis provides such a training environment: support against gravity and stabilization for increased postural stability without the delivery of support in any other direction. When the rats are positioned bipedally on a straight runway they have to initiate the forward movement by themselves by activating their impaired legs. Therefore, we hypothesized that training using the robotic postural prosthesis requires volitional control over the legs. Indeed, experiments recording neuronal activity in the motor cortex confirmed this assumption by correlation of modulation patterns with gait initiation, sustained locomotion, and corrective movements while training with the postural prosthesis. Instead, the firing rate of motor cortex neurons significantly decreased during involuntary treadmill locomotion compared with quiet standing. Additionally, bipedal position, despite of being unnatural for rats, provides important sensory information from the hip joints that alter and enhance locomotion seen in animals (Grillner & Rossignol, 1978; Slawinska *et al.*, 2012) and human SCI patients (Dietz *et al.*, 2002; Dietz & Harkema, 2004)

We consequently developed multi-system neuroprosthetic training which comprises overground step training using the postural prosthesis and electrochemical stimulation of the spinal cord to restored voluntary locomotion following paralyzing SCI. Both in rats with staggered hemisection and severe contusion, neuroprosthetic training restored voluntary overground locomotion. However, the stepping capacity of rats with staggered hemisection remained electrochemically dependent. The systemical effects of long-term application of monoaminergic drugs, though, are difficult to predict. This contrasts to electrical stimulation of the spinal cord, which was already implemented in two clinical studies. A total of four severely spinal cord injured individuals (ASIA A, B) were implanted with an electrode array over lumbar spinal segments and were trained in standing and stepping on a treadmill for seven months. After the training with epidural electrical stimulation (EES), modulation of the physiological state of the spinal circuitry enabled full-weight bearing standing, locomotor-like pattern and increased EMG activity during manually facilitated stepping. Additionally, they found the recovery of voluntary flexion of the limb when lying in supine in an individual with chronic clinically complete paralysis (ASIA B) (Harkema *et al.*, 2011). The authors conclude that EES did not induce standing by directly activating motor pools, but enabled motor function by stimulating afferent fibers in the dorsal root and engaging thereby populations of interneurons that integrated load-bearing related proprioceptive input to coordinate motor pool activity as proposed earlier *in silico* (Holsheimer, 1998; Rattay *et al.*, 2000). A recent publication confirms this assumption. Capogrosso and colleagues show in *in vivo* rat experiments and in a

computer model that the lack of direct influence of EES on motoneurons and interneurons (Capogrosso *et al.*, 2013). Further they state that EES provides excitation of lumbosacral interneurons and motorneurons, which, combined with the weak excitatory activity of residual descending axons, achieved a level of excitation that was sufficient to activate motoneurons. Harkema et al. suggested that the intense stand training and repetitive stimulation may have triggered activity-dependent neural plasticity that eventually resulted in the ability to voluntarily move the legs (Harkema *et al.*, 2011). Moreover, EES enabled volitional movements of the legs in response to verbal command in additional three patients with chronic motor complete SCI immediately after implantation of the electrode array. This suggests that descending connections to the spinal cord circuitry may have existed since the time of injury but only a higher level spinal cord excitation enabled the supraspinal command to execute the locomotor task (Angeli *et al.*, 2014b). These conclusions are consistent with findings introduced in this thesis as well as with previous results. Most importantly, this suggests that use-dependent plasticity of spared neuronal systems observed in rats may also occur in humans with severe SCI. (Courtine *et al.*, 2009c; Musienko *et al.*, 2011c; van den Brand *et al.*, 2012).

A part from gait recovery, Harkema and her colleagues reported functional gains in bladder and sexual function, as well as gain in temperature regulation as a response to stand training and electrical stimulation in one subject. A similar system-wide effect was observed after neuroprosthetic training in rats. Although mechanisms remain unclear, neuroposthetic training successfully counteracted the formation of neurogenic bladders dysfunction (Horst *et al.*, 2012)

8.2 Use-dependent plasticity

It is a well-established concept that functional recovery after partial SCI is accompanied by spontaneous reorganization of various supraspinal axonal projections in the spinal cord or the brainstem (Raineteau *et al.*, 2002; Bareyre *et al.*, 2004; Courtine *et al.*, 2008; Rosenzweig *et al.*, 2010), and even by the reorganization of sensorimotor cortex (Ghosh *et al.*, 2009; Ghosh *et al.*, 2010). In detail, functional recovery has been associated with the formation of propriospinal relay connections that bypass one or more lesion sites (Courtine *et al.*, 2008) and sprouting mechanisms of supraspinal descending fibers below lesion level (Raineteau *et al.*, 2002; Bareyre *et al.*, 2004; Rosenzweig *et al.*, 2010). However, after severe SCI, spontaneous functional recovery remains limited and such propriospinal relay connections are not formed spontaneously (Courtine *et al.*, 2008). In contrast, we showed the formation of aberrant intraspinal circuits in the lumbar spinal cord after paralyzing staggered hemisection. This neuronal degradation parallels with a degradation in gait capacity and the formation of abnormal reflex properties. Neuroposthetic training counteracts these devastating consequences and re-connects supraspinal centers with lumbosacral circuits through *de novo* thoracic intraspinal connections that bypass the SCIs. We found ubiquitous remodeling of motor cortex axonal projections, e.g. between and above the hemisections, as well as in various brainstem locomotor regions such as the nucleus gigantocellularis. Contrary to this, increased functional recovery after neuroprosthetic training in rats with severe contusion SCI seem to be mediated mainly through remodeling of spared descending reticular formation axonal projections. An increase of motor cortex projections could only be observed at the brainstem level, but not in the spinal cord. We found spontaneous sprouting of reticulospinal fibers at several thoracic and lumbar segments below the SCI. This sprouting was increased in lower thoracic and lumbar segments in trained compared to non-trained animals. Sprouting of brainstem-derived serotonergic projections, we found in trained rats both after staggered hemisection and contusion SCI. However, spontaneously, rats showed hardly increased fiber densities. Similar results were observed after cervical hemisection, where spontaneous functional recovery was not accompanied with a reorganization of the serotonergic system, neither in rats nor in primates and are in line with results obtained by other investigators (Rosenzweig *et al.*, 2010; Filli *et al.*, 2011).

It may be concluded that neuroprosthetic training triggers the reorganization of the appropriate descending supraspinal systems through which functional recovery happens.

8.3 Primate specific recovery after SCI

Although recovery could be perceived to be superior in our trained rats compared to the human patients, such semblances need to be handled with care. A comparison of scientific results from an experimental and a clinical study requires the same setting, e.g. same lesion, same intervention, and the same measurement. To better predict the clinical fruition and relevance of pre-clinical study outcomes, such insights are desirable. However, to the best of my knowledge, *chapter 7* of this thesis provides the first direct comparison of recovery extend and mechanism after SCI. The results provide an important insight into translational mechanisms of recovery after SCI. We showed that contrary to common consensus the recovery after lateralized SCI was superior in humans and in non-human primates compared to rats. Similar to results obtained in rodent studies, we uncovered that functional recovery was mediated through corticospinal tract projections below the SCI (Weidner *et al.*, 2001; Courtine *et al.*, 2008). Multivariate analyses established correlations between corticospinal tract reorganization and functional recovery. These results indicate that, corticospinal tract reorganization is a fundamental mechanism of recovery after SCI in all analyzed species. However, due to the bilateral projection patterns of corticospinal axons in higher mammals, and probably, the more advanced contribution of these inputs to motor control (Lemon & Griffiths, 2005; Nishimura *et al.*, 2007), monkeys and humans show greater functional recovery than rats after a lateral hemisection of the spinal cord - and potentially after other types of incomplete SCIs. These findings emphasize the importance of developing therapeutic interventions targeting regeneration and sprouting of the corticospinal tract (Liu *et al.*, 2010; Rosenzweig *et al.*, 2010; Oudega & Perez, 2012), and neurorehabilitation procedures to enhance the contribution of motor cortex to recovery (Nishimura *et al.*, 2007; van den Brand *et al.*, 2012). Dramatic differences between rodents and primates also highlight the value of continuing the development of non-human primate models for translational SCI research (Courtine *et al.*, 2007a; Nout *et al.*, 2012b).

8.4 Clinical implementations

Although pioneering, currently available clinical implementation of rehabilitation using EES in spinal cord injured individuals are facing critical constraints. Currently, there is a first clinical study using EES facilitated neurorehabilitation in preparation in Switzerland. The goal of this study is to address the limitations of past EES enabled training studies by ameliorate technical and rehabilitation features.

Firstly, there is no implantable stimulator available that allows multi-side stimulation pattern for stimulation of the spinal cord. The currently used stimulating system allows only the stimulation on one side (one electrode at once) and, further, does not allow differentially manipulating parameters that is needed to optimize the completion of different motor tasks. In animal models it has been shown, though, that dual-side stimulation compared to single side is more efficient in inducing stepping (Ichiyama *et al.*, 2005; Ichiyama *et al.*, 2008; Courtine *et al.*, 2009c). Further, manual tuning of multiple parameters are impractical and suboptimal. Recent experiments in the lab reveal that gait capacity can be modulated and enhanced using side-specific gait-timed phasic stimulation of the spinal cord in rats with a complete spinal cord transection. They managed to establish a mechanistic framework to personalize multisite stimulation algorithms and developed closed-loop control systems that take advantage of this paradigm to facilitate an optimal stepping pattern (Wenger et al. *in press in Science Transl. Med.*, Wenger and Musienko et al. *in preparation*). Therefore, investigators of the Swiss study are going to use a novel stimulation system which is going to allow multisite stimulation which will adapt stimulating parameters to the stepping performance of the patient through a closed-loop controller in real-time.

Secondly, in published studies neurorehabilitation was restricted to stand and bodyweight supported treadmill training (Harkema *et al.*, 2011; Angeli *et al.*, 2014b). This thesis stress the urgency, though, to use more active participation of the patient in the rehabilitation training which is increased in overground step training. Further there is evidence that gait features (Stolze *et al.*, 1997; Alton *et al.*, 1998), as well as sensory feedback (Lee & Hidler, 2008; Sloot *et al.*, 2014) are altered in naturally walking overground compared to treadmill locomotion. In the new study, patients are therefore going to be trained using an overground robotic support system, called *The FLOAT* (FLOAT, Lutz Medical Engineering, Switzerland). Like the presented postural prosthesis, this robot only supports the patient in the vertical axis but remain transparent in all other directions. Based on the results of this thesis, investigators hypothesize that overground step training is going to enhance the restoration of voluntary and natural gait functions.

Third, Rehabilitation using EES has only been tested in four patients with a motor complete SCI (ASIA A, B) so far. There is a critical need to test outcomes of such training in a bigger and more diverse cohort in order to be able to generalize clinical prognosis after EES facilitated neurorehabilitation. Additionally, Harkema et al. reported a similar recovery for sensory complete and incomplete patients and concluded that sprouting of spared sensory descending axons plays a minor part in recovery of this patient. Instead they concluded that functional recovery must have occurred through newly formed intraspinal connections that bypass the SCI (Harkema *et al.*, 2011; Angeli *et al.*, 2014b), similar to our findings in rats with staggered hemisection. Based on the fact that rehabilitation outcome increases with the number of remaining direct supraspinal fiber projections in the spinal cord (staggered hemisection as oppose to spinal cord contusion), we hypothesize that the recovery of voluntary stepping will be substantially higher in patients with remaining direct supraspinal connections. Thus, patients with motor incomplete, yet wheelchair bound (ASIA C with low motor scores) will be recruited in Switzerland.

8.5 Future approaches in spinal cord medicine

EES enabled neurorehabilitation failed so far to restore weight-bearing locomotion in individuals with severe SCIs and thereby increase substantially the life quality of these patients. One is drawn to the conclusion that EES facilitated rehabilitation alone might not be enough to free these patients from their wheelchair. The further development of neuroprosthetic systems or the combination with additional neuroregenerative therapy will most likely be critical for advancing prognosis of these individuals.

Regenerative strategies to enhance recover after SCI are diverse in approach and reach from replacement strategies like the implantation of stem cells into the lesion site (Lu *et al.*, 2012) to axonal growth-promoting strategies through reduction of glial scar formation (Bradbury *et al.*, 2002) or neural inhibitory growth proteins (Schnell & Schwab, 1990). In patients with a complete SCI, rehabilitation and neuroregenerative therapy should be optimally combined in order to have a synergistic effect of the two interventions. However, recent studies revealed complex and potentially detrimental interactions between neuroregenerative therapies and rehabilitation after SCI (Maier *et al.*, 2009), especially when rehabilitation onset was too early (Wahl *et al.*, 2014). In the acute phase without electrochemical neuromodulation, rats perform poorly during rehabilitation. In consequence, early practice of uncoordinated movements in a growth permissive environment may reinforce inappropriate or suboptimal combinations of motor circuits. Instead, our motor control using the postural interface enables interventions that restored a highly functional state in locomotor circuitries early after injury, thus opening innovative avenues to achieve synergy between neuroregenerative and neurorehabilitative therapies

The electrical neuroprosthetic approach may further be improved using the integration of a chemotrode array in order to stimulate the spinal cord not only electrically but also locally using a tailored monoaminergic drug cocktail (Musienko *et al.*, 2009; Musienko *et al.*, 2011c). Further, spinal cord stimulation could be combined using functional electrical stimulation (FES) of peripheral nerves or superficial key muscles, like the anterior tibialis to enhance dorsiflexion. Another replacing strategy is the usage of silicon-based microelectrode brain arrays (MEA) which allow high-density neuronal recording. MEAs discovered principles through which cortical networks are coordinating movement. This lead to the development of brain-machine interfaces which were shown to replace function in non-human primates (Carmena *et al.*, 2003; Velliste *et al.*, 2008) as well as in human patients (Hochberg *et al.*, 2012; Collinger *et al.*, 2013) to operate sophisticated actuators, like robotic arms. In the future, personalized neuroprosthetic

systems target to synergistically integrate restoration and replacement strategies that will allow a brain-to-body connection establishing electronic bridges to enable the direct neuromoduation of denervated spinal circuits and muscles from brain signals after sever motor disorders (for a review of available neuroprosthetic systems and future potential of neuroprosthetic systems please read more in (Borton *et al.*, 2013)).

Based on recent animal research, research presented in this thesis, and human case studies, the confidence that the translation of neuroprosthetic systems for restoring function after severe SCI into clinical practice is imminent. The implementation of such technologies require the orchestrated contribution from neurosurgeons, neurologists, physiotherapists, neuroscientists and neuroengineers to conceive complex treatments centered on the patient. Although even a well-coordinated organization of clinical and technological platforms with the goal to establish personalize neuroprosthetics that “helps the brain to help itself” might not be able to “cure” SCI, but it may become soon a treatment to improve general recovery not only after SCI but also other neuromotor disorders like Parkinson’s disease or multiple sclerosis.

9 Abbreviations

SCI	Spinal cord injury
RMV	Rückenmarksverletzung
ASIA	Americal Spinal Injury Association (http://www.asia-spinalinjury.org/)
EMG	electromyography
EES	electrical epidural stimulation
BWS	body weight support
TA	tibialis anterior
MG	medial gastrocnemius
MTP	metatarsophalangeal
TMR	Tetramethylrhodamine-conjugated dextran
vGlut1	vesicular glutamate transporter 1
vGlut2	vesicular glutamate transporter 2
C7	Cervical spinal level 7
T7	Thoracic spinal level 7
L2	Lumbar spinal level 2
S1	Sacral spinal level 1
5HT	Serotonin, 5-hydroxytryptamine
i.p.	Intraperitoneal
s.c.	Subcutaneous
BDA	Biotinulated dextran amines
CST	Cortico-spinal tract
AAV	Adeno-associated virus
eGFP	Enhanced green fluorescent protein
TRE	Tetracycline responsive element
CMV	Cytomegalovirus
HiRet	Highly efficient gene transfer lentiviral vector
eTeNT	Enhanced Tetanus Neurotoxin
rtTAV	Reverse tetracycline transactivator
PCA	Principal component analysis
NLPCA	Non-linear principal component analysis
PC 1	Principal component 1
ET-1	Endothelin-1

vGRF	Vertical ground reaction force
DoF	Degrees of freedom
GFAP	Glial fibrillary acidic protein
NMDA	N-methyl-D-aspartaic acid
FB	Fastblue
MLR	Mesencephalic locomotor region
DBS	Deep brain stimuation

10 Annex and supplementary figures

10.1 ASIA impairment scale

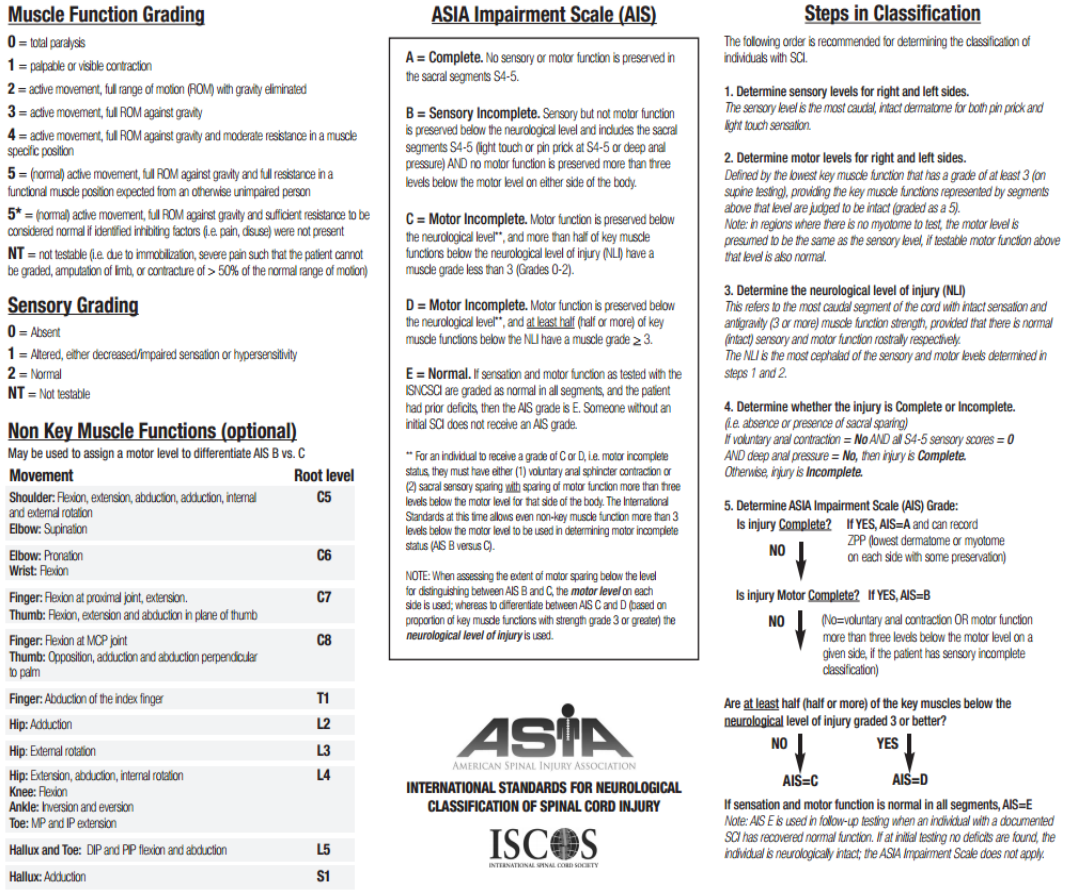

Muscle Function Grading

0 = total paralysis

1 = palpable or visible contraction

2 = active movement, full range of motion (ROM) with gravity eliminated

3 = active movement, full ROM against gravity

4 = active movement, full ROM against gravity and moderate resistance in a muscle specific position

5 = (normal) active movement, full ROM against gravity and full resistance in a functional muscle position expected from an otherwise unimpaired person

5* = (normal) active movement, full ROM against gravity and sufficient resistance to be considered normal if identified inhibiting factors (i.e. pain, disuse) were not present

NT = not testable (i.e. due to immobilization, severe pain such that the patient cannot be graded, amputation of limb, or contracture of > 50% of the normal range of motion)

Sensory Grading

0 = Absent

1 = Altered, either decreased/impaired sensation or hypersensitivity

2 = Normal

NT = Not testable

Non Key Muscle Functions (optional)

May be used to assign a motor level to differentiate AIS B vs. C

Movement	Root level
Shoulder: Flexion, extension, abduction, adduction, internal and external rotation **Elbow:** Supination	C5
Elbow: Pronation **Wrist:** Flexion	C6
Finger: Flexion at proximal joint, extension. **Thumb:** Flexion, extension and abduction in plane of thumb	C7
Finger: Flexion at MCP joint **Thumb:** Opposition, adduction and abduction perpendicular to palm	C8
Finger: Abduction of the index finger	T1
Hip: Adduction	L2
Hip: External rotation	L3
Hip: Extension, abduction, internal rotation **Knee:** Flexion **Ankle:** Inversion and eversion **Toe:** MP and IP extension	L4
Hallux and Toe: DIP and PIP flexion and abduction	L5
Hallux: Adduction	S1

ASIA Impairment Scale (AIS)

A = Complete. No sensory or motor function is preserved in the sacral segments S4-5.

B = Sensory Incomplete. Sensory but not motor function is preserved below the neurological level and includes the sacral segments S4-5 (light touch or pin prick at S4-5 or deep anal pressure) AND no motor function is preserved more than three levels below the motor level on either side of the body.

C = Motor Incomplete. Motor function is preserved below the neurological level**, and more than half of key muscle functions below the neurological level of injury (NLI) have a muscle grade less than 3 (Grades 0-2).

D = Motor Incomplete. Motor function is preserved below the neurological level**, and at least half (half or more) of key muscle functions below the NLI have a muscle grade ≥ 3.

E = Normal. If sensation and motor function as tested with the ISNCSCI are graded as normal in all segments, and the patient had prior deficits, then the AIS grade is E. Someone without an initial SCI does not receive an AIS grade.

** For an individual to receive a grade of C or D, i.e. motor incomplete status, they must have either (1) voluntary anal sphincter contraction or (2) sacral sensory sparing with sparing of motor function more than three levels below the motor level for that side of the body. The International Standards at this time allows even non-key muscle function more than 3 levels below the motor level to be used in determining motor incomplete status (AIS B versus C).

NOTE: When assessing the extent of motor sparing below the level for distinguishing between AIS B and C, the ***motor level*** on each side is used; whereas to differentiate between AIS C and D (based on proportion of key muscle functions with strength grade 3 or greater) the ***neurological level of injury*** is used.

ASIA
AMERICAN SPINAL INJURY ASSOCIATION

INTERNATIONAL STANDARDS FOR NEUROLOGICAL CLASSIFICATION OF SPINAL CORD INJURY

ISCOS
INTERNATIONAL SPINAL CORD SOCIETY

Steps in Classification

The following order is recommended for determining the classification of individuals with SCI.

1. Determine sensory levels for right and left sides.
The sensory level is the most caudal, intact dermatome for both pin prick and light touch sensation.

2. Determine motor levels for right and left sides.
Defined by the lowest key muscle function that has a grade of at least 3 (on supine testing), providing the key muscle functions represented by segments above that level are judged to be intact (graded as a 5).
Note: in regions where there is no myotome to test, the motor level is presumed to be the same as the sensory level, if testable motor function above that level is also normal.

3. Determine the neurological level of injury (NLI)
This refers to the most caudal segment of the cord with intact sensation and antigravity (3 or more) muscle function strength, provided that there is normal (intact) sensory and motor function rostrally respectively.
The NLI is the most cephalad of the sensory and motor levels determined in steps 1 and 2.

4. Determine whether the injury is Complete or Incomplete.
(i.e. absence or presence of sacral sparing)
*If voluntary anal contraction = **No** AND all S4-5 sensory scores = **0***
*AND deep anal pressure = **No,** then injury is **Complete.***
*Otherwise, injury is **Incomplete.***

5. Determine ASIA Impairment Scale (AIS) Grade:

Is injury Complete? **If YES, AIS=A** and can record ZPP (lowest dermatome or myotome on each side with some preservation)

NO ↓

Is injury Motor Complete? **If YES, AIS=B**

NO ↓ (No=voluntary anal contraction OR motor function more than three levels below the motor level on a given side, if the patient has sensory incomplete classification)

Are at least half (half or more) of the key muscles below the neurological level of injury graded 3 or better?

NO ↓ **AIS=C** YES ↓ **AIS=D**

If sensation and motor function is normal in all segments, AIS=E
Note: AIS E is used in follow-up testing when an individual with a documented SCI has recovered normal function. If at initial testing no deficits are found, the individual is neurologically intact; the ASIA Impairment Scale does not apply.

Annex 1 ASIA impairment scale. Available online on the homepage of American Spinal Injury Association (http://www.asia-spinalinjury.org/elearning/ASIA_ISCOS_high.pdf)

10.2 Supplementary information chapter 4

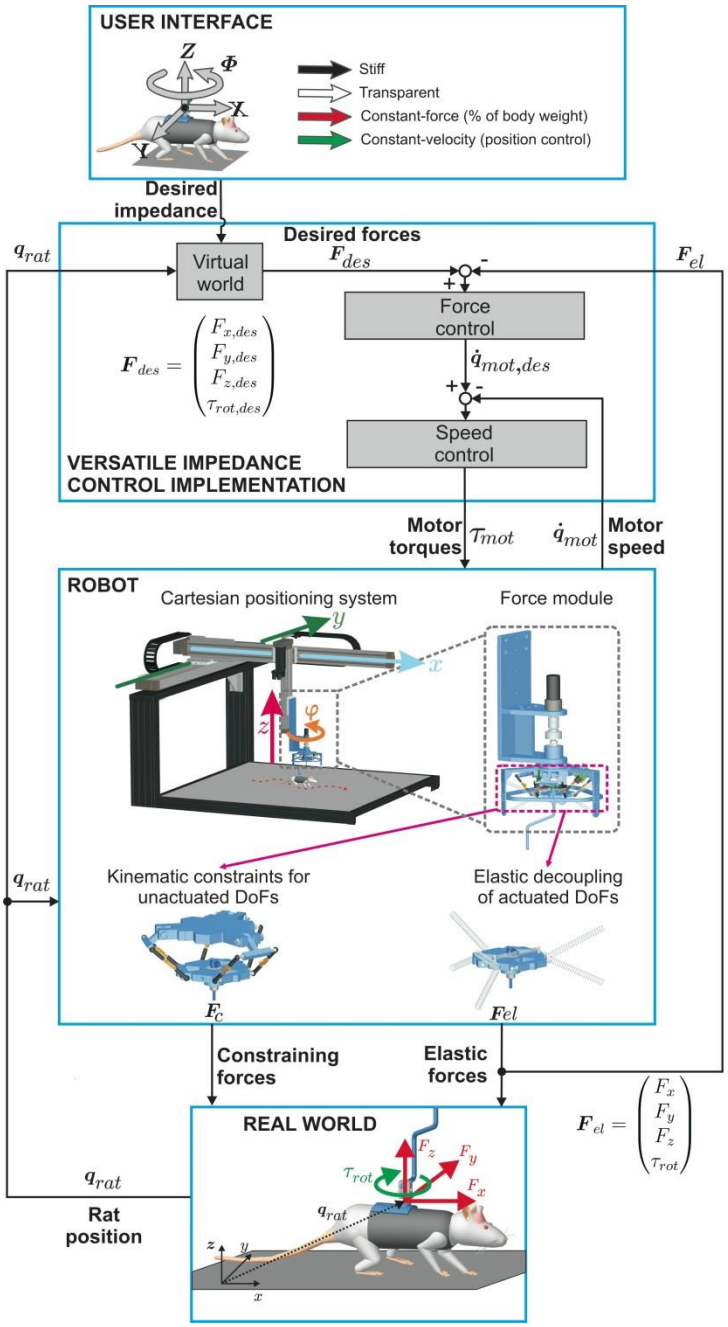

Supplementary Figure 4.1 Technical description of the robotic interface and control schemes

USER INTERFACE

A user-friendly GUI (Graphical user interface) is implemented in MATLAB/Simulink (The MathWorks, CA). The interface allows the user to create a virtual environment in

which the applied forces or the end-effector position can be adjusted for each single actuated DoF of the robot. For example, the user can independently set any of the 4 actuated axes to behave transparently. Concomitantly, the other axes can provide a constant force that is proportional to the rat's body weight, as for supporting the rat against gravity. The axes can also be configured to be stiff in order to prevent lateral fall or to guide the rat along a user-defined trajectory. Alternatively, the user can control the displacement of the end-effector (position control), as for pushing the rat in a given direction, or along a user-defined trajectory. Finally, the user can introduce sudden changes in the virtual environment. For example, a user-defined perturbation can be superimposed onto any control scheme based on external triggers or the position of the rat in the real world. The different control strategies for the various locomotor paradigms can be found in Supplementary Figure 2.

VERSATILE IMPEDANCE CONTROL IMPLEMENTATION

We implemented an impedance control scheme that can adjust the force exerted by each actuated DoF of the robotic interface independently in real-time (1kHz). The controller is cascaded: an outer loop processes the position of the rat with respect to the virtual environment; for example a world with guiding walls or gravity-reduced conditions. This algorithm translates the virtual environment defined by the user into a vector F_{des} of desired forces. A force controller adjusts the desired motor speeds $\dot{\boldsymbol{q}}_{mot,des}$ sent to the drives based upon the error between the desired forces and the forces measured through spring deflection. An inner speed controller ensures that the actual motor speed $\dot{\boldsymbol{q}}_{mot}$ tracks the desired motor speed by commanding appropriate actuator torques τ_{mot} The outer loops run on a Matlab xpc real-time operating system. The speed control runs on the actuator drives.

ROBOT

Cartesian positioning system: The robot consists of an actuated Cartesian positioning system that allows translations of the rat in the horizontal plane (*x,y*) while providing vertical support (*z*). An additional motor at the end-effector of this serial structure actuates rotation (φ). This serial configuration provides a large workspace in which forces can be applied to the animal in 4 DoFs.

Force module: To hide the inertia of the massive positioning robot and to measure the extremely small interaction forces between the robot and the rat, we developed a novel force module based on a"Series Elastic Actuator" (SEA). A SEA is composed of an actuator that is complemented with a passive compliant element in series. This compliance improves force control performance and effectively decouples actuator inertia

to achieve a transparent interface. In the force module, we extended this SEA concept to 4 DoFs by providing multidimensional compliance at the end-effector of the positioning system.

Kinematic constraints for unactuated DoF: A mechanical “Delta” linkage prevents the rat from tilting in the 2 unactuated DoF, leading to constraining forces F_c. The Delta structure also provides the means of measuring the end-effector position (rat position q_{rat}) and subsequently the interaction forces F_{el} between the robot and the rat.

Elastic decoupling of actuated DoF: The compliance for the residual DoFs is achieved by multiple linear springs attached to the suspended platform and by an additional spring pair attached to the rotating shaft within the platform.

REAL WORLD

The rat is positioned in a custom-made, skin-like jacket made of light fabrics. A Velcro strip allows attachment of the rat onto a back plate with a rigid bar coming from the robot end-effector. The rat’s position and the interaction forces with the robot are fed back to the impedance controller.

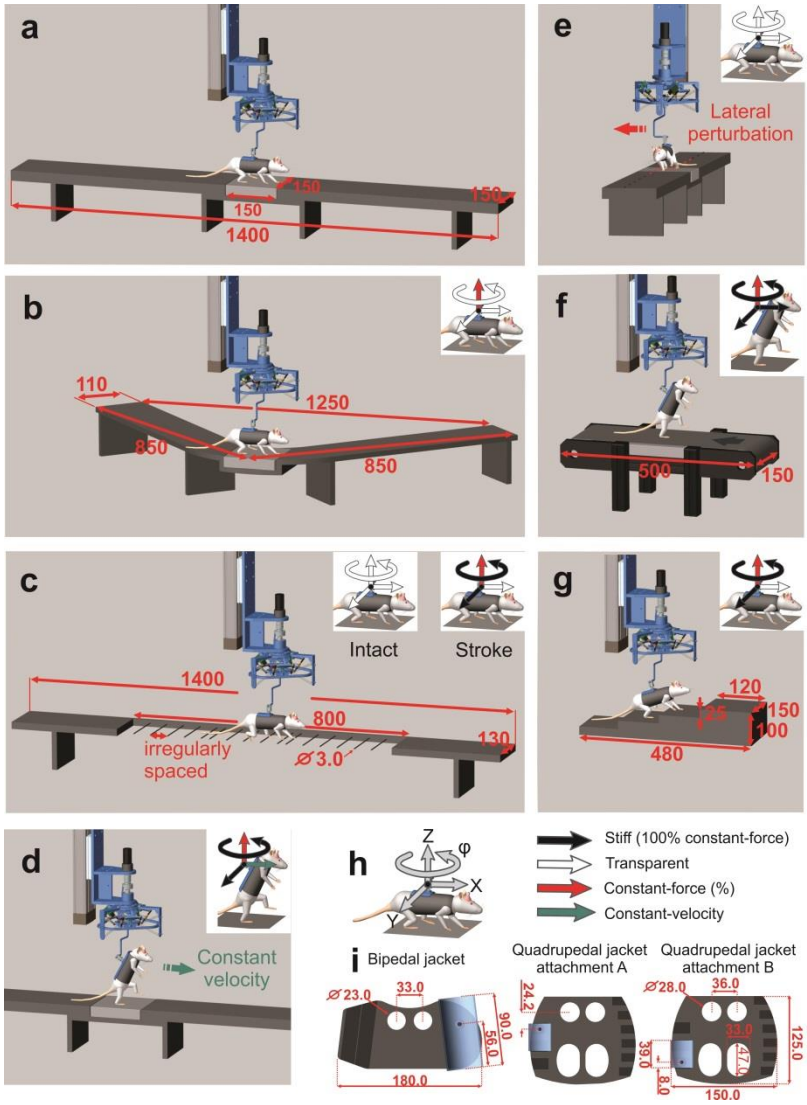

Supplementary Figure 4.2. Technical description of the locomotor testing paradigms.

Locomotor capacities of intact and motor impaired rats were evaluated in a total of 7 tasks. **a.** Quadrupedal locomotion along a straight horizontal runway. **b.** Quadrupedal locomotion along a 90deg-curved horizontal runway. **c.** Quadrupedal locomotion along a straight horizontal ladder with irregularly spaced rungs. **d.** Bipedal locomotion along a straight horizontal runway. In this task, the robot propels the rat forward at a constant velocity. **e.** Lateral perturbation (1s, 2.5N) introduced during continuous quadrupedal locomotion along a straight horizontal runway (task a). **f.** Continuous bipedal locomotion on a motorized treadmill belt. **g.** Quadrupedal locomotion along regularly spaced steps on a staircase. The various runways, stairs and ladders were made of wood but the walking surface was covered with turf to ensure a solid paw contact. The light grey box

indicates the position of the force plate that measures ground reaction forces and ground reaction torques in X, Y, Z directions. **h.** For each task, the degree of compliance was adjusted for each translational and rotational axis independently. Control strategies include: stiff control (black), zero-force control (light grey, constant-force set to 0%), adjustable constant-force (red, constant-force set to a percentage of body weight), and constant-velocity (green, position control). The behavior of each axis in each task is reported in the upper corner of each panel. **i.** Features and dimensions of the various jackets. The Velcro pads are represented in dark. The position and size of the back attachment is shown in blue. All the dimensions are reported in mm.

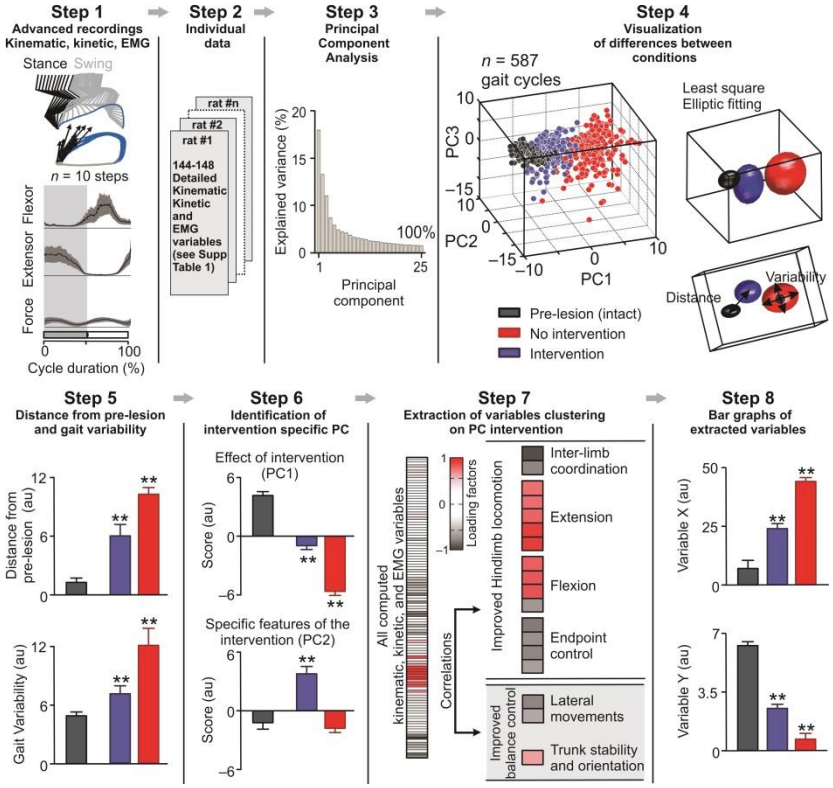

Supplementary Figure 4.3. Multi-step statistical analysis of gait parameters.

We used a set of experimental data from our database to exemplify the multi-step statistical analysis that was applied for all the experiments described in this study.**Step1:** For all the experimental conditions, we collected kinematic, kinetic and EMG data during continuous locomotion using an advanced recording system**. Step 2:** We computed a large number of parameters that provides a holistic quantification of gait features. The complete list of computed parameters can be found in **Supplementary Table 4.1**.The analytic procedures and computations are detailed in Ref (Courtine *et al.*, 2009a;

Musienko *et al.*, 2011b). **Step 3:** We applied a principal component (PC) analysis on all the variables computed from all the gait cycles from all the rats and experimental conditions. This analysis constructs new variables, i.e. PC, that linearly combine the original variables and maximize the amount of explained variance for each successive PC. Due to the high degree of correlation between gait parameters during locomotion, a few PCs are sufficient to explain a large proportion of the variance. **Step 4:** The gait cycles can be represented in the new "denoised" space created by PC1-3. In the proposed example, data points associated with each experimental condition cluster in a well-defined location, indicating that the rats exhibited intervention-specific gait patterns. Typically, PC1 powerfully differentiates gait cycles from intact rats (or pre-lesion), altered gaits from rats with SCI or stroke, and the improvement of locomotion with the robotic interface. In some instances, PC2 captures an additional feature. In the proposed example, PC2 is related to specific features of the intervention compared to intact and no intervention. In order to provide a straightforward representation of differences between conditions, we applied a least square elliptic fitting to the 3D data points. **Step 5:** To quantify the quality of gait performance, we measured the 3D geometric distance between the averaged location of gait cycles from each rat in a given condition and the average location of all gait cycles from all intact (or pre-lesion) rats. For each rat and condition, we also measured the 3D dispersion of gait cycles to provide a measure of gait variability. au, arbitrary unit. **Step 6:** The scores (position of gait cycles in the PC space) reveal which conditions are differentiated along each PC. **Step 7:** We then extracted the factor loadings, i.e. correlation between each variable and each PC. We selected the PC of interest based upon step 6, and regrouped the variables with the highest factor loading ($|value| > 0.5$, $p < 0.05$) into functional clusters, which we named for clarity. Variables that load on the same PC correlate with each other. For instance, in the proposed example, improvement of hindlimb locomotion directly correlates with improved postural control. **Step 8:** To provide a more classic representation of differences between conditions, we generated histogram plots for one variable per extracted functional cluster.

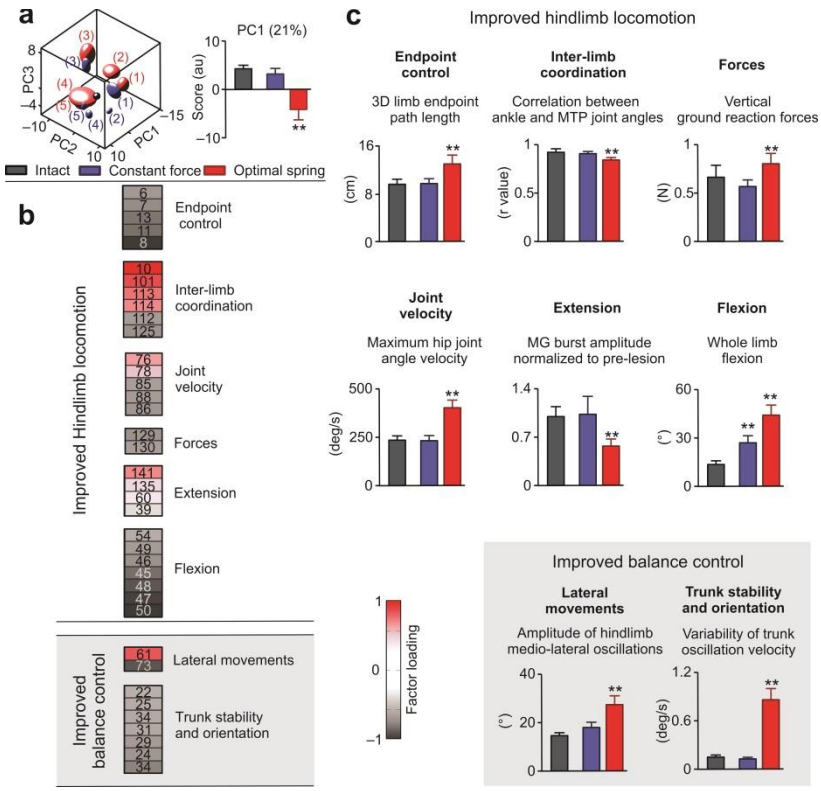

Supplementary Figure 4.4. Constant-force support leads to improved locomotor performance compared to spring-like support in rats with complete SCI.

a. PC analysis (explained variance, 48%) applied on all gait cycles and rats (n = 10 per rat and per condition). Least square fitting was performed and indexed for each rat independently. The histogram plot reports mean values (n = 5 rats) of scores on PC1 for gait cycles recorded in intact rats and in spinal rats stepping with the same level of spring-like vs. constant force vertical support. au, arbitrary unit. **b.** Variables (numbers refer to **Supplementary Table 4.1**) with the highest factor loadings on PC1 (|value|> 0.5, $p < 0.05$) were regrouped in functional clusters. **c.** Histogram plots report mean values (n = 5 rats) for one variable per functional cluster for intact rats and spinal rats stepping with spring-like vs. constant force vertical support. **, significantly different from intact at $p < 0.05$.Error bar, S.E.M.

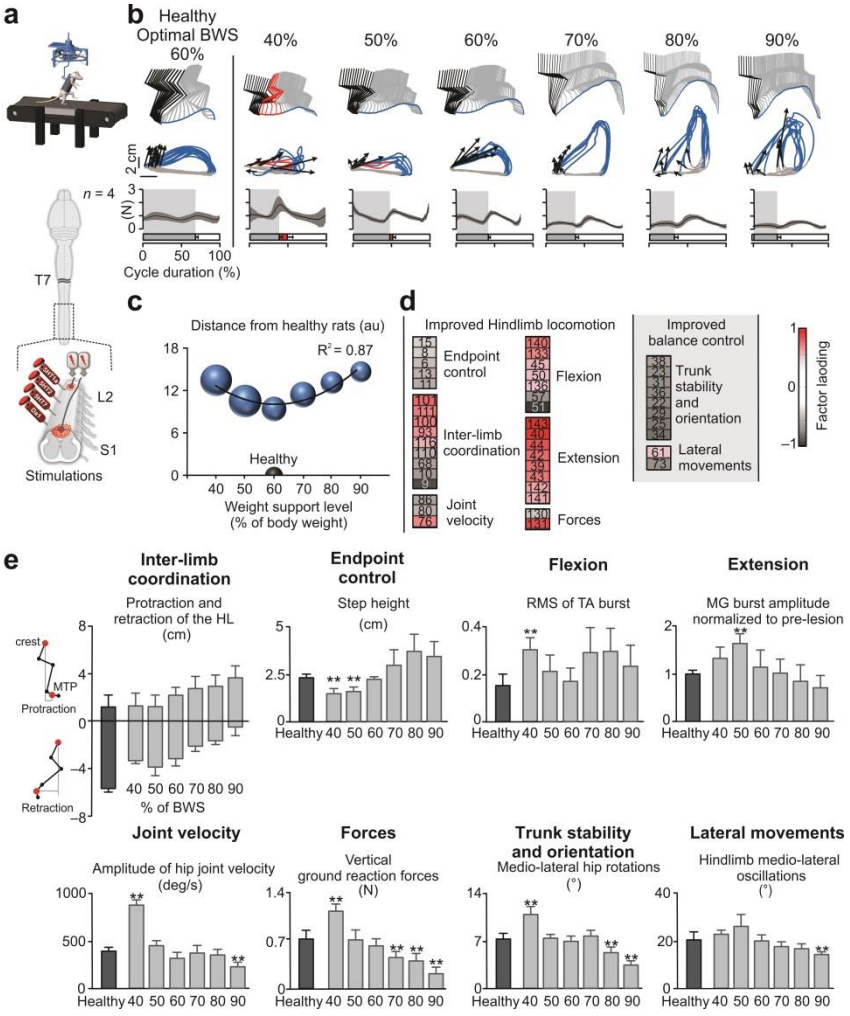

Supplementary Figure 4.5. Evaluation of the impact of weight bearing conditions on motor pattern generation in rats with complete SCI.

a. Rats (n = 4 rats) received a complete SCI. After 5 weeks of recovery, the rats received enabling factors to encourage bipedal locomotion on a treadmill (13 cm.s-1). 10 gait cycles were recorded for each level of constant-force BWS (40-90%). Locomotion was recorded in healthy rats (n = 5) at 60% of BWS, which is the weight normally carried by the hindlimbs during quadrupedal gait**. b.** Representative stick diagram decomposition of hindlimb motion during stance (black), dragging (red), and swing (light grey) for each level of BWS, as well as for an intact rat. Successive color-coded trajectories of the hindlimb endpoint (n = 10 steps) are shown together with the orientation and intensity of the foot velocity vector (arrow) at swing onset. The average (n = 10 steps, +/- S.D.) vertical ground reaction forces (left and right hindlimbs combined) and relative duration of the stance (filled box), swing (open box), and drag (red) phases of gait are displayed at the bottom. **c.** Relationship between the level of BWS and the degree of gait pattern

similarity compared to healthy rats (grey hemi-sphere), measured as the 3D distance from gait cycles in the PC analysis. The size of the spheres is proportional to gait variability, measured as the dispersion of each cluster in the PC analysis (See **Supplementary Figure 4.3**). A second-order polynomial fitting was applied to the data points to highlight the U-shaped relationship between stepping quality and BWS levels. au, arbitrary unit. **d.** Variables (numbers refer to **Supplementary Table 4.1**) with the highest factor loadings on PC1 (|value| > 0.5, $p < 0.05$) were regrouped in functional clusters. **e.** Histogram plots report mean values (n = 4 rats; error bar, S.E.M.) for one variable per functional cluster under the different levels of BWS. **, significantly different from intact at $p < 0.05$. Error bars, S.E.M.

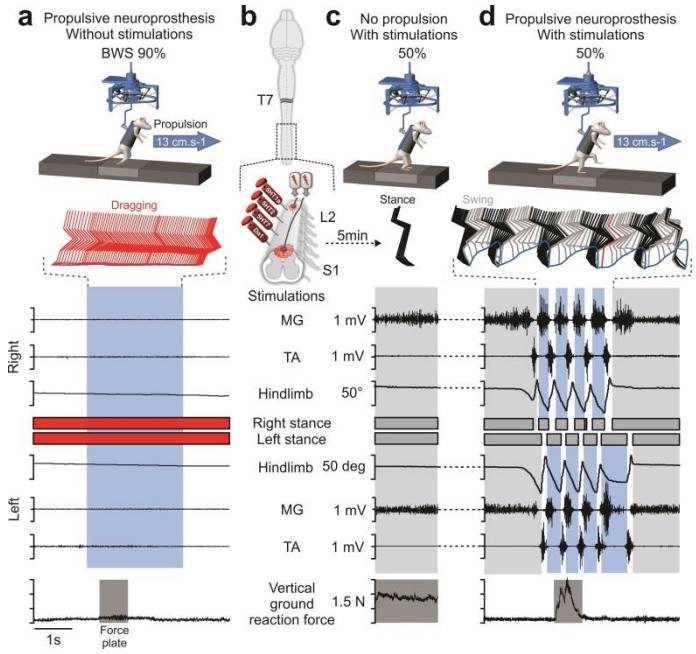

Supplementary Figure 4.6. The robotic propulsive neuroprosthesis enables coordinated overground locomotion in spinal rats.

a. Spinal rats were positioned bipedally in the robotic interface. The robot was configured to move the body forward at a constant velocity (13 cm.s–1) while providing constant-force vertical support. Below the stick diagram decomposition of hindlimb motion and limb endpoint trajectories, the traces show angular oscillations of both hindlimbs, EMG activity of left and right MG and TA muscles, and vertical forces during a representative trial performed without stimulations. **b.** To enable hindlimb locomotion, rats received tonic epidural electrical stimulation at spinal segments S1 and L2, as well as a combination of agonists to 5HT1A, 5HT2A/C, 5HT7, and DA1-like receptors. **c.** With

these stimulations, the spinal rats displayed tonic activity in left and right extensor muscles, and could stand for extensive periods of time. **d.** The animals immediately exhibited coordinated plantar stepping with alternation between both hindlimbs when the robot translated the trunk in the forward direction to replace the lost propulsive capacities.

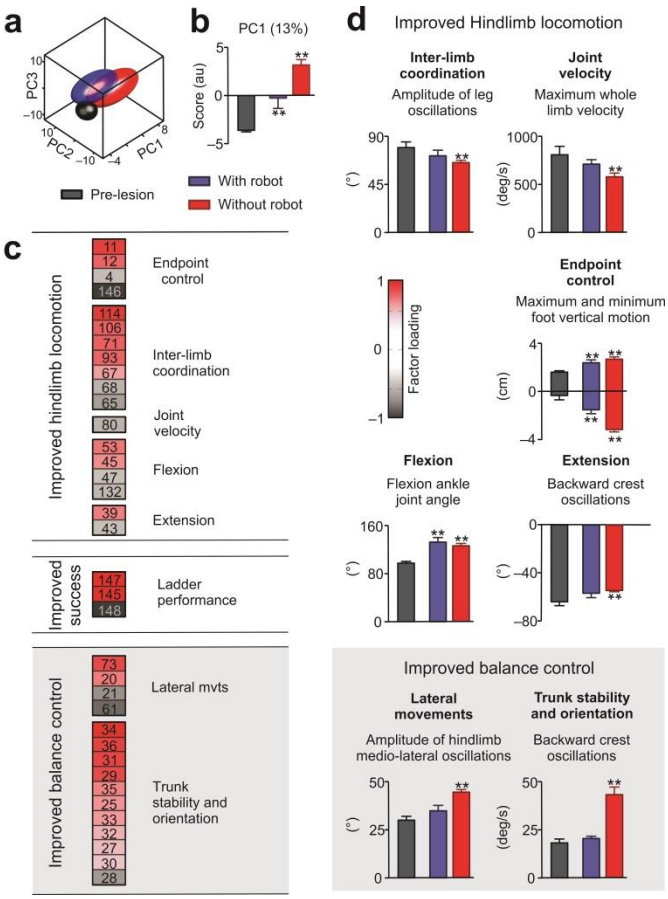

Supplementary Figure 4.7. Improved balance control with the postural neuroprosthesis correlates with improved hindlimb locomotion and performance during locomotion along a ladder with irregularly spaced rungs in rats with a cortical stroke.

a. PC analysis was applied on all gait cycles recorded along the ladder in all the rats (n = 5) before and 2 days after lesion with and without vertical constant-force robotic support. Accurate and missed steps were both included in this analysis, but undifferentiated in the plot to emphasize the contrast between the conditions with and without robot. au, arbitrary unit. **b.** The histogram plot reports the mean values (n = 5 rats) of scores on PC1. **c.** Variables (numbers refer to **Supplementary Table 4.1**) with the highest factor loadings on PC1 (|value|> 0.5, $p < 0.05$) were regrouped in functional clusters. **d.** Histogram plots report mean values (n = 5 rats) for one variable per functional

cluster, except for the improved measures of success that are reported in **Figure 3b**. **, significantly different from intact at $p < 0.05$. Error bar, S.E.M.

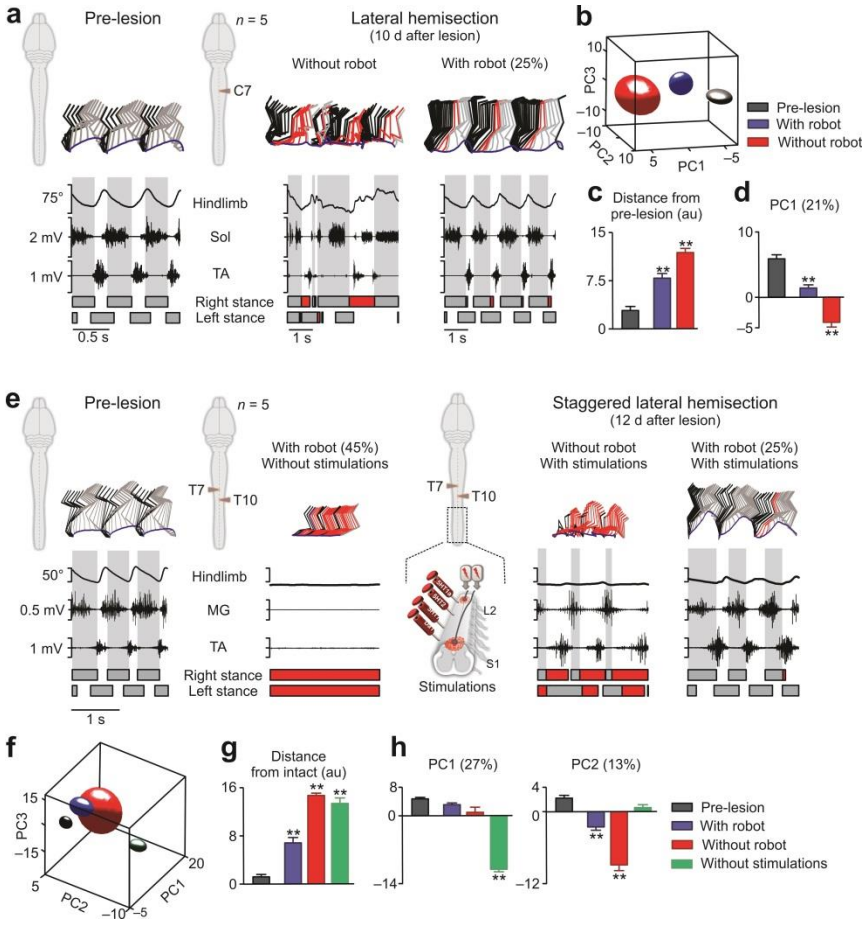

Supplementary Figure 4.8. Improved balance control with the postural neuroprosthesis correlates with improved hindlimb locomotion during straight horizontal runway locomotion in rats with moderate and severe SCI.

a. Stick diagram decomposition of hindlimb motion, hindlimb oscillations, and EMG activity of Sol and TA muscles recorded pre-lesion as well as 10 days after a lateral cervical (C7) hemisection with and without constant-force robotic support. **b.** PC analysis was applied on all gait cycles recorded in all the rats (n = 5) before and 10 days after lesion with and without robotic support. **c.** The histogram plot reports mean values (n = 5 rats) of the 3D distance from the mean location of pre-lesion gaits in the PC space. **d.** PC1scores. **e.** Hindlimb kinematics and EMG activity of MG and TA muscles recorded pre-lesion as well as 12 days after staggered lateral hemisections without enabling factors (no stimulations) as well as with stimulations without and with constant-force robotic support. **f.** PC analysis was applied on all gait cycles recorded in all the rats (n =

5) before and 10 days after lesion without stimulations as well as we with and without robotic support. **g.** The histogram plot reports mean values (n = 5 rats) of the 3D distance between the different experimental conditions and the mean location of pre-lesion gaits in the PC space. **h.** PC1 differentiates actual stepping vs. paralysis, while PC2 highlights the improvement of locomotion with the postural neuroprosthesis. **, significantly different from intact at p < 0.05. au, arbitrary unit**.** Error bar, S.E.M.

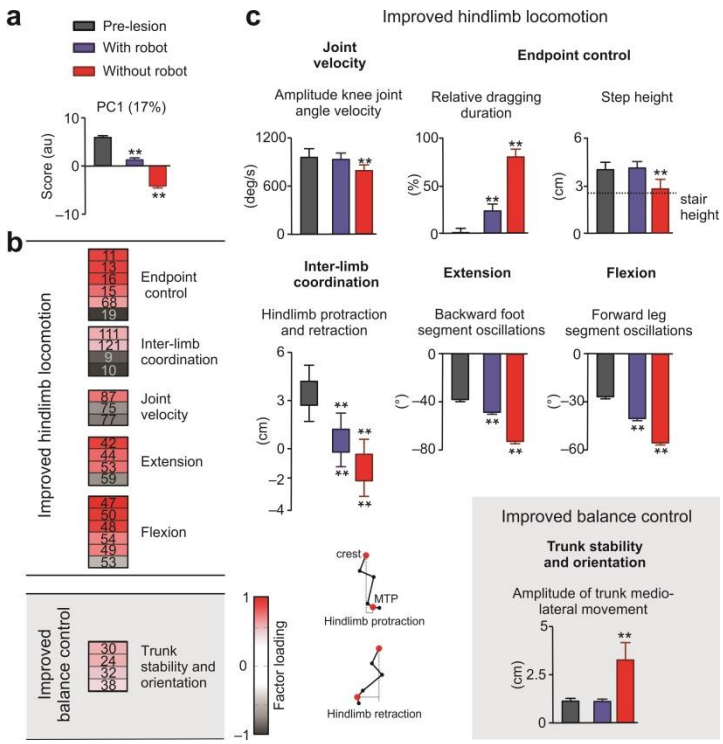

Supplementary Figure 4.9. Improved balance control with the postural neuroprosthesis correlates with improved hindlimb locomotion during locomotion on a staircase in rats with moderate SCI.

a. Histogram plots report mean values (n = 5 rats) of scores on PC1 for gait cycles recorded before as well as 10 days after a lateral cervical (C7) hemisection without and with constant-force robotic support.au arbitrary unit. **b.** Variables (numbers refer to **Supplementary Table 4.1**) with the highest factor loadings on PC1 (|value|> 0.5, p < 0.05) were regrouped in functional clusters. **c.** Histogram plots report mean values (n = 5 rats) for one variable per functional cluster. **, significantly different from intact at p < 0.05.Error bar, S.E.M.

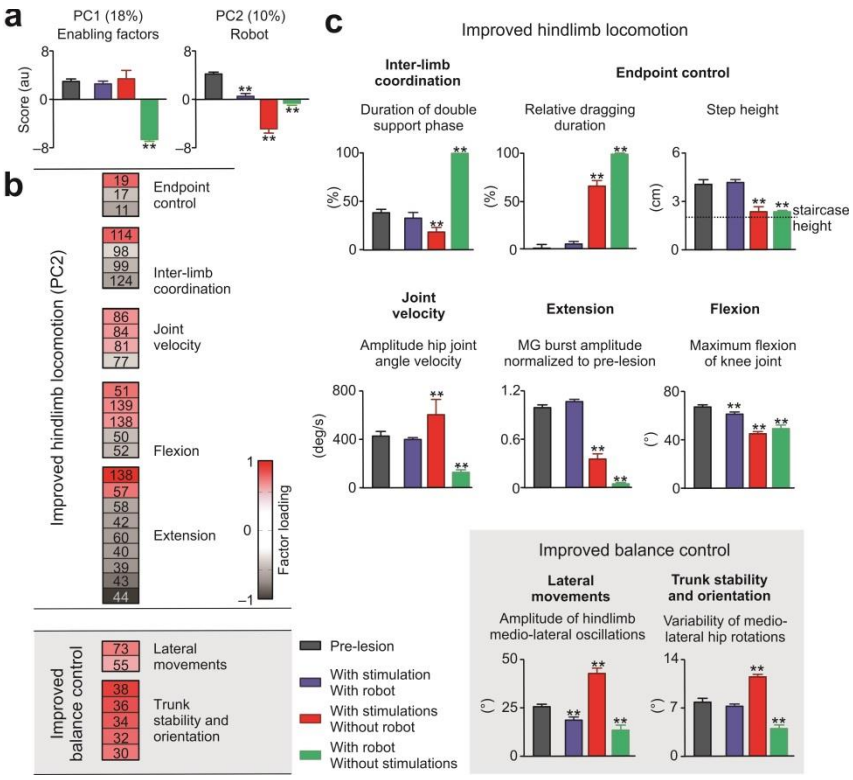

Supplementary Figure 4.10. Improved balance control with the postural neuroprosthesis correlates with improved hindlimb locomotion during locomotion on a staircase in rats with severe SCI.

a. Histogram plots report mean values (n = 5 rats) of scores on PC1 and PC2 for gait cycles recorded before the lesion and 12 days after staggered lateral hemisections under the various experimental conditions. PC1 captures the effect of motor control enabling factors, which promoted hindlimb motion in otherwise paralyzed rats. PC2 captures the improvements of hindlimb locomotion and balance control with the robotic interface. au, arbitrary unit. **b.** Variables (numbers refer to **Supplementary Table 4.1**) with the highest factor loadings on PC2 (|value|> 0.5, $p < 0.05$) were regrouped in functional clusters. **c.** Histogram plots report mean values (n = 5 rats; error bar, S.E.M.) for one variable per functional cluster under the different experimental conditions. **, significantly different from intact at $p < 0.05$. error bar, S.E.M.

Supplementary Table 1. Computed Kinematics, Kinetics, and EMG Parameters of Gait Parameters

Parameters		#	Detailed explanation
Kinematics			
Temporal features of gait			
		1	Cycle velocity
		2	Cycle duration
		3	Stance duration
		4	Relative stance duration (percent of the cycle duration)
		5	Swing duration
Limb endpoint (MTP) trajectory			
		6	Stride length
		7	Step length
		8	3D limb endpoint path length
		9	Maximum backward position
		10	Minimum forward position
		11	Step height
		12	Relative position of main peak
		13	Maximum speed during swing
		14	Relative timing of maximum velocity during swing
		15	Acceleration at swing onset
		16	Endpoint velocity
		17	Orientation of the velocity vector at swing onset
		18	Dragging
		19	Relative dragging duration (percent of swing duration)
Stability			
Base of support		20	Positioning of the foot at stance onset with respect to the pelvis
		21	Stance width
Trunk and pelvic position and oscillations		22	Variability of sagittal trunk oscillations
		23	Variability in velocity of sagittal trunk oscillations
		24	Variability of Medio-lateral hip oscillations
		25	Variability of vertical mid-point hip oscillations
		26	Variability of Medio-lateral mid-point shoulder oscillations
		27	Variability of vertical mid-point shoulder oscillations
		28	Maximum trunk vertical position
		29	Amplitude of trunk vertical movement
		30	Amplitude of trunk Medio-lateral movement
		31	Variability of vertical trunk movement
		32	Variability of Medio-lateral trunk movement
		33	Variability of Medio-laterale trunk velocity
		34	Variability of vertical trunk velocity
		35	Variability of trunk acceleration in Medio-lateral direction
		36	Variability of trunk acceleration in vertical direction
		37	Variability of Medio-lateral shoulder rotations
		38	Variability of Medio-lateral hip rotations
Joint angles and segmental oscillations			
Backward	proximal	39	Crest oscillations
		40	Thigh oscillations
		41	Leg oscillations
		42	Foot oscillations
	distal	43	Toe oscillations
	whole limb	44	Whole limb oscillations
Forward	proximal	45	Crest oscillations
		46	Thigh oscillations
		47	Leg oscillations
		48	Foot oscillations
	distal	49	Toe oscillations
	whole limb	50	Whole limb oscillations
Flexion	proximal	51	Hip joint angle
		52	Knee joint angle
		53	Ankle joint angle
	distal	54	MTP joint angle
Abduction	whole limb	55	Whole limb abduction
	distal	56	Foot abduction
Extension	proximal	57	Hip joint angle
		58	Knee joint angle
		59	Ankle joint angle
	distal	60	MTP joint angle
Adduction	whole limb	61	Whole limb adduction
	distal	62	Foot adduction
Amplitude	proximal	63	Crest oscillations
		64	Thigh oscillations
		65	Leg oscillations
		66	Foot oscillations
	distal	67	Toe oscillations
	whole limb	68	Whole limb oscillations
	proximal	69	Hip joint angle
		70	Knee joint angle
		71	Ankle joint angle
	distal	72	MTP joint angle
	whole limb	73	Whole limb medio-lateral oscillations
	distal	74	Foot abduction /adduction

Parameters		#	Detailed explanation
Kinematics			
Velocity			
Minimum	whole limb	75	Whole limb oscillation velocity
	proximal	76	Hip joint angle velocity
		77	Knee joint angle velocity
		78	Ankle joint angle velocity
	distal	79	MTP joint angle velocity
Maximum	whole limb	80	Whole limb oscillation velocity
	proximal	81	Hip joint angle velocity
		82	Knee joint angle velocity
		83	Ankle joint angle velocity
	distal	84	MTP joint angle velocity
Amplitude	whole limb	85	Whole limb angle velocity
	proximal	86	Hip joint angle velocity
		87	Knee joint angle velocity
		88	Ankle joint angle velocity
	distal	89	MTP joint angle velocity
Inter-limb coordination			
PC analysis		90	Degree of linear coupling between joint oscillations
FFT decomposition	proximal	91	Temporal coupling between crest and thigh oscillations
		92	Temporal coupling between thigh and leg oscillations
		93	Temporal coupling between leg and foot oscillations
	distal	94	Temporal coupling between foot and toe oscillations
Cross-correlation	proximal	95	Correlation between crest and tight oscillations
		96	Correlation between tight and leg oscillations
		97	Correlation between leg and foot oscillations
	distal	98	Correlation between foot and toe oscillations
Relative coupling	proximal	99	Correlation between hip and knee oscillations
		100	Correlation between knee and ankle oscillations
	distal	101	Correlation between ankle and MTP oscillations
	proximal	102	Temporal lag between backward positions of crest and thigh oscillations
		103	Temporal lag between forward positions of crest and thigh oscillations
		104	Temporal lag between backward positions of thigh and leg oscillations
		105	Temporal lag between forward positions of the thigh and leg oscillations
		106	Temporal lag between backward positions of leg and foot oscillations
		107	Temporal lag between forward positions of leg and foot oscillations
		108	Temporal lag between backward positions of foot and toe oscillations
	distal	109	Temporal lag between forward positions of foot and toe oscillations
inter-segmental coordination		110	Percentage of variance (1th eigenvector) between segmental oscillations
		111	Percentage of variance (2th eigenvector) between segmental oscillations
		112	Percentage of variance (3th eigenvector) between segmental oscillations
		113	1th eigenvector (long axis of the gait-loop) projection on thigh axis
		114	1th eigenvector (long axis of the gait-loop) projection on shank axis
		115	1th eigenvector (long axis of the gait-loop) projection on foot axis
		116	2th eigenvector (short axis of the gait-loop) projection on thigh axis
		117	2th eigenvector (short axis of the gait-loop) projection on shank axis
		118	2th eigenvector (short axis of the gait-loop) projection on foot axis
		119	3th eigenvector (normal to the the gait-loop plane) projection on thigh axis
		120	3th eigenvector (normal to the the gait-loop plane) projection on shank axis
		121	3th eigenvector (normal to the the gait-loop plane) projection on foot axis
		122	Area of the gait-loop
Left-right hindlimb coordination		123	Ratio of left to right hindlimb cycle duration
		124	Double stance duration
		125	Correlation between whole hindlimb oscillations
Forelimb and hindlimb coordination		126	Correlation between hindlimb and ipsilateral forelimb oscillations
		127	Correlation between hindlimb and contralateral forelimb oscillations
Kinetics			
		128	Medio-lateral forces
		129	Anteroposterior forces
		130	Vertical forces
		131	Weight bearing level
EMG			
Timing (relative to cycle duration, paw contact to paw contact)			
Flexor		132	Relative onset of TA EMG burst
		133	Relative end of TA EMG burst
Extensor		134	Relative onset of MG/Sol EMG burst
		135	Relative end of MG/Sol EMG burst
Duration			
Flexor		136	TA EMG burst
Extensor		137	MG/Sol EMG burst
Amplitude			
Flexor		138	Mean amplitude of TA EMG burst
		139	Integral of TA EMG burst
		140	Root mean square of TA EMG burst
Extensor		141	Mean amplitude of MG/Sol EMG burst
		142	Integral of MG/Sol EMG burst
		143	Root mean square of MG EMG burst
Antagonist co-contraction			
		144	Co-contraction of MG/Sol and TA muscles
Ladder performance			
		145	Relative horizontal position of the foot-rung during stance
		146	Relative vertical position of the foot-rung during stance
		147	Relative horizontal position of the foot (percent distance between rungs)
		148	Performance score (0 Accurate; 1 Slip; 2 Miss)

Supplementary Table 4.1 Computed kinematic, kinetic and EMG parameters

10.3 Supplementary information chapter 5

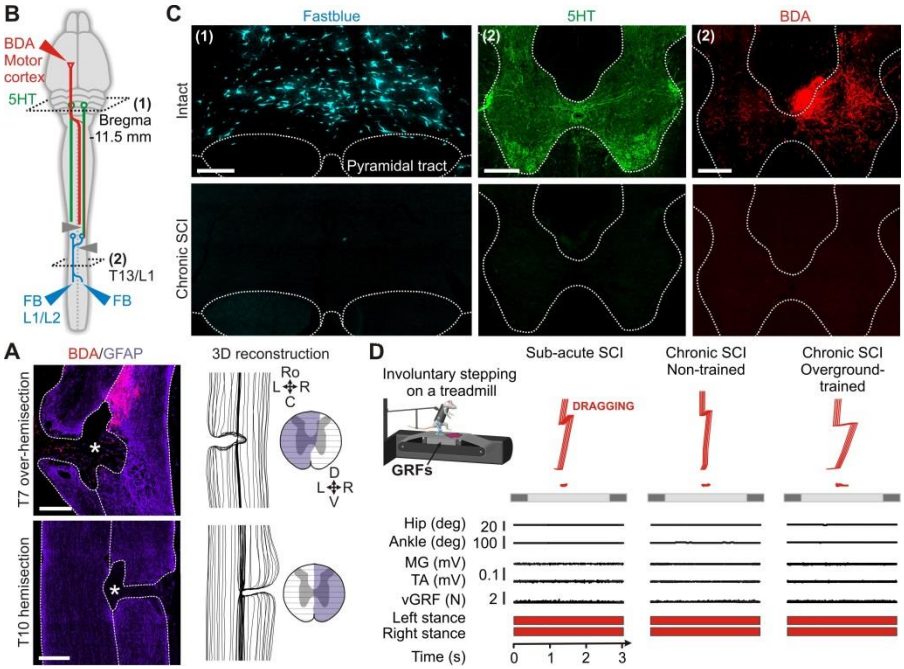

Supplementary Figure 5.1 Staggered lateral hemisections induce a complete interruption of direct supraspinal pathways, leading to a complete and permanent paralysis of both hindlimbs.

(A) Epifluorescent images as well as longitudinal and coronal views of a 3D reconstruction of the T7 lateral over-hemisection and T10 lateral hemisection. Scale bar, 500µm. We placed an over-hemisection at T7 in order to interrupt all the corticospinal fibers running in the dorsal column, thus only sparing the few (1-2%) fibers running through the right dorsolateral funiculus. **(B)**. Diagram illustrating anatomical experiments. **(C)** Combinations of retrograde (Fastblue, FB) and anterograde (biotinylated dextran amine, BDA) tracers together with immunolabeling of 5HT fibers show the complete and permanent absence of direct connections between spinal locomotor circuits and supraspinal centers. Scale bar, 300µm. **(D)** Rats were positioned in a bipedal posture above a moving treadmill belt (9 cm/s) while secured in a jacket that was attached to a robotic arm. Recordings at 1 and 9 weeks post-injury without electrochemical stimulations, both in non-trained and overground-trained rats, showed the complete and permanent absence of spontaneous hindlimb locomotor movements and vertical ground

reaction forces (vGRF), as well as the quiescent EMG activity of tibialis anterior (TA) and medial gastrocnemius (MG) muscles.

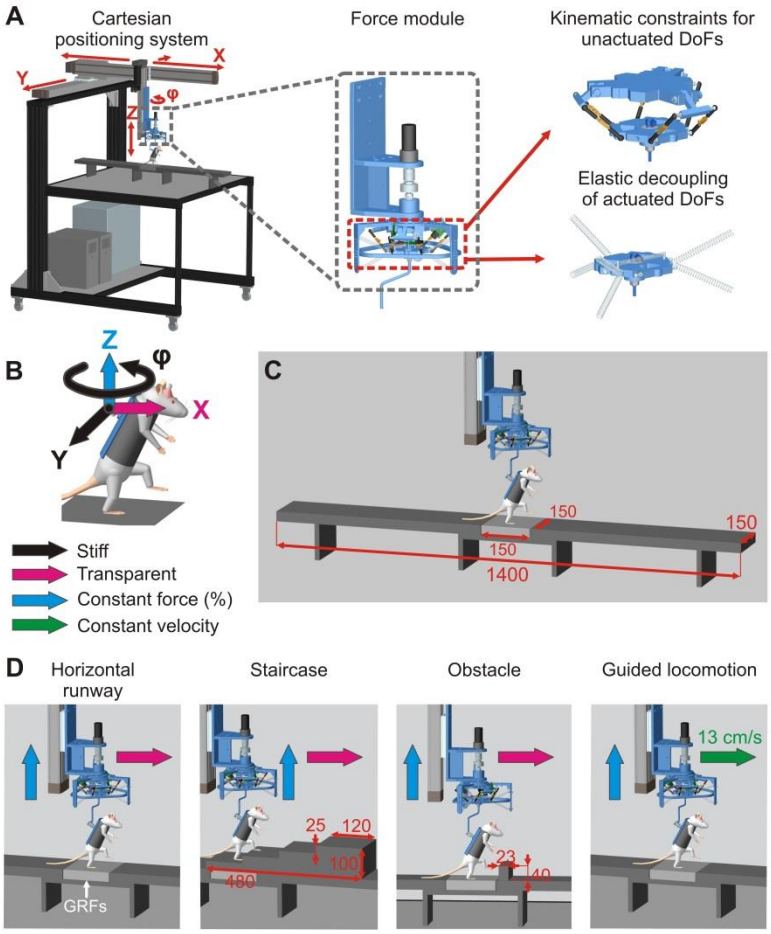

Supplementary Figure 5.2 Robotic postural interface to enable bipedal locomotion across a variety of paradigms.

(A) The robot consists of an actuated Cartesian positioning system that allows translations of the rat in the horizontal plane (X, Y) while providing vertical support (Z). An additional motor at the end-effector of this serial structure actuates rotation (φ). This serial configuration provides a large workspace in which forces can be applied to the rat in 4 degrees of freedom (DoFs). To hide the inertia of the massive positioning robot, we developed a novel force module based on a series elastic actuator (SEA). A SEA is composed of an actuator that is complemented with a passive compliant element in series. This compliant interface effectively decouples the actuator's inertia to achieve a transparent supporting system; the rat does not "feel" the presence of the robot. **(B)** The rat is positioned in a custom-made, skin-like jacket made of light fabrics. A velcro strip allows attachment of the rat onto a back plate with a rigid bar coming from the robot end-

effector. A control interface allows the user to create a virtual environment in which each of the 4 actuated DoFs can be configured independently, from stiff to fully transparent. Typically, we set the X-axis (forward direction) to behave transparently and the Z-axis to provide a constant force proportional to the rat's body weight. The lateral (Y) and rotational (φ) axes were maintained stiff to prevent lateral falls. For specific testing and training, the robot moved the rat's trunk forward at a constant velocity. Consequently, the hindlimbs moved backward and hip joint angle increased towards extension, thus creating conditions that are similar to stepping on a treadmill. Although performed overground, these stepping movements are involuntary. **(C)** Dimension of the horizontal runway. **(D)** Schematic diagrams and features of the different locomotor tasks. The light gray box indicates the position of the force plate for recordings of ground reaction forces (GRF).

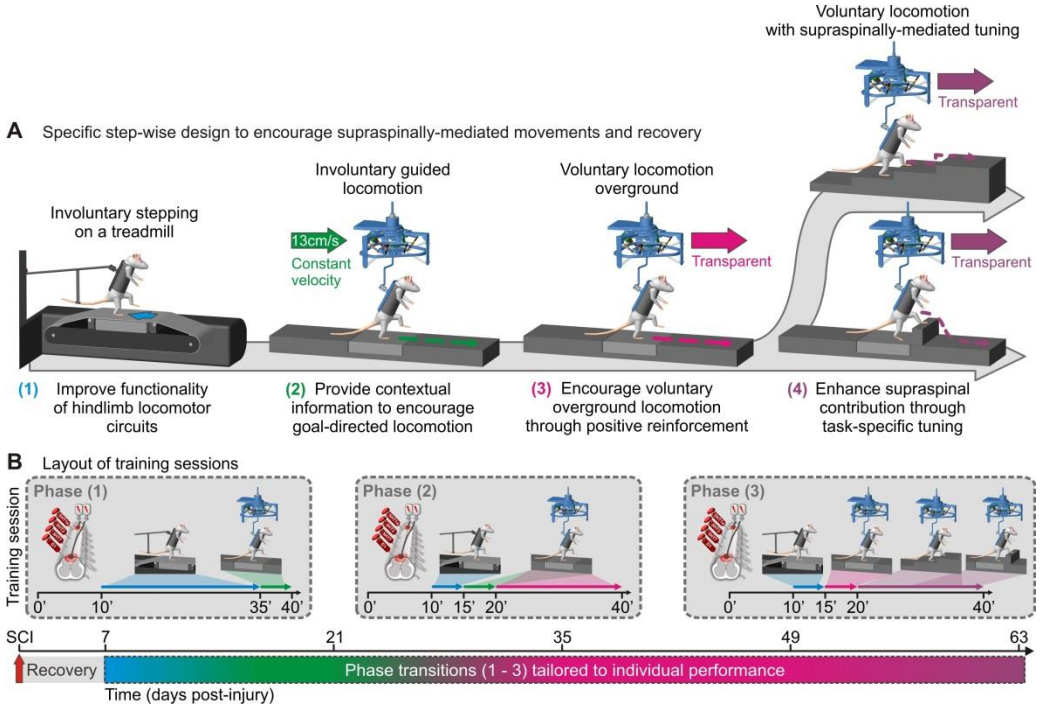

Supplementary Figure 5.3 Conceptual design of the multi-system neuroprosthetic training program.

The **training** consisted of a combination of **(A)** 4 distinct paradigms broadly divided into **(B)** 3 phases specifically tailored to the rats' performance and training objectives. To enable highly functional motor states, rats received monoamine agonists 10 min prior to training, and dual-site EES throughout the session. **Phase (1).** The primary objective of the early training phase was to optimize the functionality of lumbosacral circuits. The rats

were subjected to treadmill-based training with vertical support. Sensory input elicited by the moving treadmill belt served as a source of control for hindlimb stepping. Manual assistance was provided in an *assist-as-needed* manner in order to present appropriate sensory cues to lumbosacral circuitries. At the end of each session, we positioned the rats in the robotic postural interface and encouraged them to walk bipedally towards a target located in front of them. The robot was configured to establish optimal medio-lateral and vertical weight support. In order to provide contextual information on the requested task, the robot translated the rat forward at a constant velocity. Positive reinforcement including food rewards and motivational stimuli were used to trigger active participation. The objective was to force the brain to regain supraspinal control over the electrochemically enabled lumbosacral circuits. **Phase (2).** As the rats progressively regained the ability to produce voluntary steps, we gradually increased the duration of locomotion overground. The aim was to encourage the repetitive and quantitative activation of lumbosacral circuits by the newly formed intraspinal and supraspinal connections. However, treadmill-restricted training was still practiced daily in order to engage spinal locomotor circuits over consistent periods of time for the maintenance of their functionality. **Phase (3).** When the rats regained robust hindlimb locomotion overground, we introduced complex tasks requiring fine-tuning of hindlimb movements, i.e. stair climbing and obstacle avoidance. The goal was to promote enhanced supraspinal contribution in order to restore qualitative control over electrochemically enabled lumbosacral circuits.

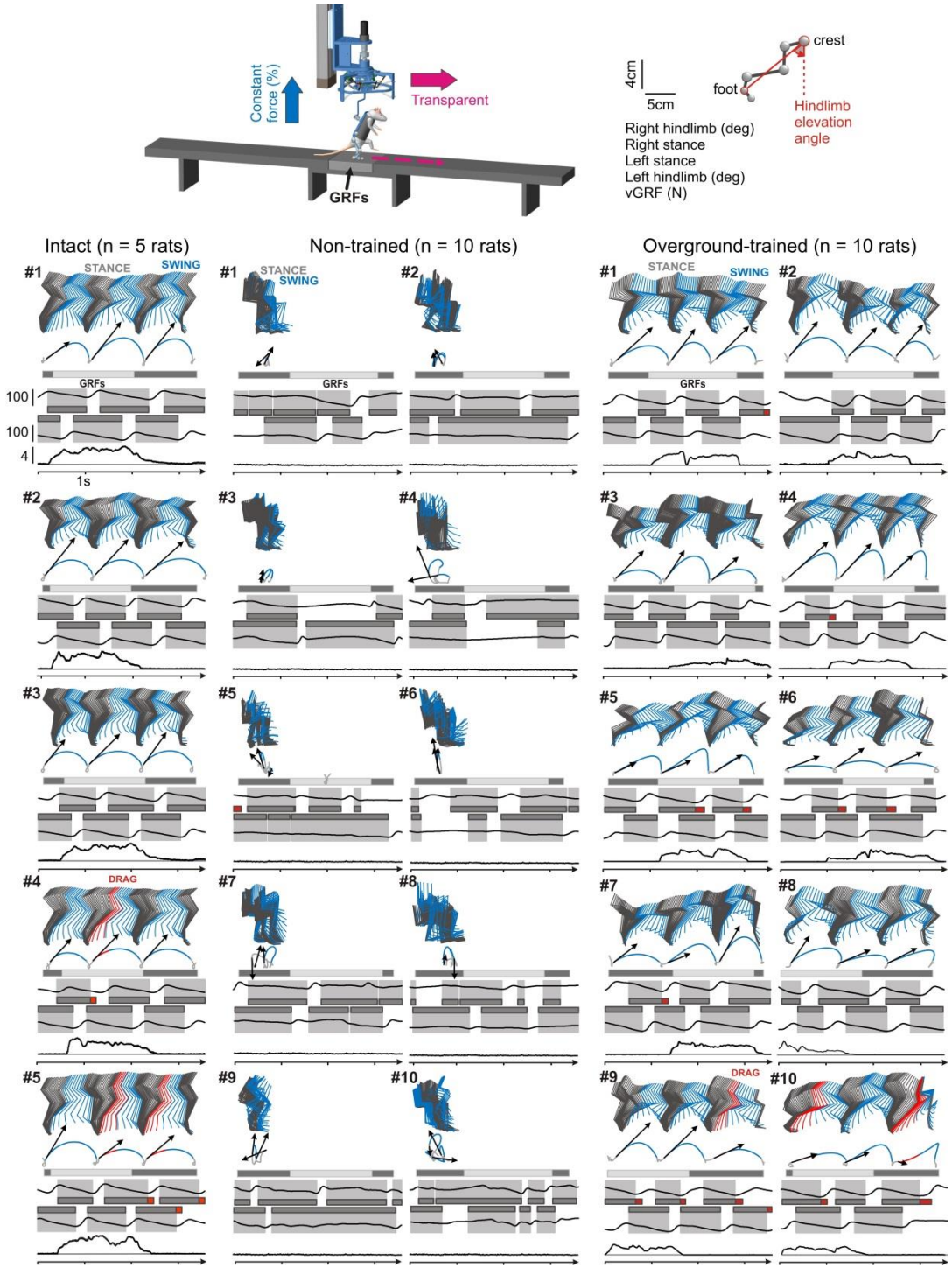

Supplementary Figure 5.4 Multi-system neuroprosthetic training restores voluntary locomotion overground in all the rats.

Representative trials are shown for five intact animals (left), as well as 9 weeks post-injury for each of the non-trained (middle) and overground-trained (right) rats. For each panel, a stick diagram decomposition of hindlimb motion is shown together with color-coded trajectories of the hindlimb endpoint. The hindlimb was defined as the virtual

segment connecting the pelvis to the foot. Vectors represent the direction and intensity of the hindlimb endpoint velocity at swing onset. The corresponding sequence of left and right hindlimb oscillations and vertical ground reaction forces (vGRF) are shown below. The light gray rectangle indicates the location of the force plate (GRFs) on the runway. Gray and red bars indicate the duration of stance and drag phases, respectively

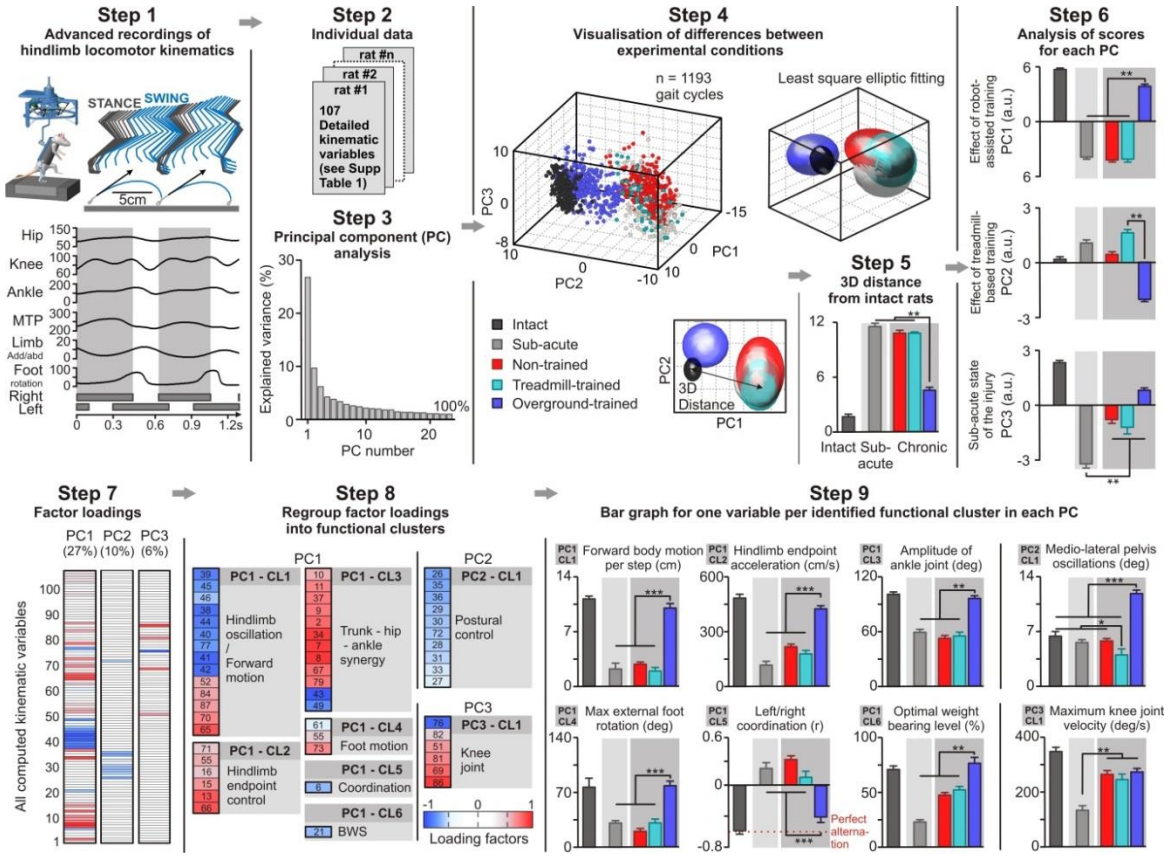

Supplementary Figure 5.5 Multi-step statistical analysis of locomotor performance and control strategies.

Step 1: Advanced recordings of hindlimb kinematics during bipedal overground locomotion. **Step 2:** We computed a large number of variables that provides a holistic quantification of gait. Variables can be found in **Table 5.1**. **Step 3:** We applied a principal component (PC) analysis on all the variables and recorded gait cycles. **Step 4:** Individual gait cycles can be represented in the new "denoised" space created by PC1-3. We applied a least square elliptic fitting to easily visualise differences between experimental groups. **Step 5:** Locomotor performances were quantified, for each rat, as the 3D Euclidean distance between the location of gait cycles and the average location of all gait cycles from all the intact rats (n = 20 rats). **Step 6:** The scores indicate which

experimental groups are differentiated by each PC. **Step 7:** Extraction of factor loadings, i.e. correlation between each gait variable and each PC. **Step 8:** We regrouped variables with the highest factor loading (|value| > 0.5, $p < 0.05$) into functional clusters (CL), which we named for clarity. **Step 9:** To highlight the functional implications of the PC analysis, we generated a histogram plot for one variable per extracted functional cluster. Conclusions: PC1 revealed that recovery of voluntary locomotion in overground-trained rats resulted from a strong synergy between ankle extension, trunk extension, and hip flexion, as well as improved interlimb coordination, increased weight bearing capacities, enhanced lateral foot motion, and near-normal control of hindlimb endpoint trajectory. PC2 indicated that treadmill-trained rats showed highly stable posture, but failed to initiate forward locomotion. In turn, overground-trained rats exhibited enhanced lateral body movements that alternatively loaded the left and right hindlimbs during locomotion, and thus helped to maintain dynamic balance. PC3 highlights the flexed posture and slow hindlimb motion of rats in the sub-acute state. a.u., arbitrary unit. **, $P < 0.01$; ***, $P < 0.001$. Error bars, s.e.m.,

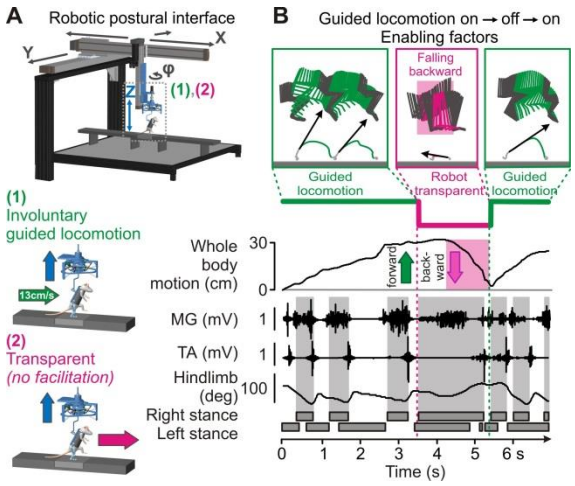

Supplementary Figure 5.6 Failure to sustain voluntary locomotion overground in treadmill-trained rats.

(A) The robotic postural interface can be operated in two modes: **(1)** *involuntary guided locomotion mode* and **(2)** *transparent mode* **(supp. fig. 5.2)**. **(B)** To test the ability of treadmill-trained rats to sustain voluntary locomotion overground, we programed a sequence during which the robotic postural interface alternated between both modes. Right hindlimb kinematics and EMG activity of right MG and TA muscles are shown according to conventions in **supp. fig. 5.6** and **Fig. 5.1**. The position of the whole body along the axis of progression is also represented. When interrupting the robotic guidance,

treadmill-trained rats failed to sustain voluntary locomotion overground despite energetic movements with the forelimbs to keep progressing towards a reward, located in front of them. Instead, due to the backward location of the body's center of mass, the rats fell backwards (shaded area). As soon as the robotic guidance was re-applied, the rats displayed coordinated, although involuntary, locomotor movements in the forward direction. These conditions are shown for a representative treadmill-trained rat at 9 weeks post-lesion, but we observed similar behaviors for all the rats in the sub-acute state (1 week post-lesion), as well as for non-trained rats at 9 weeks post-lesion.

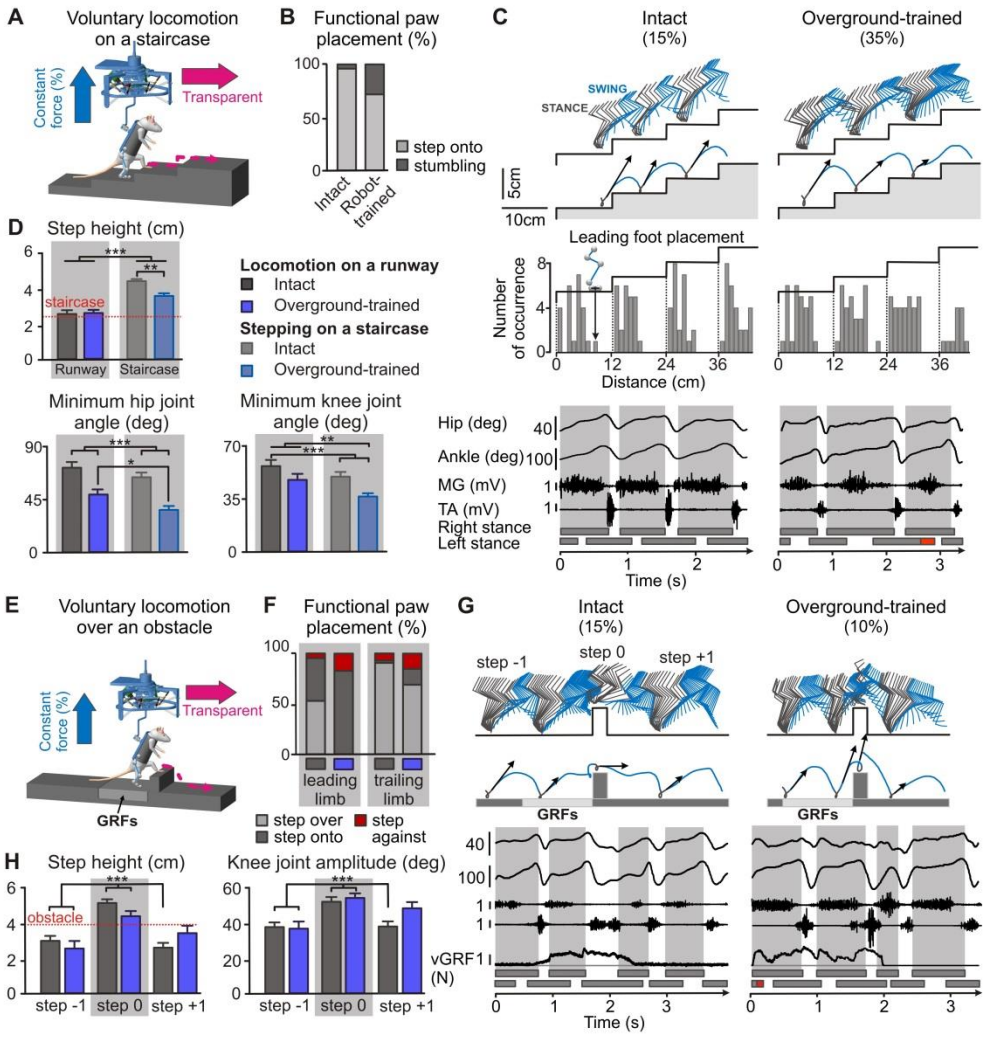

Supplementary Figure 5.7 Multi-system neuroprosthetic training restores qualitative control of hindlimb locomotor movements.

(A) Diagram illustrating bipedal locomotion on a staircase. **(B)** Histograms showing the percentage of correct (step onto) and incorrect (stumbling) hindpaw placements onto

each step of the staircase. **(C)** Bipedal locomotion on a staircase for an intact and overground-trained rat. Stick conventions are the same as **Fig. 5.1** and **supp. fig. 5.4**. The histogram plots show, for all the intact (n = 5) and overground-trained (n = 10) rats, the distribution of leading foot placements with respect to the positions of the staircases. **(D)** Histogram plots reporting step height as well as the extent of hip and knee flexion during locomotion on a runway and on a staircase for intact and overground-trained rats. **(E)** Diagram illustrating bipedal locomotion over an obstacle. **(F)** Histogram plots showing the percentage of steps performed over and onto the obstacle by the leading and trailing hindlimb for intact and overground-trained rats. **(G)** Bipedal locomotion over an obstacle for an intact and overground-trained rat. **(H)** Histogram plots reporting step height and amplitude changes of the knee joint angle before (step -1), onto (step 0), and after (step +1) the obstacle for intact (n = 5) and overground-trained (n = 10) rats. *, P < 0.05; **, P < 0.01; ***, P < 0.001. Error bars, s.e.m

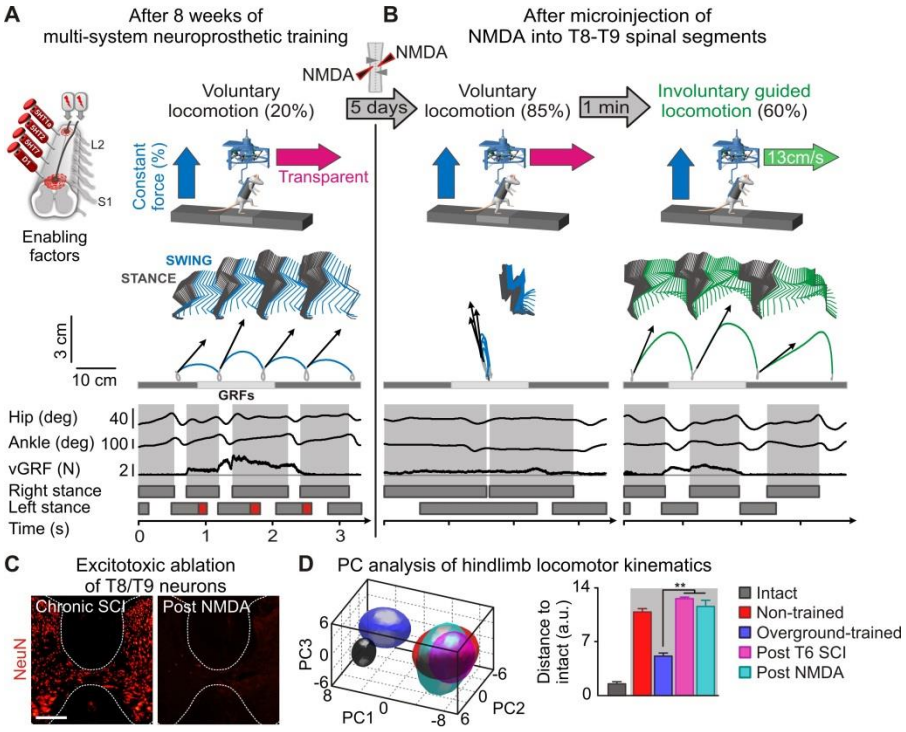

Supplementary Figure 5.8 Ablation of T8-T9 neurons abolishes voluntary locomotion overground, but leaves spinal locomotor circuitries globally unaffected.

Representative example of bipedal locomotion overground in the presence of enabling factors for a overground-trained rat **(A)** before and **(B)** 5 days after

microinjections of NMDA into T8-T9 spinal segments. Conventions are the same as in **supp. fig. 5.4**. The amount of vertical support provided by the robot is indicated in the blue arrow. After NMDA microinjections, the rats failed to initiate voluntary locomotion overground. However, all the tested rats (n = 3) displayed coordinated locomotor movements when the robot moved their body forward at a constant velocity (right panel, 13 cm/s). These results indicate that the loss of thoracic relay neurons interrupted the supraspinal control of locomotion, but did not prevent spinal locomotor circuitries from producing coordinated stepping movements. **(C)** NMDA microinjections ablated the vast majority of neurons in thoracic segments T8-T9. Scale bar, 250µm. **(D)** PC analysis of hindlimb locomotion in intact and non-trained rats, as well as overground-trained rats before the lesion, and after NMDA and complete T6 lesions. The histogram plot reports locomotor performance measured as the distance to intact rats in PC space. **, P < 0.01. a.u., arbitrary unit. Error bars, s.e.m.

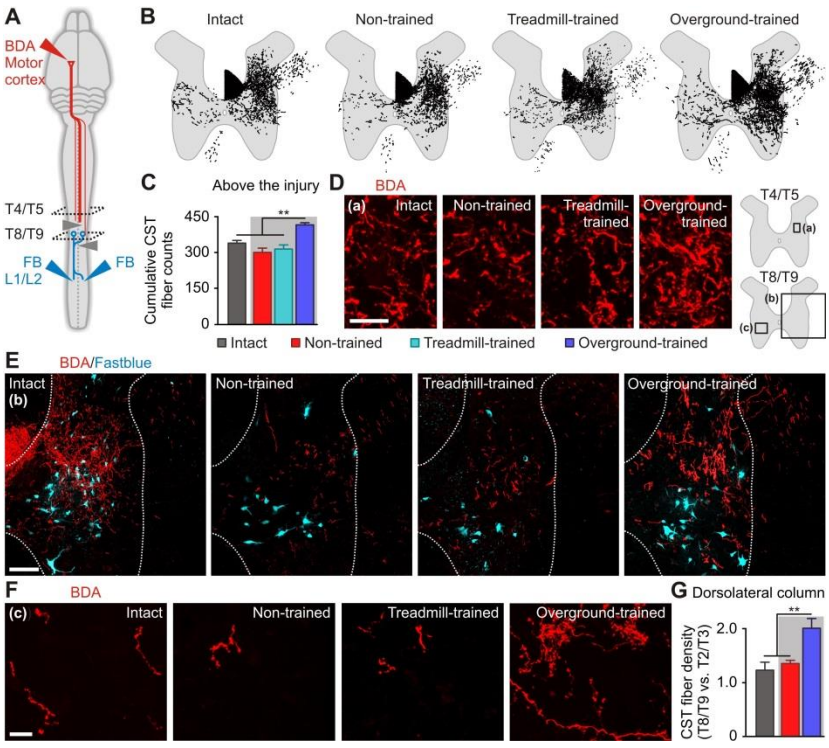

Supplementary Figure 5.9 Multi-system neuroprosthetic training promotes extensive remodeling of CST projections above and below the SCI.

(A) Diagram illustrating anatomical experiments and **analyzed regions**. **(B)** Reconstructions of CST fibers in spinal segments T4-T5, above the injury, for an intact, non-trained, treadmill-trained, and overground-trained rat. **(C)** Bar plots (n = 5 rats per

group) and **(D)** confocal images showing density of CST fibers in T4-T5 spinal segments. Scale bar, 20 µm. **(E)** Confocal images showing the density of CST fibers in the right hemicord of T8-T9 spinal segments. Scale bar, 100 µm. **(F)** Confocal images showing the density of CST fibers in the left hemicord of T8-T9 spinal segments. Scale bar, 20 µm. **(G)** Bar plot showing density of CST fibers in the right dorsolateral column (dlCST) at T8/T9 compared to T2/T3 (ratio) (n = 5 rats per group). No differences were found between the experimental groups in the density of dlCST labeling at T2-T3 (p = 0.53). **, P < 0.01. Error bars, s.e.m.

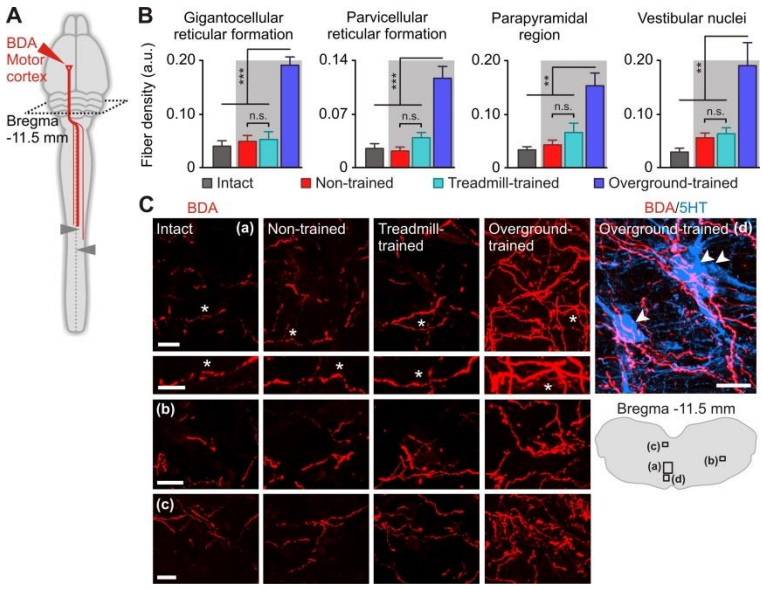

Supplementary Figure 5.10 Multi-system neuroprosthetic training promotes extensive remodeling of motor cortex axonal projections in brainstem locomotor regions.

(A) Diagram illustrating anatomical experiments **and analyzed regions**. **(B)** Bar plots (n = 5 rats per group) reporting the density of motor cortex originating fibers in the gigantocellular reticular formation, parvicellular reticular formation, parapyramidal region, and vestibular nuclei for intact, non-trained, treadmill-trained and overground-trained rats. **(C)** Representative confocal images showing the density of motor cortex originating fibers in the various brainstem locomotor regions (a) – (c). We detected unusually dense motor cortex axonal projections in the vicinity of locomotor-related serotonergic (5HT) neurons (arrows) in overground-trained rats (d). Scale bar, 20 µm. **, P < 0.01; ***, P < 0.001. n.s., non significant; a.u., arbitrary unit. Error bars, s.e.m.,

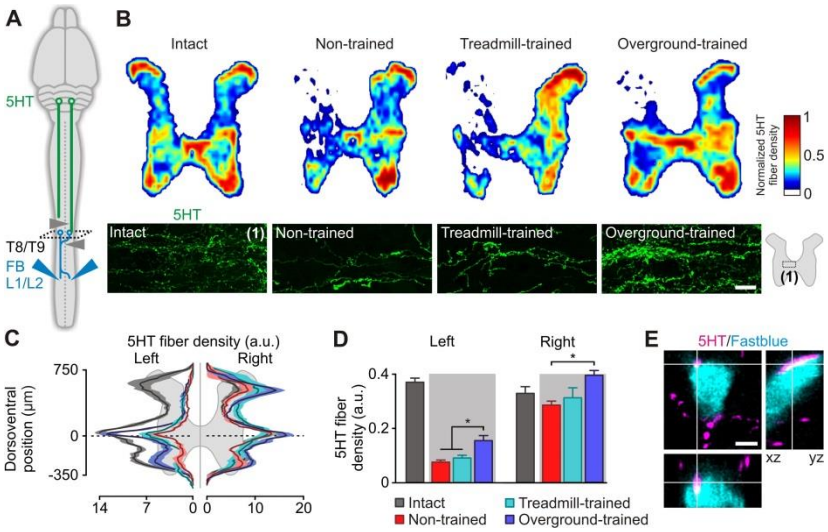

Supplementary Figure 5.11 Multi-system neuroprosthetic training promotes extensive remodeling of brainstem-derived serotonergic projections.

(A) Diagram illustrating anatomical experiments including the source of spinal 5HT projections in the brainstem. **(B)** Heat maps showing 5HT fiber density in T8-T9 segments and confocal images showing midline crossing 5HT fibers in intermediate laminae, close to the central canal. Scale bar, 20µm. **(C)** Distribution of 5HT fiber density along the dorsoventral extent of T8-T9 segments. **(D)** Bar graphs reporting 5HT fiber density in the left and right T8-T9 hemicords. **(D)** Confocal images showing close appositions between 5HT fibers and a thoracic relay neuron retrogradely labeled from L1-L2 locomotor centers in a overground-trained animal. Scale bar, 5µm. a.u., arbitrary unit. *, P < 0.05. Error bars, s.e.m.

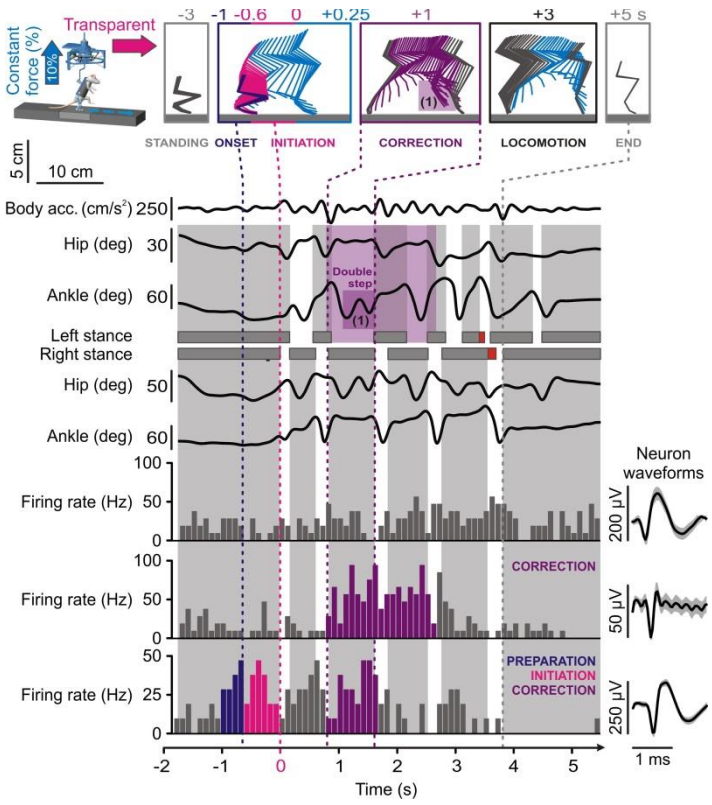

Supplementary Figure 5.12 Left motor cortex neuronal modulations correlate with gait initiation and correction.

A representative sequence including gait initiation and correction of locomotor movement is shown for a overground-trained rat. Stick diagram decompositions of hindlimb motion are displayed to highlight the various gait events. The corresponding changes in body acceleration (acc.), left and right hindlimb joint angles, and neuronal firing rates of 3 motor cortex neurons are shown below together with the duration of stance (gray), swing (empty), and drag (red). Neuron waveforms are displayed as means +/- S.D. Neuronal firing rates were estimated in 100 ms windows, and color-coded according to the period during which significant changes were found. Significance was tested by comparing the distributions of firing rates relative to *initiation* or *correction* events. If there was a significant change in firing rate within any successive pair of one-second windows from 2 s before to 1 s after the event, the neuron was classified as significantly modulated. *Initiation* was defined as the initial foot clearance. *Preparation* corresponded to the period during which a significant increase in firing rate was detected relative to standing, but no overt gait-related movement (onset, hip extension) had yet taken place. *Correction* included a sequence of three events: a step resulting in negative body acceleration superior to 80 cm/s^2, a subsequent contralateral double-step without paw placement (1), and an ipsilateral step/hop before the contralateral paw had been

fully placed. The foot clearance of the third event in this sequence was defined as the time of correction. The first neuron showed no significant modulation with respect to *initiation* or *correction*. The second neuron displayed a significant increase in firing rate 1 s before and after the *correction* event. The third neuron exhibited significant changes in firing rates 1 s before *initiation* and 1 s before *correction*.

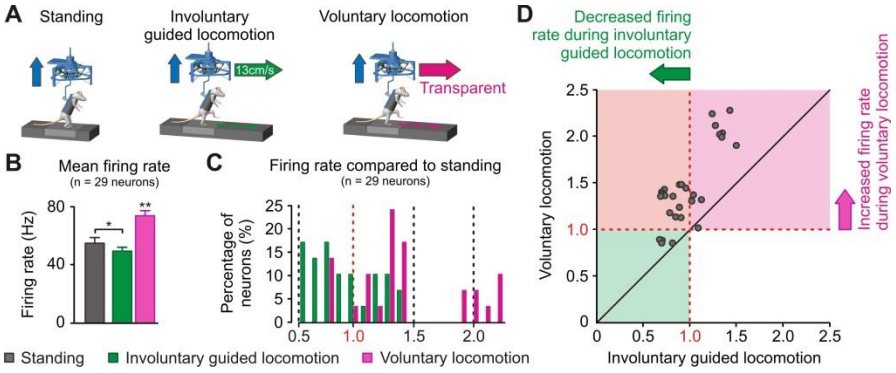

Supplementary Figure 5.13 Left motor cortex neurons showed decreased firing rate during involuntary guided locomotion.

(A) Neuronal modulations were recorded during standing, involuntary guided locomotion, and voluntary locomotion. **(B)** Bar graphs reporting average values (n = 29 neurons) of mean firing rate for each experimental condition. **(C)** Distribution of mean firing rate normalized to standing for all the recorded neurons. **(D)** Mean firing rate during involuntary guided locomotion is plotted against mean firing rate during voluntary locomotion. The majority of neurons that showed increased firing rate during voluntary locomotion exhibited a significant ($p < 0.05$) decrease in firing rate during involuntary guided locomotion (red). A cluster of neurons displayed increased firing rates during both paradigms, but the extent of the modulation was more pronounced during voluntary than involuntary locomotion (magenta). *, $P < 0.05$; **, $P < 0.01$. Error bars, s.e.m.

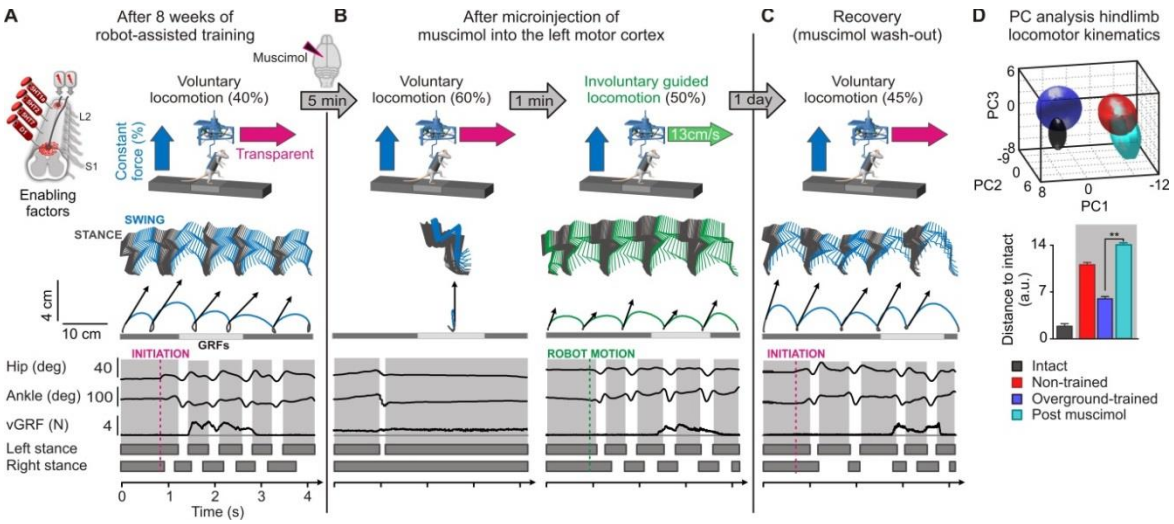

Supplementary Figure 5.14 Microinjections of muscimol into the motor cortex abolish voluntary locomotion overground, but leave spinal locomotor circuitries globally unaffected.

Representative example of bipedal locomotion overground in the presence of enabling factors for a overground-trained rat **(A)** before and **(B)** 5 min after a microinjection of muscimol into the left motor cortex. Hindlimb locomotor kinematics and vGRFs are shown using the same conventions as in **supp. fig. 5.4**. The amount of vertical support provided by the robot is indicated above each panel (%). Muscimol microinjections immediately abolished voluntary locomotion overground. However, all the tested rats (n = 3) displayed coordinated locomotor movements during involuntary guided locomotion (13 cm/s). These results indicate that the inactivation of the motor cortex suppressed the ability to initiate voluntary locomotion, but did not prevent spinal locomotor circuitries from producing coordinated stepping movements. **(C)** One day after muscimol microinjection, the rats recovered voluntary locomotion overground. **(D)** PC analysis of hindlimb locomotion in intact and non-trained rats, as well as overground-trained rats before and after muscimol microinjection. The histogram plot reports locomotor performance measured as the distance to intact rats in PC space. **, $P < 0.01$. a.u., arbitrary unit. Error bars, s.e.m.

Table S1. Computed kinematics and gait parameters for principal component (PC) analysis

Parameters		#	Detailed explanation
Kinematics			
Temporal features of gait			
		1	Cycle duration
		2	Cycle velocity
		3	Stance duration
		4	Stance duration (%)
		5	Relative stance duration (percent of the cycle duration)
		6	Interlimb coordination (cross-correlation between hindlimbs)
Limb endpoint (MTP) trajectory			
		7	Stride length
		8	Step length
		9	3D limb endpoint path length
		10	Maximum backward position
		11	Minimum forward position
		12	Step height
		13	Maximum speed during swing
		14	Relative timing of maximum velocity during swing
		15	Acceleration at swing onset
		16	Endpoint velocity
		17	Orientation of the velocity vector at swing onset
		18	Dragging
		19	Relative dragging duration (percent of swing duration)
Stability			
Base of support		20	Positioning of the foot at stance onset with respect to the pelvis
		21	Amount of robotic vertical support (%)
		22	Stance width
Trunk and pelvic position and oscillations		23	Maximum trunk vertical position
		24	Minimal trunk vertical position
		25	Amplitude of trunk vertical movement
		26	Variability of sagittal trunk oscillations
		27	Variability in velocity of sagittal trunk oscillations
		28	Variability of Medio-lateral hip oscillations
		29	Variability of vertical mid-point hip oscillations
		30	Variability of Medio-lateral mid-point shoulder oscillations
		31	Variability of vertical mid-point shoulder oscillations
		32	Variability of Medio-lateral shoulder rotations
		33	Variability of Medio-lateral hip rotations
Whole Body movement			
Displacement of the body mid-point (pelvis)		34	Forward motion
		35	Medio-lateral motion
		36	Vertical motion
		37	3D motion
Joint angles and segmental oscillations			
Backward	proximal	38	Crest oscillations
		39	Thigh oscillations
		40	Leg oscillations
		41	Foot oscillations
	distal	42	Toe oscillations
Forward	whole limb	43	Whole limb oscillations
	proximal	44	Crest oscillations
		45	Thigh oscillations
		46	Leg oscillations
		47	Foot oscillations
	distal	48	Toe oscillations
	whole limb	49	Whole limb oscillations
Flexion	proximal	50	Hip joint angle
		51	Knee joint angle
		52	Ankle joint angle
	distal	53	MTP joint angle

Parameters		#	Detailed explanation
Kinematics			
Joint angles and segmental oscillations			
Abduction	whole limb	54	Whole limb abduction
	distal	55	Foot abduction
Extension	proximal	56	Hip joint angle
		57	Knee joint angle
		58	Ankle joint angle
	distal	59	MTP joint angle
Adduction	whole limb	60	Whole limb adduction
	distal	61	Foot adduction
Amplitude	proximal	62	Crest oscillations
		63	Thigh oscillations
		64	Leg oscillations
		65	Foot oscillations
	distal	66	Toe oscillations
	whole limb	67	Whole limb oscillations
	proximal	68	Hip joint angle
		69	Knee joint angle
		70	Ankle joint angle
	distal	71	MTP joint angle
	whole limb	72	Whole limb medio-lateral oscillations
	distal	73	Foot abduction /adduction
Velocity			
Minimum	whole limb	74	Whole limb oscillation velocity
	proximal	75	Hip joint angle velocity
		76	Knee joint angle velocity
		77	Ankle joint angle velocity
	distal	78	MTP joint angle velocity
Maximum	whole limb	79	Whole limb oscillation velocity
	proximal	80	Hip joint angle velocity
		81	Knee joint angle velocity
		82	Ankle joint angle velocity
	distal	83	MTP joint angle velocity
Amplitude	whole limb	84	Whole limb angle velocity
	proximal	85	Hip joint angle velocity
		86	Knee joint angle velocity
		87	Ankle joint angle velocity
	distal	88	MTP joint angle velocity
Inter-limb coordination			
PC analysis		89	Degree of linearity in bilateral hindlimb coordination (PC analysis)
		90	Degree of linear coupling in intralimb coordination (PC analysis)
		91	Degree of linear coupling in intralimb coordination (PC analysis)
FFT decomposition	proximal	92	Temporal coupling between crest and thigh oscillations
		93	Temporal coupling between thigh and leg oscillations
		94	Temporal coupling between leg and foot oscillations
	distal	95	Temporal coupling between foot and toe oscillations
Cross-correlation	proximal	96	Correlation between crest and tight oscillations
		97	Correlation between tight and leg oscillations
		98	Correlation between leg and foot oscillations
		99	Correlation between foot and toe oscillations
		100	Correlation between hip and knee oscillations
		101	Correlation between knee and ankle oscillations
	distal	102	Correlation between ankle and MTP oscillations
Similarity to intact rats			
Cross-correlation between intact and lesioned	whole limb	103	Hindlimb
	proximal	104	Hip
		105	Knee
		106	Ankle
	distal	107	MTP

Supplementary Table 5.1: List of kinematic parameters

10.4 Supplementary information chapter 6

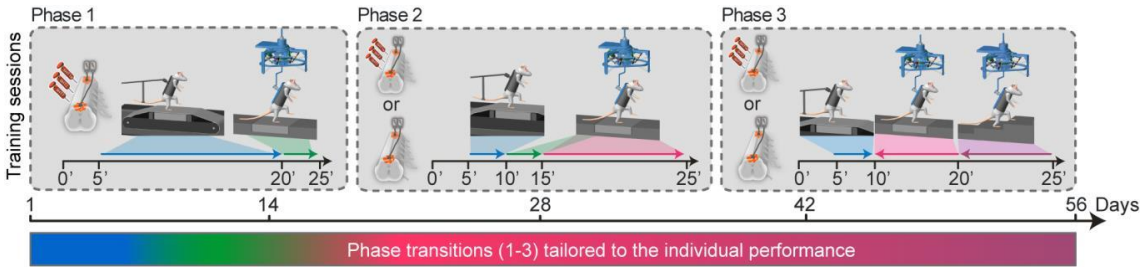

Supplementary figure 6.1 Training evolution of neuroposthetic training. Adapted from supplementary figure 4 of van den Brand et al. (van den Brand *et al.*, 2012)

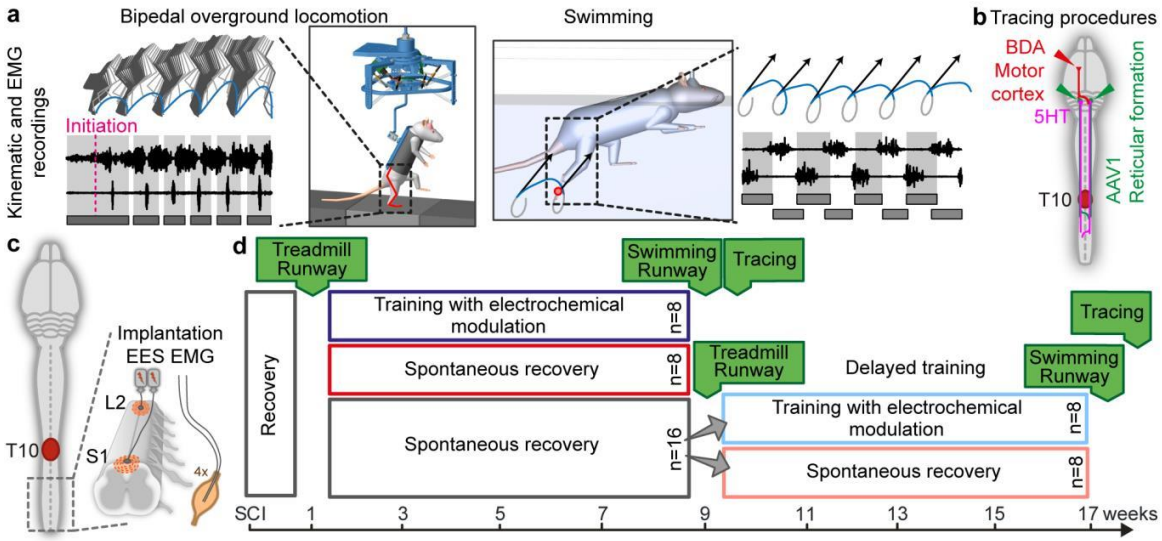

Figure 6.2 Experimental groups and used methods.

(a) Kinematic and EMG recordings during stepping and swimming motor tasks. **(b)** Schematic overview over tracing experiments and analyzed brainstem systems. Tracers were injected into the L motor cortex and bilaterally into the reticular formation. **(c)** Overview over surgical procedures; Electrodes were sutured on the dura mater over spinal segments L2 and S1, contusion SCI was induced at spinal level T10. **(d)** Experimental timeline of the different animal groups.

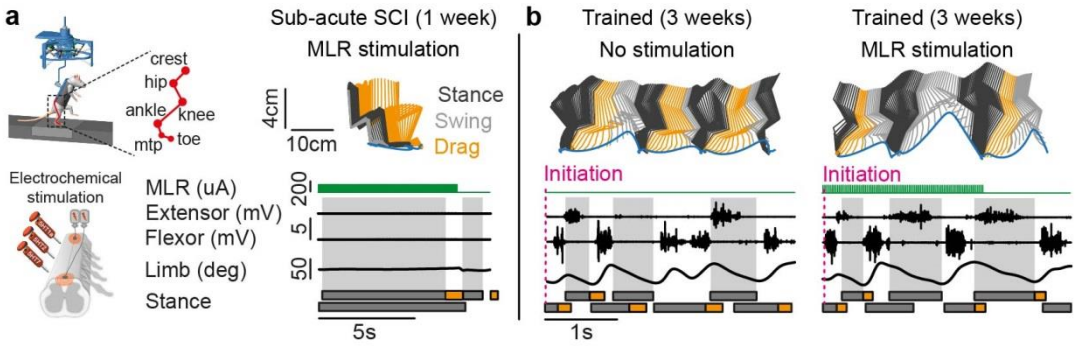

Figure 6.3 MLR DBS triggers bipedal locomotion in the robot only after voluntary stepping capacities recovered.

(a) Kinematic and EMG recordings during MLR stimulation sub-acutely after SCI. **(b)** Kinematic and EMG recordings during stepping with and without MLR stimulation 3 weeks after SCI, i.e. when voluntary stepping capacities began to recover.

10.5 Supplementary information chapter 7

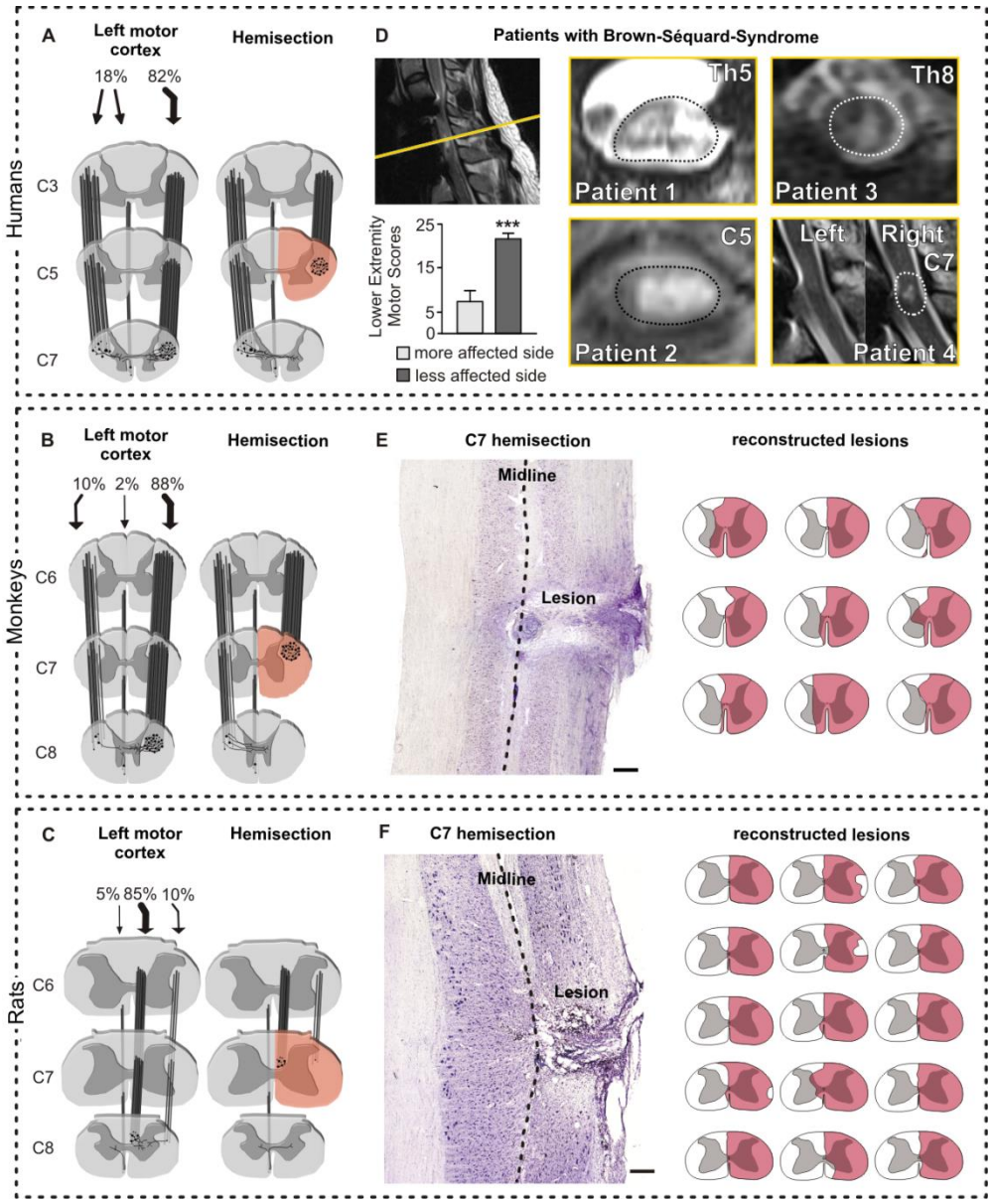

Supplementary Figure 7.1 Clinical cases and experimental models of Brown-Séquard syndrome.

(A-C) Schematic representation of corticospinal axonal projections in the spinal cord white and grey matter of humans, monkeys, and rats before injury (or healthy), and after a lateral hemisection. **(D)** MRI pictures through the transverse plane obtained in the 4 spinal-cord-injured patients who participated in the longitudinal study. Imaging was not possible for patient #5 due to an implanted pacemaker. The level of the lesion is indicated in each MRI. Bar plot displaying mean values of lower extremity scores at early time-points after the lesion. **(E-F)** Representative Nissl staining of a longitudinal section of

the hemisected spinal cord in rats and monkeys. For each experimental animal, the extent of the injured area was measured using camera lucida reconstructions. The surface of maximal damage per quarter of spinal cord was calculated to generate a measure of spared tissue. Scale bar: 1mm and 300 µm for monkeys and rats, respectively. *** denote statistical differences with p < 0.001, respectively. Error bars, s.e.m.

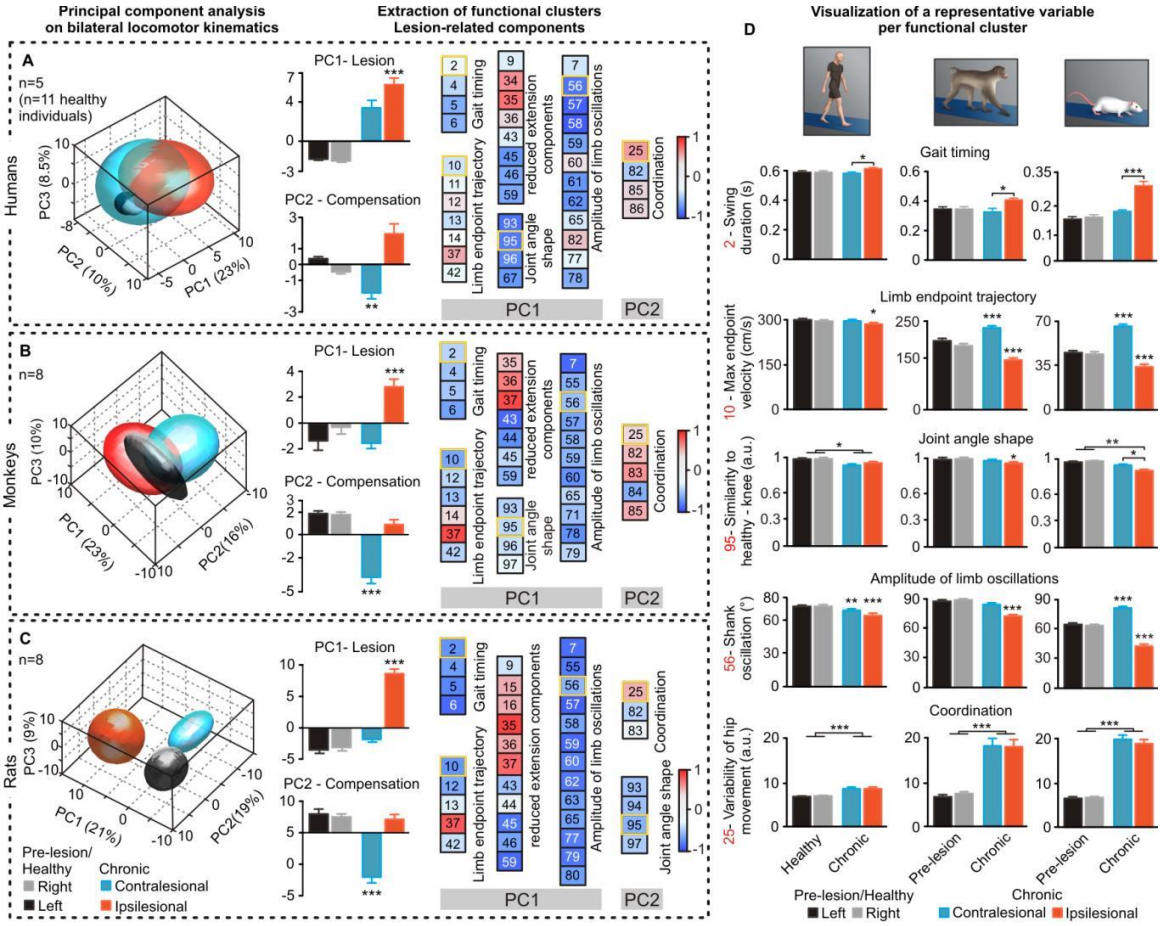

Supplementary figure 7.2. Kinematic analysis uncovers similar patterns of locomotor deficits and compensation.

(A-C) A PCA was applied on all the kinematic parameters measured for the left and right leg before the injury (or healthy), and in the chronic stage of the SCI. Left and right leg data clustered in the same space in non-injured humans **(A)**, monkeys **(B)**, and rats **(C).** In the chronic stage, gait clusters corresponding to the contralesional and ipsilesional legs moved in opposite directions, indicating side-specific alteration of gait patterns. Histogram plots report the mean values of scores for the left and right legs before the

injury (or healthy), and in the chronic stage of the lesion. For each species, PC1 and PC2 distinguished the ipsilesional and contralesional legs, respectively. We extracted the factor loadings for PC1 and PC2, and regrouped them into functional clusters that we named for clarity. The numbers refer to individual parameters that were calculated with the exact same methods in humans, monkeys, and rats (supplementary Table 7.1). Strikingly, the same list of parameters loaded on PC1 and PC2 in all the studies species. **(D)** To document gait features using more conventional representations, the histogram plots report the mean values of parameters with high factor loadings, which are framed in yellow in the functional clusters. *,**,*** denote statistical differences with $p < 0.05$, $p < 0.01$, and $p < 0.001$, respectively. Error bars, s.e.m.

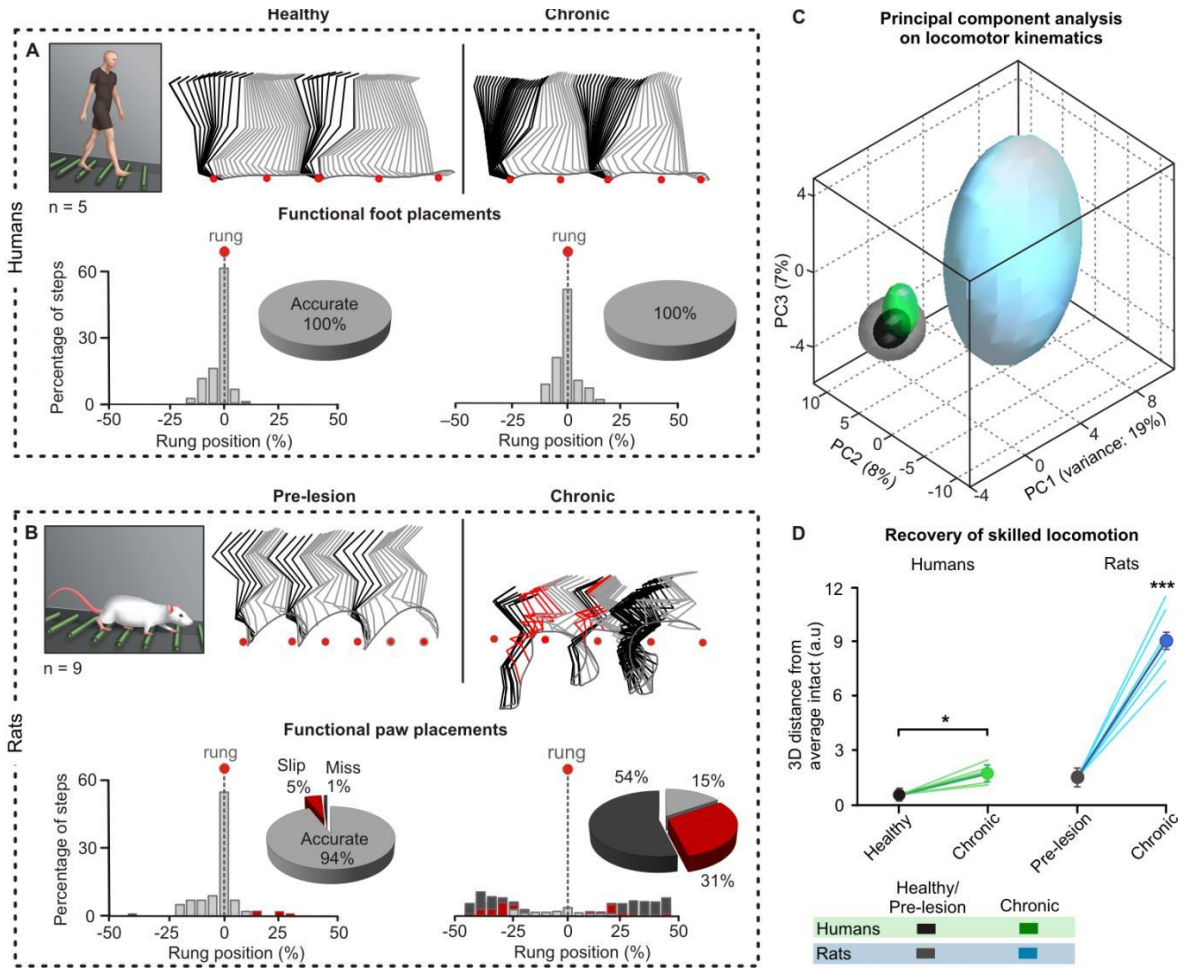

Supplementary Figure 7.3. Humans, but not rats, recovered the ability to traverse a horizontal ladder.

(A-B) Stick diagram decomposition of lower limb motion during stance (black) and swing (blue) during a continuous sequence of locomotion along the equally spaced rung (red) of a horizontal ladder. Functional foot placement was measured as the relative positioning of the ipsilesional foot with respect to two successive rung positions (red dots). The number of occurrence per 5% bin is reported together with the percentage of accurate, slipped, and missed placements. **(C)** PC analysis was applied on all the kinematic parameters (n=105) measured for the ipsilesional leg before the injury (or healthy), and in the chronic stage of the SCI. Individual (lines) and **(D)** averaged 3D distance between non-injured data points, and those measured at late time-points. *** denote conditions that were significantly different at $p < 0.001$, respectively. Error bars, s.e.m.

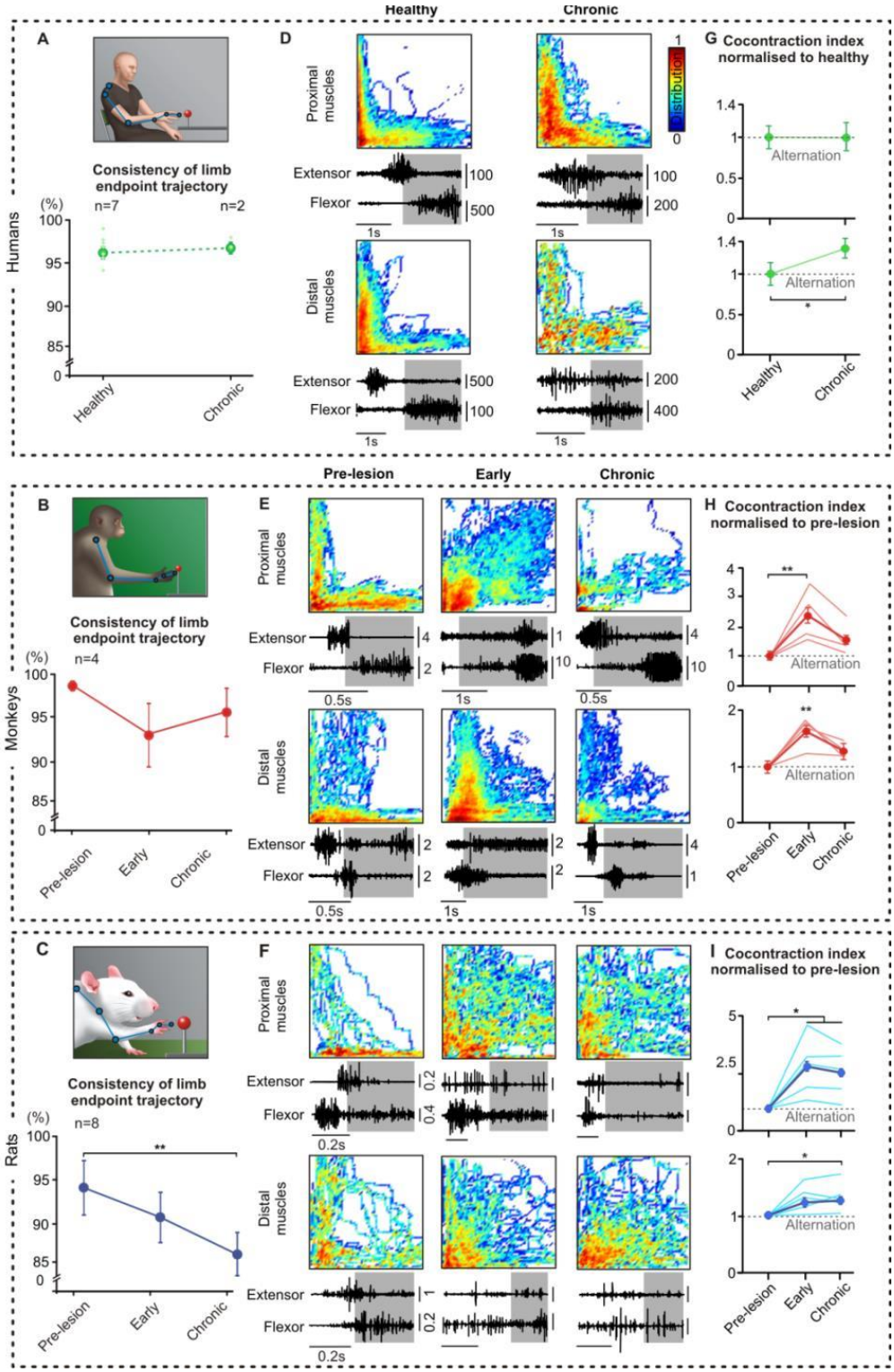

Supplementary Figure 7.4. Humans and monkeys, but not rats, recover hand kinematic and muscle activation patterns.

(A-C) The consistency of reaching movement was measured as the percent of explained variance by PC1 when applying a PC analysis on 10 successive 3D reaching

trajectories. **(D-F)** Representative example of recruitment pattern for proximal and distal pairs of antagonist muscles during a reach. The empty and shaded areas correspond to the reach and grasp phases, respectively. The color-coded plots show, for each pair of antagonistic muscles, the probability of co-activation. A L-shaped pattern indicates reciprocal activation between antagonist muscles, while a filled pattern highlights a high degree of co-activation. **(G-I)** Plots reporting the normalized values of the co-contraction index computed for proximal and distal antagonistic muscle pairs before the SCI (or healthy) and in the chronic stage. Thin lines correspond to individual data. *, ** denote significant difference at $p < 0.05$ and $p < 0.01$, respectively. Error bars, s.e.m.

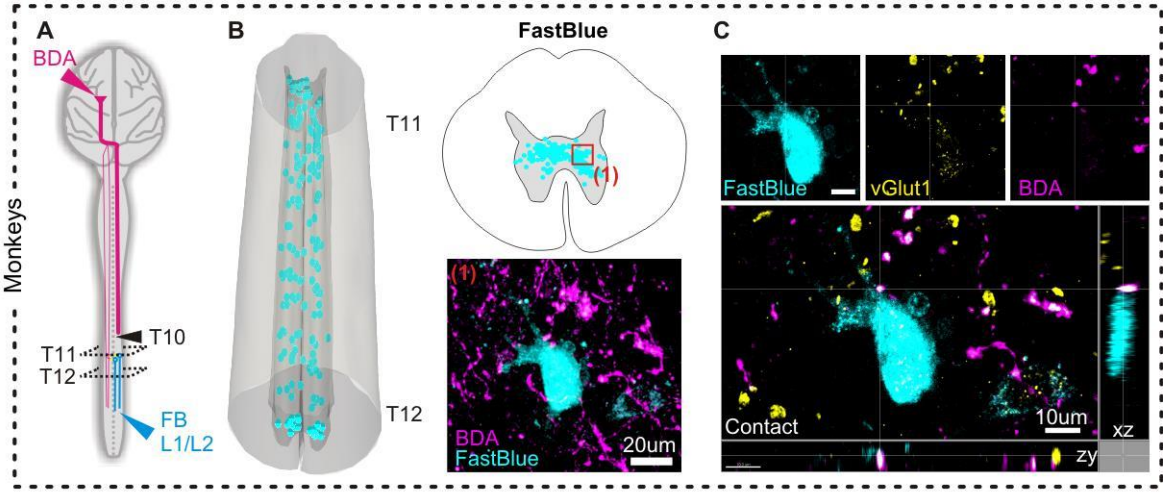

Supplementary Figure 7.5. Corticospinal fibers establish synaptic contacts with long intraspinal neurons below hemisection in monkeys.

(A) Diagram illustrating anatomical experiments and analyzed regions. **(B)** Representative photograph of corticospinal fibers surrounding a neuron retrogradelly labeled from L1/L2 segments. The photograph was taken from the intermediate laminae of T12 spinal segment, on the side of the hemisection. **(C)** Representative photographs showing 3D co-localization of BDA and vGlut1 synaptic terminals in close apposition to a neuron retrogradelly labeled form L1/L2, which demonstrate the presence of synaptic terminals onto sub-lesional corticospinal fibers that contact intraspinal neurons.

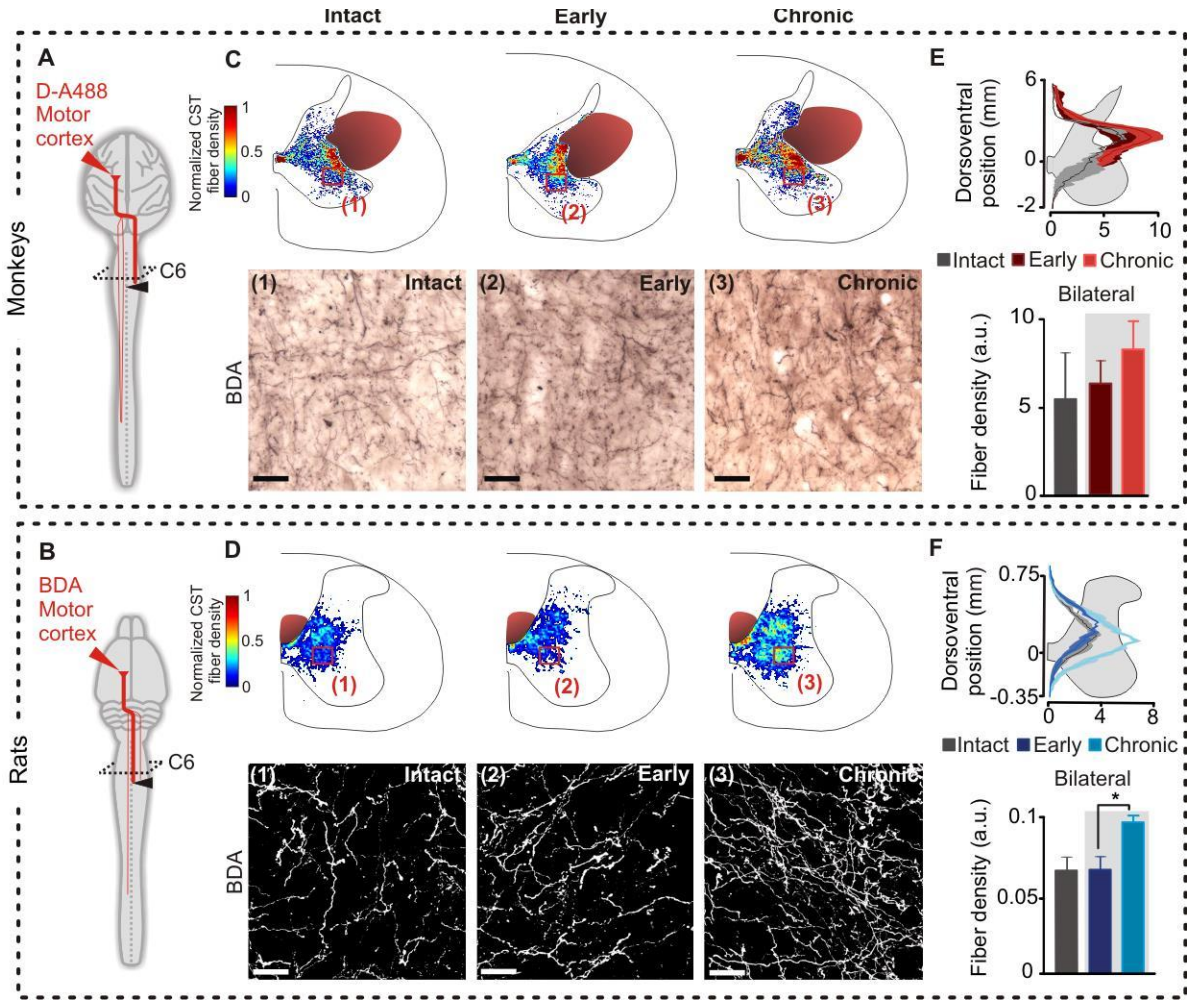

Supplementary Figure 7.6. Increased density of corticospinal fibers above hemisection in both rats and monkeys.

(A, B) Diagram illustrating anatomical experiments and analyzed regions in monkeys and rats. **(C,D)** Heat maps of corticospinal tract fiber density in the ipsilesional C6 segment, together with representative photographs of corticospinal tract fibers in monkeys and rats. **(E,F)** corticospinal tract fiber density distribution and histogram plots reporting the averaged density of corticospinal tract fibers in the analyzed C6 segment. Scale bar, 100 µm and 30 µm for monkeys and rats, respectively. *, denote significant difference at $p < 0.05$. Error bars, s.e.m

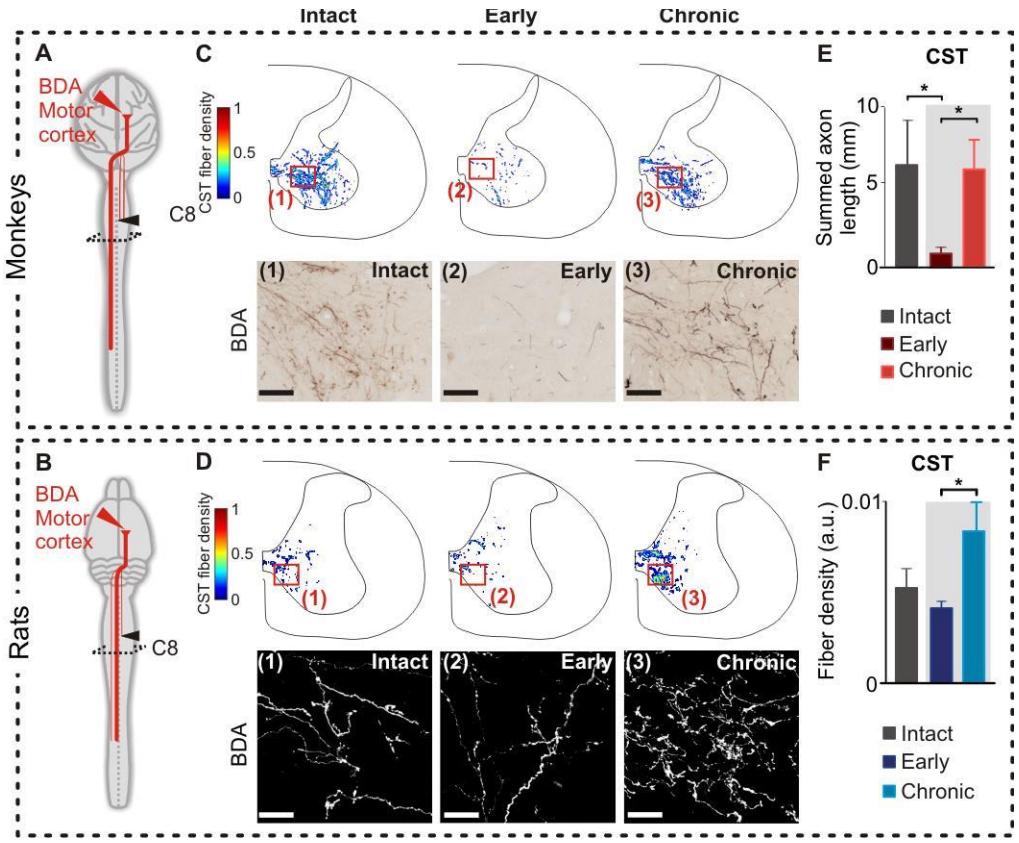

Supplementary figure 7.7 Increased density of corticospinal tract originating from the ipsilesional motor cortex fibers in segments below hemisection in both rats and monkeys.

(A,B) Diagram illustrating anatomical experiments and analyzed regions in monkeys and rats. **(C,D)** Heat maps of corticospinal tract fiber density in the ipsilesional C8 segment, below the SCI, together with representative photographs of corticospinal tract fibers in monkeys and rats. **(E,F)** Histogram plots reporting the averaged density of corticospinal tract fibers in the ipsilesional hemicord of the C8 segment. Scale bar, 100 µm for monkeys and 30 µm for rats. *, denote significant difference at $p < 0.05$. Error bars, s.e.m

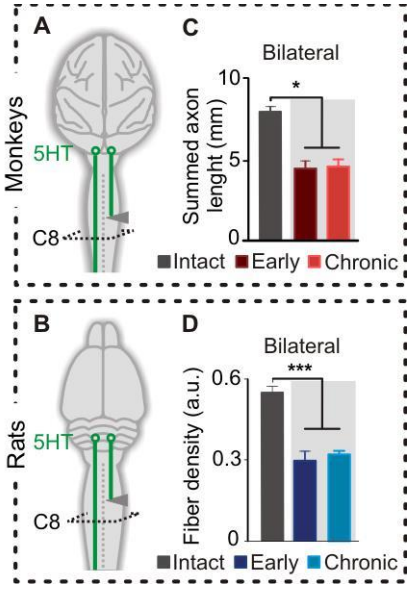

Supplementary Figure 7.8. Density of 5-HT fibers below hemisection remains unchanged in both monkeys and rats.

(A,B) Diagram illustrating anatomical experiments and analyzed regions in monkeys and rats. **(C,D)** Histogram plots reporting the averaged density of 5-HT fibers in the analyzed C8 segment, below the hemisection. *, *** denote significant difference at $p < 0.05$ and $p < 0.001$, respectively. Error bars, s.e.m.

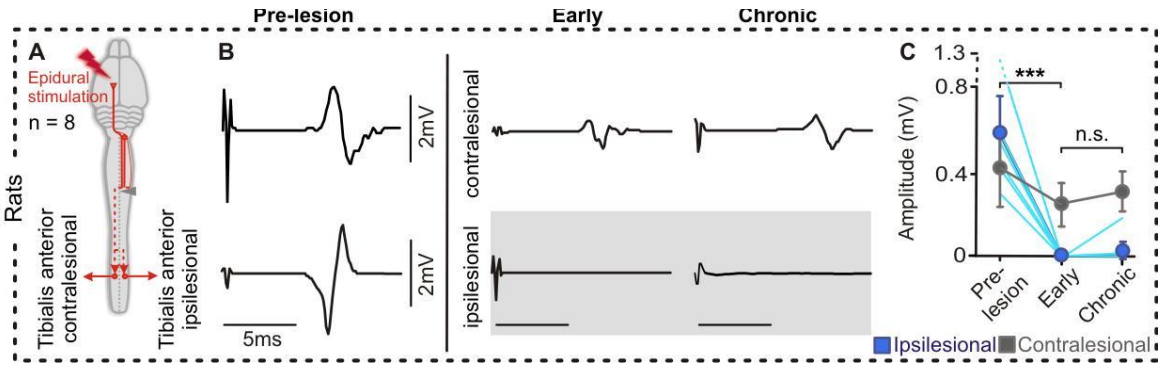

Supplementary Figure 7.9. The motor cortex fails to regain direct access to motor neurons below hemisection in rats.

(A) Diagram illustrating the electrophysiological experiment including stimulation and recording site. All the electrodes were implanted chronically. Stimulation was delivered in fully awake conditions, while the rat was standing quietly. **(B)** Motor responses elicited by a single pulse of electrical stimulation delivered over the leg area of the motor cortex. Motor responses were recorded from left and right ankle flexor muscles before, early and chronic after hemisection. **(C)** Mean values of motor response amplitudes recorded from ipsilesional and contralesional muscles before, early and chronic after hemisection. Thin lines correspond to individual data. *** denotes significant difference at $p < 0.001$. Error bars, s.e.m.

#	Computed parameters
	Gait timing
1	Stance duration
2	Swing duration
3	Relative stance duration (percent of the cycle duration)
	Limb endpoint (MTP) trajectory
4	Stride length
5	Step length
6	3D limb endpoint path length
7	Maximum backward position
8	Minimum forward position
9	Step height
10	Maximum speed during swing
11	Relative timing of maximum velocity during swing
12	Acceleration at swing onset
13	Endpoint velocity
14	Orientation of the velocity vector at swing onset
15	Dragging
16	Relative dragging duration (percent of swing duration)
	Stability
17	lateral movement of the foot during swing
18	Stance width
19	Maximum trunk lateral position
20	Minimal trunk lateral position
21	Amplitude of the lateral trunk position
22	Variability of sagittal trunk oscillations
23	Variability in velocity of sagittal trunk oscillations
24	Variability of vertical mid-point hip oscillations
25	Variability of medio-lateral hip oscillations
26	Variability of medio-lateral shoulder oscillations
27	Variability of vertical mid-point shoulder oscillations
28	Variability of Medio-lateral shoulder rotations
29	Variability of Medio-lateral hip rotations
30	Lateral oscillation of the center of mass
31	Vertical oscillation of the center of mass
32	3D oscillation of the center of mass
	Joint angles and limb segment oscillations
33	Crest oscillations (minimal elevation angle)
34	Thigh oscillations (minimal elevation angle)
35	Shank oscillations (minimal elevation angle)
36	Foot oscillations (minimal elevation angle)
37	Toe oscillations (minimal elevation angle)
38	Whole limb oscillations (minimal elevation angle)
39	Crest oscillations (maximal elevation angle)
40	Thigh oscillations (maximal elevation angle)
41	Shank oscillations (maximal elevation angle)
42	Foot oscillations (maximal elevation angle)
43	Toe oscillations (maximal elevation angle)
44	Whole limb oscillations (maximal elevation angle)
45	Hip joint angle (maximal)
46	Knee joint angle (maximal)
47	Ankle joint angle (maximal)
48	MTP joint angle (maximal)
49	Whole limb adduction
50	Foot adduction
51	Hip joint angle (minimal)

#	Computed parameters
	Joint angles and limb segment oscillations (continued)
52	Knee joint angle (minimal)
53	Ankle joint angle (minimal)
54	MTP joint angle (minimal)
55	Whole limb abduction
56	Foot abduction
57	Crest oscillations
58	Thigh oscillations
59	Leg oscillations
60	Foot oscillations
61	Toe oscillations
62	Whole limb oscillations
63	Hip joint angle
64	Knee joint angle
65	Ankle joint angle
66	MTP joint angle
67	Whole limb medio-lateral oscillations
68	Foot abduction /adduction
	Velocity
69	Whole limb angle velocity
70	Hip joint angle velocity
71	Knee joint angle velocity
72	Ankle joint angle velocity
73	MTP joint angle velocity
74	Whole limb oscillation velocity
75	Hip joint angle velocity
76	Knee joint angle velocity
77	Ankle joint angle velocity
78	MTP joint angle velocity
79	Whole limb oscillation velocity
80	Hip joint angle velocity
81	Knee joint angle velocity
82	Ankle joint angle velocity
83	MTP joint angle velocity
	Inter-limb coordination
84	Correlation between whole hindlimb oscillations
85	Degree of linear coupling between joint oscillations
86	Temporal coupling between crest and thigh oscillations
87	Temporal coupling between thigh and leg oscillations
88	Temporal coupling between leg and foot oscillations
89	Temporal coupling between foot and toe oscillations
90	Correlation between crest and tight oscillations
91	Correlation between tight and leg oscillations
92	Correlation between leg and foot oscillations
93	Correlation between foot and toe oscillations
94	Correlation between hip and knee oscillations
95	Correlation between knee and ankle oscillations
96	Correlation between ankle and MTP oscillations
	Similarity to healthy gait
97	Correlation between limb oscillation of healthy and pathological leg
98	Correlation between hip oscillation of healthy and pathological leg
99	Correlation between knee oscillation of healthy and pathological leg
100	Correlation between ankle oscillation of healthy and pathological leg
101	Correlation between MTP oscillation of healthy and pathological leg

Table 1. Computed Kinemaic parameters of the Gait

Table 7.1. List of Kinematic parameters

11 References

Ackery, A.K., A; Tator, C (2004) A Global Perspective on Spinal Cord Injury Epidemiology. *J Neurotrauma*, **21**, 1355-1370.

Ada, L., Dean, C.M., Vargas, J. & Ennis, S. (2010) Mechanically assisted walking with body weight support results in more independent walking than assisted overground walking in non-ambulatory patients early after stroke: a systematic review. *Journal of physiotherapy*, **56**, 153-161.

Agnati, L.F., Guidolin, D., Guescini, M., Genedani, S. & Fuxe, K. (2010) Understanding wiring and volume transmission. *Brain Res Rev*, **64**, 137-159.

Aguayo, A.J., Rasminsky, M., Bray, G.M., Carbonetto, S., McKerracher, L., Villegas-Perez, M.P., Vidal-Sanz, M. & Carter, D.A. (1991) Degenerative and regenerative responses of injured neurons in the central nervous system of adult mammals. *Philos Trans R Soc Lond B Biol Sci*, **331**, 337-343.

Alto, L.T., Havton, L.A., Conner, J.M., Hollis Ii, E.R., Blesch, A. & Tuszynski, M.H. (2009) Chemotropic guidance facilitates axonal regeneration and synapse formation after spinal cord injury. *Nat Neurosci*, **12**, 1106-1113.

Alton, F., Baldey, L., Caplan, S. & Morrissey, M.C. (1998) A kinematic comparison of overground and treadmill walking. *Clin Biomechanics*, **13**, 434-440.

Alvarez, F.J., Villalba, R.M., Zerda, R. & Schneider, S.P. (2004) Vesicular glutamate transporters in the spinal cord, with special reference to sensory primary afferent synapses. *J Comp Neurol*, **472**, 257-280.

Anderson, K.D. (2004) Targeting Recovery: Priorities of the Spinal Cord-Injured Population. *J Neurotrauma*, **21**, 1370-1383.

Angeli, C.A., Edgerton, V.R., Gerasimenko, Y.P. & Harkema, S.J. (2014a) Altering spinal cord excitability enables voluntary movements after chronic complete paralysis in humans. *Brain*.

Angeli, C.A., Edgerton, V.R., Gerasimenko, Y.P. & Harkema, S.J. (2014b) Altering spinal cord excitability enables voluntary movements after chronic complete paralysis in humans. *Brain*, **137**, 1394-1409.

Bachmann, L.C., Matis, A., Lindau, N.T., Felder, P., Gullo, M. & Schwab, M.E. (2013) Deep brain stimulation of the midbrain locomotor region improves paretic hindlimb function after spinal cord injury in rats. *Science translational medicine*, **5**, 208ra146.

Ballermann, M. & Fouad, K. (2006) Spontaneous locomotor recovery in spinal cord injured rats is accompanied by anatomical plasticity of reticulospinal fibers. *Eur J Neurosci*, **23**, 1988-1996.

Barbeau, H., Ladouceur, M., Norman, K.E., Pepin, A. & Leroux, A. (1999) Walking after spinal cord injury: evaluation, treatment, and functional recovery. *Arch Phys Med Rehabil*, **80**, 225-235.

Barbeau, H. & Rossignol, S. (1987) Recovery of locomotion after chronic spinalization in the adult cat. *Brain Res*, **412**, 84-95.

Bareyre, F.M., Kerschensteiner, M., Raineteau, O., Mettenleiter, T.C., Weinmann, O. & Schwab, M.E. (2004) The injured spinal cord spontaneously forms a new intraspinal circuit in adult rats. *Nat Neurosci*, **7**, 269-277.

Barriere, G., Leblond, H., Provencher, J. & Rossignol, S. (2008) Prominent role of the spinal central pattern generator in the recovery of locomotion after partial spinal cord injuries. *J Neurosci*, **28**, 3976-3987.

Barthelemy, D., Leblond, H. & Rossignol, S. (2007) Characteristics and mechanisms of locomotion induced by intraspinal microstimulation and dorsal root stimulation in spinal cats. *J Neurophysiol*, **97**, 1986-2000.

Bartus, K., James, N.D., Didangelos, A., Bosch, K.D., Verhaagen, J., Yanez-Munoz, R.J., Rogers, J.H., Schneider, B.L., Muir, E.M. & Bradbury, E.J. (2014) Large-Scale Chondroitin Sulfate Proteoglycan Digestion with Chondroitinase Gene Therapy Leads to Reduced Pathology and Modulates Macrophage Phenotype following Spinal Cord Contusion Injury. *J Neurosci*, **34**, 4822-4836.

Basso, D.M., Beattie, M.S., Bresnahan, J.C., Anderson, D.K., Faden, A.I., Gruner, J.A., Holford, T.R., Hsu, C.Y., Noble, L.J., Nockels, R., Perot, P.L., Salzman, S.K. & Young, W. (1996) MASCIS evaluation of open field locomotor scores: effects of experience and teamwork on reliability. Multicenter Animal Spinal Cord Injury Study. *J Neurotrauma*, **13**, 343-359.

Beauparlant, J., van den Brand, R., Barraud, Q., Friedli, L., Musienko, P., Dietz, V. & Courtine, G. (2013) Undirected compensatory plasticity contributes to neuronal dysfunction after severe spinal cord injury. *Brain*.

Behrman, A.L. & Harkema, S.J. (2000) Locomotor training after human spinal cord injury: a series of case studies. *Phys Ther*, **80**, 688-700.

Beres-Jones, J.A. & Harkema, S.J. (2004) The human spinal cord interprets velocity-dependent afferent input during stepping. *Brain*, **127**, 2232-2246.

Beres-Jones, J.A., Johnson, T.D. & Harkema, S.J. (2003) Clonus after human spinal cord injury cannot be attributed solely to recurrent muscle-tendon stretch. *Experimental brain research. Experimentelle Hirnforschung. Experimentation cerebrale*, **149**, 222-236.

Bernhard, M., Gries, A., Kremer, P. & Bottiger, B.W. (2005) Spinal cord injury (SCI)--prehospital management. *Resuscitation*, **66**, 127-139.

Borton, D., Micera, S., Millan Jdel, R. & Courtine, G. (2013) Personalized neuroprosthetics. *Science translational medicine*, **5**, 210rv212.

Bos, R., Sadlaoud, K., Boulenguez, P., Buttigieg, D., Liabeuf, S., Brocard, C., Haase, G., Bras, H. & Vinay, L. (2013) Activation of 5-HT2A receptors upregulates the function of the neuronal K-Cl cotransporter KCC2. *Proc Natl Acad Sci U S A*, **110**, 348-353.

Boulenguez, P., Liabeuf, S., Bos, R., Bras, H., Jean-Xavier, C., Brocard, C., Stil, A., Darbon, P., Cattaert, D., Delpire, E., Marsala, M. & Vinay, L. (2010) Down-regulation of the potassium-chloride cotransporter KCC2 contributes to spasticity after spinal cord injury. *Nat Med*, **16**, 302-307.

Bradbury, E.J., Moon, L.D., Popat, R.J., King, V.R., Bennett, G.S., Patel, P.N., Fawcett, J.W. & McMahon, S.B. (2002) Chondroitinase ABC promotes functional recovery after spinal cord injury. *Nature*, **416**, 636-640.

Brosamle, C. & Schwab, M.E. (1997) Cells of origin, course, and termination patterns of the ventral, uncrossed component of the mature rat corticospinal tract. *J Comp Neurol*, **386**, 293-303.

Brown-Sequard, C.E. (1868) Lectures on the physiology and pathology of the central nervous system and on the treatment of organic nervous affections. *Lancet*, **2**, 93-595,659-662,755-757,821-823.

Brustein, E. & Rossignol, S. (1998) Recovery of locomotion after ventral and ventrolateral spinal lesions in the cat. I. Deficits and adaptive mechanisms. *Journal of Neurophysiology*, **80**, 1245-1267.

Burke, R.E. (2007) Sir Charles Sherrington's the integrative action of the nervous system: a centenary appreciation. *Brain*, **130**, 887-894.

Bussel, B., Roby-Brami, A., Yakovleff, A. & Bennis, N. (1989) Late flexion reflex in paraplegic patients. Evidence for a spinal stepping generator. *Brain Res Bull*, **22**, 53-56.

Cai, L.L., Courtine, G., Fong, A.J., Burdick, J.W., Roy, R.R. & Edgerton, V.R. (2006a) Plasticity of functional connectivity in the adult spinal cord. *Philos Trans R Soc Lond B Biol Sci*, **361**, 1635-1646.

Cai, L.L., Fong, A.J., Otoshi, C.K., Liang, Y., Burdick, J.W., Roy, R.R. & Edgerton, V.R. (2006b) Implications of assist-as-needed robotic step training after a complete spinal cord injury on intrinsic strategies of motor learning. *J Neurosci*, **26**, 10564-10568.

Calancie, B., Alexeeva, N., Broton, J.G. & Molano, M.R. (2005) Interlimb reflex activity after spinal cord injury in man: strengthening response patterns are consistent with ongoing synaptic plasticity. *Clin Neurophysiol*, **116**, 75-86.

Calancie, B., Lutton, S. & Broton, J.G. (1996) Central nervous system plasticity after spinal cord injury in man: interlimb reflexes and the influence of cutaneous stimulation. *Electroencephalogr Clin Neurophysiol*, **101**, 304-315.

Calancie, B., Molano, M.R. & Broton, J.G. (2000) Neural plasticity as revealed by the natural progression of movement expression--both voluntary and involuntary--in humans after spinal cord injury. *Prog Brain Res*, **128**, 71-88.

Capogrosso, M., Wenger, N., Raspopovic, S., Musienko, P., Beauparlant, J., Bassi Luciani, L., Courtine, G. & Micera, S. (2013) A computational model for epidural electrical stimulation of spinal sensorimotor circuits. *J Neurosci*, **33**, 19326-19340.

Carmel, J.B., Berrol, L.J., Brus-Ramer, M. & Martin, J.H. (2010) Chronic electrical stimulation of the intact corticospinal system after unilateral injury restores skilled locomotor control and promotes spinal axon outgrowth. *J Neurosci*, **30**, 10918-10926.

Carmena, J.M., Lebedev, M.A., Crist, R.E., O'Doherty, J.E., Santucci, D.M., Dimitrov, D.F., Patil, P.G., Henriquez, C.S. & Nicolelis, M.A. (2003) Learning to control a brain-machine interface for reaching and grasping by primates. *PLoS biology*, **1**, E42.

Chen, G., Patten, C., Kothari, D.H. & Zajac, F.E. (2005) Gait differences between individuals with post-stroke hemiparesis and non-disabled controls at matched speeds. *Gait Posture*, **22**, 51-56.

Colgate, E. & Hogan, N. (1989) An analysis of contact instability in terms of passive physical equivalents *Proceedings of the IEEE International Conference on Robotics and Automation (ICRA)*, pp. 404-409.

Collinger, J.L., Wodlinger, B., Downey, J.E., Wang, W., Tyler-Kabara, E.C., Weber, D.J., McMorland, A.J., Velliste, M., Boninger, M.L. & Schwartz, A.B. (2013) High-performance neuroprosthetic control by an individual with tetraplegia. *Lancet*, **381**, 557-564.

Courtine, G., Bunge, M.B., Fawcett, J.W., Grossman, R.G., Kaas, J.H., Lemon, R., Maier, I., Martin, J., Nudo, R.J., Ramon-Cueto, A., Rouiller, E.M., Schnell, L., Wannier, T., Schwab, M.E. & Edgerton, V.R. (2007a) Can experiments in nonhuman primates expedite the translation of treatments for spinal cord injury in humans? *Nat Med*, **13**, 561-566.

Courtine, G., Gerasimenko, Y., van den Brand, R., Yew, A., Musienko, P., Zhong, H., Song, B., Ao, Y., Ichiyama, R.M., Lavrov, I., Roy, R.R., Sofroniew, M.V. & Edgerton, V.R. (2009a) Transformation of nonfunctional spinal circuits into functional states after the loss of brain input. *Nat Neurosci*, **12**, 1333-1342.

Courtine, G., Gerasimenko, Y., van den Brand, R., Yew, A., Musienko, P., Zhong, H., Song, B., Ao, Y., Ichiyama, R.M., Lavrov, I., Roy, R.R., Sofroniew, M.V., Edgerton, V.R. & Brand, R.V.D. (2009b) Transformation of nonfunctional spinal circuits into functional states after the loss of brain input. *Nature neuroscience*, **12**, 1333-1342.

Courtine, G., Gerasimenko, Y.P., van den Brand, R., Yew, A., Musienko, P., Zhong, H., Song, B., Ao, Y., Ichiyama, R.M., Lavrov, I., Roy, R.R., Sofroniew, M.V., Edgerton, V.R. & van den Brand, R. (2009c) Transformation of nonfunctional spinal circuits into functional states after the loss of brain input. *Nat Neurosci*, **12**, 1333-1342.

Courtine, G., Harkema, S.J., Dy, C.J., Gerasimenko, Y.P. & Dyhre-Poulsen, P. (2007b) Modulation of multisegmental monosynaptic responses in a variety of leg muscles during walking and running in humans. *The Journal of physiology*, **582**, 1125-1139.

Courtine, G., Roy, R.R., Raven, J., Hodgson, J., McKay, H., Yang, H., Zhong, H., Tuszynski, M.H. & Edgerton, V.R. (2005) Performance of locomotion and foot

grasping following a unilateral thoracic corticospinal tract lesion in monkeys (Macaca mulatta). *Brain*, **128**, 2338-2358.

Courtine, G., Song, B., Roy, R.R., Zhong, H., Herrmann, J.E., Ao, Y., Qi, J., Edgerton, V.R. & Sofroniew, M.V. (2008) Recovery of supraspinal control of stepping via indirect propriospinal relay connections after spinal cord injury. *Nat Med*, **14**, 69-74.

Cowley, K.C., Zaporozhets, E. & Schmidt, B.J. (2008) Propriospinal neurons are sufficient for bulbospinal transmission of the locomotor command signal in the neonatal rat spinal cord. *The Journal of physiology*, **586**, 1623-1635.

Curt, A., Keck, M.E. & Dietz, V. (1998) Functional outcome following spinal cord injury: significance of motor-evoked potentials and ASIA scores. *Arch Phys Med Rehabil*, **79**, 81-86.

Curt, A., Van Hedel, H.J., Klaus, D. & Dietz, V. (2008) Recovery from a spinal cord injury: significance of compensation, neural plasticity, and repair. *J Neurotrauma*, **25**, 677-685.

De Leon, R.D., Hodgson, J.A., Roy, R.R. & Edgerton, V.R. (1998a) Full weight-bearing hindlimb standing following stand training in the adult spinal cat. *J Neurophysiol*, **80**, 83-91.

de Leon, R.D., Hodgson, J.A., Roy, R.R. & Edgerton, V.R. (1998b) Locomotor capacity attributable to step training versus spontaneous recovery after spinalization in adult cats. *J Neurophysiol*, **79**, 1329-1340.

De Leon, R.D., Hodgson, J.A., Roy, R.R. & Edgerton, V.R. (1999a) Retention of hindlimb stepping ability in adult spinal cats after the cessation of step training. *J Neurophysiol*, **81**, 85-94.

de Leon, R.D., Tamaki, H., Hodgson, J.A., Roy, R.R. & Edgerton, V.R. (1999b) Hindlimb locomotor and postural training modulates glycinergic inhibition in the spinal cord of the adult spinal cat. *J Neurophysiol*, **82**, 359-369.

Dickinson, M.H., Farley, C.T., Full, R.J., Koehl, M.A., Kram, R. & Lehman, S. (2000) How animals move: an integrative view. *Science*, **288**, 100-106.

Dietz, V. (1992) Human neuronal control of automatic functional movements: interaction between central programs and afferent input. *Physiol Rev*, **72**, 33-69.

Dietz, V. (2009) Body weight supported gait training: from laboratory to clinical setting. *Brain Res Bull*, **78**, I-VI.

Dietz, V. (2010) Behavior of spinal neurons deprived of supraspinal input. *Nat Rev Neurol*, **6**, 167-174.

Dietz, V., Colombo, G. & Jensen, L. (1994) Locomotor activity in spinal man. *Lancet*, **344**, 1260-1263.

Dietz, V., Grillner, S., Trepp, A., Hubli, M. & Bolliger, M. (2009) Changes in spinal reflex and locomotor activity after a complete spinal cord injury: a common mechanism? *Brain*, **132**, 2196-2205.

Dietz, V. & Harkema, S.J. (2004) Locomotor activity in spinal cord-injured persons. *J Appl Physiol*, **96**, 1954-1960.

Dietz, V. & Muller, R. (2004) Degradation of neuronal function following a spinal cord injury: mechanisms and countermeasures. *Brain*, **127**, 2221-2231.

Dietz, V., Muller, R. & Colombo, G. (2002) Locomotor activity in spinal man: significance of afferent input from joint and load receptors. *Brain*, **125**, 2626-2634.

Dlouhy, B.J., Dahdaleh, N.S. & Howard, M.A., 3rd (2013) Radiographic and intraoperative imaging of a hemisection of the spinal cord resulting in a pure Brown-Sequard syndrome: case report and review of the literature. *Journal of neurosurgical sciences*, **57**, 81-86.

Dobkin, B., Barbeau, H., Deforge, D., Ditunno, J., Elashoff, R., Apple, D., Basso, M., Behrman, A., Harkema, S., Saulino, M. & Scott, M. (2007) The evolution of walking-related outcomes over the first 12 weeks of rehabilitation for incomplete traumatic spinal cord injury: the multicenter randomized Spinal Cord Injury Locomotor Trial. *Neurorehabil Neural Repair*, **21**, 25-35.

Dominici, N., Keller, U., Vallery, H., Friedli, L., van den Brand, R., Starkey, M.L., Musienko, P., Riener, R. & Courtine, G. (2012a) Versatile robotic interface to evaluate, enable and train locomotion and balance after neuromotor disorders. *Nat Med*.

Dominici, N., Keller, U., Vallery, H., Friedli, L., van den Brand, R., Starkey, M.L., Musienko, P., Riener, R. & Courtine, G. (2012b) Versatile robotic interface to evaluate, enable and train locomotion and balance after neuromotor disorders. *Nature medicine*, **18**, 1142-1147.

Donovan, W.H. (2007) Spinal Cord Injury—Past, Present, and Future. *J Spinal Cord Med*, **30**, 85-100.

Drew, T., Andujar, J.E., Lajoie, K. & Yakovenko, S. (2008) Cortical mechanisms involved in visuomotor coordination during precision walking. *Brain Res Rev*, **57**, 199-211.

Drew, T., Prentice, S. & Schepens, B. (2004) Cortical and brainstem control of locomotion. *Prog Brain Res*, **143**, 251-261.

Duschau-Wicke, A., Caprez, A. & Riener, R. (2010) Patient-cooperative control increases active participation of individuals with SCI during robot-aided gait training. *Journal of neuroengineering and rehabilitation*, **7**, 43.

Edgerton, V.R., Courtine, G., Gerasimenko, Y.P., Lavrov, I., Ichiyama, R.M., Fong, A.J., Cai, L.L., Otoshi, C.K., Tillakaratne, N.J., Burdick, J.W. & Roy, R.R. (2008) Training locomotor networks. *Brain Res Rev*, **57**, 241-254.

Edgerton, V.R. & Roy, R.R. (2009) Robotic training and spinal cord plasticity. *Brain Res Bull*, **78**, 4-12.

Edgerton, V.R., Tillakaratne, N.J., Bigbee, A.J., de Leon, R.D. & Roy, R.R. (2004) Plasticity of the spinal neural circuitry after injury. *Annu Rev Neurosci*, **27**, 145-167.

Edwards, S.B. (1975) Autoradiographic studies of the projections of the midbrain reticular formation: descending projections of nucleus cuneiformis. *J Comp Neurol*, **161**, 341-358.

Engesser-Cesar, C., Ichiyama, R.M., Nefas, A.L., Hill, M.A., Edgerton, V.R., Cotman, C.W. & Anderson, A.J. (2007) Wheel running following spinal cord injury improves locomotor recovery and stimulates serotonergic fiber growth. *Eur J Neurosci*, **25**, 1931-1939.

Fawcett, J.W., Curt, A., Steeves, J.D., Coleman, W.P., Tuszynski, M.H., Lammertse, D., Bartlett, P.F., Blight, A.R., Dietz, V., Ditunno, J., Dobkin, B.H., Havton, L.A., Ellaway, P.H., Fehlings, M.G., Privat, A., Grossman, R., Guest, J.D., Kleitman, N., Nakamura, M., Gaviria, M. & Short, D. (2007) Guidelines for the conduct of clinical trials for spinal cord injury as developed by the ICCP panel: spontaneous recovery after spinal cord injury and statistical power needed for therapeutic clinical trials. *Spinal Cord*, **45**, 190-205.

Ferguson, A.R., Irvine, K.A., Gensel, J.C., Nielson, J.L., Lin, A., Ly, J., Segal, M.R., Ratan, R.R., Bresnahan, J.C. & Beattie, M.S. (2013) Derivation of Multivariate Syndromic Outcome Metrics for Consistent Testing across Multiple Models of Cervical Spinal Cord Injury in Rats. *PloS one*, **8**, e59712.

Ferguson, A.R., Stuck, E.D. & Nielson, J.L. (2011) Syndromics: A Bioinformatics Approach for Neurotrauma Research. *Translational stroke research*, **2**, 438-454.

Filli, L., Zorner, B., Weinmann, O. & Schwab, M.E. (2011) Motor deficits and recovery in rats with unilateral spinal cord hemisection mimic the Brown-Sequard syndrome. *Brain*, **134**, 2261-2273.

Fishman, P.S. (1987) Retrograde changes in the corticospinal tract of posttraumatic paraplegics. *Archives of neurology*, **44**, 1082-1084.

Fong, A.J., Cai, L.L., Otoshi, C.K., Reinkensmeyer, D.J., Burdick, J.W., Roy, R.R. & Edgerton, V.R. (2005) Spinal cord-transected mice learn to step in response to quipazine treatment and robotic training. *J Neurosci*, **25**, 11738-11747.

Fong, A.J., Roy, R.R., Ichiyama, R.M., Lavrov, I., Courtine, G., Gerasimenko, Y., Tai, Y.C., Burdick, J. & Edgerton, V.R. (2009) Recovery of control of posture and locomotion after a spinal cord injury: solutions staring us in the face. *Prog Brain Res*, **175**, 393-418.

Freund, P., Weiskopf, N., Ashburner, J., Wolf, K., Sutter, R., Altmann, D.R., Friston, K., Thompson, A. & Curt, A. (2013) MRI investigation of the sensorimotor cortex and the corticospinal tract after acute spinal cord injury: a prospective longitudinal study. *Lancet Neurol*, **12**, 873-881.

Fuentes, R., Petersson, P., Siesser, W.B., Caron, M.G. & Nicolelis, M.A. (2009) Spinal cord stimulation restores locomotion in animal models of Parkinson's disease. *Science*, **323**, 1578-1582.

Garcia-Rill, E. & Skinner, R.D. (1987a) The mesencephalic locomotor region. I. Activation of a medullary projection site. *Brain Res*, **411**, 1-12.

Garcia-Rill, E. & Skinner, R.D. (1987b) The mesencephalic locomotor region. II. Projections to reticulospinal neurons. *Brain Res*, **411**, 13-20.

Garcia-Rill, E., Skinner, R.D., Conrad, C., Mosley, D. & Campbell, C. (1986) Projections of the mesencephalic locomotor region in the rat. *Brain Res Bull*, **17**, 33-40.

Gerasimenko, Y., Roy, R.R. & Edgerton, V.R. (2008) Epidural stimulation: comparison of the spinal circuits that generate and control locomotion in rats, cats and humans. *Exp Neurol*, **209**, 417-425.

Gerasimenko, Y.P., Ichiyama, R.M., Lavrov, I.A., Courtine, G., Cai, L., Zhong, H., Roy, R.R. & Edgerton, V.R. (2007) Epidural spinal cord stimulation plus quipazine administration enable stepping in complete spinal adult rats. *J Neurophysiol*, **98**, 2525-2536.

Gerasimenko, Y.P., Lavrov, I.A., Courtine, G., Ichiyama, R.M., Dy, C.J., Zhong, H., Roy, R.R. & Edgerton, V.R. (2006) Spinal cord reflexes induced by epidural spinal cord stimulation in normal awake rats. *J Neurosci Methods*, **157**, 253-263.

Ghosh, A., Haiss, F., Sydekum, E., Schneider, R., Gullo, M., Wyss, M.T., Mueggler, T., Baltes, C., Rudin, M., Weber, B. & Schwab, M.E. (2010) Rewiring of hindlimb corticospinal neurons after spinal cord injury. *Nat Neurosci*, **13**, 97-104.

Ghosh, A., Sydekum, E., Haiss, F., Peduzzi, S., Zorner, B., Schneider, R., Baltes, C., Rudin, M., Weber, B. & Schwab, M.E. (2009) Functional and anatomical reorganization of the sensory-motor cortex after incomplete spinal cord injury in adult rats. *J Neurosci*, **29**, 12210-12219.

Giszter, S., Patil, V. & Hart, C. (2007) Primitives, premotor drives, and pattern generation: a combined computational and neuroethological perspective. *Prog Brain Res*, **165**, 323-346.

Graham-Brown, T. (1911) The intrinsic factors in the act of progression in the mammal. . *Proc R Soc Lond B Biol Sci*, 308–319.

Grasso, R., Ivanenko, Y.P., Zago, M., Molinari, M., Scivoletto, G., Castellano, V., Macellari, V. & Lacquaniti, F. (2004) Distributed plasticity of locomotor pattern generators in spinal cord injured patients. *Brain*, **127**, 1019-1034.

Grillner, S. (1985) Neurobiological bases of rhythmic motor acts in vertebrates. *Science*, **228**, 143-149.

Grillner, S. (2006) Biological Pattern Generation: The Cellular and Computational Logic of Networks in Motion. *Neuron*, **52**, 751-766.

Grillner, S., Perret, C. & Zangger, P. (1976) Central generation of locomotion in the spinal dogfish. *Brain Res*, **109**, 255-269.

Grillner, S. & Rossignol, S. (1978) On the initiation of the swing phase of locomotion in chronic spinal cats. *Brain Res*, **146**, 269-277.

Grillner, S., Wallen, P., Saitoh, K., Kozlov, A. & Robertson, B. (2008) Neural bases of goal-directed locomotion in vertebrates--an overview. *Brain Res Rev*, **57**, 2-12.

Grillner, S. & Zangger, P. (1979) On the Central Generation of Locomotion in the Low Spinal Cat. **34**, 241-261.

Grillner, S. & Zangger, P. (1984) The effect of dorsal root transection on the efferent motor pattern in the cat's hindlimb during locomotion. *Acta Physiol Scand*, **120**, 393-405.

Gruner, J.A. & Altman, J. (1980) Swimming in the rat: analysis of locomotor performance in comparison to stepping. *Experimental brain research. Experimentelle Hirnforschung. Experimentation cerebrale*, **40**, 374-382.

Guertin, P.A. (2009) Recovery of locomotor function with combinatory drug treatments designed to synergistically activate specific neuronal networks. *Curr Med Chem*, **16**, 1366-1371.

Guyatt, G.H., Sullivan, M.J., Thompson, P.J., Fallen, E.L., Pugsley, S.O., Taylor, D.W. & Berman, L.B. (1985) The 6-minute walk: a new measure of exercise capacity in patients with chronic heart failure. *Can Med Assoc J*, **132**, 919-923.

Hagglund, M., Borgius, L., Dougherty, K.J. & Kiehn, O. (2010) Activation of groups of excitatory neurons in the mammalian spinal cord or hindbrain evokes locomotion. *Nat Neurosci*, **13**, 246-252.

Harkema, S.J. (2001) Neural plasticity after human spinal cord injury: application of locomotor training to the rehabilitation of walking. *Neuroscientist*, **7**, 455-468.

Harkema, S.J. (2008) Plasticity of interneuronal networks of the functionally isolated human spinal cord. *Brain Res Rev*, **57**, 255-264.

Harkema, S.J., Gerasimenko, Y., Hodes, J., Burdick, J., Angeli, C., Chen, Y., Ferreira, C., Willhite, A., Rejc, E., Grossman, R.G. & Edgerton, V.R. (2011) Effect of epidural stimulation of the lumbosacral spinal cord on voluntary movement, standing, and assisted stepping after motor complete paraplegia: a case study. *Lancet*, **377**, 1938-1947.

Harkema, S.J., Gerasimenko, Y., Hodes, J., Burdick, J., Angeli, C., Chen, Y., Ferreira, C.K., Rejc, E. & Edgerton, V.R. (2010) Sensory control of standing and stepping enabled by epidural stimulation after a human motor complete spinal cord injury. In Neuroscience, S.f. (ed) *2010 Neuroscience Meeting Planner*, San Diego, CA, pp. Program No. 259.251.

Harkema, S.J., Hurley, S.L., Patel, U.K., Requejo, P.S., Dobkin, B.H. & Edgerton, V.R. (1997) Human lumbosacral spinal cord interprets loading during stepping. *J Neurophysiol*, **77**, 797-811.

Hausmann, O.N. (2003) Post-traumatic inflammation following spinal cord injury. *Spinal Cord*, **41**, 369-378.

Hawthorne, A.L., Hu, H., Kundu, B., Steinmetz, M.P., Wylie, C.J., Deneris, E.S. & Silver, J. (2011) The unusual response of serotonergic neurons after CNS Injury: lack of axonal dieback and enhanced sprouting within the inhibitory environment of the glial scar. *J Neurosci*, **31**, 5605-5616.

Hebb, D.O. (1949) *The Organization of Behavior: A neuropsychological Theory*. Wiley, New York.

Hellal, F., Hurtado, A., Ruschel, J., Flynn, K.C., Laskowski, C.J., Umlauf, M., Kapitein, L.C., Strikis, D., Lemmon, V., Bixby, J., Hoogenraad, C.C. & Bradke, F. (2011) Microtubule stabilization reduces scarring and causes axon regeneration after spinal cord injury. *Science*, **331**, 928-931.

Hentall, I.D., Pinzon, A. & Noga, B.R. (2006) Spatial and temporal patterns of serotonin release in the rat's lumbar spinal cord following electrical stimulation of the nucleus raphe magnus. *Neuroscience*, **142**, 893-903.

Hiersemenzel, L.P., Curt, A. & Dietz, V. (2000) From spinal shock to spasticity: neuronal adaptations to a spinal cord injury. *Neurology*, **54**, 1574-1582.

Hochberg, L.R., Bacher, D., Jarosiewicz, B., Masse, N.Y., Simeral, J.D., Vogel, J., Haddadin, S., Liu, J., Cash, S.S., van der Smagt, P. & Donoghue, J.P. (2012) Reach and grasp by people with tetraplegia using a neurally controlled robotic arm. *Nature*, **485**, 372-375.

Holsheimer, J. (1998) Computer modelling of spinal cord stimulation and its contribution to therapeutic efficacy. *Spinal Cord*, **36**, 531-540.

Horst, M., Heutschi, J., den Brand, R., Andersson, K.E., Gobet, R., Sulser, T., Courtine, G. & Eberli, D. (2012) Multi-System Neuroprosthetic Training Improves Bladder Function After Severe Spinal Cord Injury. *The Journal of urology*.

Hou, S., Duale, H., Cameron, A.A., Abshire, S.M., Lyttle, T.S. & Rabchevsky, A.G. (2008) Plasticity of lumbosacral propriospinal neurons is associated with the development of autonomic dysreflexia after thoracic spinal cord transection. *J Comp Neurol*, **509**, 382-399.

Hou, S., Duale, H. & Rabchevsky, A.G. (2009) Intraspinal sprouting of unmyelinated pelvic afferents after complete spinal cord injury is correlated with autonomic dysreflexia induced by visceral pain. *Neuroscience*, **159**, 369-379.

Hubli, M., Dietz, V. & Bolliger, M. (2012) Spinal reflex activity: a marker for neuronal functionality after spinal cord injury. *Neurorehabil Neural Repair*, **26**, 188-196.

Hughes, J.T. (1988) The Edwin Smith Surgical Papyrus: an analysis of the first case reports of spinal cord injuries. *Paraplegia*, **26**, 71-82.

Hultborn, H. (2001) State-dependent modulation of sensory feedback. *The Journal of physiology*, **533**, 5-13.

Hultborn, H. (2006) Spinal reflexes, mechanisms and concepts: from Eccles to Lundberg and beyond. *Prog Neurobiol*, **78**, 215-232.

Iannotti, C.A., Clark, M., Horn, K.P., van Rooijen, N., Silver, J. & Steinmetz, M.P. (2011) A combination immunomodulatory treatment promotes neuroprotection and locomotor recovery after contusion SCI. *Exp Neurol*, **230**, 3-15.

Ichiyama, R.M., Broman, J., Roy, R.R., Zhong, H., Edgerton, V.R. & Havton, L.A. (2011) Locomotor training maintains normal inhibitory influence on both alpha- and

gamma-motoneurons after neonatal spinal cord transection. *J Neurosci*, **31**, 26-33.

Ichiyama, R.M., Courtine, G., Gerasimenko, Y.P., Yang, G.J., van den Brand, R., Lavrov, I.A., Zhong, H., Roy, R.R. & Edgerton, V.R. (2008) Step training reinforces specific spinal locomotor circuitry in adult spinal rats. *J Neurosci*, **28**, 7370-7375.

Ichiyama, R.M., Gerasimenko, Y.P., Zhong, H., Roy, R.R. & Edgerton, V.R. (2005) Hindlimb stepping movements in complete spinal rats induced by epidural spinal cord stimulation. *Neurosci Lett*, **383**, 339-344.

James, N.D., Bartus, K., Grist, J., Bennett, D.L., McMahon, S.B. & Bradbury, E.J. (2011) Conduction failure following spinal cord injury: functional and anatomical changes from acute to chronic stages. *J Neurosci*, **31**, 18543-18555.

Jankowska, E. & Edgley, S.A. (2006) How can corticospinal tract neurons contribute to ipsilateral movements? A question with implications for recovery of motor functions. *Neuroscientist*, **12**, 67-79.

Jordan, L.M. (1998) Initiation of locomotion in mammals. *Annals of the New York Academy of Sciences*, **860**.

Jordan, L.M., Liu, J., Hedlund, P.B., Akay, T. & Pearson, K.G. (2008) Descending command systems for the initiation of locomotion in mammals. *Brain Res Rev*, **57**, 183-191.

Kakulas, B.A. (1999) A review of the neuropathology of human spinal cord injury with emphasis on special features. *J Spinal Cord Med*, **22**, 119-124.

Kapitza, S., Zorner, B., Weinmann, O., Bolliger, M., Filli, L., Dietz, V. & Schwab, M.E. (2012) Tail spasms in rat spinal cord injury: changes in interneuronal connectivity. *Exp Neurol*, **236**, 179-189.

Kinoshita, M., Matsui, R., Kato, S., Hasegawa, T., Kasahara, H., Isa, K., Watakabe, A., Yamamori, T., Nishimura, Y., Alstermark, B., Watanabe, D., Kobayashi, K. & Isa, T. (2012) Genetic dissection of the circuit for hand dexterity in primates. *Nature*, **487**, 235-238.

Kirov, S.A. & Harris, K.M. (1999) Dendrites are more spiny on mature hippocampal neurons when synapses are inactivated. *Nat Neurosci*, **2**, 878-883.

Kitzman, P. (2006) Changes in vesicular glutamate transporter 2, vesicular GABA transporter and vesicular acetylcholine transporter labeling of sacrocaudal motoneurons in the spastic rat. *Exp Neurol*, **197**, 407-419.

Kitzman, P. (2007) VGLUT1 and GLYT2 labeling of sacrocaudal motoneurons in the spinal cord injured spastic rat. *Exp Neurol*, **204**, 195-204.

Kosofsky, B.E. & Molliver, M.E. (1987) The serotoninergic innervation of cerebral cortex: different classes of axon terminals arise from dorsal and median raphe nuclei. *Synapse*, **1**, 153-168.

Krenz, N.R. & Weaver, L.C. (1998) Sprouting of primary afferent fibers after spinal cord transection in the rat. *Neuroscience*, **85**, 443-458.

Kuypers, H.G. (1964) The Descending Pathways to the Spinal Cord, Their Anatomy and Function. *Prog Brain Res*, **11**, 178-202.

Kwakkel, G., Kollen, B.J. & Krebs, H.I. (2008) Effects of robot-assisted therapy on upper limb recovery after stroke: a systematic review. *Neurorehabil Neural Repair*, **22**, 111-121.

Lammertse, D., Dungan, D., Dreisbach, J., Falci, S., Flanders, A., Marino, R. & Schwartz, E. (2007) Neuroimaging in traumatic spinal cord injury: an evidence-based review for clinical practice and research. *J Spinal Cord Med*, **30**, 205-214.

Landry, E.S., Lapointe, N.P., Rouillard, C., Levesque, D., Hedlund, P.B. & Guertin, P.A. (2006) Contribution of spinal 5-HT1A and 5-HT7 receptors to locomotor-like movement induced by 8-OH-DPAT in spinal cord-transected mice. *Eur J Neurosci*, **24**, 535-546.

Landry, M., Bouali-Benazzouz, R., El Mestikawy, S., Ravassard, P. & Nagy, F. (2004) Expression of vesicular glutamate transporters in rat lumbar spinal cord, with a note on dorsal root ganglia. *J Comp Neurol*, **468**, 380-394.

Lapointe, N.P. & Guertin, P.A. (2008) Synergistic effects of D1/5 and 5-HT1A/7 receptor agonists on locomotor movement induction in complete spinal cord-transected mice. *J Neurophysiol*, **100**, 160-168.

Lavrov, I., Courtine, G., Dy, C.J., van den Brand, R., Fong, A.J., Gerasimenko, Y., Zhong, H., Roy, R.R. & Edgerton, V.R. (2008a) Facilitation of stepping with epidural stimulation in spinal rats: role of sensory input. *J Neurosci*, **28**, 7774-7780.

Lavrov, I., Dy, C.J., Fong, A.J., Gerasimenko, Y., Courtine, G., Zhong, H., Roy, R.R. & Edgerton, V.R. (2008b) Epidural stimulation induced modulation of spinal locomotor networks in adult spinal rats. *J Neurosci*, **28**, 6022-6029.

Lavrov, I., Gerasimenko, Y.P., Ichiyama, R.M., Courtine, G., Zhong, H., Roy, R.R. & Edgerton, V.R. (2006) Plasticity of spinal cord reflexes after a complete transection in adult rats: relationship to stepping ability. *J Neurophysiol*, **96**, 1699-1710.

Lee, B.B., Cripps, R.A., Fitzharris, M. & Wing, P.C. (2014) The global map for traumatic spinal cord injury epidemiology: update 2011, global incidence rate. *Spinal Cord*, **52**, 110-116.

Lee, S.J. & Hidler, J. (2008) Biomechanics of overground vs. treadmill walking in healthy individuals. *J Appl Physiol (1985)*, **104**, 747-755.

Lemon, R.N. (2008) Descending pathways in motor control. *Annu Rev Neurosci*, **31**, 195-218.

Lemon, R.N. & Griffiths, J. (2005) Comparing the function of the corticospinal system in different species: organizational differences for motor specialization? *Muscle Nerve*, **32**, 261-279.

Levi, A.D., Tator, C.H. & Bunge, R.P. (1996) Clinical syndromes associated with disproportionate weakness of the upper versus the lower extremities after cervical spinal cord injury. *Neurosurgery*, **38**, 179-183; discussion 183-175.

Lewicki, M.S. (1998) A review of methods for spike sorting: the detection and classification of neural action potentials. *Network: Computation in Neural Systems*, **9**.

Lin, C.S., Macefield, V.G., Elam, M., Wallin, B.G., Engel, S. & Kiernan, M.C. (2007) Axonal changes in spinal cord injured patients distal to the site of injury. *Brain*, **130**, 985-994.

Linting, M., Meulman, J.J., Groenen, P.J. & van der Koojj, A.J. (2007) Nonlinear principal components analysis: introduction and application. *Psychological methods*, **12**, 336-358.

Little, J.W. & Halar, E. (1985) Temporal course of motor recovery after Brown-Sequard spinal cord injuries. *Paraplegia*, **23**, 39-46.

Liu, J. & Jordan, L.M. (2005) Stimulation of the parapyramidal region of the neonatal rat brain stem produces locomotor-like activity involving spinal 5-HT7 and 5-HT2A receptors. *J Neurophysiol*, **94**, 1392-1404.

Liu, K., Lu, Y., Lee, J.K., Samara, R., Willenberg, R., Sears-Kraxberger, I., Tedeschi, A., Park, K.K., Jin, D., Cai, B., Xu, B., Connolly, L., Steward, O., Zheng, B. & He, Z. (2010) PTEN deletion enhances the regenerative ability of adult corticospinal neurons. *Nature neuroscience*, **13**, 1075-1081.

Lovely, R.G., Gregor, R.J., Roy, R.R. & Edgerton, V.R. (1986) Effects of training on the recovery of full-weight-bearing stepping in the adult spinal cat. *Exp Neurol*, **92**, 421-435.

Lu, P., Wang, Y., Graham, L., McHale, K., Gao, M., Wu, D., Brock, J., Blesch, A., Rosenzweig, E.S., Havton, L.A., Zheng, B., Conner, J.M., Marsala, M. & Tuszynski, M.H. (2012) Long-distance growth and connectivity of neural stem cells after severe spinal cord injury. *Cell*, **150**, 1264-1273.

Lunenburger, L., Bolliger, M., Czell, D., Muller, R. & Dietz, V. (2006) Modulation of locomotor activity in complete spinal cord injury. *Experimental brain research. Experimentelle Hirnforschung. Experimentation cerebrale*, **174**, 638-646.

Macpherson, J.M., Fung, J. & Jacobs, R. (1997) Postural orientation, equilibrium, and the spinal cord. *Adv Neurol*, **72**, 227-232.

Maegele, M., Muller, S., Wernig, A., Edgerton, V.R. & Harkema, S.J. (2002) Recruitment of spinal motor pools during voluntary movements versus stepping after human spinal cord injury. *J Neurotrauma*, **19**, 1217-1229.

Maier, I.C., Ichiyama, R.M., Courtine, G., Schnell, L., Lavrov, I., Edgerton, V.R. & Schwab, M.E. (2009) Differential effects of anti-Nogo-A antibody treatment and treadmill training in rats with incomplete spinal cord injury. *Brain*, **132**, 1426-1440.

Martin, G.F., Vertes, R.P. & Waltzer, R. (1985) Spinal projections of the gigantocellular reticular formation in the rat. Evidence for projections from different areas to

laminae I and II and lamina IX. *Experimental brain research. Experimentelle Hirnforschung. Experimentation cerebrale*, **58**, 154-162.

Matsuyama, K., Mori, F., Nakajima, K., Drew, T., Aoki, M. & Mori, S. (2004) Locomotor role of the corticoreticular-reticulospinal-spinal interneuronal system. *Prog Brain Res*, **143**, 239-249.

McKay, W.B., Ovechkin, A.V., Vitaz, T.W., Terson de Paleville, D.G. & Harkema, S.J. (2011) Long-lasting involuntary motor activity after spinal cord injury. *Spinal Cord*, **49**, 87-93.

Metz, G.A., Curt, A., van de Meent, H., Klusman, I., Schwab, M.E. & Dietz, V. (2000) Validation of the weight-drop contusion model in rats: a comparative study of human spinal cord injury. *J Neurotrauma*, **17**, 1-17.

Micera, S., Sabatini, A.M., Dario, P. & Rossi, B. (1999) A hybrid approach to EMG pattern analysis for classification of arm movements using statistical and fuzzy techniques. *Medical engineering & physics*, **21**, 303-311.

Minassian, K., Jilge, B., Rattay, F., Pinter, M.M., Binder, H., Gerstenbrand, F. & Dimitrijevic, M.R. (2004) Stepping-like movements in humans with complete spinal cord injury induced by epidural stimulation of the lumbar cord: electromyographic study of compound muscle action potentials. *Spinal Cord*, **42**, 401-416.

Molander, C., Xu, Q. & Grant, G. (1984) The cytoarchitectonic organization of the spinal cord in the rat. I. The lower thoracic and lumbosacral cord. *J Comp Neurol*, **230**, 133-141.

Mori, S., Matsui, T., Kuze, B., Asanome, M., Nakajima, K. & Matsuyama, K. (1996) Cerebellar-induced locomotion: reticulospinal control of spinal rhythm generating mechanism in cats. *Annals of the New York Academy of Sciences*, **860**.

Mullner, A., Gonzenbach, R.R., Weinmann, O., Schnell, L., Liebscher, T. & Schwab, M.E. (2008) Lamina-specific restoration of serotonergic projections after Nogo-A antibody treatment of spinal cord injury in rats. *Eur J Neurosci*, **27**, 326-333.

Murray, K.C., Nakae, A., Stephens, M.J., Rank, M., D'Amico, J., Harvey, P.J., Li, X., Harris, R.L., Ballou, E.W., Anelli, R., Heckman, C.J., Mashimo, T., Vavrek, R., Sanelli, L., Gorassini, M.A., Bennett, D.J. & Fouad, K. (2010) Recovery of motoneuron and locomotor function after spinal cord injury depends on constitutive activity in 5-HT2C receptors. *Nat Med*, **16**, 694-700.

Mushahwar, V.K., Guevremont, L. & Saigal, R. (2006) Could cortical signals control intraspinal stimulators? A theoretical evaluation. *IEEE Trans Neural Syst Rehabil Eng*, **14**, 198-201.

Mushahwar, V.K. & Horch, K.W. (2000) Muscle recruitment through electrical stimulation of the lumbo-sacral spinal cord. *IEEE Trans Rehabil Eng*, **8**, 22-29.

Mushahwar, V.K., Jacobs, P.L., Normann, R.A., Triolo, R.J. & Kleitman, N. (2007) New functional electrical stimulation approaches to standing and walking. *J Neural Eng*, **4**, S181-197.

Musienko, P., Heutschi, J., Friedli, L., den Brand, R.V. & Courtine, G. (2011a) Multi-system neurorehabilitative strategies to restore motor functions following severe spinal cord injury. *Exp Neurol*.

Musienko, P., Heutschi, J., Friedli, L., van den Brand, R. & Courtine, G. (2012) Multi-system neurorehabilitative strategies to restore motor functions following severe spinal cord injury. *Exp Neurol*, **235**, 100-109.

Musienko, P., van den Brand, R., Maerzendorfer, O., Larmagnac, A. & Courtine, G. (2009) Combinatory electrical and pharmacological neuroprosthetic interfaces to regain motor function after spinal cord injury. *IEEE Trans Biomed Eng*, **56**, 2707-2711.

Musienko, P., van den Brand, R., Marzendorfer, O., Roy, R.R., Gerasimenko, Y., Edgerton, V.R. & Courtine, G. (2011b) Controlling Specific Locomotor Behaviors through Multidimensional Monoaminergic Modulation of Spinal Circuitries. *J Neurosci*, **31**, 9264-9278.

Musienko, P., van den Brand, R., Marzendorfer, O., Roy, R.R., Gerasimenko, Y., Edgerton, V.R. & Courtine, G. (2011c) Controlling specific locomotor behaviors through multidimensional monoaminergic modulation of spinal circuitries. *J Neurosci*, **31**, 9264-9278.

Musienko, P.E., Bogacheva, I.N. & Gerasimenko Iu, P. (2005) [Significance of peripheral feedback in stepping movement generation under epideral spinal cord stimulation]. *Ross Fiziol Zh Im I M Sechenova*, **91**, 1407-1420.

Musienko, P.E., Bogacheva, I.N. & Gerasimenko, Y.P. (2007) Significance of peripheral feedback in the generation of stepping movements during epidural stimulation of the spinal cord. *Neurosci Behav Physiol*, **37**, 181-190.

Musienko, P.E., Gerasimenko Iu, P., Van den Brand, R., Roy, R.R., Zhong, H., Edgerton, V. & Courtine, G. (Year) Monoaminergic modulation of locomotion facilitated by epidural stimulation (ES) in spinal rats. In: Planner, N.M. (ed), Society for Neuroscience. City. p. Program No 573.572.

Musienko, P.E., Van den Brand, R., Märzendorfer, O., Gerasimenko, Y., Roy, R.R., Edgerton, V. & Courtine, G. (In press) Controlling specific locomotor behaviors through multidimensional monoaminergic modulation of spinal circuitries. *J Neurosci*.

Musienko, P.E., Zelenin, P.V., Orlovsky, G.N. & Deliagina, T.G. (2010) Facilitation of postural limb reflexes with epidural stimulation in spinal rabbits. *J Neurophysiol*, **103**, 1080-1092.

Musselman, K., Brunton, K., Lam, T. & Yang, J. (2011a) Spinal cord injury functional ambulation profile: a new measure of walking ability. *Neurorehabil Neural Repair*, **25**, 285-293.

Musselman, K., Brunton, K., Lam, T. & Yang, J. (2011b) Spinal cord injury functional ambulation profile: a new measure of walking ability. *Neurorehabil Neural Repair*, **25**, 285-293.

Nahar, J., Lett, K.M. & Schulz, D.J. (2012) Restoration of descending inputs fails to rescue activity following deafferentation of a motor network. *J Neurophysiol*, **108**, 871-881.

Nessler, J.A., Timoszyk, W., Merlo, M., Emken, J.L., Minakata, K., Roy, R.R., de Leon, R.D., Edgerton, V.R. & Reinkensmeyer, D.J. (2005) A robotic device for studying rodent locomotion after spinal cord injury. *IEEE Trans Neural Syst Rehabil Eng*, **13**, 497-506.

Nicol, D.J., Granat, M.H., Baxendale, R.H. & Tuson, S.J. (1995) Evidence for a human spinal stepping generator. *Brain Res*, **684**, 230-232.

Nishimura, Y., Onoe, H., Morichika, Y., Perfiliev, S., Tsukada, H. & Isa, T. (2007) Time-dependent central compensatory mechanisms of finger dexterity after spinal cord injury. *Science*, **318**, 1150-1155.

Noga, B.R., Kettler, J. & Jordan, L.M. (1988) Locomotion produced in mesencephalic cats by injections of putative transmitter substances and antagonists into the medial reticular formation and the pontomedullary locomotor strip. *J Neurosci*, **8**, 2074-2086.

Norenberg, M.D., Smith, J. & Marcillo, A. (2004) The pathology of human spinal cord injury: defining the problems. *J Neurotrauma*, **21**, 429-440.

Nout, Y.S., Ferguson, A.R., Strand, S.C., Moseanko, R., Hawbecker, S., Zdunowski, S., Nielson, J.L., Roy, R.R., Zhong, H., Rosenzweig, E.S., Brock, J.H., Courtine, G., Edgerton, V.R., Tuszynski, M.H., Beattie, M.S. & Bresnahan, J.C. (2012a) Methods for Functional Assessment After C7 Spinal Cord Hemisection in the Rhesus Monkey. *Neurorehabil Neural Repair*.

Nout, Y.S., Rosenzweig, E.S., Brock, J.H., Strand, S.C., Moseanko, R., Hawbecker, S., Zdunowski, S., Nielson, J.L., Roy, R.R., Courtine, G., Ferguson, A.R., Edgerton, V.R., Beattie, M.S., Bresnahan, J.C. & Tuszynski, M.H. (2012b) Animal models of neurologic disorders: a nonhuman primate model of spinal cord injury. *Neurotherapeutics : the journal of the American Society for Experimental NeuroTherapeutics*, **9**, 380-392.

Oliveira, A.L., Hydling, F., Olsson, E., Shi, T., Edwards, R.H., Fujiyama, F., Kaneko, T., Hokfelt, T., Cullheim, S. & Meister, B. (2003) Cellular localization of three vesicular glutamate transporter mRNAs and proteins in rat spinal cord and dorsal root ganglia. *Synapse*, **50**, 117-129.

Orlovsky, G.N., Deliagina, T.G. & Grinllner, S. (1999) *Neuronal control of locomotion: from mollusc to man*. Oxford University Press, Oxford.

Oudega, M. & Perez, M.A. (2012) Corticospinal reorganization after spinal cord injury. *The Journal of physiology*, **590**, 3647-3663.

Pearson, K.G. (2004) Generating the walking gait: role of sensory feedback. *Prog Brain Res*, **143**, 123-129.

Persson, S., Boulland, J.L., Aspling, M., Larsson, M., Fremeau, R.T., Jr., Edwards, R.H., Storm-Mathisen, J., Chaudhry, F.A. & Broman, J. (2006) Distribution of vesicular

glutamate transporters 1 and 2 in the rat spinal cord, with a note on the spinocervical tract. *J Comp Neurol*, **497**, 683-701.

Philippson, M. (1905) L'autonomie et la centrilasation dans le système nerveux des animaux. *Trav. Lab. Physiol. Inst. Solvay. (Bruxelle)*, **7**, 1-208.

Pratt, G.A., Williamson, M.M., Dillworth, P., Pratt, J., Ulland, K. & Wright, A. (1995a) Stiffness Isn't Everything *International Symposium on Experimental Robotics (ISER)* Springer, Stanford, USA.

Pratt, G.A., Williamson, M.M., Dillworth, P., Pratt, J., Ulland, K. & Wright, A. (Year) Stiffness Isn't Everything,. International Symposium on Experimental Robotics (ISER). City.

Prochazka, A., Mushahwar, V.K. & McCreery, D.B. (2001) Neural prostheses. *The Journal of physiology*, **533**, 99-109.

Quiroga, R.Q., Nadasdy, Z. & Ben-Shaul, Y. (2004) Unsupervised spike detection and sorting with wavelets and superparamagnetic clustering. *Neural Comput*, **16**, 1661-1687.

Raineteau, O., Fouad, K., Bareyre, F.M. & Schwab, M.E. (2002) Reorganization of descending motor tracts in the rat spinal cord. *Eur J Neurosci*, **16**, 1761-1771.

Raineteau, O. & Schwab, M.E. (2001) Plasticity of motor systems after incomplete spinal cord injury. *Nat Rev Neurosci*, **2**, 263-273.

Ramon y Cajal, S. (1928) *Degeneration and Regeneration of the Nervous System*. :Oxford University Press, American Branch, New York.

Rattay, F., Minassian, K. & Dimitrijevic, M.R. (2000) Epidural electrical stimulation of posterior structures of the human lumbosacral cord: 2. quantitative analysis by computer modeling. *Spinal Cord*, **38**, 473-489.

Reinkensmeyer, D.J., Aoyagi, D., Emken, J.L., Galvez, J.A., Ichinose, W., Kerdanyan, G., Maneekobkunwong, S., Minakata, K., Nessler, J.A., Weber, R., Roy, R.R., de Leon, R., Bobrow, J.E., Harkema, S.J. & Edgerton, V.R. (2006) Tools for understanding and optimizing robotic gait training. *Journal of rehabilitation research and development*, **43**, 657-670.

Riegger, T., Conrad, S., Schluesener, H.J., Kaps, H.P., Badke, A., Baron, C., Gerstein, J., Dietz, K., Abdizahdeh, M. & Schwab, J.M. (2009) Immune depression syndrome following human spinal cord injury (SCI): a pilot study. *Neuroscience*, **158**, 1194-1199.

Rosenzweig, E.S., Brock, J.H., Culbertson, M.D., Lu, P., Moseanko, R., Edgerton, V.R., Havton, L.A. & Tuszynski, M.H. (2009) Extensive spinal decussation and bilateral termination of cervical corticospinal projections in rhesus monkeys. *J Comp Neurol*, **513**, 151-163.

Rosenzweig, E.S., Courtine, G., Jindrich, D.L., Brock, J.H., Ferguson, A.R., Strand, S.C., Nout, Y.S., Roy, R.R., Miller, D.M., Beattie, M.S., Havton, L.A., Bresnahan, J.C., Edgerton, V.R. & Tuszynski, M.H. (2010) Extensive spontaneous plasticity of

corticospinal projections after primate spinal cord injury. *Nat Neurosci*, **13**, 1505-1510.

Rossignol, S., Dubuc, R. & Gossard, J.P. (2006) Dynamic sensorimotor interactions in locomotion. *Physiol Rev*, **86**, 89-154.

Rossignol, S., Giroux, N., Chau, C., Marcoux, J., Brustein, E. & Reader, T.A. (2001) Pharmacological aids to locomotor training after spinal injury in the cat. *The Journal of physiology*, **533**, 65-74.

Roth, E.J., Park, T., Pang, T., Yarkony, G.M. & Lee, M.Y. (1991) Traumatic cervical Brown-Sequard and Brown-Sequard-plus syndromes: the spectrum of presentations and outcomes. *Paraplegia*, **29**, 582-589.

Roy, R.R. & Edgerton, V.R. (2012) Neurobiological perspective of spasticity as occurs after a spinal cord injury. *Exp Neurol*, **235**, 116-122.

Ryczko, D. & Dubuc, R. (2013) The multifunctional mesencephalic locomotor region. *Current pharmaceutical design*, **19**, 4448-4470.

Scheff, S.W., Rabchevsky, A.G., Fugaccia, I., Main, J.A. & Lumpp, J.E., Jr. (2003) Experimental modeling of spinal cord injury: characterization of a force-defined injury device. *J Neurotrauma*, **20**, 179-193.

Schnell, L. & Schwab, M.E. (1990) Axonal regeneration in the rat spinal cord produced by an antibody against myelin-associated neurite growth inhibitors. *Nature*, **343**, 269-272.

Schomburg, E.D., Steffens, H. & Kniffki, K.D. (1999) Contribution of group III and IV muscle afferents to multisensorial spinal motor control in cats. *Neurosci Res*, **33**, 195-206.

Schubert, M., Curt, A., Jensen, L. & Dietz, V. (1997) Corticospinal input in human gait: modulation of magnetically evoked motor responses. *Experimental brain research. Experimentelle Hirnforschung. Experimentation cerebrale*, **115**, 234-246.

Schucht, P., Raineteau, O., Schwab, M.E. & Fouad, K. (2002) Anatomical Correlates of Locomotor Recovery Following Dorsal and Ventral Lesions of the Rat Spinal Cord. *Experimental Neurology*, **176**, 143-153.

Schwab, J.M., Brechtel, K., Mueller, C.A., Failli, V., Kaps, H.P., Tuli, S.K. & Schluesener, H.J. (2006) Experimental strategies to promote spinal cord regeneration--an integrative perspective. *Prog Neurobiol*, **78**, 91-116.

Sherrington, C. (1910a) Flexion-reflex of the limb, crossed extension reflex, and reflex stepping and standing. *J Physiol (Lond)*, **40**, 28-121.

Sherrington, C.S. (1910b) Flexion-reflex of the limb, crossed extension-reflex, and reflex stepping and standing. *The Journal of physiology*, **40**, 28-121.

Shik, M.L., Severin, F.V. & Orlovsky, G.N. (1969) Control of walking and running by means of electrical stimulation of the mesencephalon. *Electroencephalogr Clin Neurophysiol*, **26**, 549.

Singh, A., Balasubramanian, S., Murray, M., Lemay, M. & Houle, J. (2011) Role of spared pathways in locomotor recovery after body-weight-supported treadmill training in contused rats. *J Neurotrauma*, **28**, 2405-2416.

Slawinska, U., Majczynski, H., Dai, Y. & Jordan, L.M. (2012) The upright posture improves plantar stepping and alters responses to serotonergic drugs in spinal rats. *The Journal of physiology*, **590**, 1721-1736.

Sloot, L.H., van der Krogt, M.M. & Harlaar, J. (2014) Effects of adding a virtual reality environment to different modes of treadmill walking. *Gait Posture*, **39**, 939-945.

Soares, S., Barnat, M., Salim, C., von Boxberg, Y., Ravaille-Veron, M. & Nothias, F. (2007) Extensive structural remodeling of the injured spinal cord revealed by phosphorylated MAP1B in sprouting axons and degenerating neurons. *Eur J Neurosci*, **26**, 1446-1461.

Steeves, J.D. & Jordan, L.M. (1980) Localization of a descending pathway in the spinal cord which is necessary for controlled treadmill locomotion. *Neurosci Lett*, **20**, 283-288.

Steeves, J.D. & Jordan, L.M. (1984) Autoradiographic demonstration of the projections from the mesencephalic locomotor region. *Brain Res*, **307**, 263-276.

Steeves, J.D., Lammertse, D., Curt, A., Fawcett, J.W., Tuszynski, M.H., Ditunno, J.F., Ellaway, P.H., Fehlings, M.G., Guest, J.D., Kleitman, N., Bartlett, P.F., Blight, A.R., Dietz, V., Dobkin, B.H., Grossman, R., Short, D., Nakamura, M., Coleman, W.P., Gaviria, M. & Privat, A. (2007) Guidelines for the conduct of clinical trials for spinal cord injury (SCI) as developed by the ICCP panel: clinical trial outcome measures. *Spinal Cord*, **45**, 206-221.

Steward, O., Zheng, B. & Tessier-Lavigne, M. (2003) False resurrections: distinguishing regenerated from spared axons in the injured central nervous system. *J Comp Neurol*, **459**, 1-8.

Steward, O., Zheng, B., Tessier-Lavigne, M., Hofstadter, M., Sharp, K. & Yee, K.M. (2008) Regenerative growth of corticospinal tract axons via the ventral column after spinal cord injury in mice. *J Neurosci*, **28**, 6836-6847.

Stolze, H., Kuhtz-Buschbeck, J.P., Mondwurf, C., Boczek-Funcke, A., Jöhnk, K., Deuschl, G. & Illert, M. (1997) Gait analysis during treadmill and overground locomotion in children and adults.pdf>. *Electroencephalogr Clin Neurophysiol*, **105**, 490-497.

Sun, F., Park, K.K., Belin, S., Wang, D., Lu, T., Chen, G., Zhang, K., Yeung, C., Feng, G., Yankner, B.A. & He, Z. (2011) Sustained axon regeneration induced by co-deletion of PTEN and SOCS3. *Nature*.

Tan, A.M., Chakrabarty, S., Kimura, H. & Martin, J.H. (2012) Selective corticospinal tract injury in the rat induces primary afferent fiber sprouting in the spinal cord and hyperreflexia. *J Neurosci*, **32**, 12896-12908.

Tan, A.M., Stamboulian, S., Chang, Y.W., Zhao, P., Hains, A.B., Waxman, S.G. & Hains, B.C. (2008) Neuropathic pain memory is maintained by Rac1-regulated dendritic spine remodeling after spinal cord injury. *J Neurosci*, **28**, 13173-13183.

Thomas, S.L. & Gorassini, M.A. (2005) Increases in corticospinal tract function by treadmill training after incomplete spinal cord injury. *J Neurophysiol*, **94**, 2844-2855.

Tillakaratne, N.J., de Leon, R.D., Hoang, T.X., Roy, R.R., Edgerton, V.R. & Tobin, A.J. (2002) Use-dependent modulation of inhibitory capacity in the feline lumbar spinal cord. *J Neurosci*, **22**, 3130-3143.

Timoszyk, W.K., Nessler, J.A., Acosta, C., Roy, R.R., Edgerton, V.R., Reinkensmeyer, D.J. & de Leon, R. (2005) Hindlimb loading determines stepping quantity and quality following spinal cord transection. *Brain Res*, **1050**, 180-189.

Todd, A.J., Hughes, D.I., Polgar, E., Nagy, G.G., Mackie, M., Ottersen, O.P. & Maxwell, D.J. (2003) The expression of vesicular glutamate transporters VGLUT1 and VGLUT2 in neurochemically defined axonal populations in the rat spinal cord with emphasis on the dorsal horn. *Eur J Neurosci*, **17**, 13-27.

Turrigiano, G.G., Leslie, K.R., Desai, N.S., Rutherford, L.C. & Nelson, S.B. (1998) Activity-dependent scaling of quantal amplitude in neocortical neurons. *Nature*, **391**, 892-896.

Tuszynski, M.H. & Steward, O. (2012) Concepts and methods for the study of axonal regeneration in the CNS. *Neuron*, **74**, 777-791.

Vallery, H., Veneman, J., Van Asseldonk, E., Ekkelenkamp, R., Buss, M. & Van der Kooij, H. (2008) Compliant actuation of rehabilitation robots - Benefits and limitations of series elastic actuators. *Ieee Robot Autom Mag*, **15**, 60-69.

Van de Crommert, H.W., Mulder, T. & Duysens, J. (1998) Neural control of locomotion: sensory control of the central pattern generator and its relation to treadmill training. *Gait Posture*, **7**, 251-263.

van den Brand, R., Heutschi, J., Barraud, Q., DiGiovanna, J., Bartholdi, K., Huerlimann, M., Friedli, L., Vollenweider, I., Moraud, E.M., Duis, S., Dominici, N., Micera, S., Musienko, P. & Courtine, G. (2012) Restoring voluntary control of locomotion after paralyzing spinal cord injury. *Science*, **336**, 1182-1185.

Velliste, M., Perel, S., Spalding, M.C., Whitford, A.S. & Schwartz, A.B. (2008) Cortical control of a prosthetic arm for self-feeding. *Nature*, **453**, 1098-1101.

Vrieseling, E. & Arber, S. (2006) Target-induced transcriptional control of dendritic patterning and connectivity in motor neurons by the ETS gene Pea3. *Cell*, **127**, 1439-1452.

Wahl, A.S., Omlor, W., Rubio, J.C., Chen, J.L., Zheng, H., Schroter, A., Gullo, M., Weinmann, O., Kobayashi, K., Helmchen, F., Ommer, B. & Schwab, M.E. (2014) Asynchronous therapy restores motor control by rewiring of the rat corticospinal tract after stroke. *Science*, **344**, 1250-1255.

Weidner, N., Ner, A., Salimi, N. & Tuszynski, M.H. (2001) Spontaneous corticospinal axonal plasticity and functional recovery after adult central nervous system injury. *Proceedings of the National Academy of Sciences of the United States of America*, **98**, 3513-3518.

Weishaupt, N., Hurd, C., Wei, D.Z. & Fouad, K. (2013) Reticulospinal plasticity after cervical spinal cord injury in the rat involves withdrawal of projections below the injury. *Exp Neurol*, **247**, 241-249.

Wernig, A. (2005) "Ineffectiveness" of automated locomotor training. *Arch Phys Med Rehabil*, **86**, 2385-2386; author reply 2386-2387.

Wernig, A. & Muller, S. (1992) Laufband locomotion with body weight support improved walking in persons with severe spinal cord injuries. *Paraplegia*, **30**, 229-238.

Wernig, A., Muller, S., Nanassy, A. & Cagol, E. (1995) Laufband therapy based on 'rules of spinal locomotion' is effective in spinal cord injured persons. *Eur J Neurosci*, **7**, 823-829.

Wessels, M., Lucas, C., Eriks, I. & de Groot, S. (2010) Body weight-supported gait training for restoration of walking in people with an incomplete spinal cord injury: a systematic review. *Journal of rehabilitation medicine : official journal of the UEMS European Board of Physical and Rehabilitation Medicine*, **42**, 513-519.

Winter, D.A. (1990) *Biomechanics and Motor Control of Human Movement*. Wiley, New York.

Winter, D.A., MacKinnon, C.D., Ruder, G.K. & Wieman, C. (1993) An integrated EMG/biomechanical model of upper body balance and posture during human gait. *Prog Brain Res*, **97**, 359-367.

Wirth, B., van Hedel, H.J. & Curt, A. (2008) Ankle dexterity is less impaired than muscle strength in incomplete spinal cord lesion. *J Neurol*, **255**, 273-279.

Wirz, M., Zemon, D.H., Rupp, R., Scheel, A., Colombo, G., Dietz, V. & Hornby, T.G. (2005) Effectiveness of automated locomotor training in patients with chronic incomplete spinal cord injury: a multicenter trial. *Arch Phys Med Rehabil*, **86**, 672-680.

Zaaimi, B., Edgley, S.A., Soteropoulos, D.S. & Baker, S.N. (2012) Changes in descending motor pathway connectivity after corticospinal tract lesion in macaque monkey. *Brain*, **135**, 2277-2289.

Zemlan, F.P., Behrehani, M.M. & Beckstead, R.M. (1984) Ascending and descending projections from the nucleus reticularis magnocellularis and nucleus reticularis gigantocellularis: an Autoradiographic and Horseradish Peroxidase Study in the Rat. *Brain Res*, **292**, 207-220.

Zorner, B., Bachmann, L.C., Filli, L., Kapitza, S., Gullo, M., Bolliger, M., Starkey, M.L., Rothlisberger, M., Gonzenbach, R.R. & Schwab, M.E. (2014a) Chasing central nervous system plasticity: the brainstem's contribution to locomotor recovery in rats with spinal cord injury. *Brain*.

Zorner, B., Bachmann, L.C., Filli, L., Kapitza, S., Gullo, M., Bolliger, M., Starkey, M.L., Rothlisberger, M., Gonzenbach, R.R. & Schwab, M.E. (2014b) Chasing central nervous system plasticity: the brainstem's contribution to locomotor recovery in rats with spinal cord injury. *Brain*, **137**, 1716-1732.

Zorner, B., Filli, L., Starkey, M.L., Gonzenbach, R., Kasper, H., Rothlisberger, M., Bolliger, M. & Schwab, M.E. (2010a) Profiling locomotor recovery: comprehensive quantification of impairments after CNS damage in rodents. *Nat Methods*, **7**, 701-708.

Zorner, B., Filli, L., Starkey, M.L., Gonzenbach, R., Kasper, H., Rothlisberger, M., Bolliger, M. & Schwab, M.E. (2010b) Profiling locomotor recovery: comprehensive quantification of impairments after CNS damage in rodents. *Nature methods*, **7**, 701-708.

12 Acknowledgment

First of all I would like to express my sincere gratitude to Grégoire Courtine for giving me the unique opportunity to conduct this PhD work in his lab. Over the years in the lab he has not only been a supervisor to my studies but also a mentor, advisor and friend. Grégoire himself and the work in the lab gave me not only the opportunity to extensively build up my scientific knowledge and wide-field mind set, he also took big part in developing my character and a brought field of soft skills and for this I am very grateful

I would also like to thank the member of the thesis committee, Prof. Dr. Eric Rouiller, Prof. Dr. Carmen Sandi, Dr. Jocelyne Bloch and Prof. Dr. Olaf Blanke for the time and expertise of validating my thesis. A special thank goes to Prof. Dr. Olaf Blanke for being also my mentor during my time in the EPFL Neuroscience PhD program and for validating my progress reports.

I want to further express my thanks to the whole team of the G-Lab for helping realizing these studies. The number of authors on the published papers implies the conclusion that the presented work is the product of a great cooperation, both within the lab as well as with external contributors. I want to specially thank Rubia van den Brand for introducing me into the world of neurorehabilitation after SCI, Quentin Barraud for his extensive support in validating and obtaining results from anatomical experiments, Simone Duis and Laetitia Baud for their tremendous help with animal related work, and Nadia Dominici and Isabel Vollenweider for discussing biomechanical results. Most of all, I want to express my gratitude towards Janine Beauparlant-Heutschi for her cooperation, her scientific inputs, her persistent endurance, and her deep and honest friendship.

Last but not least I want to thank my family and friends that supported me during my whole study time, especially during the last year. I want to express my endless thankfulness towards my husband, Christian Wittler, who has always supported me with his true and honest love throughout my studies. My gratitude for his company and love is beyond words and completed in our daughter, Anna. Without their help, this thesis wouldn’t have been possible!

13 Curriculum Vitae

FRIEDLI WITTLER, Lucia Florinda
Bachtelstrasse 100a, 8400 Winterthur
lucia.friedliwittler@gmail.com

Education and Graduation

2010-2014	Swiss Federal Institute of Technology Lausanne (EPFL), Switzerland Neuroscience PhD program (EDNE) - PhD candidate October 2014
2004-2009	Swiss Federal Institute of Technology Zurich (ETH), Switzerland Bachelor and Master of Science ETH in Human Movement Sciences
1998-2003	Euregio Gymnasium, Romanshorn (TG), Switzerland. Federal Matura (D)

Professional Experience

2010-2014	IRP Chair for Spinal Repair, Center for Neuroprosthetics, EPFL, Lausanne, *PhD student*
2009	Experimental Neurorehabilitation Laboratory, University of Zurich, *research assistant*
2008	Makora AG - innovative health management, Zurich, *Internship*

Skills

My experience in the field of top level research taught me to hold my ground also in difficult situations, and tutor my analytic ability to integrate complex information into elegant and effective solution-oriented strategies. In the past years I thus achieved a variety of skills, specific technical as well as transferable soft skills.

Transferable and soft skills: I am skilled to lead and manage interdisciplinary research projects. Therefore, I have experience in project management within a research environment. I am further used to work in an international multi-centre (merged expertise of universities and industrial companies, see project NEUWalk) environment. As a researcher, I am familiar with the conception and planning of experiments and solving of complex problems using holistic joined-up thinking. I have excellent communication and

team management skills and I am experienced in supervising and teaching students as well as guiding technical employees.

Software: I am proficient in Microsoft Office (Word, Excel, Powerpoint), have very good knowledge in video and illustration programs (Adobe Illustrator, Premiere Pro, Corel Draw). Furthermore, I am proficient in analysis software programs (e.g. Vicon Nexus) and I am used to work with note sharing programs (Evernote, OneNote) for exchanging ideas between colleagues.

Technical skills: I am a specialist in the field of neuroscience, specifically for spinal cord injury and spinal repair. I am skilled in working with a brought field of lab techniques varying from hands-on technical skills in the field of behavioural gait analysis (in rats, non-human primates and humans) over various neurosurgical techniques (rats) to dealing with complex data matrices for analysis. I am proficient in presenting scientific results, orally (congresses, meetings, seminars) and written (grant reports, publications) to a scientific as well as to a public audience.

Publications

---

1. Reticular formation mediates motor function recovery after severe spinal cord contusion. **Friedli, L.***, Beauparlant, J.*, Martinez Gonzalez, C., Laurens, J & Courtine, G. *In preparation for Nat. Neuro.*
2. Reorganization of corticospinal function increases recovery after lateralized spinal cord injury. **L. Friedli**, E. S. Rosenzweig, Q. Barraud, M. Schubert, N. Dominici, L. Awai, J. L. Nielson, P. Musienko, H. Zhong, S. Zudnowski, R. R. Roy, EMSCI Study Group, M.S. Beattie, J.C. Bresnahan, A. R. Ferguson, A. Curt, V. R. Edgerton, M. H. Tuszynski, and G. Courtine. *Submitted to the Lancet*
3. Task-specific cortical activation underlying natural locomotion in rats. DiGiovanna, J*, Dominici, N*, **Friedli, L**, Vollenweider, I, Rigosa, J, Duis, D, Beauparlant J, Kreider, J, Schieppati, M, Micera, S and Courtine, G. *Submitted to Neuron*
4. Undirected Homeostatic Plasticity contributes to neuronal dysfunction after severe spinal cord injury. Beauparlant J, van den Brand R, **Friedli L**, Musienko P, Barraud Q, Bartholdi K. *Brain 2013*
5. Restoring Voluntary Control of Locomotion after Paralyzing Spinal Cord Injury. Van den Brand* R, Heutschi* J, Barraud Q, DiGiovanna J, Bartholdi K, Huerlimann M, **Friedli L**, Vollenweider I, Martin Moraud E, Duis S, Dominici N, Micera S, Musienko P, Courtine G. *Science 2012*

6. Versatile robotic interface to evaluate, enable and train locomotion and balance after neuromotor disorders. Dominici N, Keller U, Vallery H**, Friedli L**, van den Brand R, Starkey ML, Musienko P, Riener R, Courtine G. *Nat Med 2012*
7. Multi-system neurorehabilitation strategies to restore motor functions following severe spinal cord injury. Musienko P, Heutschi J, **Friedli L**, van den Brand R, Courtine G*. Exp. Neurol. 2011*

Attended conferences

2013 *Life Science Symposia,* Lausanne, Switzerland, poster presenter

2012 Annual Meeting of the Society for Neuroscience, New Orleans (LA), USA, poster presenter

2010 Annual Meeting of the Society for Neuroscience, San Diego (CA), USA, poster presenter

2010 *Annual NCCR neuroscience symposium* (National Center for Compentence and Research, Neuroscience) 2010, Berlingen, Switzerland, attendee

2009 Annual symposium of the Center for Neuroscience (ZNZ), Zurich, Switzerland, poster presenter

2008 Annual symposium of the Center for Neuroscience (ZNZ), Zurich, Switzerland, attendee

Extracurricular Commitments and Courses

2013 Organization committee of the EPFL networking event "*School for Life Sciences Happy Hours"*.

2012-2013 Organization committee for the "*PhD Hiring days"* of the School of Life Sciences at EPFL.

2012 Organization committee of the "Lemanic Neuroscience Annual Meeting 2012".

2011 Co-founder of the "*ZNZ PhD Social"* and co-organizer of the "*ZNZ PhD Social evening event"*.

Languages

German: native English: fluent French: intermediate Italian: basic

Personal Situation

Age 31 (18.01.1983), married, one daughter (Anna, born 20.02.2014), Swiss citizen